Low-order aeroelastic models of wind turbines for controller design

Sønderby, Ivan Bergquist; Hansen, Morten Hartvig

Publication date:
2013

Document Version
Publisher's PDF, also known as Version of record

Low-order aeroelastic models of wind turbines for controller design

Ivan Bergquist Sønderby

PhD Thesis

May, 2013

Department of Wind Energy
Technical University of Denmark

M.Sc. Ivan Bergquist Sønderby
Technical University of Denmark
Department of Wind Energy, Campus Risø
4000 Roskilde
Denmark
E-mail: ivsq@dtu.dk

Preface

This thesis is written in partial fulfillment of the requirements of obtaining the degree of PhD in mechanical engineering at the Technical University of Denmark (DTU). The work has been conducted at the Department of Wind Energy at DTU in Roskilde, Denmark. The work has been supervised by Senior Scientist Morten H. Hansen and co-supervised by Senior Scientist Bjarne Kallesøe (last-mentioned until end of 2011) at the Department of Wind Energy at DTU.

The work has been done as part of a research project: Concurrent aero-servo-elastic design of wind turbines (CASED) funded by The Danish Council for Strategic Research in the Ministry of Science, Innovation and Higher Education who is gratefully acknowledged.

The thesis contains a summary of the analysis and conclusions documented in three paper manuscripts. Two of these manuscripts are submitted for publication in the journal *Wind Energy* with one manuscript accepted for publication, with the following titles:

[P1] I. Sønderby and M.H. Hansen. Open-loop frequency response analysis of a wind turbine using a high-order linear aeroelastic model. *Wind Energy*, (accepted in revised form, March 2013)

[P2] I. Sønderby and M.H. Hansen. On order reduction of high-order linear aeroelastic models. *Wind Energy*, (submitted, April 2013).

The third manuscript is submitted for the IEEE Systems and Control Conference with the following title:

[P3] F.D. Adegas, I. Sønderby, M.H. Hansen, J. Stoustrup. Reduced-Order LPV Model of Flexible Wind Turbines from High Fidelity Aeroelastic Codes. *IEEE Systems and Control Conference 2013*, (submitted 2012)

Some additional analysis and conclusions not previously submitted for publication are documented in parts of Chapter 3 and in Chapter 4 of the thesis.

I wish to thank Senior Scientist Morten H. Hansen for consultancy, patience and fruitful discussions at countless meetings throughout the project, for good and in depth review of manuscripts and for the design of the tool HAWCStab2 used to provide aeroelastic wind turbine models.

I wish to thank my friends and office mates Witold, Leonardo, Joachim, Knud, Sri, David and Carlo for countless fruitful discussions and for various humorous and heartfelt inputs that has helped me through the project. Also, I wish to thank fellow project participant Fabiano Adegas for fruitful collaboration.

Roskilde, Denmark, 2nd of May, 2013
Ivan Bergquist Sønderby

Resumé

Moderne styringer til vindmøller designes med forskellige formål og bruges blandt andet til at reducere variationer i møllens omløbstal og den genererede effekt, samt til at reducere udmattelses- og ekstremlaster på vindmøllens komponenter. Moderne styringsdesign gøres baseret på modeller af lav orden, og for at sikre en nøjagtig styring skal disse modeller nøjagtig repræsentere det aeroelastiske respons af vindmøllen. Formålet med denne afhandling er at undersøge den nødvendige modelkompleksitet i styringsdesign til vindmøller og at undersøge og udvikle metoder til at designe vindmøllemodeller af lav orden til brug i modelbaseret styringsdesign.

Afhandlingen indeholder en karakteristik af den dynamik, der har betydning på det aeroelastiske respons af moderne vindmøller i åben-sløjfe, baseret på en højordens lineær aeroelastisk model af en vindmølle. Én af de væsentlige konklusioner i denne analyse er, at overføringsfunktionen fra kollektiv pitch-vinkel ændringer til ændringer i generator hastigheden indeholder to lavfrekvente ikke-minimum fase nulpunkter. Det vises blandt andet, at korrekt modelering af disse nulpunkter kræver frihedsgrader, der beskriver blad flap- og sideværds tårnbevægelse.

Forskellige metoder til at designe aeroelastiske modeller af vindmøller med lav orden beskrives og udvikles. Lav-ordens modeller designes ved modal trunkering ved brug af de aeroelastiske egensvingningsformer for en fuld fleksibel vindmølle. Det viser sig nødvendigt at anvende relativt mange aerodynamisk dominerede egensvingningsformer for at repræsentere effekten af det afkastede hvirveltæppe og dynamisk stall, hvilket skyldes antagelsen om uafhængige strømningsrør anvendt i Blade Element Momentum (BEM) metoden. Nøjagtige lavordens modeller er derefter designet under antagelse af kvasi-statisk aerodynamik ved trunkering med et sæt lavfrekvente egensvingningsformer. En anden reduktionsmetode kaldet balanceret trunkering viser sig at kunne beskrive effekten af det afkastede hvirveltæppe og dynamisk stall ved kun få tilstands-variable. Det vises, at et sæt reducerede modeller fundet ved forskellige operationspunkter kan forbindes ved interpolation og derfor kan anvendes i styringsdesign.

I afhandlingen foreslås en ny metode til at reducere separat antallet af strukturelle og aerodynamiske tilstands-variable i aeroelastiske modeller ved brug af strukturelle og aerodynamiske basis vektorer. Nøjagtig approksimation af det lavfrekvente bladrespons opnåes ved brug af et sæt lavfrekvente, strukturelle egensvingningsformer for et blad og ved statisk residualisering af de højfrekvente egensvingningsformer. Effekten af det afkastede hvirveltæppe og dynamisk stall kan tilnærmes ved brug af et sæ aerodynamiske svingningsformer, der er slaver af strukturelle svingningsformer. Fremtidigt arbejde er at afprøve denne teknik på andre modeller af de instationære aerodynamiske kræfter på vindmøller og at anvende de reducerede modeller til styringsdesign.

Abstract

Wind turbine controllers are used to optimize the performance of wind turbines such as to reduce power variations and fatigue and extreme loads on wind turbine components. Accurate tuning and design of modern controllers must be done using low-order models that accurately captures the aeroelastic response of the wind turbine. The purpose of this thesis is to investigate the necessary model complexity required in aeroelastic models used for controller design and to analyze and propose methods to design low-order aeroelastic wind turbine models that are suited for model-based control design.

The thesis contains a characterization of the dynamics that influence the open-loop aeroelastic frequency response of a modern wind turbine, based on a high-order aeroelastic wind turbine model. One main finding is that the transfer function from collective pitch to generator speed is affected by two low-frequency non-minimum phase zeros. To correctly predict the non-minimum phase zeros, it is shown to be essential to include lateral tower and blade flap degrees of freedom.

The thesis describes and analyzes various methods to design low-order aeroelastic models of wind turbines. Low-order models are designed by modal truncation by using the aeroelastic mode shapes of a fully flexible wind turbine. To capture the effect of shed vorticity and dynamic stall, a relatively large number of aerodynamically dominated modes are required, due to the assumption of independent annular flow tubes in the Blade Element Momentum theory (BEM). A set of accurate reduced-order models are subsequently designed assuming quasi-steady aerodynamics, by truncation with a set of low-frequency mode shapes. In a comparison, the balanced truncation method is found to be able to capture the effect of the shed vorticity and dynamic stall using only few states. A set of reduced-order models obtained at various operating points are shown to be easily connected by interpolation and are thereby suited for gain-scheduling control design.

A new method is proposed to reduce separately the number of structural and aerodynamic states in aeroelastic models by using a set of structural and aerodynamic basis functions. Accurate approximation of the low-frequency blade response is obtained using a set of purely structural blade mode shapes and by static residualization of the high-frequency blade modes. The effect of shed vorticity and dynamic stall on the blade response can be captured using a set of aerodynamic slave modes of the low-frequency structural flap modes. Future work is to test the proposed method on others models of the unsteady aerodynamic forces on wind turbines and to use the reduced models for controller design.

Contents

Chapter 1

Introduction

The purpose of modern wind turbines is to harvest the power of the wind and convert mechanical wind power into electrical energy used in households and industry. Today, the use of wind turbines to generate electrical power has become a feasible alternative to the burning of fossil fuels.

Horizontal axis wind turbines, which is the subject of this thesis, have been used to generate electricity as early as the late nineteenth century by Poul La Cour in Denmark [1]. In the beginning of the 1970's the increasing price of fossil fuels motivated further research into horizontal axis wind turbines, leading to the design of three-bladed, fixed-speed, stall-regulated wind turbines in the 1980's denoted as the 'danish' design concept [2]. Stall-regulated wind turbines were the dominating design of newly installed wind turbines for many years. Stall-regulated wind turbines benefit from the passive decrease in lift occurring at above rated wind speeds due to stall that limits the aerodynamic torque on the rotor. Stall-regulated turbines with large, flexible blades can suffer from stall-induced edgewise blade vibrations resulting in large blade root bending moments.

Today, most newly installed turbines are variable-pitch, variable-speed wind turbines using asynchronous generators. A variable-pitch, variable-speed turbine can be operated close to maximum power capture at all wind speeds. The main advantage of using variable-pitch wind turbines is the ability to actively regulate the aerodynamic torque on the rotor and thereby control the generated power and rotor speed. Another advantage is the ability to perform active load reduction with the controller using collective, cyclic and/or individual pitch. Figure 1.1 shows a photograph of a modern, horizontal axis wind turbine with three blades in operation close to the West coast of Jutland, Denmark.

Today, the trend is that wind turbines are upscaled, such that they are designed with larger rotor diameters and higher towers. The overall cost-effectiveness of wind turbine upscaling has received a lot of attention and was recently studied in the UpWind project [3] in which various suggestions are made to circumvent design challenges for wind turbines with a capacity of up to 20 MW. With increasing turbine size, the vibration of the wind turbine tower and blades becomes more low-frequent, such that the wind turbine control system is more likely to interact with the structural vibration of the flexible bodies of the wind turbine.

Active control of wind turbines is used to optimize the performance of wind turbines. The primary goal of the wind turbine controller is to limit variations in the generator speed and the generated power and this is usually done by varying the generator torque and collective blade pitching in response to a measurement of the generator speed signal. Recently a lot of focus is on designing wind turbine controllers that actively reduce loading on wind turbines, such as controllers that actively increase the damping of the drivetrain torsional vibration through generator torque control and active load reduction of the tower base bending moments by collective pitching. Proper design of a wind turbine controller can reduce power variations, fatigue and extreme loads on components and prevent instabilities to occur. Model-based controllers are suited for design of such controllers designed to achieve multiple objectives with multiple controller inputs. To meet the objectives of

Figure 1.1: Modern upwind, variable-speed, pitch-regulated, horizontal axis wind turbines in operation close to the West coast of Jutland, Denmark.

the controller, the controller must be designed on a model that correctly predicts the aero-servo-elastic response of the wind turbine. This thesis deals with the necessary complexity of such control design models and how to design low-order aeroelastic models of wind turbines suited for model-based control design.

The remainder of this chapter contains an overview of the state of the art in low-order aeroelastic models used for wind turbine control design, followed by a description of the motivation and content of the thesis.

1.1 State of the art

This section gives a short description of the concepts of unsteady aerodynamics of shed vorticity, dynamic stall and dynamic inflow, followed by a review of the low-order aeroelastic models usually used for control design.

1.1.1 Engineering models of unsteady aerodynamics

The Blade Element Momentum (BEM) theory is the prevailing method used to predict the aerodynamic forces on horizontal axis wind turbines in engineering and control design models. The BEM theory provides a method of predicting the static aerodynamic forces acting on wind turbine blades operating with constant inflow perpendicular to the rotor [4].

A wind turbine blade in operation experiences an airflow that varies in time, because of wind turbulence, wind shear and whenever the rotor is not aligned with the inflow. Another source of time-varying inflow is that of **dynamic inflow**. Dynamic inflow characterizes the dynamic changes in the induction at the rotor plane caused by the rotor wake when the

loading on the rotor changes due to changes in pitch angles or the wind speed. The effect of dynamic inflow was demonstrated in early experiments on the Tjæreborg turbine [5] by measuring the wind turbine response from a change in blade pitch. Figure 1.2 shows a time series of the measured shaft torque in response to a change in collective pitch angle from the Tjæreborg experiments, reproduced from Hansen et al. [6]. A simplified model of dynamic inflow suited for coupling with the BEM model was developed by Øye [7] using two first order filters with radially dependent time constants. The time constants used to describe the effect of dynamic inflow are on the order of the mean wind speed divided with the rotor diameter. Recent models of dynamic inflow used in aeroelastic simulation tools are similar to the model proposed by Øye and has been validated with Computational Fluid Dynamics analysis [5, 8]. Common practice is to design controllers using models where instant update of the induction is assumed [2]. The effect of including dynamic inflow in controller and estimator design has received a lot of attention as reviewed by Henriksen et al. [9] who propose a simplification to Øye's dynamic inflow model making the model suited for controller and estimator design.

When the blades sees a change in relative inflow, the aerodynamic forces are not immediately changed as predicted by the static lift and drag curves, but experience a lag. For an airfoil operating in attached flow, the aerodynamic forces are lagging because of the memory effect of circulation shed into the wake of the airfoil when the bound circulation on the airfoil changes, denoted the **shed vorticity** [11]. The influence of the shed vorticity on the aerodynamic forces on the airfoil becomes prominent when the vibrational frequency is high relative to the inflow velocity (i.e. at high *reduced frequencies*). Figure 1.3 shows an example of measured variations in lift coefficient versus angle of attack for an airfoil undergoing harmonic pitching both below and above stall, reproduced from Leishman [10]. The effect of shed vorticity is to decrease the slope of the lift curve in attached flow [12], such that the changes in the aerodynamic forces are lower than evaluated at the static lift and drag curves. **Dynamic stall** is a phenomena that occurs in stalled operation where the presence of a vortex shed from the trailing edge causes a decrease in pressure on the suction side of the airfoil and thereby much higher lift than for an airfoil in static

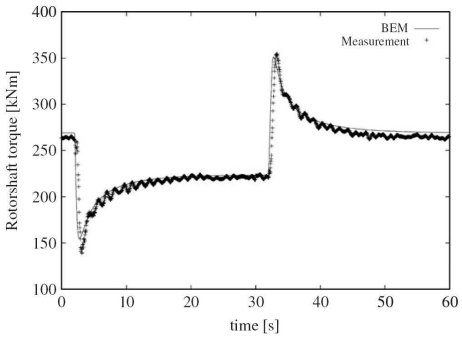

Figure 1.2: Measured time series of shaft torque in response to step changes in collective pitch of the Tjæreborg wind turbine compared with an engineering model of dynamic inflow. Reproduced from Hansen et al. [6].

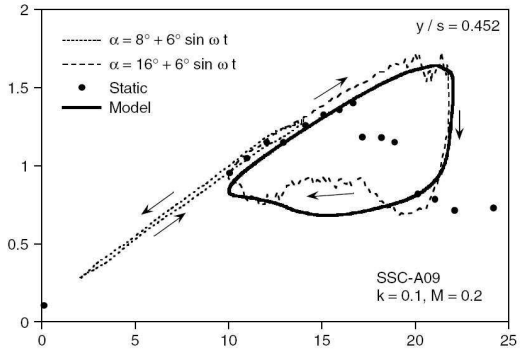

Figure 1.3: Dynamic lift coefficient versus angle of attack for an airfoil undergoing harmonic pitching at a reduced frequency of 0.1. Comparison between experiments and models. Reproduced from Leishman [10]

operation at the same angle of attack [13]. Early work by Rasmussen et al. [14] shows the importance of dynamic stall in prediction of aerodynamic damping of wind turbine blades at typical frequencies of structural vibration. In wind turbine applications it is important to predict both the effect of shed vorticity and dynamic stall [10].

There exist a limited number of state space models describing the effects of shed vorticity and dynamic stall. The dynamic stall model developed by Øye [15] is widely used in nonlinear aeroelastic simulation models of wind turbines. Hansen et al. [12] developed a model including both the effects of shed vorticity and dynamic stall, which has been linearized for use in aeroelastic modal analysis and controller design. Another example is the ONERA model [16]. These models use between one and four time constants at each blade section for all three blades to describe the aerodynamic forces which leads to high-order models that are not directly suited for controller design. Control design models typically assume quasi-steady aerodynamic forces, which means that the changes in aerodynamic forces are predicted from the static lift and drag curves at the blade sections. To the authors knowledge there are no examples of wind turbine models suited for control design that include the effects of shed vorticity and dynamic stall.

One of the drawbacks of the Blade Element Momentum theory is that it assumes that there is no aerodynamic coupling between aerodynamic forces at different radial sections of the blades, usually denoted as the strip theory. In reality, the aerodynamic forces experienced at one blade section are affected by the forces experienced in neighbouring sections. The prediction of the aerodynamic coupling effects in the spanwise blade direction can be improved in BEM models by making a 3D correction to the aerodynamic profile coefficients [17]. Models of both the shed and trailing vorticity in the near wake has been designed and coupled to the BEM model to describe the 3D aerodynamic coupling effects using indicial functions [17]. A current research topic is to couple the models used to describe the dynamic effect of the near wake on the blade loading with models of structural dynamics.

Reduced-order models of the unsteady aerodynamic forces on aircrafts has recently been designed by modal truncation using purely aerodynamic eigenmodes that describes the dominant flow structures. Reduced-order models of unsteady aerodynamics has been designed for e.g. incompressible, potential flows using a vortex-lattice model [18] and flows described by the Euler equations as reviewed by Dowell [19]. For better approximation at low frequencies, a static and dynamic correction method has been proposed [20]. The Proper Orthogonal Decomposition (POD) technique [21] is a model reduction technique that constructs a set of basis vectors that optimally describes the energy content in a number of snapshots of the flow field with a low number of states. The POD technique has been used in wind turbine analysis to describe the main effect of turbulence in the inflow [22].

1.1.2 Low-order aeroelastic models for controller design

Øye [23] proposes to tune the gains of a classical controller in the collective pitch to speed loop using a model that includes only one state describing rigid body rotation of the rotor. Changes in aerodynamic forces caused by changes in rotor speed, mean wind speed and collective pitch angles are predicted under assumption of frozen wake. Linear time-invariant aeroelastic models are obtained at various operating points by linearization of the nonlinear aerodynamics at the desired operating points. The effect of model complexity on this tuning of a classical controller is addressed by Hansen [24], who uses a high-order linear aeroelastic model including tower, drivetrain and blade flexibilty and effects of shed

vorticity and dynamic stall to tune a classical collective and cyclic pitch controller. If the gain of the proportional-integral controller is tuned using a model of a rigid turbine, then the closed-loop pole of the rigid body rotor mode has a frequency higher than that tuned for and a damping ratio much lower, due to the flexibility of the turbine.

Bossanyi [25] has investigated the necessary model complexity used for control design of a pitch-regulated, variable-speed wind turbine. When operating in generator torque control, he suggests to use a model that contains at least rigid body rotation of the drivetrain and rotor and the first torsional drivetrain mode by coupling of the rotor inertia to a generator inertia by a torsional spring. For above rated operation using collective pitch control, he suggests also to model at least the inertia of the rotor and generator, the pitch actuator and the longitudinal tower vibration. The first longitudinal tower mode must be included because the pitch-controller excites this mode through variations in aerodynamic thrust and because the pitch-controller is used to actively damped tower vibrations to reduce tower loads.

Correct modelling of the tower dynamics is also important due to the presence of a non-minimum phase zero that limits the bandwidth of the collective pitch controller of the generator speed. Leithead et al. [26] analyze the frequency response from collective pitch demand to generator speed and show existence of a non-minimum phase zero at the 1^{st} tower modes and show how to compensate for them in closed-loop operation. The non-minimum phase zero is a limitation on the bandwidth of the pitch to speed controller because of the large negative change in phase occurring at the zero which is not cancelled by the poles of the tower motion. The change in phase associated with the non-minimum phase zero makes the speed respond opposite to that of a minimum phase zero and must therefore be correctly predicted. The non-minimum phase zeros is a problem for large turbines and especially for offshore turbines, because of the low tower frequencies. Fischer [27] clarifies under what conditions that the non-minimum phase zero exists based on a simplified model including a longitudinal tower degree of freedom and one state to describe rigid body rotor rotation. Changes in the aerodynamic forces are modeled with quasi-steady gradients of rotor torque and thrust from changes in pitch and from changes in the relative wind speed seen by the rotor.

Wright & Balas [28] investigate how the complexity of the control design model influence collective pitch control of a two-bladed turbine. They find that it is important to include rigid body rotor rotation, drivetrain flexibility, the first collective flap modes and longitudinal tower bending mode. To ensure stable closed-loop behavior the controller model must include the free-free drivetrain torsion mode.

A conventional way to model the structural vibration of wind turbines in low-order models is to use the purely structural mode shapes of each of the wind turbine substructures: tower, drivetrain and blades. One common approach is to use the Component Mode Synthesis method [29, 30] in which the wind turbine is modelled using the rigid body modes and a set of structural modes describing the flexibility of the substructures, which are then subsequently connected to represent the structural dynamics of the wind turbine. Variants of the component mode synthesis method are applied in the TURBU tool [31], in Bladed [32] and in FAST [33]. TURBU can provide reduced-order models by such an order reduction scheme of a finite beam element model of tower, drivetrain and three blades that is coupled with an unsteady BEM model including aerodynamic states to describe dynamic stall. Reduced-order models provided by TURBU are utilized for extreme gust control [34] and individual pitch control [35] and one can reduce the order of the model from 600 to 100 states and conserve the frequency response up to 5 Hz [31]. To conserve the frequency

response at low frequencies it was required to "*include the quasi-steady behavior of the high-frequency modes*" in the blade and tower substructures. To the authors knowledge, order reduction is not applied of the equations describing dynamic stall.

Some order reduction techniques in Finite Element analysis of structural mechanics are reviewed by Cook [30]. One approach is to do modal expansion, where the basis is shifted and a set of generalized states are used to describe vibration of a reduced set of structural mode shapes. To achieve better approximation at low frequencies, a static correction can be applied whereby the static deflection under external excitation of the structure is ensured to be exact.

Design of linear low-order aeroelastic models for model-based control design has been extensively studied for aircrafts [21, 36]. Traditionally, the structure is assumed to vibrate in prescribed structural mode shapes and unsteady aerodynamic forces are described as slaves of these prescribed structural mode shapes. Order reduction techniques are developed to represent unsteady aerodynamic forces cast in the frequency domain by low-order rational transfer function matrices for each structural mode shape. A rational transfer function matrix can be realized in a state space formulation and be used in model-based control design. In the design of reduced-order aeroelastic models for aircrafts, Karpel [37] proposes to use a dynamic residualization scheme in which the effect of aerodynamic and structural stiffness and damping forces on high-frequency modes is retained.

Order reduction using wind turbine mode shapes is one of many order reduction techniques that can be used to generate low-order models for controller design. One property of modal order reduction is that each mode dominate the response close to the aeroelastic frequency of this mode, such that good approximation typically can be achieved in a specified frequency interval by using the modes in the region. The design of reduced-order models for control design has been extensively studied in the control engineering community. A comprehensive review of these order reduction techniques can be found in a book by Antoulas [38] described in a line of thought suited for control engineers and in a review by Ersal et al. [39]. The *balanced* reduction technique is a projection-based technique in which the original basis of the states is projected onto another basis by a similar transformation. The balanced *truncation* technique is proposed by Moore [40] and is widely used in the design of low-order linear state space models. The balanced truncation technique use a transformation onto a reduced set of basis vectors that contains most of the signal energy transmitted from a chosen set of inputs to a set of outputs in a transfer function matrix. In the case of lightly damped second order modes that typically arise in models of structural dynamics, the balanced basis converges towards the modal basis as the damping decreases [41]. The aeroelastic mode shapes of a wind turbine are however largely damped by aerodynamics and the two methods are therefore not similar in this case. Clarx & Cox [21] use balanced truncation to reduce the number of free wake vortices in a vortex-lattice model of aerodynamic forces on a typical airfoil section.

A wind turbine is operated at various conditions depending on e.g. the mean wind speed at the rotor. The models used for design of controllers and estimators must vary with the operating point, because the aerodynamic forces depend nonlinearly on the relative wind speed, and because of nonlinearities due to stall. Another reason is the effect on the local changes in aerodynamic forces due to the deflected state of the blades. The effect of blade deflection on the aeroelastic stability of a wind turbine blade is studied by Kallesøe [42], who concludes that mainly the edgewise blade modes are affected by the blade deflection through coupling with blade torsion due to the static flapwise blade bending.

The usual approach in control design to accommodate these effects is to design a controller for a set of frozen values of the scheduling variable and then interpolate the controller gains [23, 43]. Recent advances in design of gain-scheduling controllers for wind turbines are designs of a linear parameter-varying (LPV) state space model of the wind turbine that covers specific regions of the operating curve and models nonlinear changes with operation point by parameter-varying matrices in the state space model. LPV controllers are designed by Bianchi et al. [44] based on a model that includes nonlinear variations in aerodynamic torque. Østergaard et al. [45] also parameterizes aerodynamic thrust variations and includes drivetrain torsional flexibility and longitudinal tower flexibility and shows improvements in performance relative to classical controllers.

Both in the design of model-based, gain-scheduling controllers and for LPV controllers there is a need to have a set of low-order models at various operating points, that can be described by a set of system matrices which can be parameterized with a scheduling variable using a set of states that are somewhat consistent. One way to ensure that the states are consistent is to use the structural or aeroelastic modal coordinates, i.e. the generalized states that describes vibration of the structural or aeroelastic modes of the turbine, as already seen in previous LPV controllers [44, 45]. For LPV control design the set of reduced-order system matrices must be parameterized, e.g. by assuming polynomial dependency with respect to the scheduling variable, which can be done by using linear least squares optimization [46].

1.2 Motivation

The scope of this thesis is twofold:

1. To create insight into the aeroelastic response of modern horizontal axis wind turbines in response to control signals and disturbances and thereby to describe what wind turbine dynamics is relevant to include in control design models.

2. To analyze and propose methods to design low-order aeroelastic models of wind turbines that accurately approximates the aeroelastic wind turbine response and are suited for design of model-based controllers.

It is important that design and tuning of controllers and estimators is performed on aeroelastic models that characterize accurately the response of wind turbines in operation. The objectives of the controllers cannot be reached if these models are inaccurate. This thesis aims at giving a description of what influence the low-frequency, aeroelastic frequency response of wind turbines in a way that is useful in the control design based on more accurate aeroelastic models of wind turbines.

Typically, the models used in the design and tuning of controllers are very simplified models cast directly as low-order models and are not validated thoroughly with more accurate models or wind turbine measurements. More accurate models may be obtained using a similar number of states by reducing the order of high-order aeroelastic models. This thesis explores some of the existing order reduction techniques and proposes another technique to design low-order aeroelastic models of wind turbines.

The main contributions of this thesis are:

1. A thorough analysis of the aeroelastic frequency response of a modern wind turbine in open-loop, in which special attention is given to the response of the generator

speed output in response to harmonic changes in collective pitch, generator torque and in the mean wind speed. It is found that the lateral tower vibration and collective flap motion influence the prediction of two non-minimum phase zeros occurring at low frequencies.

2. An evaluation of the use of the modal truncation order reduction technique in the design of low-order linear aeroelastic wind turbine models, including a description of the influence of both the structurally and aerodynamically dominated modes on the static and dynamic frequency responses of a wind turbine.

3. A comparison of the modal truncation and balanced truncation order reduction techniques in relation to the design of a set of low-order aeroelastic models of wind turbines suited for the design of gain-scheduled model-based controllers.

4. A description and evaluation of a proposed order reduction technique that separately reduces the order of the structural degrees of freedom and the number of aerodynamic states in aeroelastic models by using a set of structural and aerodynamic basis functions, respectively.

1.3 Outline

Chapter 2 presents the results given in [P1] and contains first a description of the high-order linear aeroelastic model of a modern wind turbine used in the subsequent analysis. The linear aeroelastic model is then validated with a nonlinear aeroelastic model by comparing a set of aeroelastic frequency response functions for operation at various wind speeds. The complexity of the linear model is then varied in an open-loop frequency response analysis to clarify what must be included to capture the aeroelastic frequency response of a wind turbine.

Chapter 3 presents the results and analysis given in [P2] and [P3] and contains a description of the modal truncation order reduction method and an evaluation of the effect of the low-frequency structurally and aerodynamically dominated modes, where the latter describes the effects of shed vorticity and dynamic stall. Reduced-order models are subsequently designed by modal truncation assuming quasi-steady aerodynamics. The reduced-order models obtained by modal truncation are compared with models obtained by balanced truncation and it is shown how the components of the reduced-order system of equations are suited for interpolation with wind speed.

Chapter 4 contains a description of a new order reduction scheme using structural and aerodynamic modes to reduce separately the structural and aerodynamic states in aeroelastic models. As an example the technique is used to design low-order aeroelastic models of a wind turbine blade. Chapter 5 contains the conclusions of the thesis and gives recommendations for future work.

Chapter 2

Open-loop frequency response analysis

The purpose of this chapter is to analyze and describe the necessary model complexity that is required to describe the aeroelastic wind turbine response in control design models.

This chapter contains first a description of the high-order linear aeroelastic model of a wind turbine used in the subsequent analysis. The linear aeroelastic model is then validated with a nonlinear aeroelastic model by comparing the aeroelastic frequency response functions for small amplitude control inputs in open-loop for a turbine in normal operation at various wind speeds. The complexity of the linear model is then varied to clarify what influence the aeroelastic frequency response functions from harmonic changes in generator torque, collective pitch angle demand and in the mean wind speed to the generator speed output at various wind speeds.

2.1 High-order linear aeroelastic model

This section contains a description of the linear aeroelastic model of the NREL 5 MW onshore wind turbine defined by Jonkman et al. [47] and used for subsequent frequency response analysis. The model is identical to the available HAWC2 model [48] except that the static tilt is set to 0 deg to ensure uniform inflow. The structural damping of the drivetrain is lowered, by changing the Rayleigh parameter for stiffness proportional damping of torsional motion from 0.0184 Nm·s/Nm to 0.0120 Nm·s/Nm.

2.1.1 Model description

The high-order model used for frequency response analysis is the recent linear aeroelastic model HAWCStab2 developed in house. A more complete description of the linear aeroelastic model is provided by Hansen [24] for an isolated blade. The model is a linearization of a geometrically nonlinear finite beam element model coupled with an unsteady Blade Element Momentum model of aerodynamic forces on the blades including effects of shed vorticity and dynamic stall. So far, the model assumes frozen wake and does not include a model of dynamic inflow. A comparison is made using nonlinear time simulations to clarify the effect of dynamic inflow.

Linearization is performed analytically around a stationary deflected state of the blades obtained from an equilibrium between elastic and centrifugal forces and the static aerodynamic forces due to an assumed uniform inflow to the rotor plane. Gravity forces are neglected to obtain this stationary steady operational state for any operational point given by a mean wind speed, pitch angle and rotor speed.

The discretization used in the finite beam element model is illustrated in Figure 2.1. The number of elements used to model the tower, drivetrain and each blade are eight, four and 19 Timoshenko beam elements, respectively. Four elements are used for the drivetrain to ensure correct modeling of bending and torsion of the drivetrain. Each element has two nodes and six degrees of freedom (DOFs) per node to describe rotation and translation in all three axis. The generator and pitch bearings are modeled as frictionless bearings. Pitch

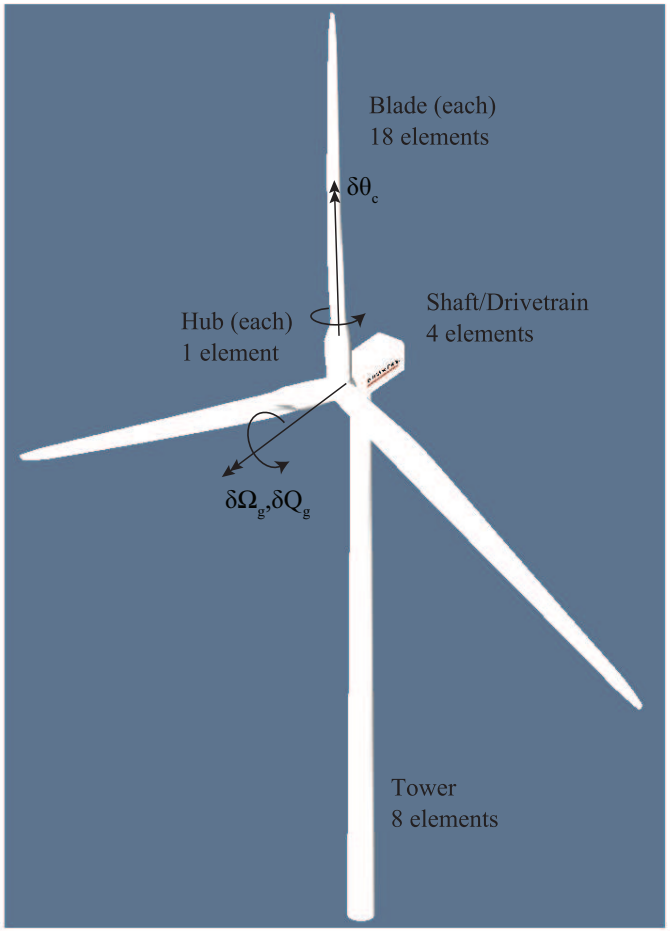

Figure 2.1: Snap shots from HAWCStab2 animation of NREL wind turbine listing the number of elements and showing the definitions of positive directions of inputs and outputs.

actuators are modeled by second order response of actual pitch to demanded input. The aeroelastic turbine dynamics is investigated without effect of actuators, and the frequency of the actuator model is therefore set so high that the demanded pitch angle is reached almost instantly for the frequency range analyzed. Aerodynamic forces on the blades are modeled by using 30 aerodynamic calculation points distributed such that they are closely spaced at the blade root and tip. The model of unsteady aerodynamics includes at each aerodynamic calculation point, two states to approximate the frequency response of the Theodorsen theory and two states are used to describe trailing edge separation and dynamic stall as described in Hansen et al. [12].

All degrees of freedom describing blade and hub motion and all aerodynamic states are transformed into multiblade coordinates by the Coleman transformation to remove dependency of the rotor azimuth angle in the system matrices. The state vector $\mathbf{z}_k$ that describes the structural and aerodynamical states for blade k in blade-fixed coordinates,

is transformed into multiblade coordinates by the Coleman transformation:

$$\mathbf{z}_k = \mathbf{a}_o + \mathbf{a}_1 \cos\left(\Omega t + \tfrac{2\pi}{3}(k-1)\right) + \mathbf{b}_1 \sin\left(\Omega t + \tfrac{2\pi}{3}(k-1)\right),\ k = 1,2,3 \tag{2.1}$$

where $\mathbf{a}_0$, $\mathbf{a}_1$ and $\mathbf{b}_1$ are the collective and the two cyclic components of $\mathbf{z}$, respectively. When the blades are identical and identically mounted (isotropic rotor) and the wind speed is uniform over the rotor and perpendicular to the rotor, then the Coleman transformation removes dependency of the azimuth angle in the system matrices of the linearized aeroelastic model [49].

2.1.2 Equations of motion

The linear high-order aeroelastic model is described by the system of equations

$$\mathbf{M}\ddot{\mathbf{z}}_s + (\mathbf{C}_s + \mathbf{G} + \mathbf{C}_a)\dot{\mathbf{z}}_s + (\mathbf{K} + \mathbf{K}_a + \mathbf{K}_{sf})\mathbf{z}_s + \mathbf{A}_f\mathbf{x}_a = \mathbf{F}_s \tag{2.2a}$$

$$\dot{\mathbf{x}}_a + \mathbf{A}_d\mathbf{x}_a + \mathbf{C}_{sa}\dot{\mathbf{z}}_s + \mathbf{K}_{sa}\mathbf{z}_s = \mathbf{F}_a \tag{2.2b}$$

where Equation (2.2a) governs structural vibration of the structural degrees of freedom in $\mathbf{z}_s$ and Equation (2.2b) describes the aerodynamic states $\mathbf{x}_a$ used to model unsteady aerodynamics on the blades. The matrices $\mathbf{M}$, $\mathbf{K}$ and $\mathbf{C}_s$ are the mass, stiffness and structural damping matrix, respectively. The stiffness matrix models both elastic stiffness and centrifugal blade stiffness. The matrix $\mathbf{G}$ models gyroscopic forces on the blades and $\mathbf{C}_a$ and $\mathbf{K}_a$ are the aerodynamic damping and stiffness matrices, respectively. The aerodynamic states couples to the structural states through the term $\mathbf{A}_f\mathbf{x}_a$ and the structural dynamics excites the aerodynamic states through both a velocity dependent term $\mathbf{C}_{sa}\dot{\mathbf{z}}_s$ and a translation/rotation dependent term $\mathbf{K}_{sa}\mathbf{z}_s$. The matrix $\mathbf{A}_d$ describes the lag on the aerodynamic forces. The terms $\mathbf{F}_s$ and $\mathbf{F}_a$ represents structural and aerodynamical forces due to actuators and changes in the wind speed. To improve the conditioning of the eigenvalue problem set up directly on the first order form of Equation (2.2), a reduced state transformation is applied using structurally undamped eigenvectors as described in [P1] but omitted here for brevity.

The system in Equation (2.2) is put on first order form:

$$\dot{\mathbf{x}} = \mathbf{A}\mathbf{x} + \mathbf{B}\mathbf{u} \tag{2.3a}$$

$$y = \mathbf{C}\mathbf{x} \tag{2.3b}$$

where, by definition:

$$\mathbf{x} = \begin{Bmatrix} \mathbf{x}_a \\ \mathbf{z}_s \\ \dot{\mathbf{z}}_s \end{Bmatrix} \quad ; \quad \mathbf{u} = \begin{Bmatrix} \delta Q_g \\ \delta\theta_c \\ \delta W \end{Bmatrix} \quad ; \quad y = \delta\Omega_g \tag{2.4}$$

$$\mathbf{A} = \begin{bmatrix} -\mathbf{A}_d & -\mathbf{K}_{sa} & -\mathbf{C}_{sa} \\ \mathbf{0} & \mathbf{0} & \mathbf{I} \\ -\mathbf{M}^{-1}\mathbf{A}_f & -\mathbf{M}^{-1}(\mathbf{K} + \mathbf{K}_a + \mathbf{K}_{sf}) & -\mathbf{M}^{-1}(\mathbf{C} + \mathbf{G} + \mathbf{C}_a) \end{bmatrix} \tag{2.5}$$

$$\mathbf{B} = \begin{bmatrix} \mathbf{0} & \mathbf{B}_{da} \\ \mathbf{0} & \mathbf{0} \\ \mathbf{M}^{-1}\mathbf{B}_{us} & \mathbf{M}^{-1}\mathbf{B}_{ds} \end{bmatrix} \quad ; \quad \mathbf{C} = \begin{bmatrix} \mathbf{0} & \mathbf{0} & 0...1...0 \end{bmatrix} \tag{2.6}$$

where $\mathbf{B}_{us}$, $\mathbf{B}_{ds}$ and $\mathbf{B}_{da}$ have been linearized with respect to the inputs and are defined from:

$$\mathbf{F}_s = \mathbf{B}_{us} \left\{ \begin{array}{c} \delta Q_g \\ \delta\theta_c \end{array} \right\} + \mathbf{B}_{ds}\delta W \quad ; \quad \mathbf{F}_a = \mathbf{B}_{da}\delta W \tag{2.7}$$

where δQ_g, $\delta\theta_c$ and δW denotes small variations in the generator torque, collective pitch angles and mean wind speed, respectively and where $\mathbf{C}$ extracts the generator speed variations $\delta\Omega_g$. Figure 2.1 shows the definitions of positive inputs and outputs. There is no gearbox model, i.e., the low speed shaft (LSS) speed of the generator is used in the analysis.

2.1.3 Changes in the model complexity

The linear model is used to analyze the frequency response functions between each input and each output. To investigate the effects of model complexity, different versions of the linear model is used: Substructures may be made rigid by removing the DOFs. In cases referred to as *purely structural*, the mean aerodynamic forces are included to find the static blade deflection, but the variation of aerodynamic forces are removed in the linear system of equations. In cases referred to as '*unst.aerodyn.*', the model includes unsteady airfoil aerodynamics, whereas quasi-steady airfoil aerodynamics is referred to as '*qs.aerodyn.*'. The assumption of quasi-steady airfoil aerodynamics is achieved by setting $\dot{\mathbf{x}}_a = \mathbf{0}$ in Equation (2.2b), solving for $\mathbf{x}_a$ and inserting the solution in (2.2a).

If all substructures are made rigid, only the generator bearing is retained, and quasi-steady aerodynamics is assumed, the linear model reduces to the simple 1st order model proposed by Bossanyi [25] and often used in control design models:

$$I_r\delta\dot{\Omega}_g = \delta Q_g + \left.\frac{\partial Q}{\partial\Omega}\right|_0 \delta\Omega_g + \left.\frac{\partial Q}{\partial\theta}\right|_0 \delta\theta_c \tag{2.8}$$

where I_r is the total rotational inertia of the drivetrain and rotor and Q is the aerodynamic torque on the rotor. The frequency responses predicted with the high-order linear model are compared with the predictions using this 1st order model and the gradients of the aerodynamic torque assumes that the wake is frozen such that there is no change in the induction for changes away from the operation point to be able to compare with the linear model.

2.2 Validation with time simulations using nonlinear model

This section presents a validation of the aeroelastic frequency response predicted by the linear model with the response predicted by the nonlinear aeroelastic model HAWC2 [50]. Validation is done on the frequency response from generator torque and collective pitch to generator speed for the NREL 5 MW wind turbine operating at 8 and 20 m/s for small amplitude input signals. The effects of dynamic inflow are clarified by validation with the nonlinear model. The linear aeroelastic model is then used to perform aeroelastic modal analysis to explain the sources of resonances in the frequency responses.

2.2.1 Frequency response

The frequency response functions predicted by the linear model given by Equation (2.3) is found from the transfer function matrix $\mathbf{G}(s)$, which is the ratio of the Laplace transform

of the output $Y(s)$ to the Laplace transform of the inputs $\mathbf{U}(s)$:

$$\mathbf{G}(s) = \frac{Y(s)}{\mathbf{U}(s)} = \mathbf{C}(s\mathbf{I} - \mathbf{A})^{-1}\mathbf{B} \tag{2.9}$$

where s is the complex Laplace variable. The steady amplitude and phase shift relative to the input is found by matrix inversion as the modulus and phase of $\mathbf{G}(i\omega)$, where $i = \sqrt{-1}$ and ω is the excitation frequency.

The nonlinear aeroelastic model used in the simulations includes geometrical nonlinearities due to large deflections, nonlinear unsteady and wake aerodynamics and nonlinear couplings between structural degrees of freedom and aerodynamic states. Structural damping is modeled as Rayleigh type damping where damping is assumed proportional to structural stiffness and inertia. Spectral damping is used in the linear model, where a damping matrix is deduced that gives a specific damping ratio to each structural mode. Structural damping in the linear model is tuned to approximate the structural damping in the nonlinear model at standstill. The nonlinear aeroelastic model includes dynamic inflow modeled as two 1^{st} order filters with radial dependent time constants. The two filters models the dynamic contribution to the induction from the far wake and the near wake, respectively [8, 50].

Figure 2.2 shows a typical time series of variations in generator LSS speed used for the extraction of the frequency response function from HAWC2. The left diagram shows the time series at start up and until reaching close to steady state. The large overshoot on the speed during the initial transients has no influence on the present analysis. Excitation from gravity forces, wind shear, tower shadow and wind turbulence are removed to reach close to stationary state. The rotor accelerates until generator torque and collective pitch control actions limits the rotational speed to around 12.1 rpm. At $t = 200$ s, the pitch angles are fixed to the desired value which is slightly different than that set by the controller, thereby causing a slight disturbance on the speed signal which is dampened by the generator torque control. At $t = 295$ s, generator torque is fixed and harmonic signal is overlayed at $t = 300$

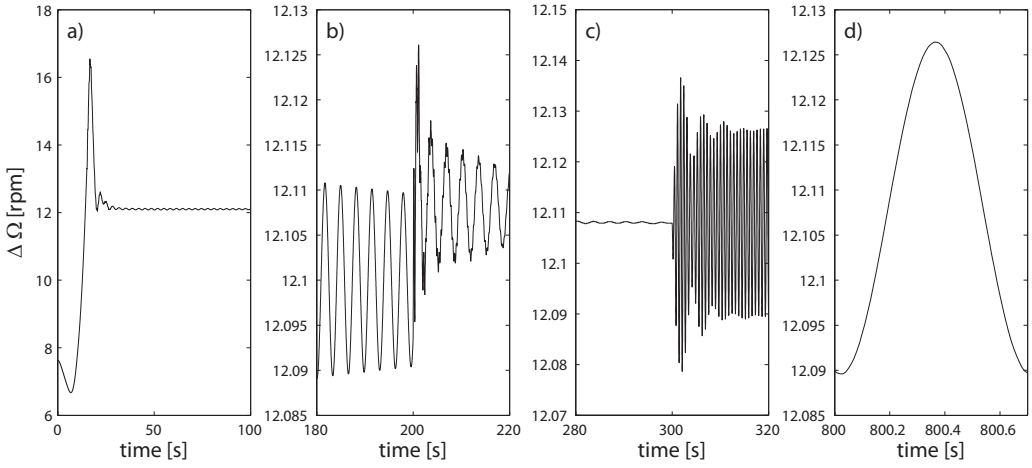

Figure 2.2: Typical time series of generator speed from simulations using nonlinear aeroelastic model by subsequent FFT analysis a) at start up, b) before and after pitch angle is fixed, c) before and after harmonic excitation is initiated and d) of the assumed stationary variation.

s on static generator torque and collective pitch separately, until the end of the simulation. The overlayed harmonic changes in generator torque and collective pitch has amplitudes of 48.5 kNm on the low speed shaft and 0.5 deg, respectively. A total of 205 simulations has been performed for each operation point and input type using harmonic excitation at different frequencies, such that the frequency response can be obtained in an interval $[0, 3]$ Hz.

After transients have dampened out a Fourier transformation is done on a time signal spanning one period at the excitation frequency. In simulations where the generator torque and collective pitch angles are varied at frequencies below 0.1 Hz, the signal is extracted from $t = 1300$ s. For excitation frequencies above 0.1 Hz, the signal is extracted from $t = 800$ s. Figure 2.2d shows the time-series used for Fourier transformation. The time step size is set such that one period at the excitation frequency includes 2^N samples, where $N \in [6; 14]$ depending on the excitation frequency. It is ensured that the sampling frequency is always higher than 50 Hz for excitation frequencies below 0.1 Hz and always higher than 100 Hz for excitation frequencies above 0.1 Hz, to avoid damping and frequency shifts introduced by the Newmark time integration scheme used in HAWC2.

Estimates of the linear frequency response are achieved by taking the Fourier amplitude and phase at the excitation frequency, whereby remaining nonlinear and transient effects are minimized. Figures 2.3 and 2.4 show comparisons of the frequency response from generator torque and collective pitch demand to generator speed, respectively, predicted by the linear and nonlinear models at 8 m/s and 20 m/s.

The response predicted by the linear model is similar to the response obtained from nonlinear time simulations for small excitation amplitudes. The responses deviates around 1.6 Hz and 2.7 Hz, which can be explained by differences in the models of structural damping of the 1^{st} and 2^{st} drivetrain modes, because the responses can be made to fit, separately at 8 m/s and 20 m/s, by applying small changes in the structural drivetrain damping in the linear model. Note the large phase drop at the tower frequency in Figure 2.4 which is 720 deg and 360 deg for operation at 8 m/s and 20 m/s, respectively, due to the non-minimum phase zeros as discussed later.

The time simulations with the nonlinear model include effects of dynamic inflow whereas the linear model assumes frozen wake. Dynamic inflow has no significant effect on the frequency response from generator torque to speed at both 8 m/s and 20 m/s, but it affects the frequency response from collective pitch to speed for operation at lower wind speeds. At 8 m/s, Figure 2.4a shows that dynamic inflow affects the response around the 1^{st} tower modes at 0.32 Hz and below by decreasing the amplitude and increasing the phase relative to frozen wake response. The reason is that the axial induction increases when pitching to stall such that the inflow velocity decreases. Thus, the influence of dynamic inflow is to give a negative change in aerodynamic rotor torque, which counteracts the positive change in torque due to higher angles of attack. As a result, a lower change in rotor speed is needed at 0 Hz to establish zero net variations in the aerodynamic torque on the rotor. At high wind speeds the axial induction factors are small and therefore the effect of the wake dynamics is small already at 14 m/s (not shown).

2.2.2 Aeroelastic modal analysis

The linear aeroelastic model is used to determine the aeroelastic modes responsible for the dynamics in the frequency response shown in Figures 2.3 and 2.4. The homogenous solution to Eq. (4.15a) is:

$$\mathbf{x} = \mathbf{v}e^{\lambda t} = \mathbf{v}e^{\alpha t}(\cos\omega t + i\sin\omega t) \tag{2.10}$$

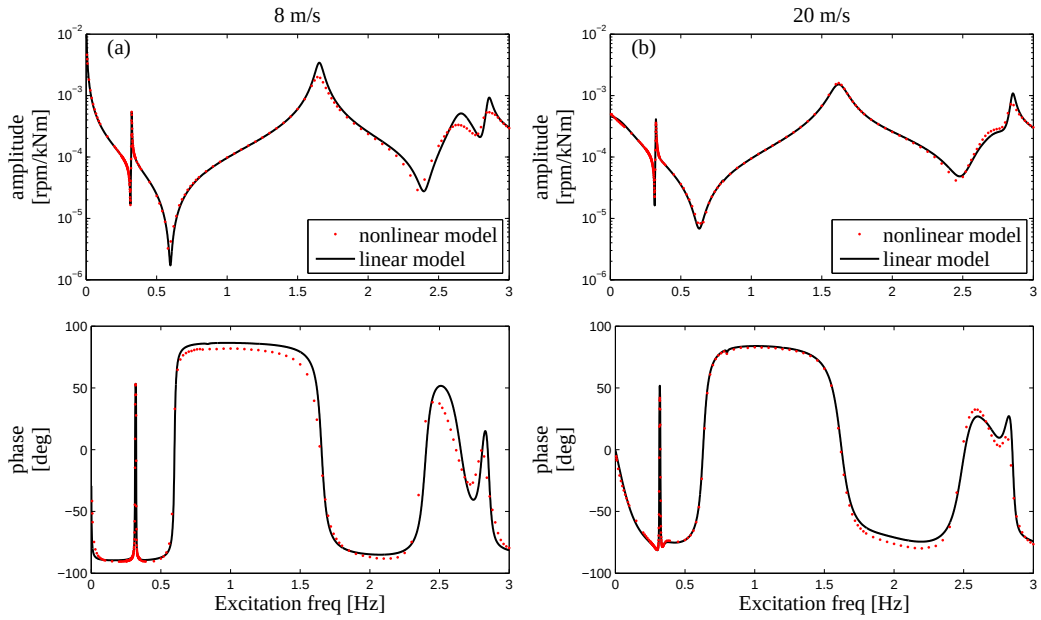

Figure 2.3: Aeroelastic frequency response from generator torque δQ_g to generator speed $\delta\Omega_g$ for NREL 5 MW wind turbine in operation at 8 and 20 m/s. Validation of aeroelastic frequency response predicted by linear model with time simulations using nonlinear aeroelastic model.

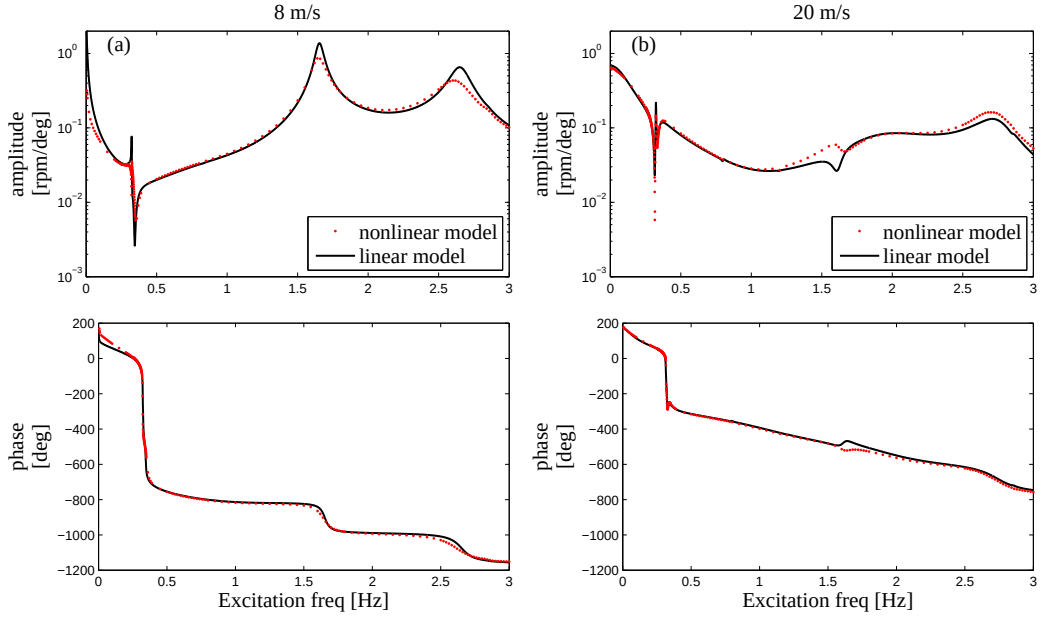

Figure 2.4: Aeroelastic frequency response from collective pitch angle $\delta\theta_c$ to generator speed $\delta\Omega_g$ for NREL 5 MW wind turbine in operation at 8 and 20 m/s. Validation of aeroelastic frequency response predicted by linear model with time simulations using nonlinear aeroelastic model.

where $\mathbf{v}$ and λ are solutions to the algebraic eigenvalue problem:

$$(\mathbf{A} - \lambda\mathbf{I})\mathbf{v} = \mathbf{0} \tag{2.11}$$

and $\mathbf{v}$ is an eigenvector and $\lambda = \alpha + i\beta$ the corresponding eigenvalue.

The solution to the eigenvalue problem (2.11) consists of structurally and aerodynamically dominated modes. The structurally dominated modes consist mainly of pairs of complex conjugated eigenvectors and eigenvalues and are characterized by the aeroelastic damping ratio ξ and aeroelastic frequency ω given by:

$$\omega = \mathrm{Im}\{\lambda\} \qquad \xi = -\mathrm{Re}\{\lambda\}/|\lambda| \tag{2.12}$$

Table 2.1 lists the aeroelastic frequencies and damping of structurally dominated modes ordered according to the aeroelastic frequency for operation at 8 m/s, 14 m/s and 20 m/s. Due to the free generator bearing, there is a mode, that describes rigid body rotation of the drivetrain and rotor in the generator bearing. This rigid body rotation mode is a 1^{st} order mode at 8 m/s and 14 m/s and a highly damped 2^{nd} order mode at 20 m/s. In operational points where the blades are pitched, rigid body rotation of drivetrain and rotor couple structurally with collective flap motion, such that vibrational energy in the rotor rotation is transferred to collective flap vibration, which is not entirely limited by aerodynamic damping, whereby the rigid body rotation mode becomes a 2^{nd} order mode. Most modern wind turbines have the same order of some of the structurally dominated modes. The 1^{st} tower modes will typically have lower frequency than the 1^{st} collective flap mode, because of large rotor inertia in the tower motion.

Each of the aerodynamically dominated modes (**not** listed in Table 2.1) describe variations in aerodynamic forces in local sections along the blade span due to the four by four block diagonal form of the $\mathbf{A}_d$ matrix. The BEM model assumes that changes in

ω [**Hz**]	ξ [%]	ω [**Hz**]	ξ [%]	ω [**Hz**]	ξ [%]	**Description**
8 m/s		14 m/s		20 m/s		
λ = -0.0112 rad/s		λ = -0.0184 rad/s		0.035	95.9	Rigid body rotation of rotor
0.32	0.38	0.32	0.44	0.32	0.61	1^{st} lateral tower
0.33	6.19	0.33	7.30	0.33	7.98	1^{st} longitudinal tower
0.57	64.1	0.60	77.3	0.63	80.0	1^{st} backward whirling blade flap
0.84	54.8	0.80	0.69	0.80	0.56	1^{st} backward whirling blade edge
0.78	1.45	0.81	68.1	0.84	71.4	1^{st} collective blade flap
0.91	47.9	0.99	60.8	1.01	65.2	1^{st} forward whirling blade flap
1.18	1.76	1.20	1.11	1.20	0.81	1^{st} forward whirling blade edge
1.55	16.4	1.52	20.9	1.53	21.7	2^{nd} backward whirling blade flap
1.65	2.4	1.65	2.43	1.62	3.14	1^{st} collective edge/drivetrain torsion
1.92	12.5	1.93	17.0	1.93	16.6	2^{nd} collective blade flap
1.89	13.7	1.93	15.3	1.94	16.3	2^{nd} forward whirling blade flap
2.63	1.92	2.64	2.04	2.62	2.10	2^{nd} longitudinal tower
2.65	3.62	2.68	3.76	2.73	3.89	2^{nd} collective edge/drivetrain torsion
2.76	3.34	2.77	3.77	2.75	3.65	1^{st} tower torsion (yaw)
2.85	0.71	2.85	0.70	2.85	0.62	2^{nd} lateral tower

Table 2.1: Open-loop aeroelastic frequencies and damping of structurally dominated mode shapes with low aeroelastic frequency for NREL 5 MW turbine operating at 8, 14 and 20 m/s.

aerodynamic forces at one aerodynamic calculation point does not couple with changes in aerodynamic forces at neighboring calculation points, except weakly through structural motion, whereby the eigenvectors of the aerodynamically dominated modes are only weakly coupling in the aerodynamic state variables across the calculation points.

Figure 2.5 shows the variations of cut-off frequencies with blade radius of time delays modeling shed vorticity and dynamic stall for NREL 5 MW turbine in normal operation at 8 m/s, 14 m/s and 20 m/s found under assumption of no coupling of the delays with structural states. The cut-off frequencies in Figure 2.5 are the eigenvalues of the four by four diagonal blocks of the $\mathbf{A}_d$ matrix obtained directly from the steady state BEM solution. The dashed horizontal line shows the aeroelastic frequency of the 1$^{\text{st}}$ longitudinal tower mode for comparison. The figure shows cut-off frequencies of two of the four time delays at each blade section; one that characterizes the effect of shed vorticity below stall and one characterizing the pressure lag in the boundary layer in stalled flow [12]. The cut-off frequencies increase with blade radius, because the relative inflow velocities increase, causing a faster update of the aerodynamic forces because the shed vorticity is faster convected away from the airfoil and the movement of the separation point of the dynamic stall becomes faster. The cut-off frequencies have an order of magnitude similar to the aeroelastic frequency of the 1$^{\text{st}}$ tower modes at some sections, and the delays may couple to the rigid body rotor rotation mode and the 1$^{\text{st}}$ tower modes.

2.3 Relevant frequency range for approximation

This section describes at what frequency intervals it is desirable to have good approximation of the response of generator speed in response to control actions from generator torque and collective pitch demands in the design of a generator speed and power controller.

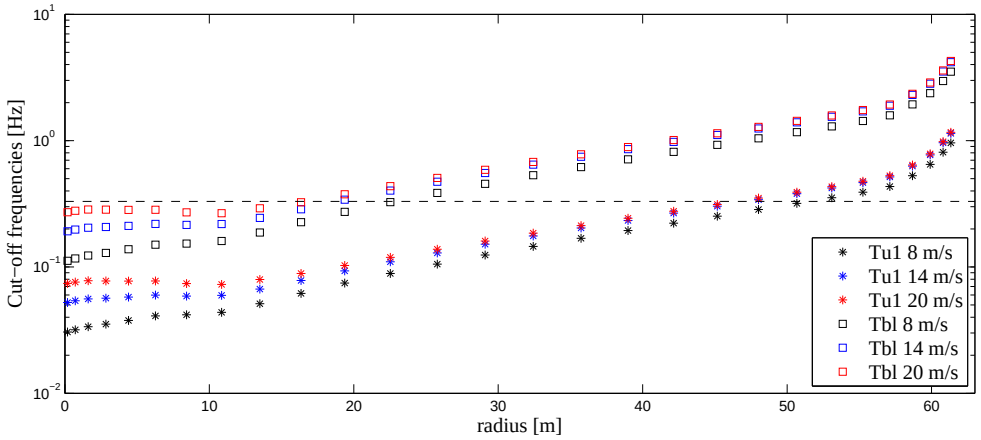

Figure 2.5: Variation of cut-off frequencies with blade radius of time delays modeling lag on aerodynamic forces due to shed vorticity and dynamic stall in separate blade sections for NREL 5 MW blade in normal operation at 8 m/s, 14 m/s and 20 m/s, where T_{u1} denotes one of two time delays describing shed vorticity below stall and T_{bl} denotes pressure lag in the boundary layer in stalled flow [12]. Cut-off frequencies are found under the assumption that there is no coupling to structural states. The dashed horizontal line shows the aeroelastic frequency of the 1$^{\text{st}}$ longitudinal tower mode for comparison.

Accurate approximation of the frequency response from control signals to measured output is desired at frequencies where the control signals in closed-loop are high. A series of closed-loop simulations has been made, using the nonlinear simulation code HAWC2 of the model of the NREL 5 MW turbine in closed-loop with a classical proportional-integral (PI) controller with Class B normal turbulence. The simulations are performed using a Newmark time integration scheme with a time step of 0.02 s using a time series spanning 300 s. The controller is designed to maintain constant generator speed and power as described by Hansen [24]. A measurement of the generator speed is used by the controller to generate collective pitch angle and generator torque demands using two PI controllers. The generator torque controller is designed to actively damped the torsional drivetrain vibrations using a notch filter.

Figure 2.6 shows the Fourier amplitudes of time series of generator speed, collective pitch angle demands and generator torque demands in closed-loop for the NREL 5 MW turbine in normal operation at the above rated wind speed 19 m/s. The black points in Figure 2.6 show the Fourier amplitudes for a fully flexible turbine with a static tilt of 5.0 deg. The blue points in Figure 2.6 show the Fourier amplitudes for a fully rigid turbine in which the rotor tilt is set to zero and tower shadow, wind shear and gravity forces are removed. The blue points are included to understand what cause the different peaks in the Fourier amplitudes.

The spectral content of the collective pitch, generator torque and generator speed signals for a fully flexible turbine are all characterized by a peak close to 0 Hz due to rigid body rotation of the rotor, a peak at around the 1$^{\text{st}}$ tower modes at 0.3 Hz and a peak at around 1.7 Hz at the closed-loop frequency of the 1$^{\text{st}}$ drivetrain torsion mode. All three signals also show a peak at 3P, where P is the rotational frequency of the rotor. For a fully rigid turbine with no static tilt, wind shear, gravity and tower shadow (blue points) there are also peaks at 3P in all three signals, and the peak at 3P can be explained by the rotational sampling of turbulence [51], giving 1P loads at the blade root and 3P variations in the generator speed which feeds back into the control signals. Good accuracy is therefore desired both at the frequency of the rigid-body rotor mode, the 1$^{\text{st}}$ tower modes, the 1$^{\text{st}}$ drivetrain torsion mode and at around 3P due to sampling of turbulence.

2.4 Frequency response analysis using high-order linear model

In this section, the complexity of the linear model is varied by changing the number of state variables to clarify what must be included in a model to capture the aeroelastic frequency response of a modern wind turbine, exemplified by analyzing the frequency responses from harmonic variations in the generator torque, collective pitch angle demand and mean wind speed to the generator speed output. For generator torque and collective pitch inputs, the purely structural response due to the actuator input is investigated before the aeroelastic response, to see the effect of structural dynamics and a separate section is in each case used to analyze the response at the 1$^{\text{st}}$ tower modes.

2.4.1 Mean wind speed to generator speed

Figure 2.7 shows the aeroelastic frequency response from mean wind speed harmonic variations to generator speed at 14 m/s and 20 m/s predicted using unsteady aerodynamics (filled line) and quasi-steady aerodynamics (dotted line). Note, that in the frequency response we assume instant change in the mean wind speed; the unsteady aerodynamic model does not describe dynamics related to how fast the mean wind speed changes in

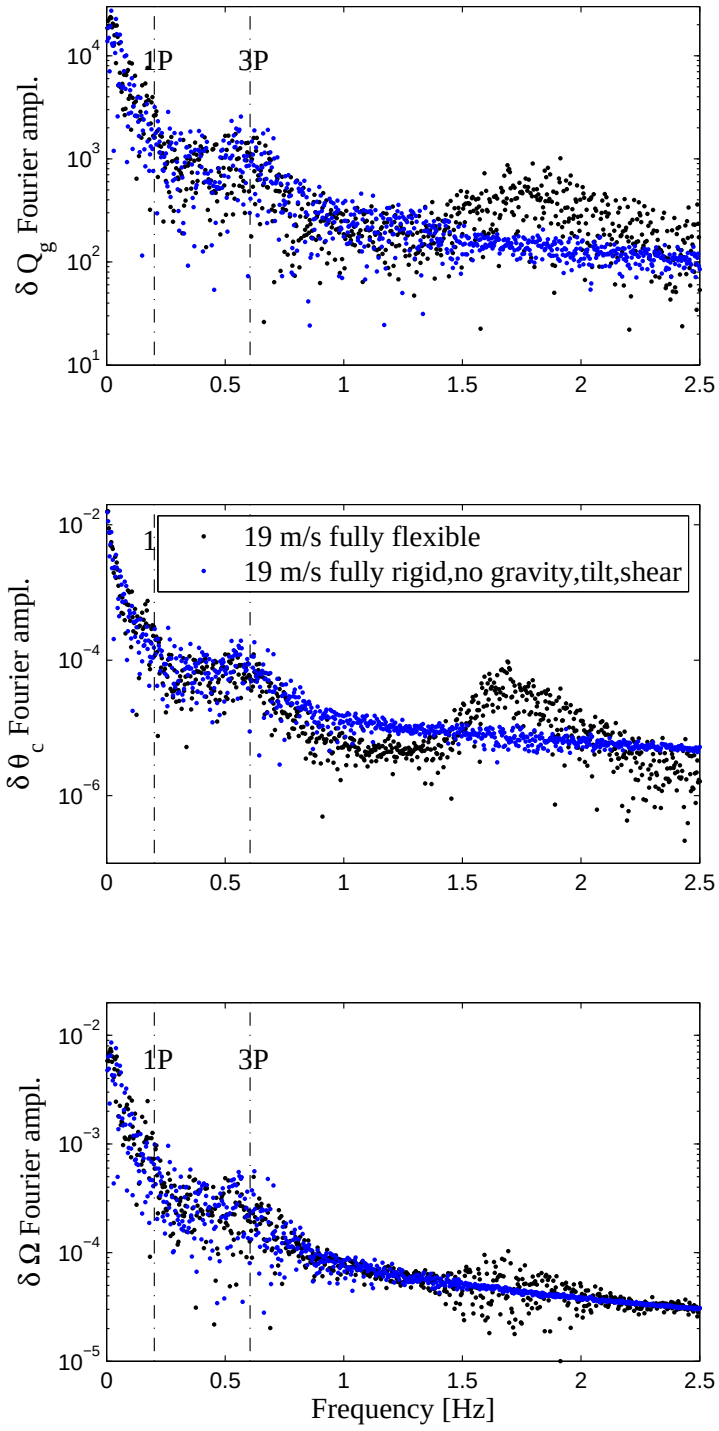

Figure 2.6: Fourier amplitudes of closed-loop time series of collective pitch angle demand, generator torque demand and generator speed for the NREL 5 MW wind turbine in normal operation at 19 m/s. Comparison between control signals and generator speed response for a fully flexible turbine and a rigid turbine with and without effects of gravity, wind shear and tower shadow.

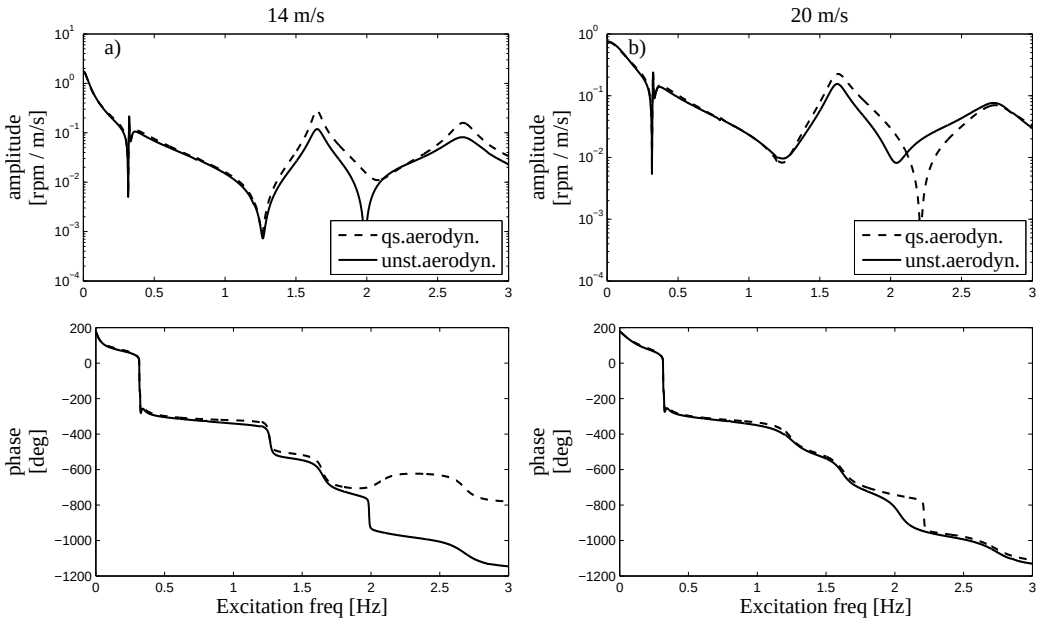

Figure 2.7: Aeroelastic frequency response from changes in mean wind speed to generator speed for NREL 5 MW turbine at normal operation at 14 m/s and 20 m/s. Comparison between the response predicted by the full-order model with unsteady aerodynamics (filled lines) and with quasi-steady aerodynamics (dashed lines).

for example a gust. The full-order response of generator speed of harmonic variations in mean wind speed is similar to that of collective pitch excitation below 1.0 Hz; a change in mean wind speed changes the angle of attack and thereby the aerodynamic forces similar to a change in pitch angle.

At both 14 m/s and 20 m/s, there are two non-minimum phase zeros at 1.2 Hz and 2.0 Hz causing negative phase shifts of -180 deg. At the zero at 1.2 Hz, the changes in mean wind speed excites the 1st torsional drivetrain mode, which couples with the 1st edgewise blade bending mode. An increase in mean wind speed gives a positive change in lift forces at the blade sections which forces the blade to bend relative to the hub positive clockwise. The edgewise blade vibration in the 1st drivetrain torsion mode changes the relative velocities at the blade sections, causing decreasing angle of attack and lift, that counteracts the change in lift from the mean wind speed increase, such that there is little net change in aerodynamic torque. The zero at 2.0 Hz exist due to coupling between collective blade vibration in the 1st drivetrain mode and in the 2nd drivetrain mode, such that the net change in aerodynamic rotor torque is close to zero.

The effect of assuming quasi-steady aerodynamics (dotted lines in Figure 2.7) is to increase the amplitude of the generator speed signal at the 1st drivetrain mode, because the model predicts too large changes in aerodynamic torque for a change in wind speed in attached flow due to the neglected effect of shed vorticity. The aeroelastic frequency response from generator torque, collective pitch and mean wind speed inputs to generator speed output all show little effect of assuming quasi-steady aerodynamics at excitation frequencies below the 1st drivetrain mode, because at these low frequencies lag on aerodynamic forces appears only at the inner blade sections that have no large contribution to

the overall changes in aerodynamic rotor torque and thrust.

2.4.2 Generator torque to generator speed

Figure 2.8 shows the purely structural frequency response from generator torque to speed for various cases of model complexity for the NREL 5 MW turbine in normal operation at 8 m/s and 20 m/s. The only difference in the conditions at 8 m/s and 20 m/s is the blade pitch, the mean rotational speed of the drivetrain and rotor, and the static blade deformation about which the geometrically nonlinear structural model has been linearized. The green curves in Figure 2.8 show the structural frequency response for a fully rigid turbine. Rigid-body rotation of the drivetrain and rotor can explain the response up to around the natural frequency of the 1st lateral tower mode at 0.32 Hz. The response of a rigid turbine equals the response of the 1st order model: $I_r \delta\dot{\Omega}_g = \delta Q_g$ and the rotational inertia causes a phase of 90 deg at all frequencies and a drop in amplitude with frequency.

When the tower is made flexible (red curves), the generator torque is in resonance with the 1st and 2nd lateral tower modes at 0.32 Hz and 2.9 Hz at both wind speeds. The lateral tower modes are excited by the generator reaction torque and are observable on the speed signal because of nacelle roll relative to the tower top. The 1st and 2nd lateral tower modes cause two zeros to appear very close to these modes at 0.315 Hz and 1.8 Hz. At the zero at 0.315 Hz, the change in rotor speed caused by the nacelle roll associated with the lateral tower motion counteracts the rigid-body rotation caused by the generator action torque. The zero nearly cancels the pole at 0.32 Hz creating a zero net phase shift across the 1st tower modes. After resonance of the 1st lateral tower mode, the response is

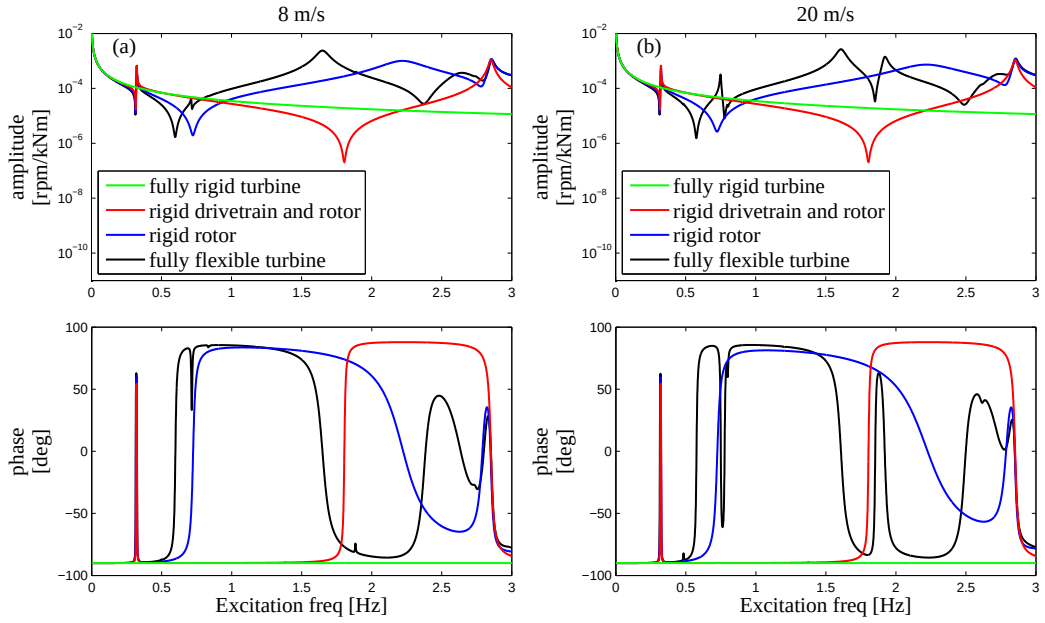

Figure 2.8: Purely structural frequency response from generator torque to generator speed for NREL 5 MW wind turbine operating at 8 and 20 m/s. Comparisons of frequency response predicted with models with no aerodynamic forces and with a fully rigid turbine (green), rigid drivetrain and rotor (red), rigid rotor (blue) and fully flexible turbine (black).

again governed by rigid-body rotation of the drivetrain and rotor. The similar phenomena occurs at the zero located at 1.8 Hz where it is nacelle roll associated with the 2nd lateral tower mode that cancels the rigid-body rotor rotation in the generator speed output.

The blue curves in Figure 2.8 show the structural frequency response when the tower and drivetrain are flexible and the rotor is rigid. The 1st torsional mode of the drivetrain leads to resonance at 2.2 Hz and a zero at 0.72 Hz at both 8 m/s and 20 m/s. At the zero at 0.72 Hz, the rotor is moving while the generator end of the drivetrain is stationary, because the generator torque is counterbalanced by rotor inertia forces.

The black curves in Figure 2.8 show the purely structural frequency response for a fully flexible turbine. Due to the added blade flexibility, the 1st drivetrain mode now couples with the 1st collective edge blade mode, whereby the resonance frequency is decreased from 2.2 Hz to 1.6 Hz. The zero at 0.59 Hz at both wind speeds is also shifted from 0.72 Hz due to blade flexibility. At 20 m/s, the 1st and 2nd collective flap modes influence the frequency response close to their modal frequencies of 0.75 Hz and 1.92 Hz due to the static blade pitch and are accompanied by two zeros very close to these frequencies at 0.78 Hz and 1.86 Hz. The zeros and poles related to each of the 1st and 2nd collective flap modes make phase shifts that cancels each other. At the zero at 0.78 Hz, the generator torque excites both the 1st drivetrain mode and the 1st collective flap mode in a motion where edgewise blade bending relative to the hub in clockwise rotor direction is in phase with flapwise bending downstreams and in phase with the applied generator torque. The inertia forces from blade vibration in both the 1st drivetrain mode and the 1st collective flap mode counteracts the applied generator torque. Similarly, at the zero at 1.86 Hz, the generator torque excites the 1st drivetrain mode and the 2nd collective flap mode, and the inertia forces from this motion counteracts the generator torque to form a zero in the generator speed output.

Figure 2.9 shows a comparison between the purely structural response (magenta curves) and the aeroelastic response (black curves) for a fully flexible turbine. The main effects of including aerodynamic forces is seen at 20 m/s below the 1st tower modes and around the 1st and 2nd collective flap modes.

The response predicted by the simple 1st order model in Equation (4.26a) with rigid structure and quasi-steady aerodynamics (blue curves) predicts the correct tendencies below the 1st tower modes. At 20 m/s aerodynamic forces decrease the amplitude at low frequencies and create a positive phase shift of 90 deg at 0 Hz compared to the purely structural response, because aerodynamic damping forces dominate the inertia forces that vanish at 0 Hz. At 8 m/s, the aerodynamic damping of the rotor is low and the response is dominated by inertia until very close to 0 Hz. Although not seen for the present turbine, the static change in blade deflection caused by static changes in aerodynamic forces at 0 Hz, could cause that the aerodynamic gradients predicted for a rigid rotor are wrong. The aerodynamic gradients could in particular be predicted wrongly by a rigid-rotor assumption for a swept blade, because changes in steady state aerodynamic forces from a change in e.g. generator torque could cause high blade torsion.

Around the 1st and 2nd collective flap modes, the amplitude is reduced, due to large aerodynamic damping of flap vibration. The influence of the collective flap modes is seen from Figure 2.10 that shows a pole-zero map of the transfer functions in Figure 2.9. The figure shows poles and zeros that influence the frequency response and that does not cancel out in the transfer function. There are zero-pole cancelations of all asymmetric flap and edgewise modes. There are no zero-pole cancelations of the 1st and 2nd drivetrain modes at all wind speeds because the generator torque excites the drivetrain modes. There is zero-pole cancelation of the 1st collective flap mode at both 8 m/s and 20 m/s. The 2nd collective

flap mode is canceled by a zero at 8 m/s and is nearly canceled at 20 m/s indicating that aerodynamic damping does not entirely limit vibration of the 2nd collective flap mode and is responsible for the phase difference of 10 deg seen around 2.2 Hz in Figure 2.9. Generally, it can be concluded, that the collective flap modes are not essential to include to model the transfer function from generator torque to speed because of aerodynamic damping.

For excitation frequencies below 3 Hz, there is no significant difference between using unsteady and quasi-steady aerodynamics (not shown) on the response from generator torque to generator speed because the modes that influence the response are mainly modes characterized by vibration in the rotor plane where the effect of aerodynamic forces is small, except on the rigid-body rotor mode. There is no effect of lag on lift and drag on the rigid-body rotor mode because the frequency of vibration is so low, that lag only occurs at blade sections close to the blade root, where the components to the overall changes in aerodynamic rotor torque are small compared to sections closer to the blade tip.

The results shown above are for the NREL 5 MW turbine in onshore operation. For another turbine the ordering of the aeroelastic frequencies of the 1st and 2nd collective flap modes are likely to change relative to the zero at 0.72 Hz and the 1st drivetrain mode at 1.6 Hz, respectively, but without any significant effect on the response due to large aerodynamic damping of these modes.

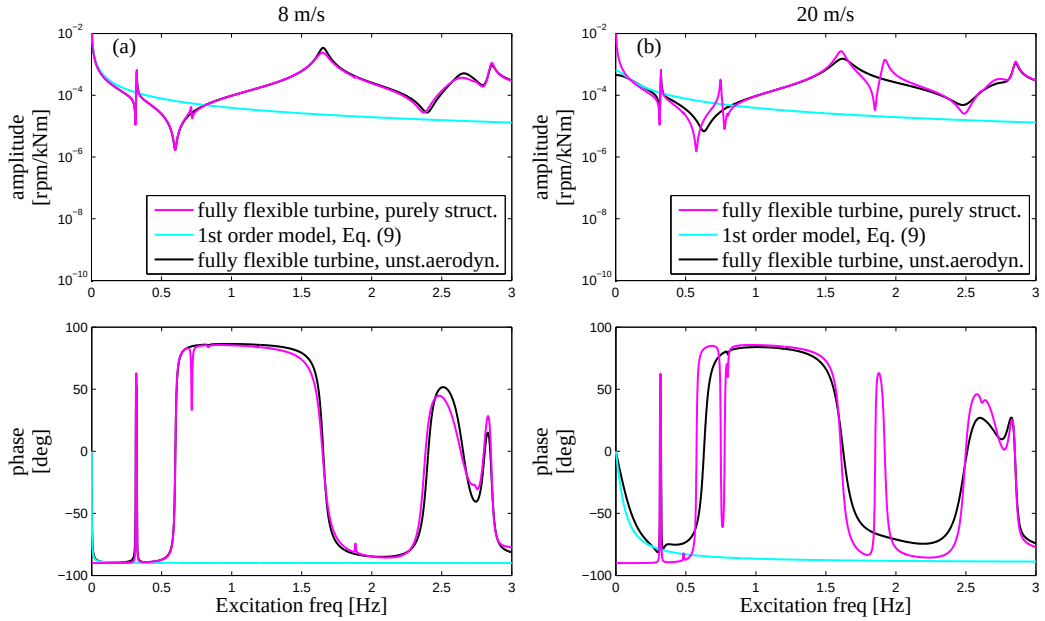

Figure 2.9: Aeroelastic frequency response from generator torque to generator speed for NREL 5 MW wind turbine operating at 8 m/s and 20 m/s. Comparisons of frequency response predicted with fully flexible structure and no aerodynamic forces (magenta), with the 1st order model in Equation (4.26a) (cyan) and with fully flexible turbine with unsteady aerodynamic forces (black).

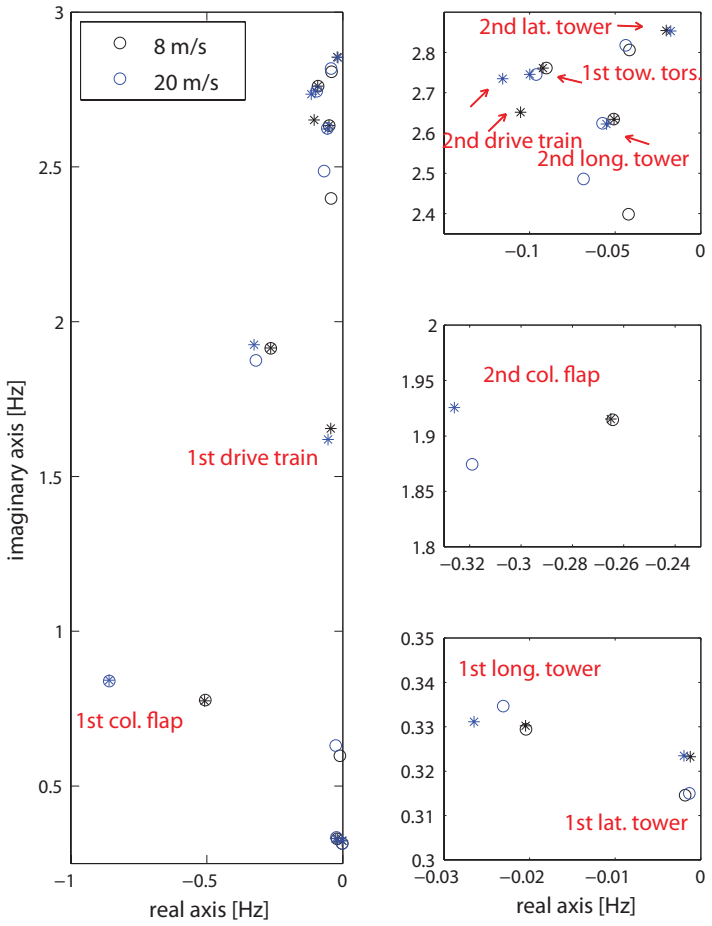

Figure 2.10: Aeroelastic poles and zeros of minimal realization of transfer function from generator torque to generator speed for NREL 5 MW wind turbine operating at 8 m/s and 20 m/s. ($*$ poles, $\circ$ zeros).

Effect of longitudinal tower vibration

The influence of longitudinal tower motion on the response from generator torque to generator speed is illustrated in Figure 2.11. The figure shows the aeroelastic frequency response close to the 1st tower modes for a turbine with a tower that is very stiff in longitudinal direction (blue curves) and for a fully flexible turbine (black curves) operating at 8 m/s and 20 m/s. The vertical lines show the aeroelastic frequencies of the 1st tower modes for a fully flexible turbine. For a fully flexible turbine, there is a zero at 0.315 Hz and a pole at 0.323 Hz due to nacelle roll associated with the 1st **lateral** tower mode. There are no changes in amplitude or any phase shifts occurring across the frequency of the 1st **longitudinal** mode at 0.33 Hz which shows that the 1st longitudinal tower mode has no influence. Thus, any deviations between the blue and black curves arise due to longitudinal tower motion in the 1st lateral tower mode. It can be seen that longitudinal tower vibration has a small influence only at 20 m/s, which is seen as larger phase shifts

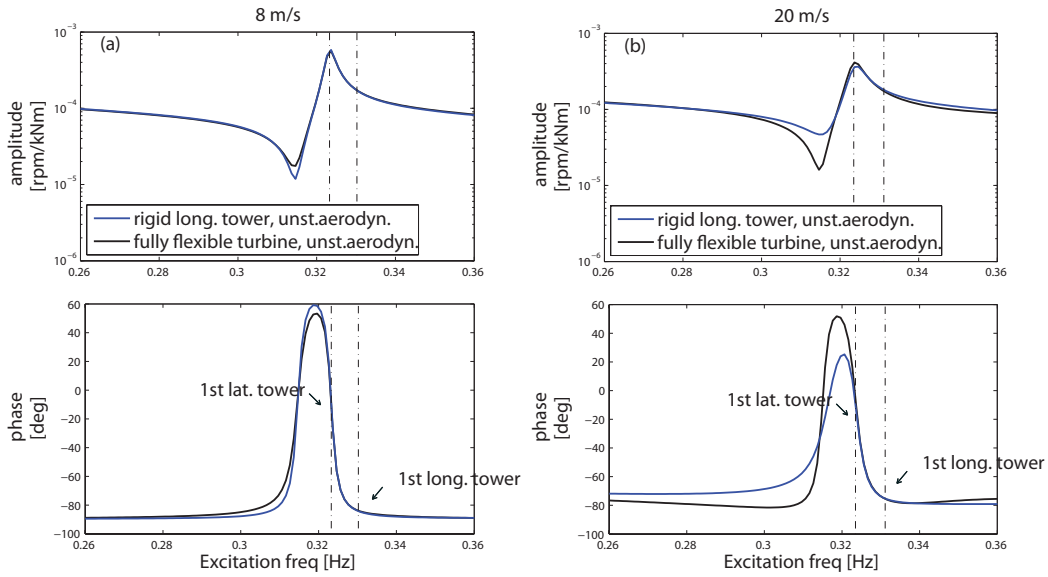

Figure 2.11: Aeroelastic frequency response at frequencies close to the 1st tower modes from generator torque to generator speed for NREL 5 MW wind turbine operating at 8 m/s and 20 m/s. Comparisons of frequency response predicted for a turbine with a tower that is very stiff in longitudinal direction (blue) and for a fully flexible turbine (black).

across the zero at 0.315 Hz and at the 1st lateral tower mode.

The small changes due to the increased longitudinal tower stiffness occurring at 20 m/s are caused by removal of longitudinal tower motion in the 1st lateral tower mode. Figure 2.12 shows the tower top motion in the 1st longitudinal and lateral tower modes for a fully flexible turbine with no aerodynamic forces (a), a turbine with rigid drivetrain and rotor and quasi-steady aerodynamics (b) and for a fully flexible turbine with unsteady aerodynamic forces (c) for the NREL turbine in normal operation at 8 m/s, 14 m/s and 20 m/s. Without aerodynamic forces, the 1st lateral and longitudinal tower modes consist of purely lateral and longitudinal tower motion, respectively. Thus, gyroscopic forces due to rotor tilting in the 1st longitudinal tower mode does not provide large coupling between lateral and longitudinal tower motion. For a turbine with a rigid drivetrain and rotor with aerodynamic forces (b), the 1st lateral tower mode has a component in the longitudinal direction that changes with operation point. The similar trend is seen for a fully flexible turbine (c). Thus, the coupling of the 1st lateral tower mode to longitudinal tower motion must be through aerodynamics, indicating that lateral tower vibration changes the aerodynamic thrust.

2.4.3 Collective pitch demand to generator speed

Figure 2.13 shows the purely structural frequency response from collective pitch to generator speed for various cases of model complexity for the NREL 5 MW turbine operating at the above rated wind speeds 14 m/s and 20 m/s. The green curves show the structural response for a fully rigid turbine, where the pitching inertia forces of the flapwise bent blades, makes the amplitude increase with the square of frequency and gives a phase of -90 deg except very close to 0 Hz. Because the blades are bent downwind, the pitching

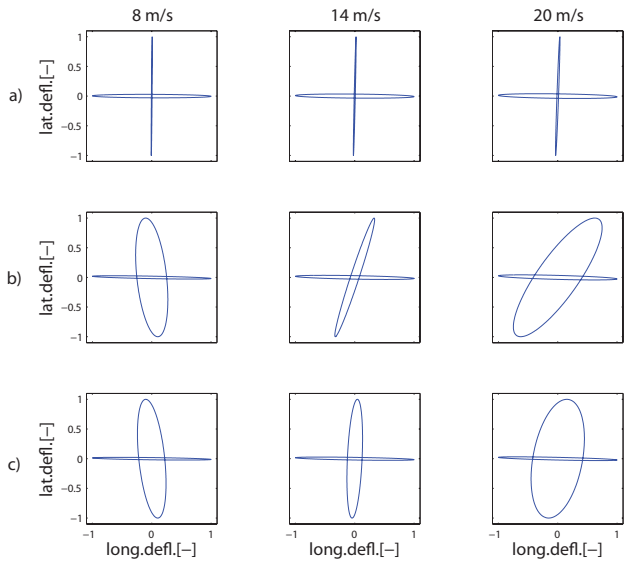

Figure 2.12: Tower top motion of the 1st lateral and longitudinal modes for a) a fully flexible turbine without aerodynamic forces, b) a fully flexible turbine and unsteady aerodynamics and for c) a turbine with rigid drivetrain and rotor and unsteady aerodynamics in normal operation at 8 m/s, 14 m/s and 20 m/s. Tower is seen from above and positive longitudinal tower deflection is defined to be upstreams, i.e. the wind is coming from the right of the plots.

inertia forces have a positive torque creating component in the positive direction of δQ_g for a positive pitch towards stall leading to a phase of -90 deg. The amplitude is slightly higher at 14 m/s than at 20 m/s, because of the larger static flap deflection.

The blue curves in Figure 2.13 shows the purely structural frequency response when the drivetrain is flexible and tower and rotor are rigid. Drivetrain flexibility causes a resonance with the 1st drivetrain mode at 2.2 Hz. The drivetrain mode is excited by the pitch actuator due to misalignment between the center of gravity and the pitching axis. The phase shifts -180 deg across the frequency of the 1st drivetrain mode at 14 m/s and 20 m/s.

The black curves in Figure 2.13 shows the structural response for a fully flexible turbine. The pitch actuator excites the 1st collective flap mode at 0.74 Hz, because the centers of gravity along the blade are not aligned with the pitch axis. The 1st collective flap mode is accompanied by a minimum-phase zero at 0.73 Hz, where collective pitching excites both the 1st drivetrain mode and the 1st collective flap mode. At this zero, the vibration of the 1st collective flap mode causes a torque to act on the rotor in the negative direction of δQ_g for a change in pitch towards stall, that counteracts the pitching inertia forces such that the net torque variations are zero. The zero nearly cancels the phase shift due to the 1st collective flap mode. The 1st drivetrain mode is in resonance at 1.6 Hz, shifted from 2.2 Hz due to added blade flexibility and is accompanied again by a phase shift of -180 deg. The 2nd collective flap mode at 1.9 Hz highly influence the response at both 14 m/s and 20 m/s. The amplitude at the 2nd collective flap mode is much higher than at the 1st collective flap mode, because the pitching inertia forces are larger at higher excitation frequencies, and because the 2nd collective flap mode lies close to the 1st drivetrain mode, where rotor

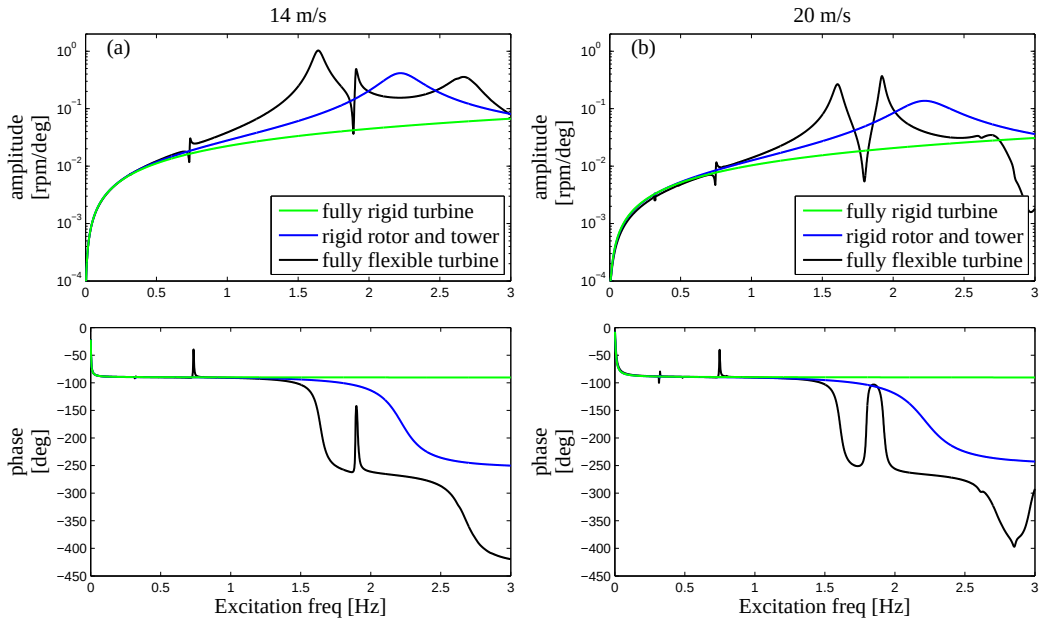

Figure 2.13: Purely structural frequency response from collective pitch to generator speed for NREL 5 MW wind turbine operating at 14 and 20 m/s. Comparisons of frequency response predicted from models assuming no aerodynamic forces and fully rigid turbine (green), rigid rotor and tower (blue) and a fully flexible turbine (black).

speed variations are larger, which provides larger excitation of the 2$^{\text{nd}}$ collective flap mode. Resonance of the 2$^{\text{nd}}$ collective flap mode is accompanied by a zero at 1.89 Hz and 1.80 Hz at 14 m/s and 20 m/s, respectively. At these zeros, collective pitching excites both the 1$^{\text{st}}$ drivetrain mode and the 2$^{\text{nd}}$ collective flap mode. The 2$^{\text{nd}}$ collective flap mode couples to rotor rotation when the blades are pitched and is excited such that it creates a torque in the negative direction of δQ_g for a change in pitch towards stall and thereby counteracts the torque created due to vibration of the 1$^{\text{st}}$ drivetrain mode, such that there are no net generator speed variations. This coupling is more significant at 20 m/s where the blades are more pitched.

A comparison has been made of the pitching inertia forces for a rigid blade undergoing harmonic pitch angle variations around the undeformed state and statically deflected state of the NREL blade in normal operation at various wind speeds to clarify the effect of static blade deflection. The pitching inertia forces are measured as the amplitude of forces in the rotational direction of the rotor arising from harmonic variations in pitch angle at frequency ω_θ and amplitude A_θ. The total pitching inertia forces for the blade are found by summing up over the number of blade elements assuming constant structural properties over each element. The amplitude of pitching inertia forces $A_{p,i}$ for element i can be written

$$A_{p,i} = \omega_\theta^2 m_i l_i \sin\phi_{0,i} A_\theta \tag{2.13}$$

where $\phi_{0,i}$ and l_i are the polar coordinates of the element centre of gravity in the blade system, m_i is the element mass and $A_{p,i}$ is the amplitude of pitching inertia forces.

Figure 2.14 shows the total amplitude A_p of pitching inertia forces versus wind speed

for the NREL 5 MW turbine blade in the undeformed and statically deformed state in response to harmonic pitching with an amplitude of 1 deg at a frequency of 1 Hz together with the static position of the centre of gravity at the blade tip in the rotor coordinate system. The pitching inertia forces are larger than of the undeflected blade at wind speeds below 22 m/s because the blades are highly deflected downstreams in the flap direction and peaks at 11 m/s where the thrust forces are highest. For blades with a significant prebend upstreams, the pitching inertia forces are expected to be lower, because the static position of the centre of gravity in the flap direction is further upstreams than for a non-prebended blade.

The influence of aerodynamic forces on the frequency response is now analyzed. Figure 2.15 shows a comparison of the response for a fully rigid turbine without and with quasi-steady aerodynamic forces and the response predicted by the simplified model in Equation (4.26a). At 0 Hz, the effect of including aerodynamic forces is to increase the amplitude and shift the phase with 180 deg because of changes in aerodynamic torque caused by pitching. The steady state effect of a constant change in collective pitch is that the generator speed settles at a new equilibrium between the steady state generator torque and the aerodynamic torque on the rotor. Pitching towards feather gives less aerodynamic torque because of lower angles of attack, whereby the rotor speed decreases. The decrease in rotor speed gives an additional inflow velocity component, that increases the angle of attack and thereby the aerodynamic torque, such that the net variation in aerodynamic

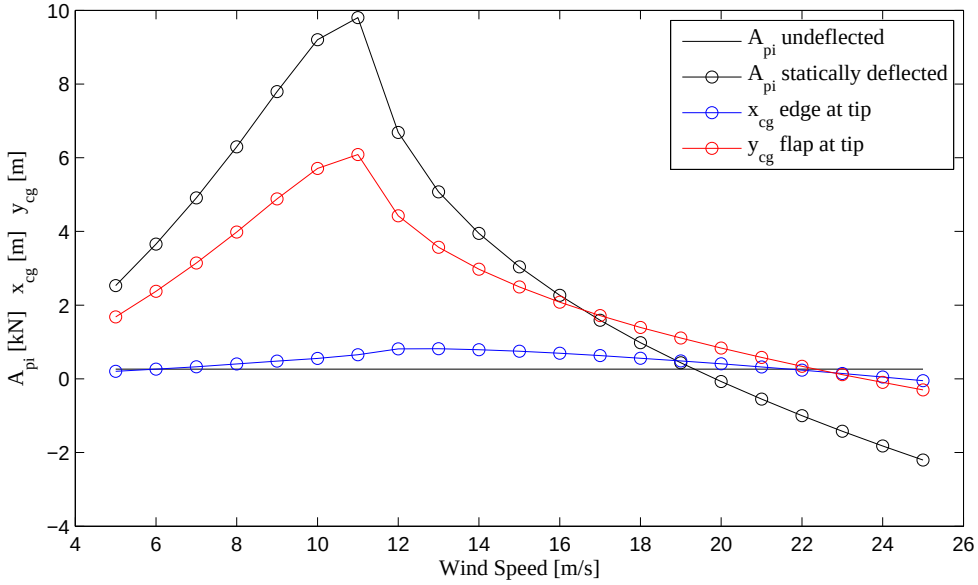

Figure 2.14: Amplitude of pitching inertia forces in the edgewise blade direction positive towards rotational direction of the rotor for a rigid NREL 5 MW blade undergoing harmonic pitch angle variations with amplitude of 1 deg and frequency of 1 Hz. Comparison of pitching inertia forces for undeflected blade and statically deflected blade for normal operation at various wind speeds. Static position of the centre of gravity at the blade tip in the blade coordinate system (x:positive towards rotational direction,y:positive downstreams).

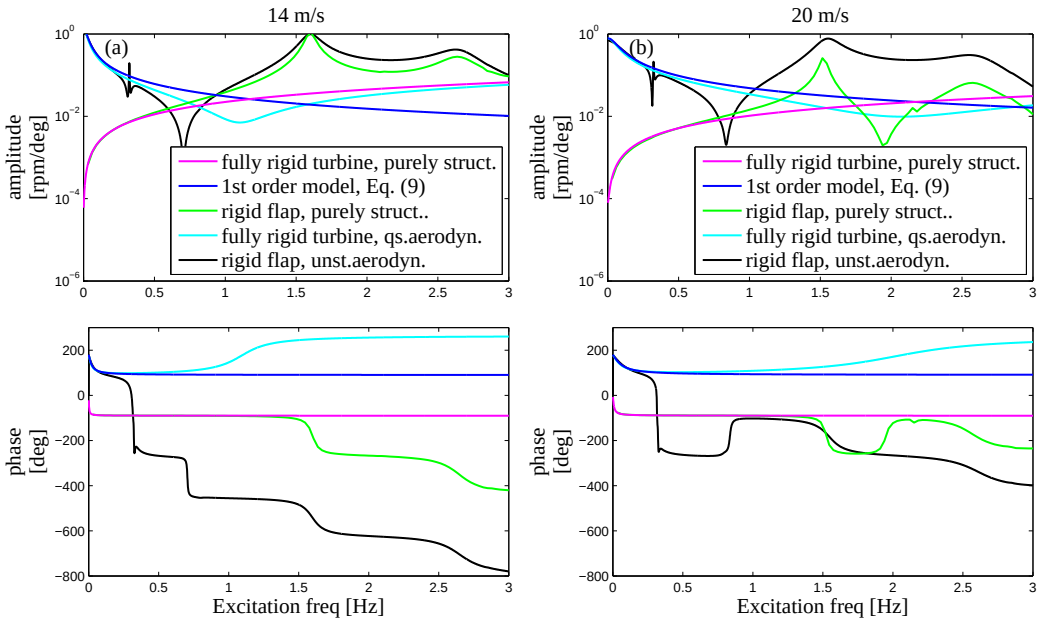

Figure 2.15: Purely structural and aeroelastic frequency response from collective pitch to generator speed for NREL 5 MW wind turbine operating at 14 m/s and 20 m/s. Comparisons of frequency response with models including a fully rigid turbine with no aerodynamic forces (magenta), the 1st order model in Equation (4.26a) (blue), turbine with rigid flap and no aerodynamic forces (green), a fully rigid turbine with quasi-steady aerodynamics (cyan) and a turbine with blades rigid in flap direction and unsteady aerodynamics (black).

rotor torque is zero at 0 Hz.

The response predicted with a fully rigid turbine with quasi-steady aerodynamics (cyan curves) has a minimum-phase zero at 1.1 Hz and 2.1 Hz at 14 m/s and 20 m/s, respectively, where there is a positive phase shift of around 180 deg, due to pitching inertia forces. Under harmonic collective pitch angle variations, the pitching inertia forces gives a torque on the rotor in positive direction of δQ_g for a change in pitch towards stall, whereas the aerodynamic torque gives a higher torque in the negative direction and thus excites the rotor in the opposite direction as the pitching inertia forces. The pitching inertia forces grows with excitation frequency and above the zeros at 1.1 Hz and 2.1 Hz at 14 m/s and 20 m/s, respectively, they are large enough to dominate the response over variations in aerodynamic torque.

The black curves in Figure 2.15 show the frequency response for a turbine with rigid blades in the flap direction. At 0.32 Hz, collective pitching now couples with the 1st tower modes to create a minimum phase and a non-minimum phase zero at 14 m/s and 20 m/s that causes the phase to shift approximately 360 deg crossing the frequencies of the 1st tower modes, because of 180 deg phase shift over the non-minimum phase zero and -180 deg over the lateral tower mode. The longitudinal tower mode introduce a zero and a pole with phase shifts that cancels each other. The minimum-phase zero at 0.71 Hz and 0.84 Hz for 14 m/s and 20 m/s, respectively, are shifted from 1.1 Hz and 2.1 Hz. To illustrate why the added drivetrain and edge flexibility causes these zeros to shift to a lower

frequency, the purely structural response for a turbine with rigid flap is shown in Figure 2.15 (magenta curves). Collective pitching excites the 1st drivetrain mode structurally and vibration of this mode excites the rotor in phase with the pitching inertia forces, such that the variations in aerodynamic torque are suppressed at lower excitation frequencies.

Figure 2.17 shows a map of poles and zeros that does not cancel out of the transfer function from collective pitch to generator speed for the turbine where the blades are made rigid in the flap direction. There are pole-zero cancelations of all asymmetric flap and edgewise modes (not shown), no zero-pole cancelations of the 1st and 2nd collective flap modes, and a lowly damped zero exist at 0.71 Hz and 0.84 Hz for 14 m/s and 20 m/s, respectively. At 14 m/s the zero is non-minimum phase and causes a -180 deg phase shift in the black curves in Figure 2.15, and at 20 m/s it is a minimum phase zero causing a positive phase shift of 180 deg.

Figure 2.16 shows a comparison of the response for a fully flexible turbine without aerodynamic forces (blue curves) and with quasi-steady aerodynamic forces (cyan curves). The response predicted by the simplified model in Equation (4.26a) is also included (green curves) to show that it captures the steady state response well at 0 Hz at both 14 m/s and 20 m/s.

Compared to the response of a turbine where blades are rigid in the flap direction (black curves in Figure 2.15), there is a large change in phase between the 1st tower modes and the 1st drivetrain mode, which must be due to the added flapwise blade flexibility. To explain this observation, the aeroelastic poles and zeros for the fully flexible turbine has been plotted in Figure 2.17. The pole-zero map shows that the lowly damped zeros

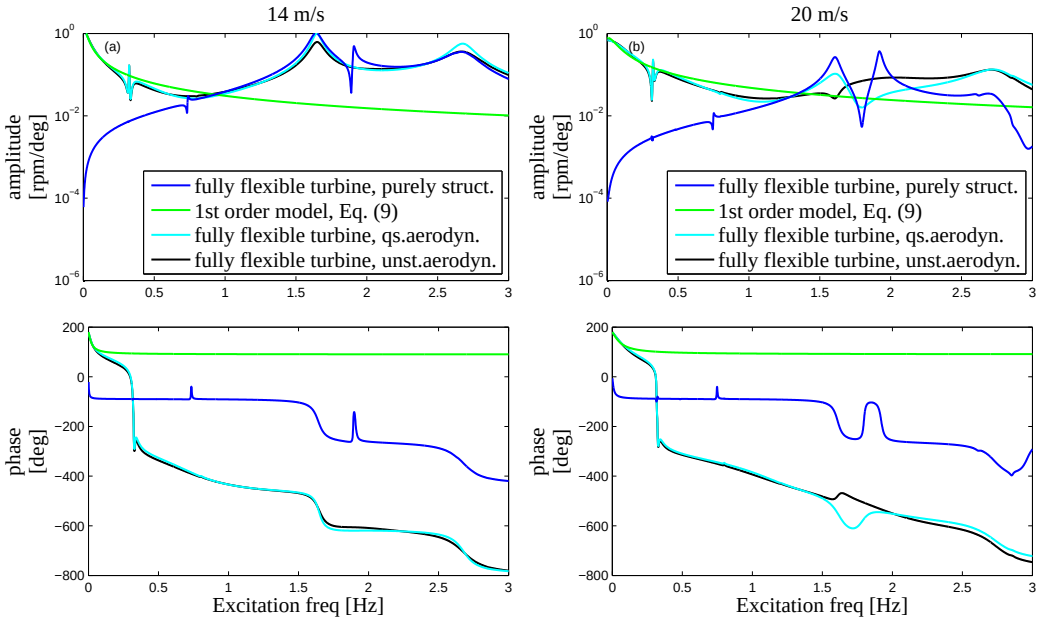

Figure 2.16: Aeroelastic frequency response from collective pitch to generator speed for NREL 5 MW wind turbine operating at 14 m/s and 20 m/s. Comparisons of frequency response with models including a fully flexible turbine with no aerodynamic forces (blue), the 1st order model in Equation (4.26a) (green), a fully flexible turbine with quasi-steady aerodynamics (cyan) and a fully flexible turbine with unsteady aerodynamics (black).

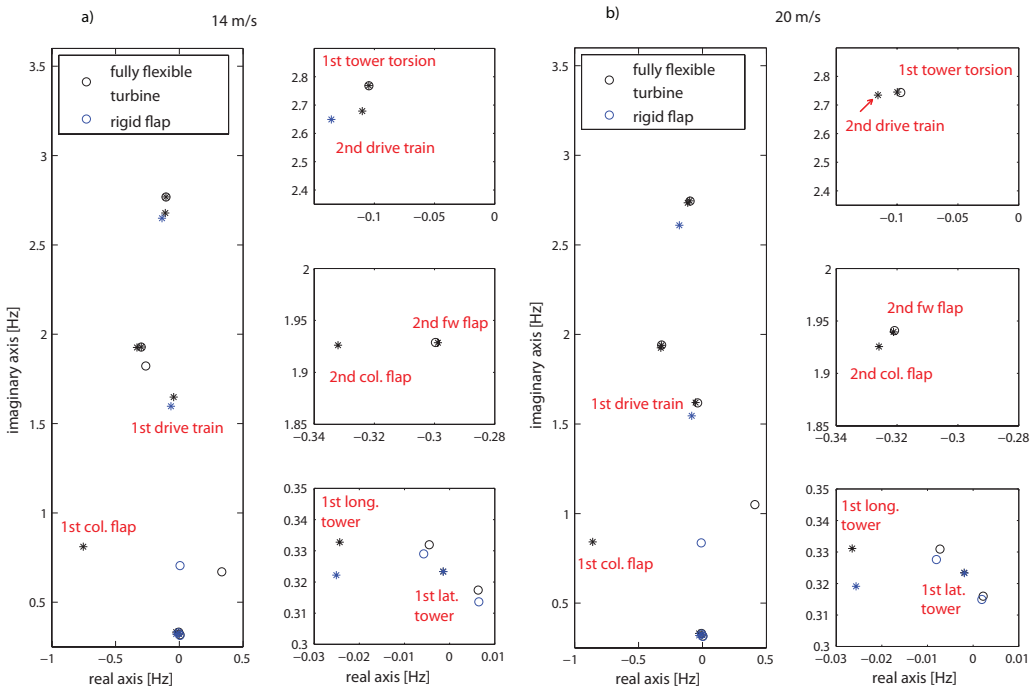

Figure 2.17: Aeroelastic poles and zeros of minimal realization of transfer function from collective pitch demand to generator speed for NREL 5 MW wind turbine operating at 14 m/s and 20 m/s. Comparison between pole-zero map for fully flexible turbine with unsteady aerodynamics (black) and turbine with blades rigid in flap direction with unsteady aerodynamics (blue) ($*$ poles, $\circ$ zeros).

at 0.71 Hz and 0.84 Hz at 14 m/s and 20 m/s, respectively, which are predicted for a turbine with rigid flap, are replaced by two highly damped non-minimum phase zeros at 0.67 Hz and 1.1 Hz. These non-minimum phase zeros creates a phase shift of -180 deg in the cyan curves in Figure 2.16 which occurs over a large frequency interval. It can be concluded that collective flap DOFs must be included to correctly predict existence of the non-minimum phase zeros at 0.67 Hz and 1.1 Hz for 14 m/s and 20 m/s, respectively.

The cyan curves in Figure 2.16 shows, that quasi-steady aerodynamic forces changes the structural response at the 1^{st} drivetrain mode and the 2^{nd} collective flap modes by adding damping that lowers the response at these modes. The 1^{st} drivetrain mode is mainly damped by aerodynamics at 20 m/s, because at larger pitch angles, the 1^{st} drivetrain mode couples more with collective flap vibration. The zero located in between at 1.89 Hz and 1.80 Hz at 14 m/s and 20 m/s, respectively, is also damped by aerodynamic forces and the effect of the zero on the frequency response is not visible at 14 m/s, but can still be seen at 1.80 Hz at 20 m/s.

The effect of using unsteady aerodynamics instead of quasi-steady aerodynamics is seen by comparing the magenta and black curves in Figure 2.16. At 14 m/s there is no clear difference, whereas at 20 m/s a clear difference is observed at the 1^{st} drivetrain mode and the 2^{nd} collective flap mode. To explain this change, a pole-zero map has been plotted in Figure 2.18 for a fully flexible turbine with quasi-steady aerodynamics (blue points) and with unsteady aerodynamics (black points), that shows the poles of the 1^{st}

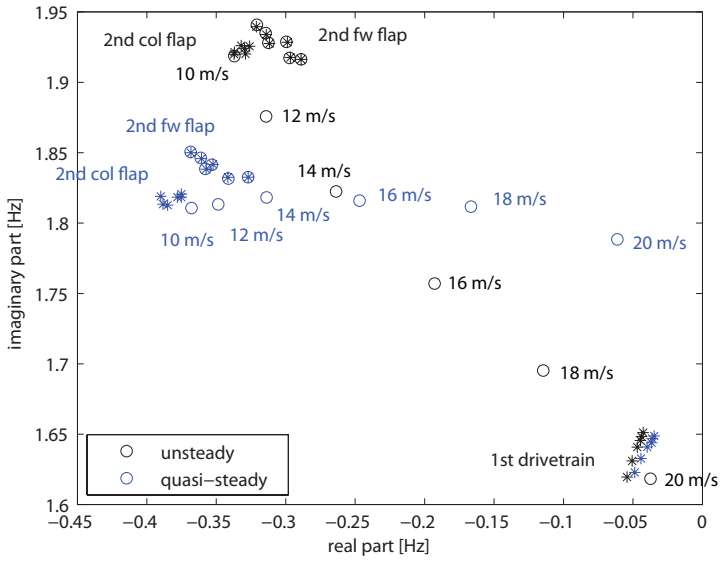

Figure 2.18: Aeroelastic poles and zeros of transfer function from collective pitch demand to generator speed for NREL 5 MW wind turbine operating at 14 m/s and 20 m/s with frequencies close to the 1st drivetrain mode. Comparison between pole-zero map for fully flexible turbine with quasi-steady aerodynamics (blue) and unsteady aerodynamics (black) ($*$ poles, $\circ$ zeros).

drivetrain mode and the 2nd collective flap mode at various wind speeds together with the zero with a frequency between these poles. The quasi-steady aerodynamic model predicts correct location of the poles of the 1st drivetrain mode, but estimates a too low aeroelastic frequency of the 2nd collective flap mode. At 10 m/s the 2nd collective flap mode tends to cancel with a zero, such that there is no influence of 2nd collective flap mode at this wind speed, because of lower pitch angles. With increasing wind speed the zero moves and does not cancel the pole. With unsteady aerodynamics a similar trend is seen, but at 20 m/s the zero has moved close to the 1st drivetrain mode, thereby almost cancelling the pole of the 1st drivetrain mode and creating a drop in amplitude at the frequency of the 1st drivetrain mode at 20 m/s in the black curves in Figure 2.16.

To understand what causes the zeros shown in Figure 2.18, Figure 2.19 shows the frequency response from collective pitch (positive towards stall) to the generator speed and rotor speed (left) and the collective blade tip velocities in the flap and edgewise blade directions relative to the hub (right) for the NREL 5 MW wind turbine in normal operation at 8 m/s and 20 m/s. The results shown in Figure 2.19 are obtained by Fourier transformation of the nonlinear time simulations which were used for validation previously.

The response at the resonance peak at 1.64 Hz at 8 m/s in Figure 2.19 characterizes the 1st drivetrain torsional mode. The 1st drivetrain mode is characterized by a generator speed and rotor speed that are in phase, where the rotor speed variations have slightly lower amplitudes due to drivetrain torsion. The figure shows, that the collective edgewise blade velocity relative to the hub (positive towards the rotational direction) in the 1st drivetrain mode is nearly in opposite phase as the rotor speed variations, which is due to the inertia of the blades relative to the hub.

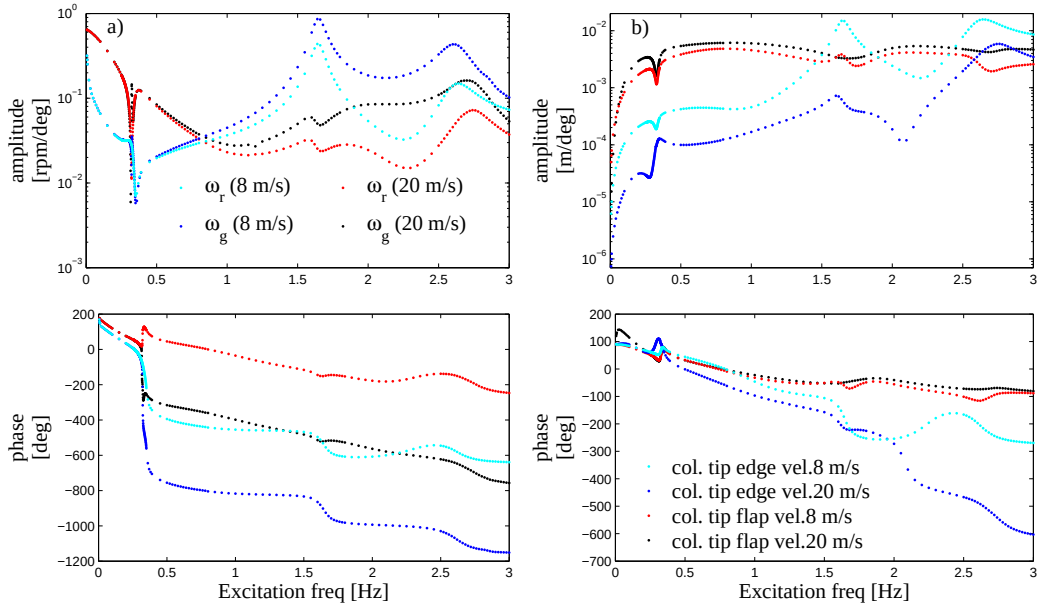

Figure 2.19: Aeroelastic frequency response functions from collective pitch angle demand (positive towards stall) to generator speed and rotor speed variations (a) and to the collective blade tip velocities relative to the hub in the pitched blade root coordinate systems (b) for the NREL 5 MW wind turbine in normal operation at 8 m/s and 20 m/s. The responses are predicted by Fourier transformation of nonlinear time simulations using HAWC2. Edgewise blade velocities positive towards rotational direction and flapwise velocities positive downstream.

Figure 2.18 showed that at 20 m/s the poles of the 2$^{\text{nd}}$ collective flap mode does not cancel with the nearby zero, which is because the collective flapwise blade vibration couples to rigid body rotor rotation through the inertia and aerodynamic damping forces of the collective flap motion relative to the hub. Figure 2.19 shows that exactly at the frequency of the zero at 1.66 Hz at 20 m/s, the collective flapwise blade tip velocity (positive downstream) is out of phase with the rotor speed changes with a relative phase of around -150 deg mainly because of the inertia forces on the blades from collective flapwise blade vibration relative to the hub. What happens at the zero at 1.66 Hz at 20 m/s is that the inertia forces caused by collective flap vibration in the 2$^{\text{nd}}$ collective flap mode counteracts the increased aerodynamic rotor torque caused by the increasing angles of attack from collective pitching.

Figure 2.18 shows that a model including the effects of shed vorticity and dynamic stall predicts that the zeros are placed closer to the pole of the 1$^{\text{st}}$ drivetrain mode at high wind speeds relative to a model with quasi-steady aerodynamics. This trend can be explained from the lower aerodynamic damping of the flap motion predicted with unsteady aerodynamics, causing higher flapwise blade motion relative to the hub and thereby larger inertia forces that are completely out of phase with the positive change in aerodynamic torque caused by pitching.

Non-minimum phase zero at the 1st tower modes

Controllability of generator speed with collective pitch is affected by a non-minimum phase zero close to the frequency of the 1st tower bending modes. Figure 2.20 shows the real part of zeros with frequency close to the 1st tower modes for normal operation at below rated wind speed up to 25 m/s. The zeros are calculated for three different models including only longitudinal tower flexibility and quasi-steady aerodynamics (as Fischer [27]), both longitudinal and lateral tower flexibility, rigid drivetrain and rotor and quasi-steady airfoil aerodynamics and for a fully flexible turbine and unsteady aerodynamics. The figure shows that a model that only includes longitudinal tower flexibility and rigid-body rotation of the rotor predicts that there are non-minimum phase zeros below 15 m/s and the non-minimum phase zeros turns into minimum phase zeros above 15 m/s. Collective pitching excites the longitudinal tower vibrations through changes in thrust forces. At the 1st longitudinal tower mode, the thrust forces are in resonance with the longitudinal tower mode and the tower top deflection and velocity in the longitudinal direction shift with a phase of -180 deg across the 1st longitudinal tower mode. The longitudinal tower motion change the inflow and below 15 m/s the resulting change in aerodynamic torque is large enough to counterbalance the effect on the aerodynamic torque from the change in angle of attack caused by pitching the blades. The change in inflow caused by longitudinal tower vibration, cause the aerodynamic torque to experience a phase shift of -180 deg across the 1st longitudinal tower mode, following the phase shift of the longitudinal tower velocity and causing the non-minimum phase zero at the generator speed output. Above 15 m/s, the steady state relative velocities increase such that the effect on the aerodynamic torque of longitudinal tower vibration decrease. The changes in aerodynamic torque from a change in collective pitch angle is thereby mainly determined by the change in angle of attack caused by pitching the blades. As a results, the non-minimum phase zero change to a minimum-phase zero, that nearly cancels the effect of the 1st longitudinal tower mode.

When lateral tower flexibility is included (blue curves in Figure 2.20, the single zero becomes two zeros and one of them is a non-minimum phase zero for all wind speeds. It can be concluded that it is important to include lateral tower degree of freedom to predict correctly that there are non-minimum phase zeros. Below rated wind speed, the model with fully flexible turbine and unsteady aerodynamics predicts existence of up to three non-minimum phase zeros at the 1st tower modes. At 8 m/s, the pole of the 1st longitudinal mode and three non-minimum phase zeros gives a total phase drop of -720 deg, as seen previously in Figure 2.3a.

Under collective pitch angle variations, the tower vibrates in both lateral and longitudinal directions, which is illustrated in Figure 2.21 that shows the aeroelastic frequency response from collective pitch demand to tower top lateral and longitudinal deflections for the NREL 5 MW turbine with rigid drivetrain and rotor in normal operation at 14 m/s and 20 m/s. The figure shows a comparison of lateral tower top deflection predicted for a turbine with rigid drivetrain and rotor and for a turbine with rigid drivetrain and rotor where the tower is made very stiff in the longitudinal direction, to analyze the effect of longitudinal vibration on forces in the lateral direction. For a positive change in pitch angle (towards stall) the thrust forces increase and results in fore-aft deflection in phase with the change in pitch angle, except close to 0 Hz where rigid-body rotor rotation results in small phase differences. Lateral tower deflection hugely increase at the 1st tower modes, along with longitudinal tower vibration and results in lateral tower deflection equal in size to longitudinal deflection at 0.3 Hz. At the 1st tower modes the lateral tower deflection is shifted with a phase of approximately -90 deg relative to the longitudinal deflection,

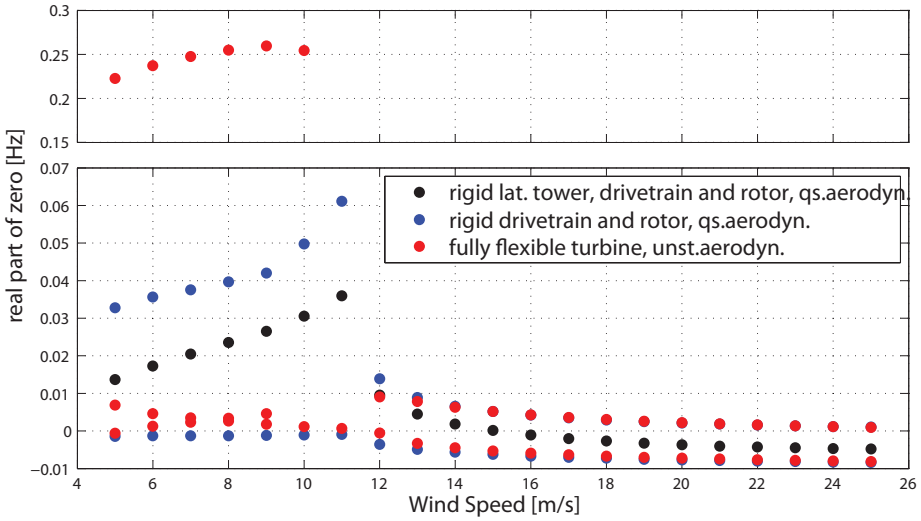

Figure 2.20: Variation of real part of zeros close to the 1$^{\text{st}}$ tower modes in transfer function from collective pitch to generator speed for NREL 5 MW wind turbine in normal operation at various wind speeds. Comparisons between transfer function zeros predicted by linear models assuming rigid tower in lateral direction and rigid drivetrain and rotor and quasi-steady aerodynamics (black), rigid drivetrain and rotor and quasi-steady aerodynamics (blue) and for fully flexible turbine with unsteady aerodynamics (red).

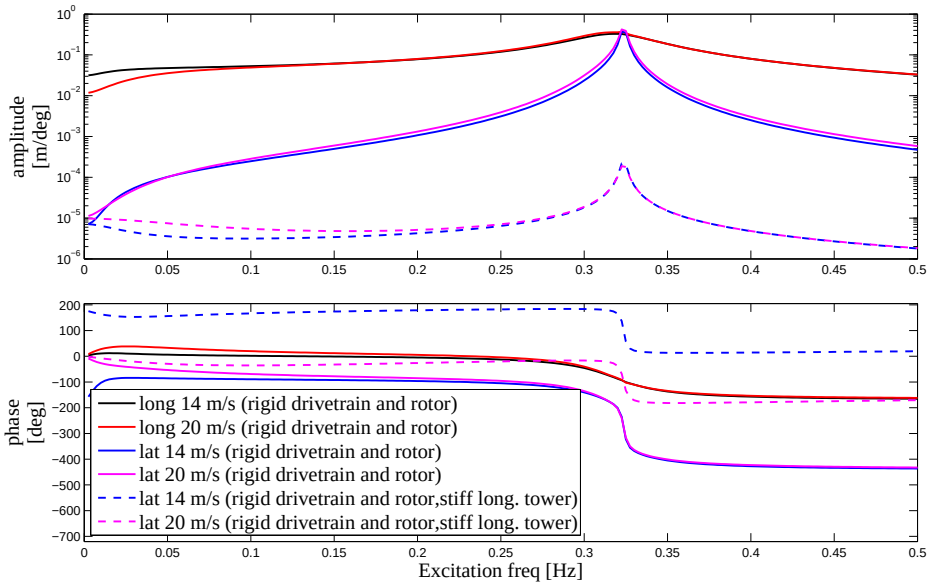

Figure 2.21: Aeroelastic frequency response from collective pitch demand to longitudinal and lateral tower top displacement for the NREL 5 MW turbine in normal operation at 14 m/s and 20 m/s. Comparison between the response for a turbine with a rigid drivetrain and rotor and a turbine with rigid drivetrain and rotor where the tower is made very stiff in the longitudinal direction.

showing that forces acting on the tower in the sideways direction are in phase with the longitudinal tower velocity. The excitation of the lateral tower vibrations through collective pitching can be explained by the fact that the 1st lateral tower mode couples to the longitudinal tower mode. The dotted lines show that the lateral tower top deflection is order of magnitudes smaller if the tower is made stiff in the longitudinal direction, which can be explained by the removed longitudinal tower motion in the 1st lateral tower mode.

Figure 2.22 shows the frequency response from collective pitch to generator speed close to the 1st tower modes for operation at 14 m/s and 20 m/s as predicted by three different linear models including 1) only tower longitudinal tower flexibility and quasi-steady aerodynamics, 2) lateral and longitudinal tower flexibility and quasi-steady aerodynamics and 3) for a fully flexible turbine with unsteady aerodynamics. The figure also shows the response of generator speed measured at the generator bearing and at the generator end of the shaft found by the nonlinear time-simulations using HAWC2 for a fully flexible turbine. At 14 m/s, the model that only includes longitudinal tower flexibility (red curves) predicts that there is a non-minimum phase zero at 0.32 Hz where phase drops almost -360 deg over the shown narrow frequency range. At 20 m/s, the same model predicts a minimum-phase zero at 0.32 Hz, giving a net phase shift of approximately 0 deg across the shown frequency interval, because of 180 deg phase shift of the minimum-phase zero

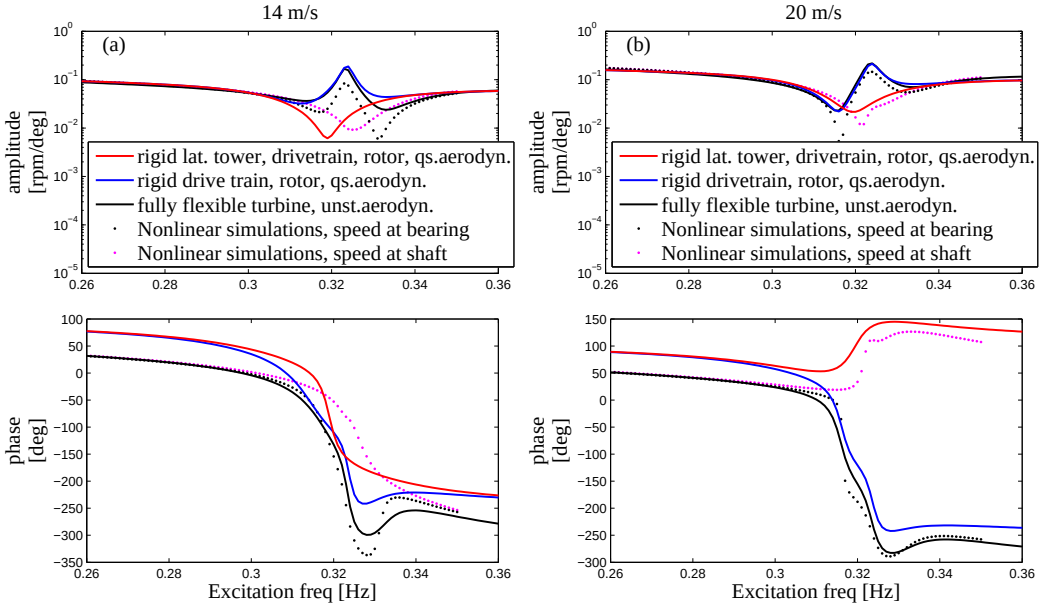

Figure 2.22: Aeroelastic frequency response from collective pitch demand to generator speed at the frequency of the 1st tower mode for NREL 5 MW wind turbine operating at 14 m/s and 20 m/s. Comparisons of frequency response predicted by linear models assuming rigid tower in lateral direction, rigid drivetrain and rotor and quasi-steady aerodynamics (red), rigid drivetrain and rotor and quasi-steady aerodynamics (blue) and for a fully flexible turbine with unsteady aerodynamics (black curve). Comparison between generator speed response measured at bearing output and at shaft end from nonlinear time-simulations with a fully flexible turbine.

and -180 deg phase shift of the 1st longitudinal tower mode. With lateral tower flexibility included, the frequency response is affected by a non-minimum phase zero at 0.32 Hz resulting in a phase drop of approximately -360 deg at both 14 m/s and 20 m/s.

The dotted black and magenta curves in Figure 2.22 compares the generator speed response measured at the generator bearing and at the generator end of the shaft found from the nonlinear time-simulations using HAWC2. There is no non-minimum phase zero at the speed measured on the shaft at 20 m/s, showing that the detected influence of lateral tower motion is caused by nacelle roll associated with lateral tower vibration. The nacelle roll cause a change in the generator speed output that counteracts the increased speed due to the larger aerodynamic rotor torque arising from blade pitching, and the nacelle roll thereby promotes existence of the non-minimum phase zeros.

So, it has been shown to be essential to include lateral tower dynamics besides what is included in the model suggested by Fischer [27]. It is important for correct prediction of non-minimum phase zeros, to include static blade torsion when predicting the gradients of thrust and torque, because blade torsion directly changes the angle of attack. Correct predictions of structural damping of both lateral and longitudinal tower motion may influence predictions of non-minimum phase behavior, because damping influence the amount of vibration of these modes.

2.5 Chapter summary

The open-loop aeroelastic frequency response of a wind turbine from generator torque and collective pitch control actions to generator speed is analyzed based on a recently developed high-order linear aeroelastic model. The frequency response is analyzed for the onshore NREL 5 MW wind turbine in normal operation at various wind speeds. The analysis exemplifies the aeroelastic frequency response of most non-floating, three-bladed, upwind wind turbines, because the ordering of the 1st tower, collective flap and drivetrain/collective edge modes is the same. The linear aeroelastic model is shown to be valid for small amplitude inputs compared to the response of generator speed predicted by time-simulations with the nonlinear aeroelastic model HAWC2.

The aeroelastic frequency response from generator torque to variations in generator speed is shown to be affected by mainly rigid-body rotor rotation and by resonance of the 1st drivetrain torsional mode, which is coupled with collective edgewise blade vibration. The lateral tower modes affects the response close to their aeroelastic frequencies due to nacelle roll, whereas the effect of longitudinal tower vibration is insignificant. Inertia forces acting on the blades due to variations in the rotational speed excites the collective flap modes, mostly at high wind speeds where the blades are pitched. However, due to large aerodynamic damping the influence of the collective flap modes on the transfer function from generator torque to generator speed is insignificant.

The aeroelastic response from collective pitch demand to generator speed is determined by rigid body rotation of drivetrain and rotor below the frequencies of the 1st tower modes. At the 1st tower modes there are up to three non-minimum phase zeros below rated wind speed and one non-minimum phase zero above rated. For correct prediction of the non-minimum phase zero above rated, it is shown to be important to include both the 1st lateral and longitudinal tower modes. Between the 1st tower modes and the 1st drivetrain mode, the frequency response is affected by a highly damped non-minimum phase zero at above rated wind speeds. To correctly predict existence of this zero it is shown to be necessary to model correctly the influence of pitching inertia forces due to flapwise bent blades and to include the 1st drivetrain mode, and collective flap degrees of freedom. It is

important to include aerodynamic damping of the 1st drivetrain mode mainly at high pitch angles. At 14 m/s, there is no difference in the response predicted with a quasi-steady and an unsteady model of airfoil aerodynamics. At 20 m/s, the quasi-steady response deviates at the 1st drivetrain mode, where it fails to predict the correctly influence of a minimum-phase zero, that nearly cancels the pole of the 1st drivetrain mode.

Chapter 3

Order reduction by modal and balanced truncation

This chapter shows how to design low-order aeroelastic models of a wind turbine suited for model-based control design. Low-order models are designed by order reduction of a high-order linear aeroelastic wind turbine model containing structural degrees of freedom that describes the flexibility of tower, drivetrain and blades and aerodynamic states that describes the influence of unsteady aerodynamic forces on the blades.

Order reduction is done by the modal truncation technique using aeroelastic wind turbine mode shapes. Instead of the common approach, which is to reduce the number of structural degrees of freedom of each subcomponent of the turbine and subsequently assemble these models [31, 32, 52, 53], reduced-order models are designed here using the aeroelastic mode shapes of a fully flexible wind turbine. These mode shapes each includes the couplings between the substructures and the aeroelastic couplings between structural blade vibration and the resulting changes in the aerodynamic forces on the blades. Order reduction is done using both the structurally and aerodynamically dominated modes predicted by the high-order, linear aeroelastic model, and a description is given of the influence of the aerodynamically dominated mode shapes. Subsequently, the order is reduced using aeroelastic mode shapes in which quasi-steady aerodynamics is assumed and it is shown that the system matrices of the reduced-order models are suited for interpolation with a scheduling variable.

The reduced-order models obtained by modal truncation are compared to models obtained by the balanced truncation technique in terms of how many states must be used to capture the aeroelastic low-frequency response of a wind turbine. It is analyzed how the balanced truncation technique can capture the effect of shed vorticity and dynamic stall, which is shown to require relatively many states in the modal truncation technique. It is shown how the reduced-order models obtained by the balanced truncation technique can be easily interpolated and therefore also are suited for design of gain-scheduling controllers. The system matrices of the two sets of models are compared using a unique form of the system of equations.

As an example, reduced-order models are designed using the high-order linear aeroelastic wind turbine model called HAWCStab2 [54]. The model is identical to the model described previously and used for frequency response analysis in Chapter 2. The reduced-order models are evaluated on how well the models predict the aeroelastic frequency response from generator torque, collective pitch angle demands and changes in the mean wind speed to the generator speed output predicted by the high-order model. The reduced-order models designed by the balanced reduction technique are also evaluated on how they capture the aeroelastic frequency and damping and mode shapes of the low-frequency wind turbine modes.

This chapter contains first a mathematical description of the modal truncation method. It is then shown how some of the aerodynamically dominated modes influence the frequency response through coupling with rigid body rotor rotation and longitudinal tower

vibration. Subsequently, reduced-order models are designed by modal truncation under assumption of quasi-steady aerodynamics. This is followed by a description of the balanced reduction technique, a description of the required number of balanced states and a comparison of the two sets of system matrices obtained by modal and balanced truncation, showing that the reduced-order system matrices are suited for interpolation with wind speed. The chapter is finally concluded by a chapter summary.

3.1 Order reduction by modal truncation

Before reduced-order models are designed in later sections, a short description is given of the modal truncation technique.

3.1.1 Reduction by modal truncation

Order reduction by modal truncation [38] is done by first applying a full-order state transformation: $\mathbf{x} = \mathbf{\Phi q}$ where $\mathbf{\Phi}$ is denoted the *modal matrix* and contains all the eigenvectors of $\mathbf{A}$ in columns. By this state transformation, a linear time-invariant system of equations on first order form, such as (2.3), can be written:

$$\dot{\mathbf{q}} = \mathbf{\Lambda q} + \mathbf{\Phi}^{-1}\mathbf{B u} \tag{3.1a}$$

$$y = \mathbf{C\Phi q} \tag{3.1b}$$

where $\mathbf{q}$ is the new state vector with generalized states that each describes the motion of a mode shape and $\mathbf{\Lambda}$ is the Jordan form of $\mathbf{A}$. For any square matrix $\mathbf{A}$, the Jordan form is a block diagonal matrix that consist of Jordan blocks. If all eigenvectors of $\mathbf{A}$ are linearly independent, then the Jordan form is a diagonal matrix with the eigenvalues of $\mathbf{A}$ in the diagonal such that each Jordan block is of size 1×1. For all systems used in the present analysis, the modal matrix $\mathbf{\Phi}$ has full rank and thus $\mathbf{A}$ has a diagonal Jordan form.

The state describing the azimuth rotation angle of the rotor $\delta\theta_{azi}$ has been removed from the system of equations prior to the eigenvalue decomposition in Equation (3.1) to ensure that the modal matrix has full rank. This state has no effect on the response from inputs to outputs and represents the pure integrator mode $\dot{\delta\theta}_{azi} = \delta\Omega$ which shows up as a mode with zero eigenvalue $\lambda = 0$ giving a singular modal matrix.

The eigenvalue decomposed form (3.1) is then partitioned:

$$\begin{Bmatrix} \dot{\mathbf{q}}_1 \\ \dot{\mathbf{q}}_2 \end{Bmatrix} = \begin{bmatrix} \mathbf{\Lambda}_1 & \mathbf{0} \\ \mathbf{0} & \mathbf{\Lambda}_2 \end{bmatrix} \begin{Bmatrix} \mathbf{q}_1 \\ \mathbf{q}_2 \end{Bmatrix} + \begin{bmatrix} \left[\mathbf{\Phi}^{-1}\right]_1 \\ \left[\mathbf{\Phi}^{-1}\right]_2 \end{bmatrix} \mathbf{B u} \tag{3.2a}$$

$$y = \mathbf{C} \begin{bmatrix} \mathbf{\Phi}_1 & \mathbf{\Phi}_2 \end{bmatrix} \begin{Bmatrix} \mathbf{q}_1 \\ \mathbf{q}_2 \end{Bmatrix} \tag{3.2b}$$

where indices 1 and 2 denote subcomponents of the matrices. Order reduction by modal truncation is done by representing the full-order model by the subcomponents of the system matrices with index 1, that corresponds to low-frequency aeroelastic modes and by neglecting all other subcomponents denoted with index 2, such that the reduced-order system of equations are given by:

$$\dot{\mathbf{q}}_1 = \mathbf{\Lambda}_1\mathbf{q}_1 + \left[\mathbf{\Phi}^{-1}\right]_1 \mathbf{B u} \tag{3.3a}$$

$$y = \mathbf{C\Phi}_1\mathbf{q}_1 \tag{3.3b}$$

This scheme of a full-order state transformation followed by reduction is applied instead of using a classical modal expansion $\mathbf{x} \approx \Phi_r \mathbf{q}_r$ to get the diagonal structure of $\mathbf{\Lambda}$, which ensures that only the chosen subset of modes are excited by the inputs and measured at the outputs. The modal matrix $\mathbf{\Phi}$ is not orthonormal, regardless of normalization of the eigenvectors, i.e. $\mathbf{\Phi}^{-1} \neq \mathbf{\Phi}^*$, where $*$ denotes the conjugate transpose.

The components of the reduced-order system matrices in Equation (3.3) are complex but are made real by using a coordinate transformation into the real and imaginary parts of the generalized states $\mathbf{q}_1$. For each set i of complex-conjugated eigenvalues and eigenvectors, the transformed system is written:

$$\dot{\mathbf{q}}_{r,i} = \mathbf{A}_{r,i}\mathbf{q}_{r,i} + \mathbf{B}_{r,i}\mathbf{u} \quad ; \quad y = \mathbf{C}_{r,i}\mathbf{q}_{r,i} \tag{3.4a}$$

$$\mathbf{A}_{r,i} = \begin{bmatrix} -\xi\omega_n & -\omega_d \\ \omega_d & -\xi\omega_n \end{bmatrix} ; \mathbf{B}_{r,i} = \begin{bmatrix} \mathbf{B}_{r,i,\alpha} \\ \mathbf{B}_{r,i,\beta} \end{bmatrix} = \begin{bmatrix} \left[\mathbf{\Phi}^{-1}\right]_{i,\alpha}\mathbf{B} \\ \left[\mathbf{\Phi}^{-1}\right]_{i,\beta}\mathbf{B} \end{bmatrix} \tag{3.4b}$$

$$\mathbf{C}_{r,i} = \begin{bmatrix} \mathbf{C}_{r,i,\alpha} \\ \mathbf{C}_{r,i,\beta} \end{bmatrix}^T = 2\mathbf{C}\begin{bmatrix} \mathbf{\Phi}_{i,\alpha} \\ -\mathbf{\Phi}_{i,\beta} \end{bmatrix}^T \tag{3.4c}$$

where $\mathbf{q}_{r,i} = \begin{Bmatrix} \mathrm{Re}(\mathbf{q}_{1,i}) & \mathrm{Im}(\mathbf{q}_{1,i}) \end{Bmatrix}^T$ and where ω_n is the undamped frequency of mode i found as $\omega_n = |\lambda_i|$, where λ_i is the i'th eigenvalue of $\mathbf{A}$. In Equations (3.4) ω_d and ξ are the damped frequency and the damping ratio of mode i, respectively, as defined previously in Equation (2.12). The indices α and β denote the real and imaginary parts, respectively. The factor $2\mathbf{C}$ in the output matrix in (3.4c) arise because the total output equals twice the real part of the output for one of the complex-conjugated poles.

3.1.2 Modal truncation including unsteady aerodynamics

In this section, two examples are used to describe the influence of aerodynamically dominated modes on the aeroelastic frequency response of a wind turbine. The aerodynamically dominated modes investigated here are those arising from shed vorticity and dynamic stall as exemplified by the predictions of the high-order linear aeroelastic model described in Chapter 2, see Figure 2.5.

Influence of aerodynamically dominated modes on steady state responses

Figure 3.1 shows a comparison between the aeroelastic frequency response from generator torque to generator speed predicted by the high-order model (black) and by a reduced-order model obtained by modal truncation including the rigid body rotor rotation mode (blue) at 8 m/s and 20 m/s. The reduced-order model is seen to accurately approximate the response below the 1$^{\text{st}}$ tower modes at 8 m/s but not at 20 m/s, where it predicts too large amplitude at 0 Hz. The red curves in Figure 3.1 are obtained when including five aerodynamically dominated modes as discussed later.

To find out what modes might cause that the rigid body rotor mode predicts an offset at 0 Hz, the influence of each mode on the frequency response has been determined. For each of the transfer functions, the importance of each mode is evaluated by the maximum amplification in the frequency response predicted by each modal subsystem in Equation (3.1), denoted the modal H_∞ norm. Figure 3.2 shows the modal H_∞ norms versus aeroelastic frequencies and cut-off frequencies of purely real eigenvalues for the transfer function from generator torque to generator speed of all structurally dominated modes (black) and all collective aerodynamically dominated modes (red) at 8 m/s, 14 m/s and 20 m/s.

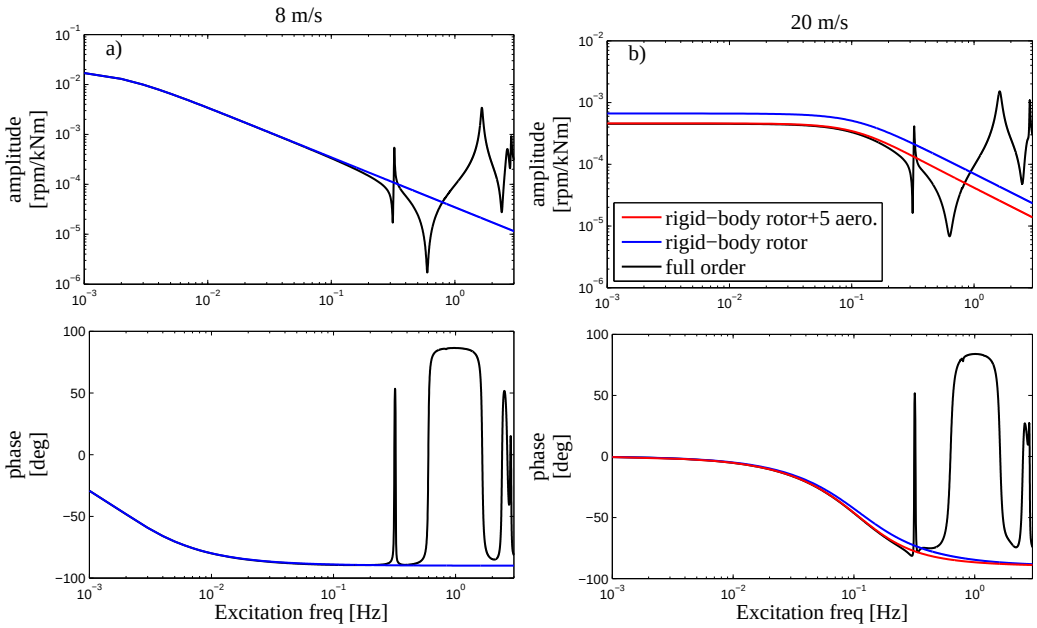

Figure 3.1: Aeroelastic frequency response from generator torque to generator speed for NREL 5 MW wind turbine in normal operation at 8 m/s and 20 m/s predicted by the full-order model (black) and a reduced-order model including the rigid body rotor mode (blue) and a model including the rigid body rotor mode and five collective aerodynamically dominated modes (red).

At 20 m/s in Figure 3.2c, five to ten collective aerodynamically dominated modes with cut-off frequencies below 0.3 Hz have modal norms close to that of the rigid body mode, which is located at $\omega_d = 0.035$ Hz at 20 m/s, and are therefore expected to significantly change the frequency response. At lower wind speeds, the modal norms of the collective aerodynamically dominated modes decrease and therefore also the influence of these modes. A similar influence of the aerodynamically dominated modes is seen in the frequency response from collective pitch angle demand and mean wind speed to generator speed (not shown). A reduced-order model that includes the rigid body rotor mode and the five most important aerodynamically dominated modes which are highlighted by red squares in Figure 3.2c, predicts the frequency response in the red curves in Figure 3.1. The inclusion of these modes in the reduced-order model significantly improves the approximation to the steady state generator speed response to generator torque variations.

To evaluate how many aerodynamically dominated modes are needed, reduced-order models has been designed that includes the rigid body rotor mode and from zero to ten of the most important aerodynamically dominated modes. Figure 3.3 shows the relative error on the amplitude at 0 Hz predicted by the eleven reduced-order models at 20 m/s for the transfer functions from generator torque, collective pitch angle demand and mean wind speed to generator speed. Without any aerodynamically dominated modes the amplitude at 0 Hz deviates with up to 100% relative to the high-order response. A static error below 20% in the response from collective pitch demand to generator speed is achieved by including at least five aerodynamically dominated modes.

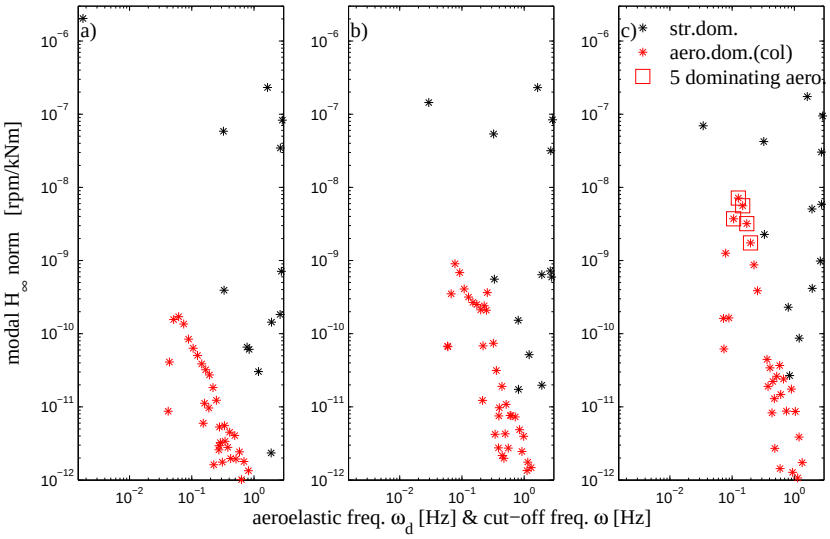

Figure 3.2: H_∞ norms of each aeroelastic modal subsystem of the system of equations (3.1) of each structurally dominated modes (black) and collective aerodynamically dominated modes (red) in the transfer function from generator torque to generator speed for the NREL 5 MW wind turbine in normal operation at a) 8 m/s, b) 14 m/s and c) 20 m/s. The red squares in c) show the five most dominating aerodynamically dominated modes at 20 m/s.

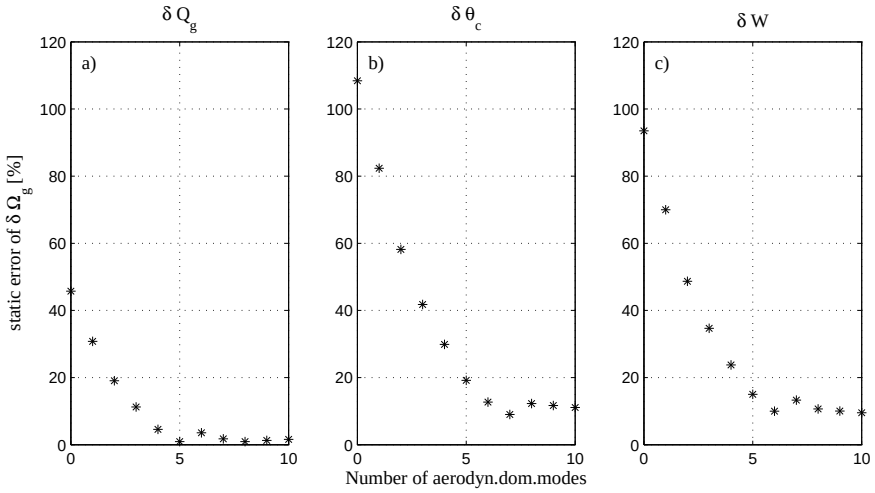

Figure 3.3: Relative error on the amplitude at 0 Hz in the transfer functions from generator torque, collective pitch angle demand and mean wind speed to generator speed versus number of collective aerodynamically dominated modes included in reduced-order model. The reduced-order model includes the rigid body rotor mode and from zero to ten aerodynamically dominated modes for the NREL 5 MW wind turbine in normal operation at 20 m/s.

To explain the effect of the collective aerodynamically dominated modes, Figure 3.4 shows the variations in aerodynamic forces along a blade in the direction perpendicular to the chord axis, denoted δF_c^*, for the most important aerodynamically dominated mode at 8 m/s, 14 m/s and 20 m/s, respectively. The force variations are determined from the eigenvectors of these modes, which are normalized such that the generator speed components are positive and such that the maximum absolute value is unity. At 8 m/s and 14 m/s the most important aerodynamic modes characterize changes in aerodynamic forces only in one calculation point, whereas the mode at 20 m/s shows variation in aerodynamic forces at many sections along the blade because of coupling with rigid body rotor rotation, as explained in the following.

The aerodynamically dominated modes are excited by a change in the angle of attack, caused e.g. by blade pitching, flapwise bending, or change of wind speed. At low wind speed a change in angle of attack will cause only small changes in aerodynamic forces because of low relative velocities. For increasing wind speeds, a change in angle of attack will cause large variations in the aerodynamic rotor torque and thrust and the aerodynamically dominated modes will therefore couple with rigid body rotation of the rotor and the flapwise blade bending modes, causing a change in aerodynamic forces at all sections along the blade. Figure 3.4 shows that at 20 m/s the structural coupling with rigid body rotor rotation and flapwise blade bending modes gives a change in relative velocities that decrease the angle of attack - giving higher lift forces - in the inner part of the blade because of stall, and giving lower lift at mid- and outer part where the blades operate in attached flow.

The aerodynamically dominated modes that influence the generator speed variations at 0 Hz at high wind speeds are all characterized by a large variation in aerodynamic forces at the blade mid-span. This observation can be explained by the facts, that the aerodynamically dominated modes at the blade mid-span contributes more to the aerodynamic rotor torque than modes close to the blade root and close to the blade tip, because of low relative velocities and thereby low changes in lift at the blade root and because of low inflow angles at the blade tip causing that changes in lift mainly changes the thrust

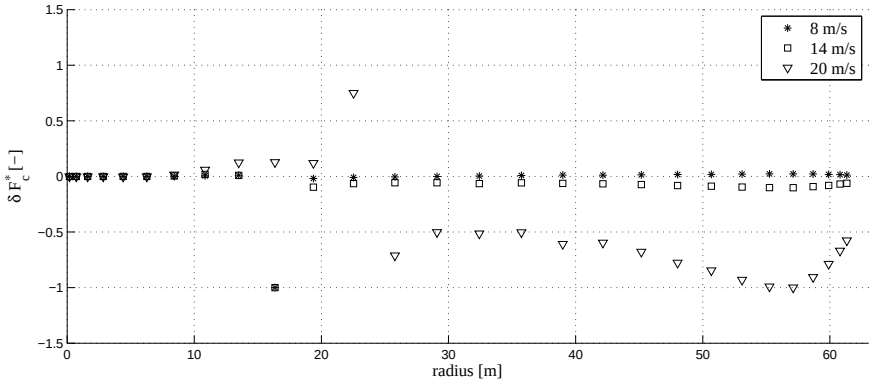

Figure 3.4: Normalized changes in aerodynamic forces perpendicular to local chord direction versus blade radius of three aerodynamically dominated modes with cut-off frequencies of 0.062 Hz, 0.077 Hz and 0.13 Hz for NREL 5 MW wind turbine in normal operation at 8 m/s, 14 m/s and 20 m/s, respectively. Each of the three modes has the highest influence on rotor speed output of all aerodynamically dominated modes at the specific wind speeds.

forces.

It has now been shown that some aerodynamically dominated modes couple with rigid body rotor rotation and thereby are important in predicting the response of generator speed variations at 0 Hz. Vice versa, the rigid body rotor mode will couple to some of the aerodynamically dominated modes at above rated wind speeds. Figure 3.1 showed that approximation with the rigid body rotor mode alone predicts too high amplitude at 0 Hz in the transfer function from generator torque to speed at 20 m/s, which is because the rigid body rotor mode couples with some of the aerodynamically dominated modes. The rigid body rotor mode approximates the changes in rotor speed at 0 Hz too high, because the effective changes in lift when the rotor speed changes are predicted too small in this mode.

Influence of aerodynamically dominated modes on dynamic responses

The last section showed that five to ten aerodynamically dominated modes must be included to achieve good approximation of the response at frequencies below the 1st tower modes. This section shows that other aerodynamically dominated modes affect accurate prediction of the non-minimum phase zeros at the 1st longitudinal tower mode in the response from collective pitch to generator speed [26]. These aerodynamically dominated modes are necessary to include in modal truncation, because the 1st longitudinal tower mode couples to these modes. However, it has previously been shown, that a model assuming rigid drivetrain and rotor, and quasi-steady aerodynamics can correctly predict the existence of non-minimum phase zeros at above rated wind speeds in the transfer function from collective pitch to generator speed.

Figure 3.5 shows the aeroelastic frequency response from collective pitch angle demand to generator speed for the NREL 5 MW wind turbine in normal operation at 14 m/s and 20 m/s as predicted by the high-order model (black) and by reduced-order models designed by modal truncation including different aeroelastic modes. All reduced-order models in this section include the rigid body rotor mode and the ten most dominating aerodynamically dominated modes to ensure accurate prediction of changes in aerodynamic torque at 0 Hz.

The red curves in Figure 3.5 show that a model including also the 1st longitudinal and lateral tower modes predicts existence of a minimum phase zero at 0.31 Hz at both 14 m/s and 20 m/s at the aeroelastic frequency of the 1st longitudinal tower mode. The green curves in Figure 3.5 shows, that when furthermore the 1st collective flap mode is included, the model predicts a non-minimum phase zero at 0.32 Hz at 14 m/s but not at 20 m/s.

The reason why the 1st collective flap mode must be included, when it is previously shown that a rigid rotor can predict the non-minimum phase zero, is because the 1st longitudinal tower mode couples with the 1st collective flap mode. In the forced response of collective pitching at the 1st tower mode, the flap motion is however somewhat limited by the changes in thrust forces associated with the variation in collective pitch. The 1st longitudinal tower mode couples with the 1st collective flap mode, because of the changes in aerodynamic forces at the blades due to changes in relative velocities caused by the longitudinal tower motion. The 1st longitudinal tower mode is characterized by a motion where a positive tower velocity in the downwind direction is in phase with a collective flapwise deflection velocity relative to the hub in the upwind direction, due to the changes in aerodynamic forces on the blades associated with the longitudinal tower motion. The reason why the model without the 1st collective flap mode cannot correctly predict the non-minimum phase zero at the 1st tower modes is because of too small changes in aerodynamic torque and thrust predicted with these modes, due to the collective flap vibration in the

1^{st} longitudinal tower mode.

The cyan curves in Figure 3.5b show, that the non-minimum phase can be correctly predicted at 20 m/s by including four collective aerodynamically dominated modes with cut-off frequencies of $\omega_c = 0.41$ Hz, 0.45 Hz, 0.60 Hz and 0.75 Hz. The cut-off frequencies are slightly higher than of those aerodynamically dominated modes already included, because these modes are characterized by changes in aerodynamic forces at the blade tip where the inflow velocities are higher and the cut-off frequencies therefore higher. Figure 3.6 shows snap shots of variation in aerodynamic forces of the aerodynamically dominated mode with a cut-off frequency of 0.75 Hz. The chosen mode is characterized by high changes in thrust forces at the blade tip, which can be explained by the relative small inflow angles at the blade tip. The changes in thrust forces associated with the aerodynamically dominated modes at the blade tip, makes these modes important for correct prediction of the non-minimum phase zero at the 1^{st} longitudinal tower mode.

3.1.3 Modal truncation including quasi-steady aerodynamics

An assumption of quasi-steady aerodynamics has been found to give accurate predictions of the aeroelastic frequency response from changes in generator torque, collective pitch angles and in mean wind speed, except at around the 1^{st} drivetrain torsion mode in the response from collective pitch to speed, where a quasi-steady aerodynamic model fails to

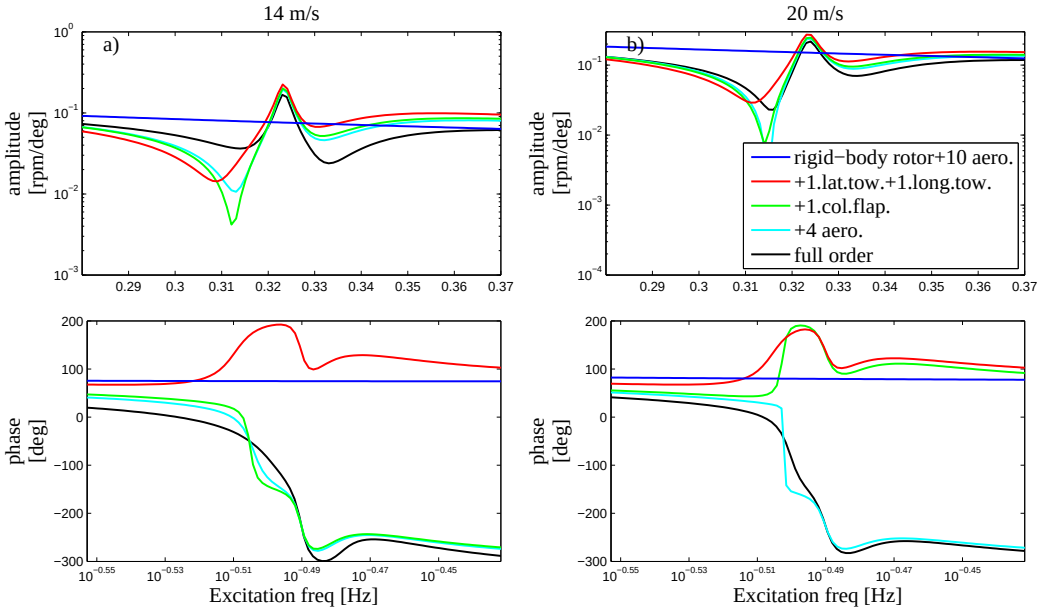

Figure 3.5: Aeroelastic frequency response from collective pitch angle demand to generator speed predicted by the full-order model with unsteady aerodynamics (black) and predicted by a reduced-order model including the rigid body mode and ten collective aerodynamically dominated modes (blue), and by reduced-order models including **also** the 1^{st} lateral and longitudinal tower modes (red), including **also** the 1^{st} collective flap mode (green) and including **also** four collective aerodynamically dominated modes characterizing unsteady aerodynamics at the blade tip (cyan).

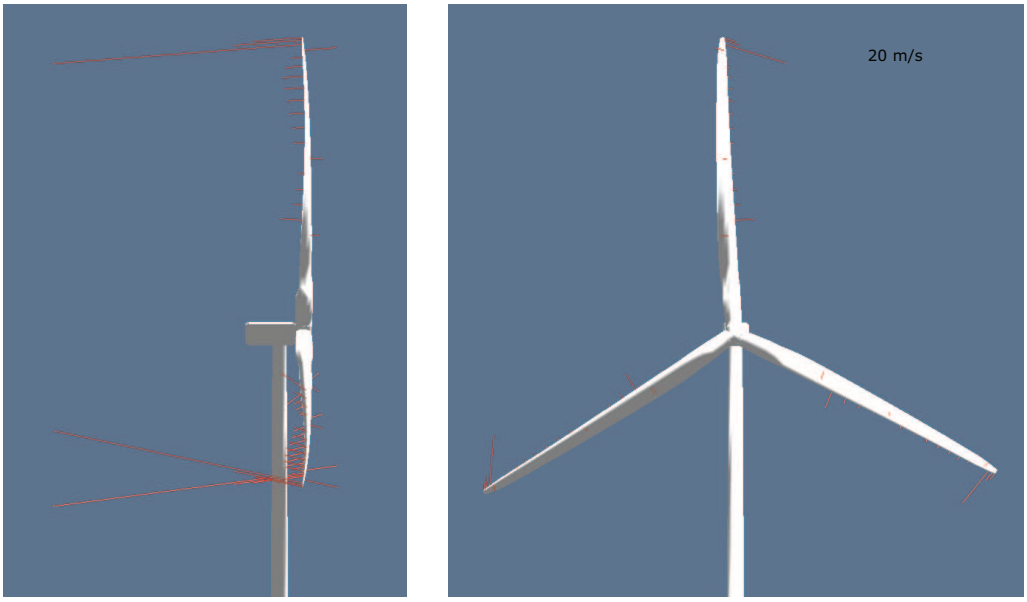

Figure 3.6: Snap shots of variations in aerodynamic forces of one collective aerodynamically dominated mode with cut-off frequency of $\omega_c = 0.75$ Hz for the NREL 5 MW in normal operation at 20 m/s. This mode is characterized by unsteady aerodynamics in a blade section close to the tip, where a change in angle of attack produces high changes in thrust.

correctly predict a zero located close to the pole of this mode. Limitations of the pitch actuator may limit the changes in actual pitch angles at variations in the pitch angle demands at the frequencies of the 1st drivetrain mode and thereby also the influence of the unsteady aerodynamics at these frequencies.

Order reduction is now performed by modal truncation using aeroelastic mode shapes in which quasi-steady aerodynamics is assumed. It is shown how each of the transfer functions from generator torque, collective pitch angle demands and mean wind speed to generator speed can be approximated by gradually increasing the number of aeroelastic modes in the reduced-order model. Before the design of reduced-order models, the following section gives a modal analysis with quasi-steady aerodynamics.

Aeroelastic modal analysis with quasi-steady aerodynamics

Figure 3.7 shows the eigenvalues corresponding to aeroelastic modes with low frequency predicted with quasi-steady aerodynamics. Figure 3.7a shows the real part of the eigenvalues and Figure 3.7b the positive imaginary part of the eigenvalues. The black curves in Figure 3.7 show the real and imaginary parts of the pole of the rigid body rotor mode, where the dashed black line is for the rigid body rotor mode predicted by a simplified model assuming rigid lateral tower, rigid drivetrain and rotor and quasi-steady aerodynamics. This simplified model is used for comparison to study the effects of flexibility of the rotor and drivetrain and the effects of lateral tower flexibility.

Below 15 m/s there is no significant difference between the pole of the rigid body rotor mode predicted from the high-order model with quasi-steady aerodynamics and from that predicted using the simplified model, whereas above 15 m/s the eigenvalue of the rigid

body rotor mode becomes more negative than that predicted with a model assuming rigid rotor, because the rigid body rotor mode couples with the 1st collective flap mode. Above 24 m/s the rigid body mode couples with the 1st collective flap mode to form a 2nd order mode with real value of approximately −0.25 Hz and non-zero imaginary value.

The red curves in Figure 3.7 show the real and imaginary parts of the eigenvalues of the 1st collective flap mode. Both the dotted red curves (•) and red curves marked with circles (○) are associated with the 1st collective flap mode. Below 16 m/s, the 1st collective flap mode consists of a set of complex-conjugate poles. Up to 16 m/s, the real part of the pole of the 1st collective flap mode decrease and the aeroelastic frequency decrease, because the aerodynamic damping of this mode increase with wind speed due to higher relative inflow velocities [55]. Above 16 m/s the 1st collective flap mode becomes overdamped and the set of complex-conjugated eigenvalues of the 1st collective flap mode shift to become two poles with purely real and distinct eigenvalues. The assumption of quasi-steady aerodynamics causes that the aerodynamic damping of the 1st collective flap mode is larger than when unsteady aerodynamics is included, see Table 2.1. The green, blue and cyan curves in Figure 3.7 show the poles of the 1st lateral and longitudinal tower modes and the 1st drivetrain torsional mode.

Frequency response from generator torque to generator speed

Table 3.1 lists the content of the various reduced-order models designed to approximate the low-frequency aeroelastic wind turbine response.

Figure 3.8 shows the aeroelastic frequency response from generator torque to generator speed predicted by a full-order model with quasi-steady aerodynamics (black) and by four

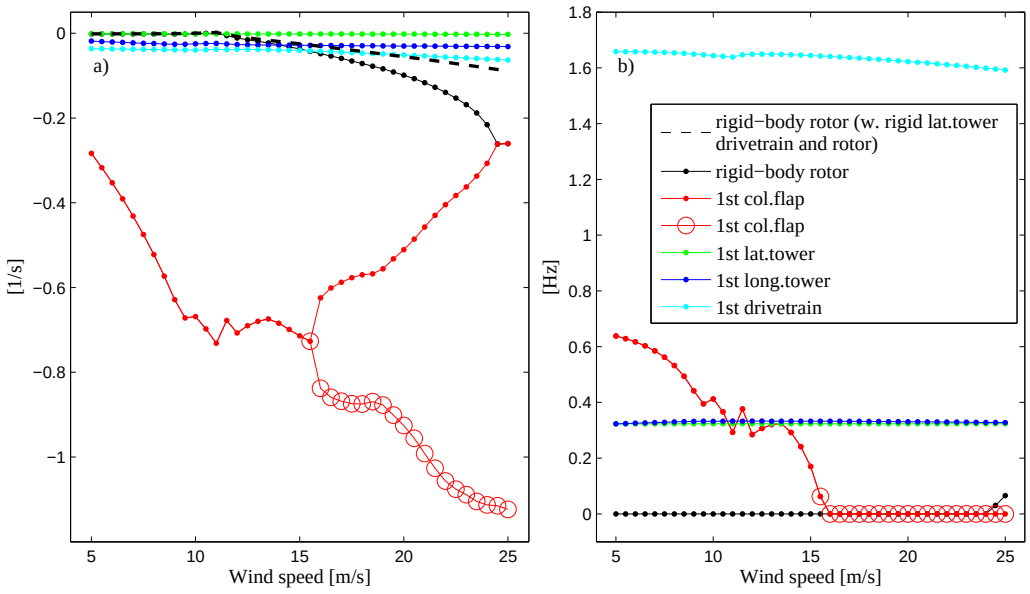

Figure 3.7: Poles of low-frequency aeroelastic mode shapes for the NREL 5 MW wind turbine in normal operation at wind speeds from 5 m/s to 25 m/s equidistant with 0.5 m/s under assumption of quasi-steady aerodynamics. Figure (a) shows the real part of the eigenvalues and Figure (b) the imaginary part, which is equal to the aeroelastic frequency.

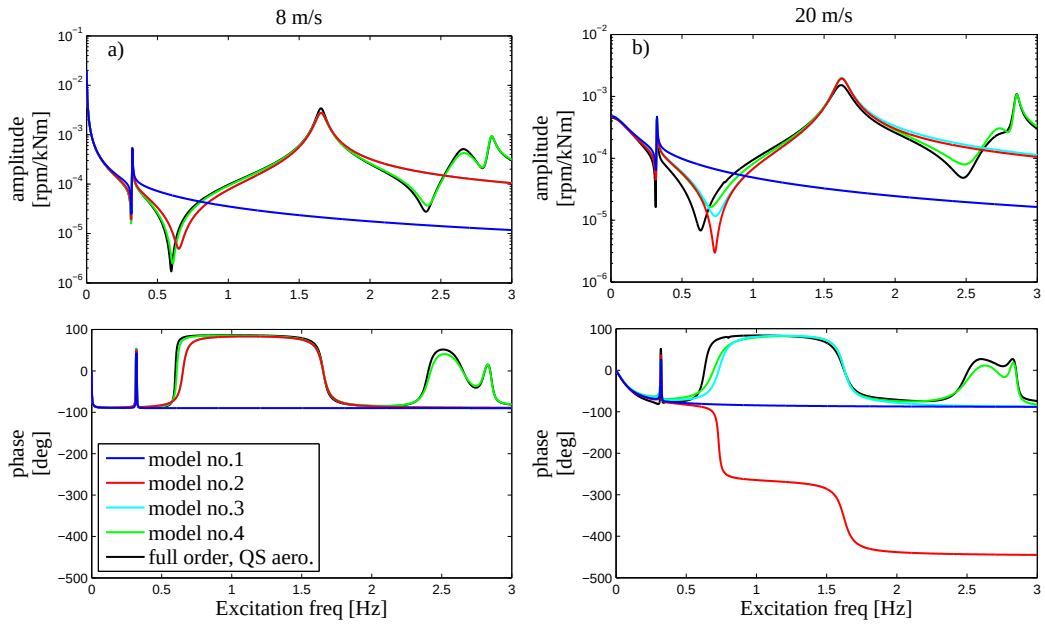

Figure 3.8: Aeroelastic frequency response from generator torque to generator speed for NREL 5 MW turbine in normal operation at 8 m/s and 20 m/s. Comparison between responses predicted by a model assuming quasi-steady aerodynamics (black) and predicted by reduced-order models obtained by modal truncation including the aeroelastic modes in model no. 1 to 4 defined in Table 3.1.

different reduced-order models denoted by model no. 1 to 4 defined in Table 3.1.

Model no.	**Aeroelastic modes included in model**
1	rigid body rotor, 1^{st} lateral tower
2	rigid body rotor, 1^{st} lateral tower, 1^{st} drivetrain
3	rigid body rotor, 1^{st} lateral tower, 1^{st} drivetrain, 2^{nd} collective flap
4	rigid body rotor, 1^{st} lateral tower, 1^{st} drivetrain, 2^{nd} collective flap, 2^{nd} drivetrain, 2^{nd} lateral tower
5	rigid body rotor
6	rigid body rotor, 1^{st} collective flap
7	rigid body rotor, 1^{st} lateral tower, 1^{st} longitudinal tower, 1^{st} collective flap
8	rigid body rotor, 1^{st} lateral tower, 1^{st} longitudinal tower, 1^{st} collective flap, 1^{st} drivetrain
9	rigid body rotor, 1^{st} lateral tower, 1^{st} longitudinal tower, 1^{st} collective flap, 1^{st} drivetrain, 2^{nd} collective flap, 2^{nd} drivetrain

Table 3.1: Description of the aeroelastic modes included in the various reduced-order models used to approximate the aeroelastic frequency response of the NREL 5 MW turbine. The aeroelastic modes are determined using quasi-steady aerodynamics.

The reduced-order model no. 1, that includes the rigid body rotor mode and the 1st lateral tower mode estimates correctly the high gain at 0 Hz, see blue curves in Figure 3.8. The model correctly predicts the zero at 0.315 Hz and the resonance peak at 0.32 Hz at both 8 m/s and 20 m/s, because they exist due to nacelle roll associated with the 1st lateral tower mode.

The red curves in Figure 3.8 show the response predicted by the reduced-order model no. 2 including also the 1st drivetrain mode. At 8 m/s, the model captures correctly the presence of the minimum-phase zero at 0.72 Hz and the resonance peak at the 1st drivetrain mode. At 20 m/s, the model 2 predicts a non-minimum phase zero at 0.72 Hz that causes a negative phase shift of -180 deg. By including also the 2nd collective flap mode (model no. 3), the zero at 0.72 Hz becomes a minimum-phase zero at 20 m/s, whereas at 8 m/s there is no visible change in the response. The prediction of a non-minimum phase zero of the reduced-order model no. 2 at 0.72 Hz, can be explained by a coupling of the 1st drivetrain mode with the 2nd collective flap mode at high wind speeds due to the larger pitch angles. The 2nd collective flap mode (model no. 3) compensates for the flap motion already included with the 1st drivetrain mode. By additionally including the 2nd drivetrain and the 2nd lateral tower modes (model no. 4), the reduced-order model can correctly predict the response up to 3 Hz.

Frequency response from collective pitch and mean wind speed to generator speed

Figures 3.9 and 3.10 show the aeroelastic frequency response from collective pitch angle demand and mean wind speed, respectively, to generator speed for the NREL 5 MW turbine in normal operation at 14 m/s and 20 m/s, predicted by the full-order model with unsteady airfoil aerodynamics (black), under assumption of instant update in the mean wind speed, and with quasi-steady aerodynamics (dashed black) and by five different reduced-order models that includes the aeroelastic modes given in model no. 5 to 9 in Table 3.1.

The blue curves in Figures 3.9 and 3.10 show the responses predicted by the model no. 5 that includes the rigid body rotor mode. At 14 m/s, the model correctly predicts the response at 0 Hz whereas at higher wind speeds , e.g. 20 m/s, it predicts too high amplitude for both pitch and wind speed inputs, as already described in Section 3.1.2 for the model including unsteady aerodynamics. A correct amplitude and phase is achieved at up to the aeroelastic frequency of the 1st tower modes by including also the 1st collective flap mode in model no. 6, shown with red curves. The rigid body rotor mode couples with the 1st collective flap mode at high wind speed when quasi-steady aerodynamics is assumed, such that the rigid body rotor mode alone predicts too high gain at 0 Hz because flap vibration lowers the aerodynamic damping of this mode due to the effect of the flapwise blade motion on the angle of attack in the velocity triangle.

The dashed red curves in Figures 3.9 and 3.10 show the aeroelastic response predicted by the model no. 7 that includes also the 1st tower modes. At both 14 m/s and 20 m/s and for both inputs, the negative phase shift of -360 deg caused by the non-minimum phase zero at the 1st longitudinal tower mode is captured by the model.

The green curves in Figures 3.9 and 3.10 show the response of the reduced-order model no. 8, where also the 1st drivetrain mode is included. For collective pitch inputs, the model approximates well both amplitude and phase up to the frequency of the 1st drivetrain mode, except that it predicts too low amplitude at frequencies in between the 1st tower modes and the 1st drivetrain mode mainly at 20 m/s. For mean wind speed inputs, the

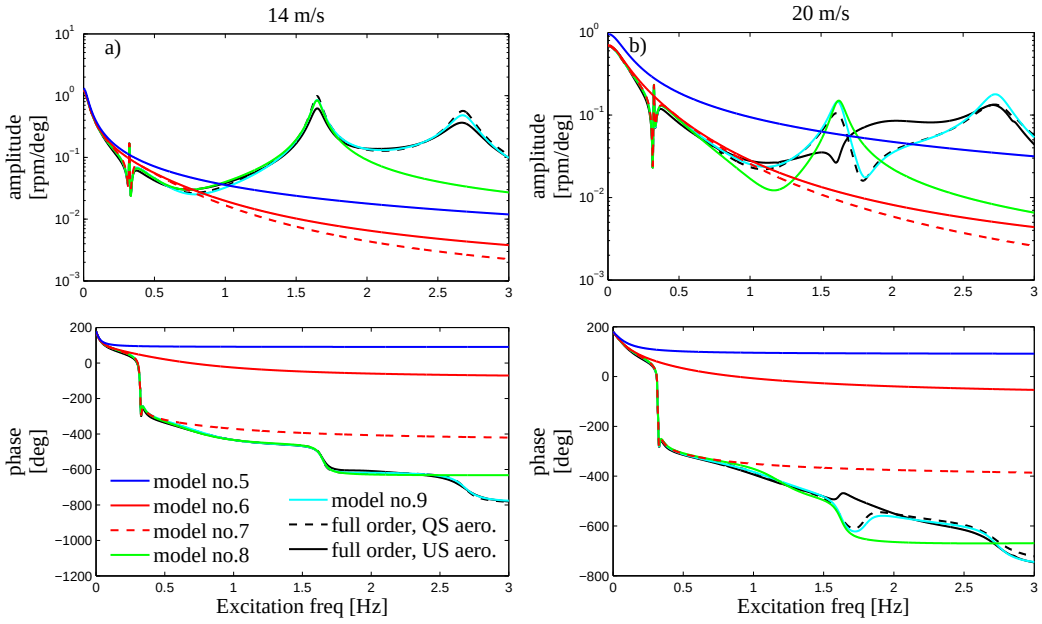

Figure 3.9: Aeroelastic frequency response from collective pitch demand to generator speed for NREL 5 MW turbine in normal operation at 14 m/s and 20 m/s. Comparison between responses predicted by a model assuming quasi-steady aerodynamics (black curves) and predicted by reduced-order models obtained by modal truncation including the aeroelastic modes in model no. 5 to 9 listed in Table 3.1.

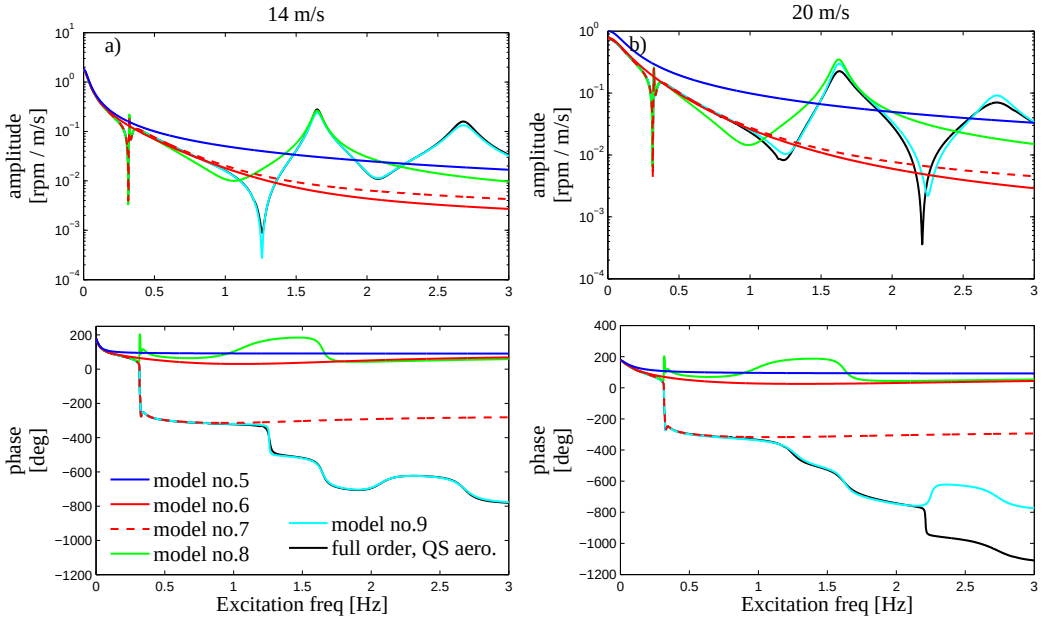

Figure 3.10: Aeroelastic frequency response from changes in mean wind speed to generator speed for NREL 5 MW turbine in normal operation at 14 m/s and 20 m/s. Comparison between responses predicted by a model assuming quasi-steady aerodynamics (black curves) and predicted by reduced-order models obtained by modal truncation including the aeroelastic modes in model no. 5 to 9 listed in Table 3.1.

model no. 8 (green curves in Figure 3.10) does not capture correctly the non-minimum phase zero at the 1st longitudinal tower mode, which can be explained by the collective flap motion introduced by the 1st drivetrain mode.

The cyan curves in Figures 3.9 and 3.10 show the response predicted by model no. 9 including the 2nd collective flap mode and the 2nd drivetrain mode and a total of thirteen states. The combined effect of adding the 2nd collective flap mode and the 2nd drivetrain mode leads to a good approximation of the full order response with quasi-steady aerodynamics up to 3 Hz at both 14 m/s and 20 m/s for both inputs.

3.2 Balanced order reduction

The aim of this section is to compare the modal truncaton reduction technique with the balanced truncation reduction technique in terms of how many states are required to capture the aeroelastic low-frequency response of wind turbines. Attention is given to how many states are required in the balanced truncation technique to capture the effect of the unsteady aerodynamic forces due to shed vorticity and dynamic stall, which in the modal truncation technique requires a relatively large number of aerodynamically uncoupled modes, due to the assumption of independent annular flow tubes in the BEM theory.

As an example, the balanced truncation reduction technique is used to design reduced-order models based on the high-order wind turbine model used previously and the reduced-order models are evaluated on how well the models predict the aeroelastic frequency response from generator torque, collective pitch angle demands and changes in the mean wind speed to the generator speed output. The reduced-order models are also evaluated on how they capture the aeroelastic frequency and damping and the mode shapes of the low-frequency structurally dominated wind turbine modes.

One way of using the balanced reduction technique to generate low-order models suited for gain-scheduling controllers has been investigated in the collaborate paper Adegas et al. [P3]. In the paper, order reduction is done by extracting all structurally and aerodynamically dominated modes with aeroelastic frequency or cut-off frequency below a certain threshold and then subsequently use the balanced reduction technique to decrease the order of this intermediate size reduced-order model. In the collaborate paper, the reduced-order models are finally prepared for interpolation by realizing the reduced-order system of equations on a unique companion form, as explained in the paper.

Here, reduced-order models are also designed by extracting all structurally and aerodynamically dominated modes with aeroelastic frequencies and cut-off frequencies lower than a certain threshold into an intermediate size model using the modal truncation method. A low-order model is subsequently designed by balanced truncation. The present analysis provides a description of how the reduced-order models obtained by balanced truncation approximates the eigenvalues and mode shapes of some of the low-frequency modes predicted by the full-order model.

This section contains first a description of the balanced model reduction technique. Then it is analyzed how many balanced states are needed in the reduced-order models to achieve good accuracy. It is then shown how the components of the reduced-order system matrices vary with operating point and it is described how the reduced-order models obtained by balanced order reduction approximate the aeroelastic frequency and damping of the low-frequency aeroelastic mode shapes.

3.2.1 Balanced reduction technique

Order reduction by *balanced truncation* is suggested by Moore [40], who propose to design low-order models by using a set of balanced states that most efficiently represents the response from a set of inputs to a set of outputs for a linear time-invariant state space model on the form:

$$\dot{\mathbf{x}}(t) = \mathbf{A}\,\mathbf{x}(t) + \mathbf{B}\,\mathbf{u}(t) \tag{3.5a}$$

$$\mathbf{y}(t) = \mathbf{C}\,\mathbf{x}(t) + \mathbf{D}\,\mathbf{u}(t) \tag{3.5b}$$

where $\mathbf{x}$ is the state vector, $\mathbf{u}$ a set of inputs, $\mathbf{y}$ a set of outputs and $\mathbf{A}$, $\mathbf{B}$, $\mathbf{C}$ and $\mathbf{D}$ the corresponding system matrices. A *balanced realization* is a full-order realization of the system of equations, where each state characterize dynamics of a 'shape' that is defined to be equally controllable or reachable from the inputs $\mathbf{u}$ and observable from the outputs $\mathbf{y}$. Balanced truncation is performed by subsequently removing balanced states that are least controllable and observable, because these states do not contribute to the input-output response.

A balanced realization is achieved based on specific measures of the observable 'energy' measured at the outputs and the control 'energy' used to control or reach the states from the inputs. Moore [40] propose to define the observable energy E_o and the control energy E_c as

$$E_o = \int_0^\infty \mathbf{y}^T\mathbf{y}dt \quad \text{where} \quad \mathbf{y}(t) = \mathbf{C}e^{\mathbf{A}t}\mathbf{x}(0) \tag{3.6a}$$

$$E_c = \int_0^\infty \mathbf{x}^T\mathbf{x}dt \quad \text{where} \quad \mathbf{x}(t) = e^{\mathbf{A}t}\mathbf{B} \tag{3.6b}$$

where $\mathbf{y}(t)$ is defined as the output response to a non-zero initial state ($\mathbf{x}(0) \neq \mathbf{0}$) and zero input ($\mathbf{u} = \mathbf{0}$) and where $\mathbf{x}(t)$ is defined as the state response with zero initial conditions ($\mathbf{x}(0) = \mathbf{0}$) and a unit disturbance in the input, c.f. [56].

The observable energy E_o and control energy E_c in Equation 3.6 can be written as:

$$E_o = \mathbf{x}^T(0)\mathbf{W}_o\mathbf{x}(0) \qquad E_c = \text{trace}[\mathbf{W}_c] \tag{3.7}$$

where $\mathbf{W}_o$ is the *observability Gramian* and $\mathbf{W}_c$ is the *controllability Gramian* defined as

$$\mathbf{W}_o = \int_0^\infty e^{\mathbf{A}^T t}\mathbf{C}^T\mathbf{C}e^{\mathbf{A}t}dt \quad ; \quad \mathbf{W}_c = \int_0^\infty e^{\mathbf{A}t}\mathbf{B}\mathbf{B}^T e^{\mathbf{A}^T t}dt \tag{3.8}$$

The components of the observability Gramian denotes how much each state contributes to the output energy E_o and the components of the controllability Gramian denotes how much energy E_c is transferred from the inputs to each state in the model.

The balanced realization is then defined as the realization of the system of equations (3.5) where the observability and controllability Gramians are identical and diagonal; identical, because then the states are equally controllable and observable; diagonal, because then the total observable energy and control energy can be written as a sum of contributions from each of the balanced states, ensuring that we gradually improve the approximation of the frequency response from the inputs to the outputs when more balanced states are added to the model.

The observability and controllability Gramians in Equation 3.8 are solutions to the two following Lyapunov equations

$$\mathbf{A}^T\mathbf{W}_o + \mathbf{W}_o\mathbf{A} = -\mathbf{C}^T\mathbf{C} \tag{3.9a}$$

$$\mathbf{A}\mathbf{W}_c + \mathbf{W}_c\mathbf{A}^T = -\mathbf{B}\mathbf{B}^T \tag{3.9b}$$

and the problem of finding a balanced realization is to find a new system of equations defined by the system matrices $\mathbf{A}_b$, $\mathbf{B}_b$, $\mathbf{C}_b$ and $\mathbf{D}_b$, that gives solutions to the two Lyapunov equations that are identical and diagonal.

The balanced realization of the full-order system of equations can be written as a full-order similar transformation: $\mathbf{x} = \mathbf{T}\mathbf{q}_b$ where $\mathbf{q}_b$ are the generalized balanced states and $\mathbf{T}$ is the basis-shift transformation matrix with balanced 'shapes' in columns, giving a full-order system which is:

$$\dot{\mathbf{q}}_b = \mathbf{A}_b\mathbf{q}_b + \mathbf{B}_b\mathbf{u} \tag{3.10a}$$

$$\mathbf{y} = \mathbf{C}_b\mathbf{q}_b + \mathbf{D}_b\mathbf{u} \tag{3.10b}$$

where $\mathbf{A}_b = \mathbf{T}^{-1}\mathbf{A}\mathbf{T}$, $\mathbf{B}_b = \mathbf{T}^{-1}\mathbf{B}$, $\mathbf{C}_b = \mathbf{C}\mathbf{T}$ and $\mathbf{D}_b = \mathbf{D}$. Different algorithms exist to find the transformation matrix $\mathbf{T}$ and thereby the balanced realization, as reviewed by Antoulas [38]. In the present analysis, the algorithm proposed by Laub et al. [57] is used to obtain the balanced realization.

The diagonals of the observability and controllability Gramians of the balanced realization contain the *Hankel singular values*, which are direct measures of how much each generalized state in the balanced realization contributes to the input-output response. If the first k balanced states with largest Hankel singular values are included in the reduced-order model, there is a guaranteed bound on the H_∞ norm on the error system [58] given by

$$\| \mathbf{G}(s) - \mathbf{G}_r(s) \|_\infty \leq 2 \sum_{i=k+1}^{n} \sigma_i \tag{3.11}$$

where $\mathbf{G}$ and $\mathbf{G}_r$ are the full-order and reduced-order transfer function matrices, respectively, s is the Laplace variable and σ_i is the i'th Hankel singular value. Thus, the sum of the Hankel singular values of balanced states that are not included in the reduced-order model denotes an upper limit to how large error there is on any of the three transfer functions investigated here. Equation (3.11) shows that the balanced reduction technique will try and decrease the H_∞ norm on the error between the original and the reduced-order transfer function matrices. Thus, the balanced reduction technique will try and fit the high-amplitude peaks in one or more of the frequency response functions from the three inputs to the generator speed output, dependent on the applied input scaling done prior to balancing.

Order reduction by balanced truncation is performed by removing the balanced states which are least controllable and observable, i.e. the states with the smallest Hankel singular values such that the system of equations are represented by the subcomponents related to the balanced states with highest Hankel singular values. The reduced-order system of equations obtained by balanced truncation can then be written as:

$$\dot{\mathbf{q}}_{b,tt} = \mathbf{A}_{b,tt}\mathbf{q}_{b,tt} + \mathbf{B}_{b,tt}\mathbf{u} \tag{3.12a}$$

$$\mathbf{y} = \mathbf{C}_{b,tt}\mathbf{q}_{b,tt} + \mathbf{D}_b\mathbf{u} \tag{3.12b}$$

where $\mathbf{q}_{b,tt}$ denotes the vector of balanced states included in the reduced-order model and where matrices $\mathbf{A}_{b,tt}$, $\mathbf{B}_{b,tt}$, $\mathbf{C}_{b,tt}$ are the subcomponents of the matrices of the balanced realization corresponding to these balanced states.

3.2.2 Low-order models by balanced truncation

Order reduction is done here based on the linear aeroelastic model of the NREL 5 MW, which is described in Chapter 2 and used previously in this chapter to design reduced-order models by modal truncation with generator torque, collective pitch angle and mean wind speed as inputs and generator speed as output. Balanced reduction is here done on a model which is already reduced in order by modal truncation including all modes with a cut-off frequency or undamped frequency below a chosen threshold of 3.0 Hz resulting in a model including around 300 states, that fully captures the low-frequency response. Modal truncation is done before balanced reduction to ensure that the balanced states describes low-frequency dynamics and has a similar effect as frequency weighting of inputs and/or outputs [38]. Without frequency weighting, the balanced reduction may try to capture high-frequency dynamics, which are not relevant to include.

Scaling

Balanced reduction is done on a system of equations, in which the inputs and output are scaled using the scaling matrices $\mathbf{W}_u$ and $\mathbf{W}_y$ defined by

$$\mathbf{u} = \mathbf{W}_u \hat{\mathbf{u}} \qquad \text{and} \qquad y = \mathbf{W}_y \hat{y} \tag{3.13}$$

where $\hat{\mathbf{u}}$ and $\hat{y}$ are the scaled input vector and the scaled output, respectively. Then, balanced reduction is done on the new scaled system of equations defined by:

$$\dot{\mathbf{x}} = \mathbf{A}\mathbf{x} + \mathbf{B}\mathbf{W}_u \hat{\mathbf{u}} \tag{3.14a}$$

$$\hat{\mathbf{y}} = W_y^{-1}\mathbf{C}\mathbf{x} + W_y^{-1}\mathbf{D}\mathbf{W}_u \hat{\mathbf{u}} \tag{3.14b}$$

The choice of input and output scaling matrices determines directly which of the three single-input single-output transfer functions that the balanced reduction technique will try and approximate. The aim of a controller could typically be to decrease the effect of a mean wind speed disturbance on the generator speed response, such that good accuracy is required of the frequency response from mean wind speed to generator speed. For the control inputs, the scaling should correspond to how the weighting of the control inputs is done in the design of the controller, such that it is ensured, that the response of the actual control input used to limit variations in the generator speed is well approximated.

The usual procedure is to scale the generator torque and collective pitch control inputs with the typical allowed changes of these control inputs in closed loop, and to scale the wind speed disturbance input with typical changes in this input. The input and output scaling matrices are defined as:

$$\mathbf{W}_u = \begin{bmatrix} 200 \text{ kNm} & 0 & 0 \\ 0 & 1 \text{ deg} & 0 \\ 0 & 0 & 1 \text{ m/s} \end{bmatrix} \quad ; \quad W_y = 1 \text{ rpm} \tag{3.15}$$

The generator torque input is scaled with 200 kNm which is 1/20 of the static generator torque acting at stationary operation at 20 m/s found to be approximately 4000 kNm. A similar ratio is used in scaling of the two other inputs.

Figure 3.11 shows a comparison of the scaled frequency response of the three transfer functions from generator torque, collective pitch demand and from mean wind speed to generator speed for the NREL 5 MW turbine in normal operation at 14 m/s and 20 m/s predicted by the full-order model including unsteady aerodynamics. At both 14 m/s and 20 m/s, the highest Hankel singular values of the balanced model will aim at capturing the response of collective pitch and variations in the mean wind speed up to around 1 Hz, whereas around the frequency of the 1st drivetrain mode, it will aim at capturing the response of collective pitching and generator torque variations at 14 m/s and of mean wind speed variations and generator torque variations at 20 m/s, due to the high amplitudes of the scaled frequency responses of these inputs shown in Figure 3.11.

Reduced-order models: Accuracy and interpretation

Figure 3.12 shows the 20 highest Hankel singular values for the scaled transfer function matrix from generator torque, collective pitch angle and mean wind speed to generator speed for the models of the NREL 5 MW turbine in normal operation at 8 m/s, 14 m/s and 20 m/s obtained by modal truncation including around 300 states. These Hankel singular values represents the 20 balanced states, that are found most efficiently to describe the frequency response from the scaled generator torque, collective pitch demand and mean wind speed variations to the generator speed output. The figure shows that at 8 m/s and 14 m/s there are three balanced states and at 20 m/s there is one balanced state which has significantly higher Hankel singular values and thus are expected to capture the principal effect of the transfer functions. Figure 3.12 shows that between Hankel singular value number 14 and 15 of the intermediate size models of the NREL 5 MW turbine at both 8 m/s, 14 m/s and 20 m/s, there is a clear jump in the Hankel singular values, showing that the balanced states corresponding to the highest 14 Hankel singular values are expected to capture the primary and secondary effects of the investigated transfer function matrices.

Figures 3.13-3.15 show the aeroelastic frequency response from generator torque, collective pitch angle demands and mean wind speed to generator speed for the NREL 5 MW

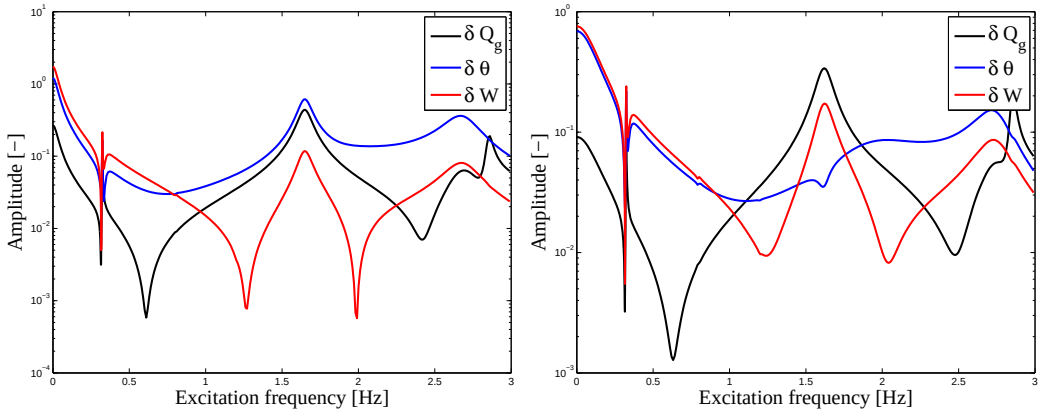

Figure 3.11: Aeroelastic frequency response amplitudes of transfer functions from generator torque, collective pitch demand and mean wind speed inputs to generator speed output for scaled inputs and outputs of NREL 5 MW wind turbine in normal operation at 14 m/s (left) and 20 m/s (right).

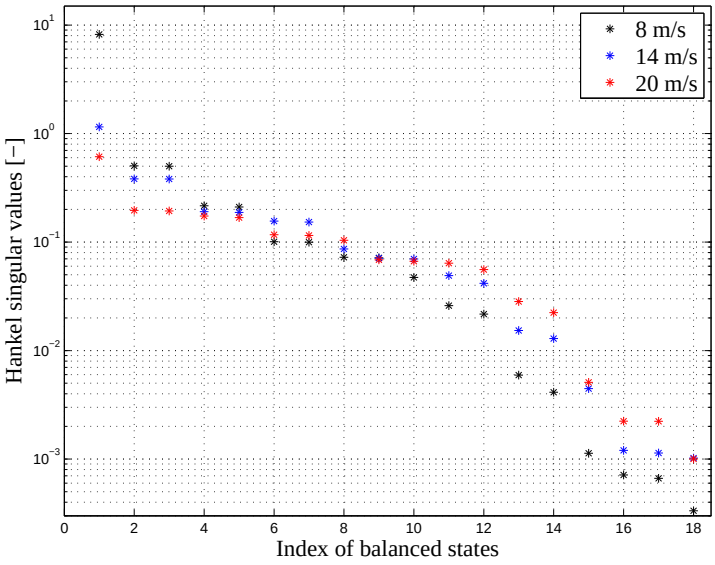

Figure 3.12: The highest 20 Hankel singular values in descending order of the scaled transfer function matrix from generator torque, collective pitch angle and mean wind speed to generator speed for an intermediate size model of the NREL 5 MW wind turbine in normal operation at 8 m/s, 14 m/s and 20 m/s obtained by modal truncation of all structurally and aerodynamically dominated modes with frequencies below 3 Hz.

turbine in normal operation at 14 m/s and 20 m/s predicted by the full-order models and for reduced-order models obtained by balanced truncation containing different number of balanced states.

The red curves in Figures 3.13-3.15 show the frequency responses predicted by a model including the three balanced states corresponding to the three highest singular values. This model captures the response at 0 Hz for all three transfer functions at both 14 m/s and 20 m/s, except for some small deviations for generator torque inputs at 20 m/s and captures the response at the 1$^{\text{st}}$ drivetrain mode. Thus, these three balanced states are thereby found to have a similar effect as the three generalized states of the rigid body rotor mode and the 1$^{\text{st}}$ drivetrain mode used in the modal truncation technique. The balanced reduction technique aims at approximating the response of these modes because the scaled amplitudes are relatively large at these frequencies in Figure 3.11. The three-state model does not capture the response at the 1$^{\text{st}}$ tower modes, and thereby fails to predict the large change in phase at 0.3 Hz in the response of collective pitching and mean wind speed inputs.

The blue curves in Figures 3.13-3.15 show the response predicted with a model including ten balanced states. The main effect of including the additional seven balanced states compared to the previous 3$^{\text{rd}}$ order model, is better approximation of the response at the 1$^{\text{st}}$ lateral and longitudinal tower modes and of the response at the 2$^{\text{nd}}$ drivetrain mode at around 2.7 Hz, such that the models now captures the non-minimum phase response at the 1$^{\text{st}}$ tower modes for collective pitch and mean wind speed inputs. However, the model predicts wrongly a -360 deg phase shift in the generator speed response at the 1$^{\text{st}}$ tower mode for generator inputs.

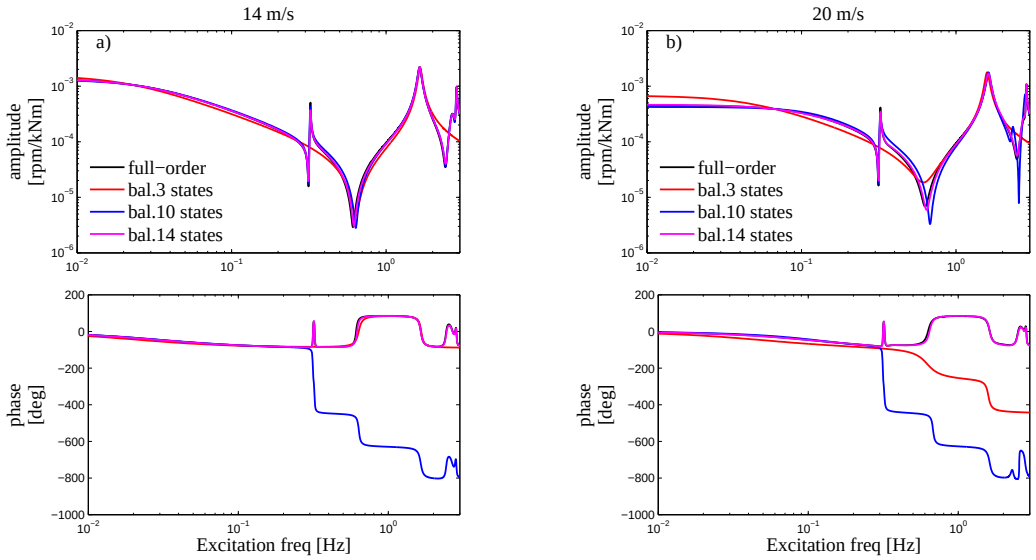

Figure 3.13: Aeroelastic frequency response from generator torque to generator speed for NREL 5 MW turbine in normal operation at 14 m/s and 20 m/s. Comparison of response predicted by the full-order model with unsteady aerodynamics (black) and response of reduced-order models obtained by balanced reduction using various number of balanced states.

The magenta curves in Figures 3.13-3.15 show the frequency response predicted with a model including 14 balanced states, which is seen to capture accurately the frequency responses for all three inputs at both 14 m/s and 20 m/s. The four additional balanced states that has been included in this model relative to the previous model, mainly affects the response at the 1^{st} tower modes for generator torque inputs and at the 1^{st} drivetrain mode; for collective pitch angle demand inputs at 20 m/s the model captures accurately the zero close to this mode, which was previously found to be affected by the lag from shed vorticity and dynamic stall (see Figure 3.9).

The content of the reduced-order models obtained by balanced truncation is further described from how the models predicts the aeroelastic poles and some of the aeroelastic mode shapes relative to the full-order model.

Figure 3.16 shows the real and imaginary parts of the eigenvalues corresponding to the low-frequency modes of the NREL 5 MW wind turbine in normal operation at various wind speeds. The figure shows a comparison between the eigenvalues predicted by the full-order model and predicted by the reduced-order models designed previously including 14 balanced state. The left column shows the real parts of the eigenvalues corresponding to these modes, and the right column shows the positive imaginary part of the eigenvalues. The top row of diagrams in Figure 3.16 shows the eigenvalues corresponding to the rigid body rotor mode and a new aerodynamically dominated mode, as explained later. The bottom row in Figure 3.16 shows the eigenvalues corresponding to the 1^{st} lateral and longitudinal tower modes, the 1^{st} and 2^{nd} collective flap modes and the 1^{st} drivetrain torsion mode predicted by the full-order models and estimated by the reduced-order models obtained by balanced truncation, as explained in the following. The figure shows the poles

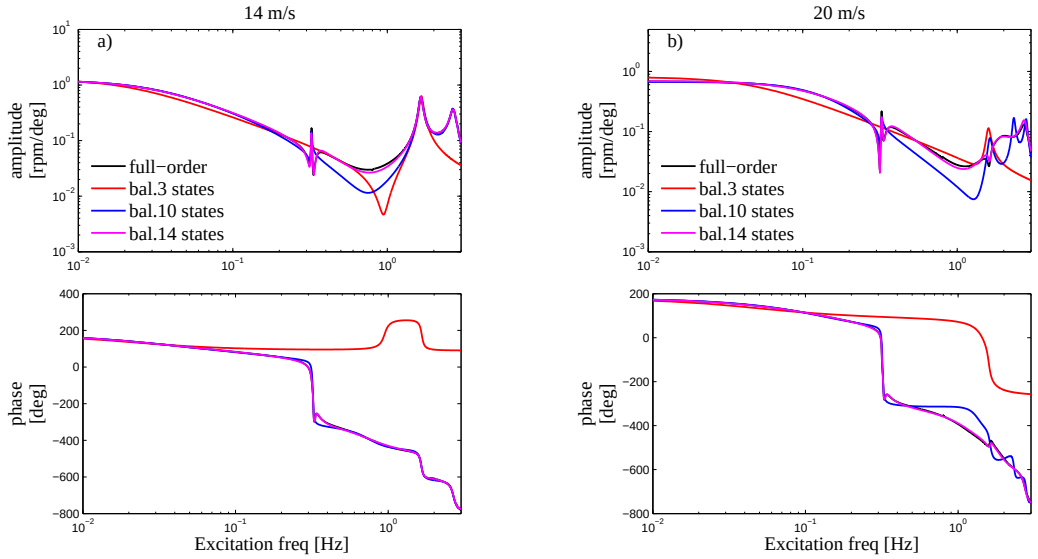

Figure 3.14: Aeroelastic frequency response from collective pitch angle demand to generator speed for NREL 5 MW turbine in normal operation at 14 m/s and 20 m/s. Comparison of response predicted by the full-order model with unsteady aerodynamics (black) and response of reduced-order models obtained by balanced reduction using various number of balanced states.

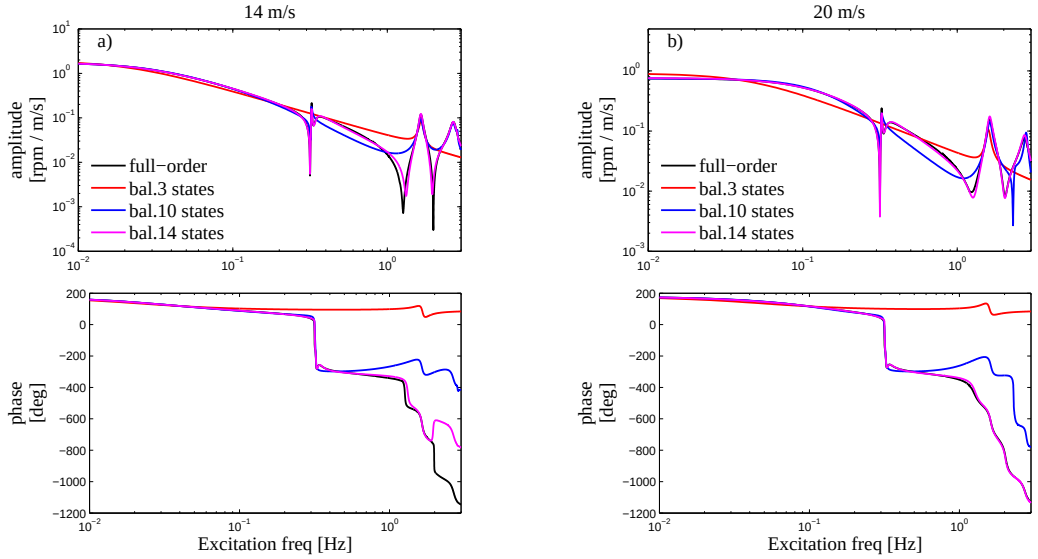

Figure 3.15: Aeroelastic frequency response from mean wind speed to generator speed for NREL 5 MW turbine in normal operation at 14 m/s and 20 m/s. Comparison of response predicted by the full-order model with unsteady aerodynamics (black) and response of reduced-order models obtained by balanced reduction using various number of balanced states.

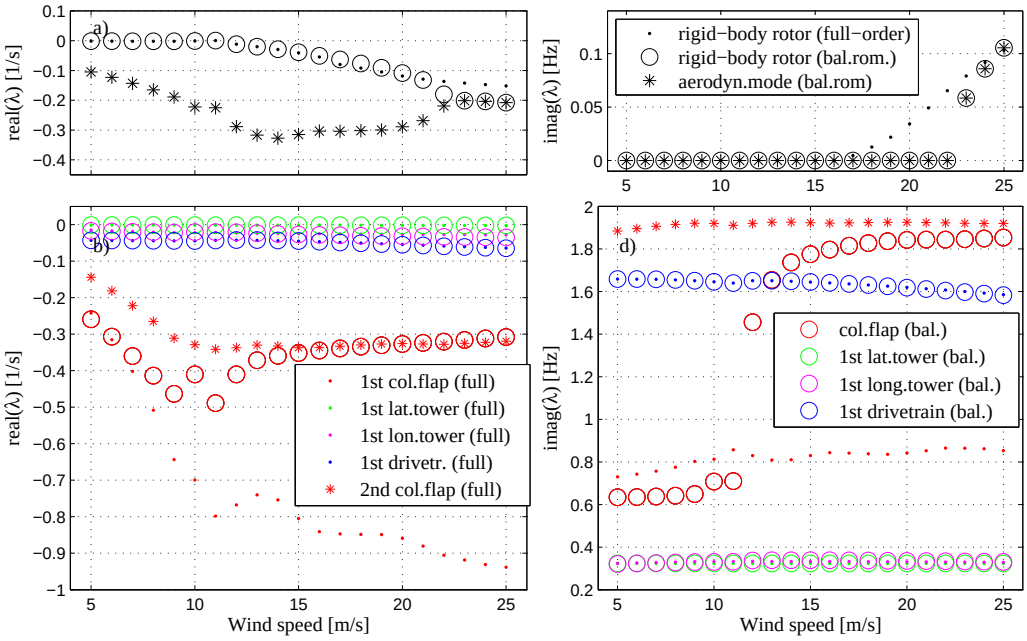

Figure 3.16: Poles of low-frequency aeroelastic mode shapes of the NREL 5 MW wind turbine in normal operation at various wind speeds predicted by reduced-order models obtained by balanced truncation included 14 balanced states and compared with the poles predicted by the full-order aeroelastic model.

corresponding to ten of the fourteen poles of the balanced reduced-order models. The remaining four poles (not shown) have eigenvalues similar to the 2$^{\text{nd}}$ drivetrain torsion mode and the 2$^{\text{nd}}$ lateral mode predicted by the full-order model.

The reduced-order models captures the eigenvalues of the rigid body rotor mode (black points and circles in Figure 3.16) accurately up to around 15 m/s, where the full-order model predicts that the rigid body rotor mode becomes a 2$^{\text{nd}}$ order mode. The reduced-order models predicts that the rigid body rotor mode couples to a 1$^{\text{st}}$ order aerodynamically dominated mode above 23 m/s to form a 2$^{\text{nd}}$ order mode. That the rigid body rotor mode couples with the aerodynamically dominated mode at high wind speeds and not the 1$^{\text{st}}$ collective flap mode - as seen previously with the quasi-steady aerodynamic model - is in agreement with how the modes couples in the full-order model.

The eigenvalues shown with black asterisks in Figure 3.16 correspond to a new aerodynamically dominated mode found by the balanced reduction technique, that represents the effects of the large number of collective aerodynamically dominated poles of the full-order model.

The red circles in Figure 3.16 shows another pole of the reduced-order model, which is characterized by a high damping ratio that grows up to around rated wind speed and then decrease with wind speed, and an aeroelastic frequency (Figure 3.16d) that is close to 0.7 Hz below rated and then at rated increase to around 1.8 Hz. The red points ($\bullet$) and asterisks ($*$) in Figure 3.16 shows the poles of the 1$^{\text{st}}$ and 2$^{\text{nd}}$ collective flap modes predicted by the full-order model. It is observed that below rated this pole of the reduced-order model resembles the 1$^{\text{st}}$ collective flap mode, whereas above rated the pole resembles

the 2nd collective flap mode, indicating that above rated the 2nd collective flap mode has a larger influence on the generator speed response than the 1st collective flap mode.

Figure 3.16 shows, that the reduced-order model with the 14 balanced states captures fully the poles of the 1st lateral and longitudinal tower modes and the 1st drivetrain mode predicted by the full-order model.

Some attention is now given to how the reduced-order models captures the mode shapes of the corresponding modes of the full-order model.

Figure 3.17 shows the variations in the collective aerodynamic forces in the new aerodynamically dominated mode shown with black asterisks in Figure 3.16 for operation at 8 m/s, 14 m/s and 20 m/s. The figure shows the variations in the aerodynamic forces in this mode perpendicular to the local chord directions at the aerodynamic calculation points versus blade radius. The forces shown in Figure 3.17 are found by transforming the eigenvector corresponding to this mode given in the basis of the balanced 'shapes' back into the original basis of nodal degrees of freedom and aerodynamic states. This transformation can be written as: $\phi_o = \mathbf{T}_r \phi_b$, where ϕ_b is the eigenvector given in the balanced basis, ϕ_o is the eigenvector given in the original basis and $\mathbf{T}_r$ is the reduced-order transformation matrix, which consists of the columns of $\mathbf{T}$ used in the balanced realization (3.12) corresponding to the highest Hankel singular values.

The aerodynamic forces in Figure 3.17 of the aerodynamically dominated mode are continuously distributed over the blade, opposite to those of the full-order model shown previously in Figures 3.4 and have the same trend as the force-variations on the rigid body rotor mode: steadily increasing variations in aerodynamic forces with blade radius, due to the higher changes in relative inflow velocity, except at the tip where the chord is small. Instead of the large number of uncoupled aerodynamically dominated modes of the full-order model, analyzed e.g. in Figure 3.4, the balanced truncation technique efficiently describes the influence of the lag caused by shed vorticity and dynamic stall by a single state.

Figure 3.18 shows the collective blade deflections in the 'collective flap' mode shape predicted by the reduced-order models corresponding to the red circles in Figure 3.16. The mode shapes of the reduced-order models are compared with the mode shapes of the 1st

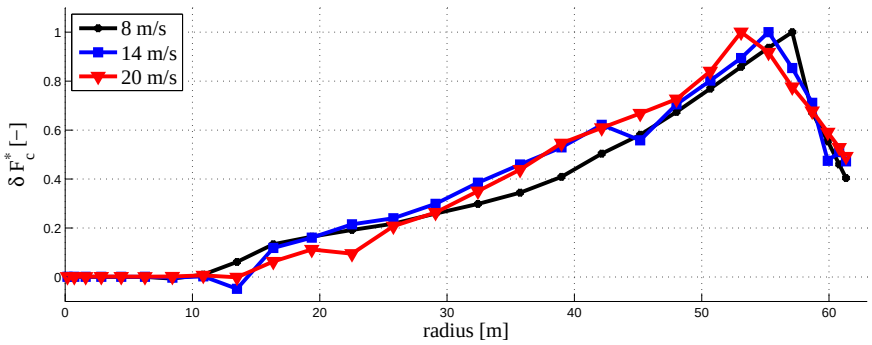

Figure 3.17: Normalized changes in aerodynamic forces perpendicular to local chord direction versus blade radius of an aerodynamically dominated mode of the reduced-order model obtained by balanced truncation for the NREL 5 MW wind turbine in normal operation at 8 m/s, 14 m/s and 20 m/s, respectively.

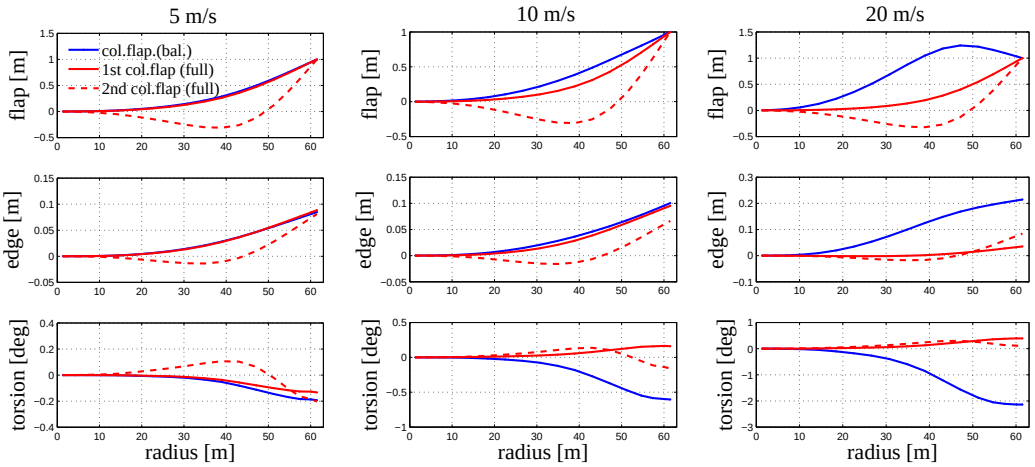

Figure 3.18: Aeroelastic mode shape of a 'collective flap mode' predicted by a reduced-order model obtained by balanced truncation. This mode has an aeroelastic frequency close to that of the 1st and 2nd collective flap modes below and above rated wind speed, respectively. The figure shows the collective blade deflections in the flap and edge directions relative to the hub and the torsional rotation around the local elastic axis versus blade radius of this mode compared to the mode shapes of the 1st and 2nd collective flapwise mode shapes predicted by the full-order model. Example: NREL 5 MW wind turbine in normal operation at 5 m/s, 14 m/s and 20 m/s.

and 2nd collective flap modes predicted by the full-order model. At 5 m/s, the 'collective flap' mode shape predicted by the reduced-order model is very similar to the shape of the 1st collective flap mode. At 10 m/s, the 'collective flap mode' predicted by the reduced-order model is still mainly characterized by vibration in the 1st collective flap mode, but includes larger variations in the blade torsion than in either of the collective flap modes of the full-order model. At 20 m/s, the 'collective flap mode' contains more of the 2nd collective flap motion than at low wind speeds, but the edgewise deflection and torsional rotation of this mode does not accurately represent that of the 2nd collective flap mode of the full-order model. Thus, although the eigenvalues of the mode predicted by balanced truncation are very close to that of the 2nd collective flap mode at high wind speeds in Figure 3.16, the mode shape does not accurately represent the actual mode shapes of the 2nd collective flap mode.

If we compare how many balanced states are required compared to modal states in the modal reduction technique, it is generally observed that the balanced reduction technique is very efficient in capturing the effect of the large number of aerodynamically dominated time constants, whereas it requires approximately the same number of states to capture the effect of the structurally dominated modes.

The chosen input scaling performed prior to the design of the reduced-order models affects the content of the reduced-order models. If reduced-order models are designed based only on the generator input, the reduced-order models obtained by balanced truncation tends to include a 'collective flap mode' with an eigenvalue close to the 2nd flap mode at all wind speeds. If only the collective pitch angle demand input is used, the models obtained by balanced truncation tend to include the 2nd collective flap mode at all wind speeds, and

two additional 1st order modes at and above rated wind speed, somewhat characterizing the 1st collective flap mode.

3.3 Reduced-order models for controller design

In this section, it is described that the system matrices of the reduced-order models obtained by modal truncation and balanced truncation are suited for interpolation or parametrization with a gain-scheduling variable characterizing changing operating point of the wind turbine. As an example, it is chosen to study the changes in the system matrices happening along the desired operational points of a wind turbine characterized by a specific variation of the rotor speed and collective pitch angles as the mean wind speed changes.

The reduced-order models are put on the eigenvalue decomposed form to ensure that the system matrices are suited for interpolation. To make this form unique it is proposed to normalize the eigenvectors relative to the generator speed output component of each mode. There exist other methods to obtain a realization of models at different parameters that are suited for interpolation or parametrization than the one proposed here. One approach is to use one of the companion forms of the systems of equations, as proposed in [P3].

3.3.1 Unique representation

To ensure that the components of the reduced-order matrices vary smoothly with operating point, we choose to represent the system of equations in its eigenvalue decomposed form, i.e. in the diagonal form given in Equation (3.1). The reduced-order models obtained by modal truncation are already realized on diagonal form. The reduced-order models obtained by balanced truncation given by Equations (3.12) are diagonalized, such that the reduced-order system of equations can be written:

$$\dot{\mathbf{q}} = \mathbf{\Lambda}\mathbf{q} + \mathbf{\Phi}_b^{-1}\mathbf{B}_b\mathbf{u} \tag{3.16a}$$

$$\mathbf{y} = \mathbf{C}_b\mathbf{\Phi}_b\mathbf{q} + \mathbf{D}\mathbf{u} \tag{3.16b}$$

where $\mathbf{\Lambda}$ is the diagonal spectral matrix that consist of the eigenvalues of $\mathbf{A}_b$ in the diagonal and $\mathbf{\Phi}_b$ is the modal matrix consisting of the eigenvectors of $\mathbf{A}_b$ in columns. The reduced-order models designed here by balanced truncation all have a matrix $\mathbf{A}_b$ with distinct eigenvalues and therefore a modal matrix of full rank, such that the inverse of the modal matrix can be found. The system matrices of the reduced-order models obtained by balanced truncation are made real-valued in the same way as done in the modal truncation technique as given by Equations (3.4) with new definitions of the input and output matrices $\mathbf{B}_{r,i}$ and $\mathbf{C}_{r,i}$:

$$\mathbf{A}_{r,i} = \begin{bmatrix} -\xi\omega_n & -\omega_d \\ \omega_d & -\xi\omega_n \end{bmatrix} \tag{3.17a}$$

$$\mathbf{B}_{r,i} = \begin{bmatrix} \mathbf{B}_{r,i,\alpha} \\ \mathbf{B}_{r,i,\beta} \end{bmatrix} = \begin{bmatrix} \left[\mathbf{\Phi}^{-1}\right]_{b,i,\alpha} \\ \left[\mathbf{\Phi}^{-1}\right]_{b,i,\beta} \end{bmatrix} \mathbf{B}_b \tag{3.17b}$$

$$\mathbf{C}_{r,i} = \begin{bmatrix} \mathbf{C}_{r,i,\alpha} & \mathbf{C}_{r,i,\beta} \end{bmatrix} = 2\mathbf{C}_b \begin{bmatrix} \mathbf{\Phi}_{b,i,\alpha} & -\mathbf{\Phi}_{b,i,\beta} \end{bmatrix} \tag{3.17c}$$

The components of the reduced-order input matrix $\mathbf{B}_r$ and of the reduced-order output matrix $\mathbf{C}_r$ depends on how the eigenvectors of $\mathbf{A}$ are normalized prior to the eigenvalue

decomposition. Here, the eigenvectors are normalized such that the generator speed output from this mode becomes:

$$[\mathbf{C}_b\phi_i]_\Omega = \omega_d\big(\frac{\xi}{\sqrt{1-\xi^2}} + j2\big) \qquad \text{and} \qquad [\mathbf{C}_b\bar{\phi}_i]_\Omega = \omega_d\big(\frac{\xi}{\sqrt{1-\xi^2}} - j2\big) \tag{3.18}$$

where ϕ_i and $\bar{\phi}_i$ are the two eigenvectors related to each 2$^{\text{nd}}$ order mode and where $j = \sqrt{-1}$ and ω_d and ξ are the aeroelastic frequency and damping ratio of the corresponding mode, respectively. This specific normalization of the eigenvectors is convenient, because it ensures that the components of the reduced-order input and output matrices can be given a physical interpretation. Using the normalization given in Equation (3.18), the reduced-order output matrix for the specific mode is found from Equations (2.6) and (3.4c) to be:

$$\mathbf{C}_{r,i} = \begin{bmatrix} 2\text{Re}(\phi_{i,\Omega}) & -2\text{Im}(\phi_{i,\Omega}) \end{bmatrix} = \begin{bmatrix} 2\omega_n\xi & -4\omega_d \end{bmatrix} \tag{3.19}$$

where ω_n is the undamped frequency of this mode found as $\omega_n = |\lambda_i|$, where λ_i is the i'th eigenvalue of $\mathbf{A}$. Similarly, the eigenvectors of the 1$^{\text{st}}$ order modes are normalized prior to order reduction, such that their generator speed output equals: $[\mathbf{C}_b\phi_i]_\Omega = -2\lambda_i$. The component of the output matrix $\mathbf{C}_{r,i}$ for the 1$^{\text{st}}$ order modes is then:

$$\mathbf{C}_{r,i} = -2\lambda_i \tag{3.20}$$

The components of $\mathbf{C}_{r,i}$ given in Equations (3.19) and (3.20) are the scaled real and imaginary parts of the eigenvalues related to the corresponding mode, which makes the output matrix suited for parametrization, as shown in the following.

The reduced-order input matrix $\mathbf{B}_r$ consist of modal blocks of $\mathbf{B}_{r,i}$, defined in Equations (3.4) and (3.17), that each describes the external excitation of the i'th mode. With the specific normalization defined in Equations (3.19) and (3.20), the components of $\mathbf{B}_{r,i}$ can be given a physical interpretation which is related to how much the specific mode contributes to the amplitude in the three frequency response functions considered here.

The transfer function matrix from the three inputs to the generator speed output of the i'th modal subsystem in Equations (3.3) and (3.16) is denoted $\mathbf{G}_{r,i}(s)$ and is defined as

$$\mathbf{G}_{r,i}(s) = \mathbf{C}_{r,i}(s\mathbf{I} - \mathbf{A}_{r,i})^{-1}\mathbf{B}_{r,i} \tag{3.21}$$

for both 1$^{\text{st}}$ and 2$^{\text{nd}}$ order modes, where s is the Laplace variable and the matrices $\mathbf{A}_{r,i}$, $\mathbf{B}_{r,i}$ and $\mathbf{C}_{r,i}$ are the system matrices of the i'th modal subsystem. The amplitude of the frequency response of $\mathbf{G}_{r,i}(s)$ at 0 Hz for 1$^{\text{st}}$ order modes and at ω_d for 2$^{\text{nd}}$ order modes are found to be:

$$|\mathbf{G}_{r,i}(0)| = -2\mathbf{B}_{r,i} \tag{3.22}$$

$$|\mathbf{G}_{r,i}(j\omega_d)|^2 = \frac{4}{\xi^2}\Big(\mathbf{B}_{r,i,\alpha}^2 + (1-\xi^2)\mathbf{B}_{r,i,\beta}^2 - 2\xi\sqrt{1-\xi^2}\mathbf{B}_{r,i,\alpha}\mathbf{B}_{r,i,\beta}\Big) \tag{3.23}$$

for 1$^{\text{st}}$ and 2$^{\text{nd}}$ order modes, respectively, where $\mathbf{B}_{r,i,\alpha}$ and $\mathbf{B}_{r,i,\beta}$ are the components of the modal input matrix for 2$^{\text{nd}}$ order modes.

Equation (3.22) shows that for 1$^{\text{st}}$ order modes, we can understand the components of

the input matrix $\mathbf{B}_{r,i}$ as the amplitude at 0 Hz in the frequency response of this mode scaled with a factor of 1/2, i.e. $\mathbf{B}_{r,i}$ denotes how much the i'th mode contributes to the amplitude at 0 Hz in the frequency response from each inputs to the generator speed output.

Equation (3.23) shows that the components $\mathbf{B}_{r,i,\alpha}$ and $\mathbf{B}_{r,i,\beta}$ of the input matrix for 2^{nd} order modes denotes the amplitude in the frequency response of this modal subsystem evaluated at the resonance peak at $\omega = \omega_d$. For modes that are lowly damped, the last term in (3.23) can be neglected, showing that whenever the amplitude at the resonance peak in the modal frequency response either decrease or increase so does the magnitudes of both $\mathbf{B}_{r,i,\alpha}$ and $\mathbf{B}_{r,i,\beta}$.

To summarize, it is proposed to realize the reduced-order system of equations on the eigenvalue decomposed form in Equation (3.17) and to normalize the eigenvectors of the reduced-order $\mathbf{A}_r$ matrix according to a chosen output which is the generator speed in the present case. Normalization of the eigenvectors from Equation (3.18) could be done based on other outputs, such as the longitudinal tower top deflection in each mode. The components of the input matrix would then again have the interpretation given in Equations (3.22) and (3.23), just with the longitudinal tower top deflection as the output.

3.3.2 Reduced-order system matrices

This section describes and compares the reduced-order system matrices obtained by modal truncation and balanced truncation previously in this chapter and shows that these models are suited for interpolation with wind speed. Both sets of models are represented on the unique form described in the previous section.

A set of reduced-order models of the type no. 8, see Table 3.1, obtained by modal truncation using quasi-steady aerodynamics and including the rigid body rotor mode, the 1^{st} lateral and longitudinal tower modes, the 1^{st} drivetrain mode and the 1^{st} collective flap mode, i.e. five modes in total, has been designed for the NREL 5 MW turbine in normal operation at wind speeds from 5 m/s to 25 m/s. The model no.8 is used here for brevity, although this model not accurately predicts the phase of the response of mean wind speed changes, see Figure 3.10. The results however still apply for models of higher complexity, because the subset of the matrices corresponding to the states of the modes in model no.8 remains unchanged in model no.9. The system matrices obtained by modal truncation are compared to the system matrices obtained by balanced truncation with the 14 balanced states used above. The modes included in the reduced-order models are ordered according to their mode shape to make the models suited for interpolation.

The reduced-order matrices $\mathbf{A}_r$ are on block diagonal form and consists of matrices $\mathbf{A}_{r,i}$ of each of the modes in the reduced-order models given in Equations (3.4b) and (3.17a). The components of $\mathbf{A}_{r,i}$ are the real and imaginary parts of the eigenvalues of mode i and are shown previously in Figure 3.7 for the models obtained by modal truncation and in Figure 3.16 for models obtained by balanced truncation.

The real and imaginary parts of the eigenvalues of the rigid body rotor mode, the 1^{st} lateral and longitudinal tower modes and the 1^{st} drivetrain mode predicted by both modal and balanced truncation all vary smoothly with wind speed. The components for the 1^{st} collective flap mode included by modal truncation, Figure 3.7, show some discontinuities at 11 m/s, where the blades operates close to stall. As described previously, the 1^{st} col-

lective flap mode shifts from a 2nd order mode into two 1st order modes at 16 m/s and the components of $\mathbf{A}_{r,i}$ for this mode can be interpolated also close to 16 m/s. The real and imaginary parts of the 'collective flap mode' predicted by balanced truncation, Figure 3.16, can also easily be interpolated, despite the large shift in the poles of this mode at around rated wind speed.

Figure 3.19 shows the components of the reduced-order output matrices $\mathbf{C}_{r,i}$ obtained by both modal truncation and balanced truncation, extracting the generator speed output from the generalized states of the rigid body rotor mode, the 1st lateral and longitudinal tower modes and the 1st drivetrain mode for the NREL 5 MW wind turbine in normal operation at wind speeds from 5 m/s to 25 m/s. The figure also shows the components of the output matrix corresponding to the 1st collective flap mode in the model obtained by modal truncation and the 'collective flap mode' and the aerodynamically dominated mode predicted by balanced truncation. For comparison, the output matrices for a fully flexible turbine are compared to the output matrix corresponding to the 1st longitudinal tower mode and the rigid body rotor mode for a turbine with rigid lateral tower, drivetrain and rotor including quasi-steady aerodynamics.

The black points ($\bullet$) and black circles in Figure 3.19 show the components of the output matrix corresponding to the generalized state of the rigid body rotor mode, denoted $C_{r,1}$ and obtained by modal truncation and balanced truncation, respectively. The components related to the rigid body rotor mode obtained by balanced truncation are very similar to those obtained by modal truncation. The black dashed line in Figure 3.19 shows $C_{r,1}$ predicted by a model with rigid rotor, drivetrain and rigid lateral tower. Both for a fully flexible turbine and a turbine with e.g. rigid rotor, the components $C_{r,1}$ increase with wind speed above rated, because the aerodynamic damping of the rigid body rotor motion increase with wind speed, due to the increased blade pitch angles and higher damping gives lower time constants and thereby lower eigenvalues in Equation (3.20). The components in $C_{r,1}$ are higher for a fully flexible turbine than for a turbine with rigid rotor. This observation can be explained by decreasing inertia in the rigid body rotor mode due to coupling with collective flap blade vibration, causing the time constant of the rigid body rotor mode to decrease.

The black asterisks ($*$) in Figure 3.19 show the components corresponding to the aerodynamically dominated mode found by balanced truncation. The components related to the aerodynamically dominated mode vary smoothly with wind speed, except at around 22 m/s, where there is an abrupt change, because here the aerodynamically dominated modes couples with the rigid body rotor mode to become a 2nd order mode.

The red points and red asterisks in Figure 3.19 show the components of the output matrix corresponding to the 1st collective flap mode, denoted $C_{r,2}$ and $C_{r,3}$. Up to 16 m/s, the 1st collective flap mode is a 2nd order mode, as previously explained, and the two components $C_{r,2}$ and $C_{r,3}$ are equal to the first and second components of $\mathbf{C}_{r,i}$ in Equation (3.19), respectively. Both $C_{r,2}$ and $C_{r,3}$ increase up to 16 m/s, because the aerodynamic damping of the flap mode increase. The component $C_{r,2}$ is continuous across 16 m/s, where the flap mode change into two 1st order modes, because the specific normalization of the eigenvectors ensures this; i.e. $C_{r,2}$ can be written as $2\omega_n\xi = -2\mathrm{Re}(\lambda)$, which is identical to the output component for the 1st order mode: -2λ when the eigenvalue becomes purely real at 16 m/s.

The red circles in Figure 3.19 show the components of the output matrix related to the 'collective flap' mode predicted by balanced truncation that vary smoothly with wind

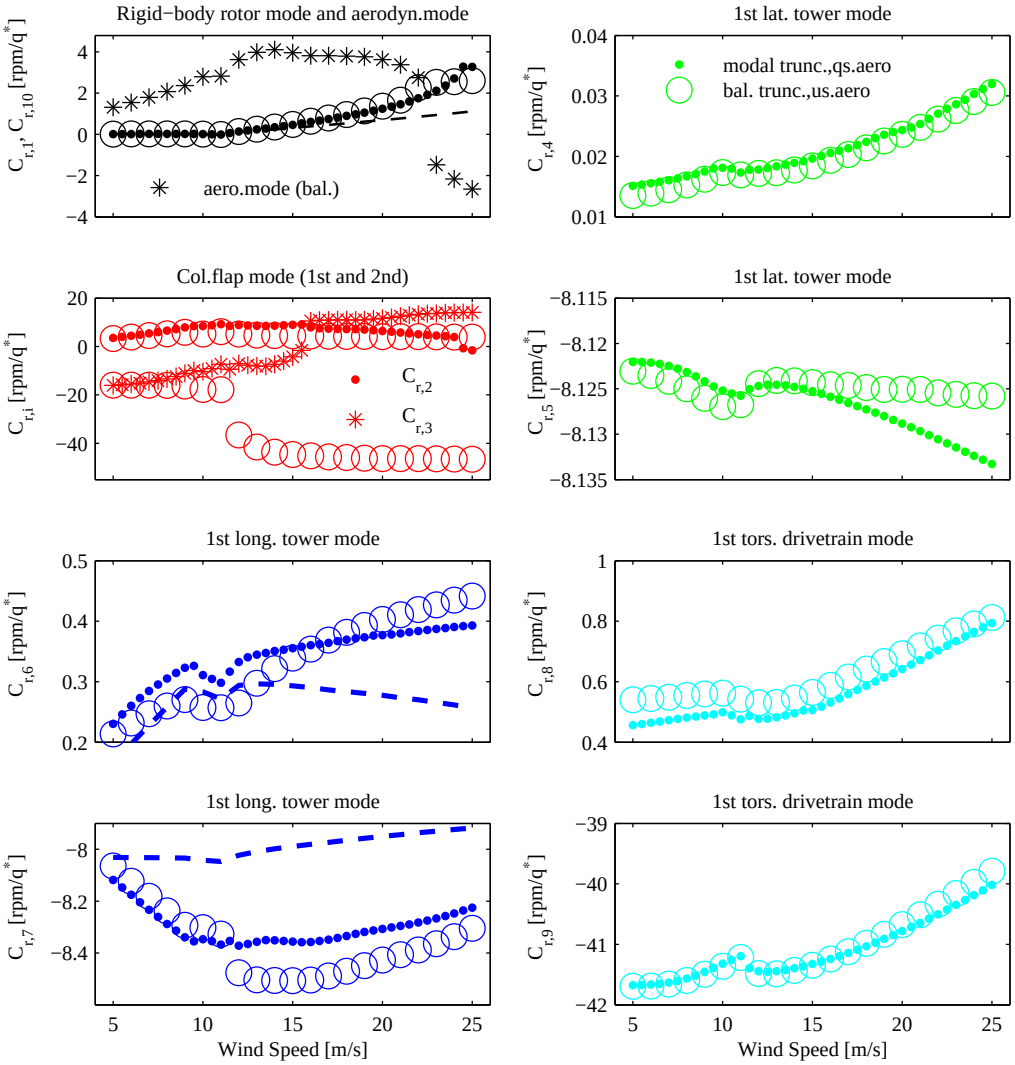

Figure 3.19: Components of the reduced-order output matrix $\mathbf{C}_r$ for the generator speed output for the NREL 5 MW wind turbine in normal operation at various wind speeds for a set of reduced-order models including 14 balanced states on Jordan form (◯). Comparison with output matrix for reduced-order models obtained by modal truncation with quasi-steady aerodynamics (•) and with components for a turbine with rigid rotor, drivetrain and rigid lateral tower and quasi-steady aerodynamics (dashed lines).

speed. Above rated speed at around 10 m/s, the components found by balanced truncation varies from $C_{r,2}$ and $C_{r,3}$ obtained by modal truncation, because here the pole shifts to resemble that of the 2$^{\text{nd}}$ collective flap mode.

The green points and green circles in Figure 3.19 show the components of the output matrix corresponding to the states of the 1$^{\text{st}}$ lateral tower mode obtained by modal and balanced truncation, respectively. The components are denoted $C_{r,4}$ and $C_{r,5}$ and correspond to the first and second component of $\mathbf{C}_{r,i}$ in (3.19). The components predicted by the modal truncation and balanced truncation are nearly the same. The component $C_{r,4}$ increase slightly with wind speed. This observation can be explained by the increasing aeroelastic damping of the 1$^{\text{st}}$ lateral tower mode caused by coupling to longitudinal tower motion, as explained previously in Chapter 2. The other component $C_{r,5}$ is almost constant with wind speed.

The blue points and blue circles in Figure 3.19 show the two components of the generator speed output matrix related to the state of the 1$^{\text{st}}$ longitudinal tower mode predicted by modal and balanced truncation, respectively. The two components are denoted $C_{r,6}$ and $C_{r,7}$ and equals the first and second components of $\mathbf{C}_{r,i}$ in (3.19), respectively. The figure shows a comparison between $C_{r,6}$ and $C_{r,7}$ for a fully flexible turbine and a turbine with rigid lateral tower, drivetrain and rotor. The components predicted by modal and balanced truncation show a similar trend and vary slightly both below and above rated wind speed. The model with a rigid rotor predicts components with magnitudes below that for a fully flexible turbine. This observation can be explained by the fact that the aeroelastic damping of the 1$^{\text{st}}$ longitudinal tower mode is higher for a rigid rotor than for a flexible one because of collective flap vibration out of phase with longitudinal tower top vibration.

The cyan points and circles in Figure 3.19 show the components of $\mathbf{C}_{r,i}$ for the 1$^{\text{st}}$ torsional drivetrain mode predicted by modal and balanced truncation, respectively. These components are denoted $C_{r,8}$ and $C_{r,9}$ and correspond to the first and second components of $\mathbf{C}_{r,i}$ in (3.19), respectively. The components $C_{r,8}$ and $C_{r,9}$ increase gradually with wind speed in both sets of models, which can be explained by the larger aerodynamic damping of the rotor rotation motion in this mode, due to higher pitch angles.

Figure 3.20 shows the magnitude of the components of the reduced-order input matrix $\mathbf{B}_{r,i}$ obtained by modal truncation from the three inputs: generator torque, collective pitch angle and mean wind speed to the generalized states of the rigid body rotor mode, denoted $B_{r,1}$. The figure shows a comparison with the input matrix predicted with a model with rigid lateral tower, rigid rotor and drivetrain and quasi-steady aerodynamics, which are shown with black points. The black points and circles deviates highly at around rated wind speed and above 20 m/s. Recall, that the interpretation of $B_{r,1}$ is given by Equation (3.22) as the forced amplitude of the generator speed at 0 Hz caused by each of the three inputs. The large deviations at around rated wind speed in Figure 3.20 shows that an assumption of rigid rotor gives two large variations in the generator speed at 0 Hz compared to a fully flexible turbine. This observation can be explained by the large static flap deflection at around rated wind speed, that cause the blades to deflect torsionally when they are e.g. pitched and the aerodynamic forces on the blades thereby are changed. This observation indicates that the gradients of aerodynamic rotor torque to changes in pitch and mean wind speed changes predicted for a rigid rotor are too large.

For collective pitch and mean wind speed inputs above 20 m/s, the input $\mathbf{B}_{r,i}$ increase

relative to that of a turbine with rigid rotor because the rigid body rotor mode couples with the 1st collective flap mode at high wind speeds, causing the aerodynamic damping of this mode to decrease and thereby the amplitude of the generator speed output at 0 Hz to increase, as shown previously in Figures 3.9 and 3.10.

Figure 3.21 shows the magnitude of the components of the reduced-order input matrix corresponding to the states of the rigid body rotor mode and the 1st collective flap mode for the model obtained by modal truncation, and corresponding to the states of the rigid body rotor mode, the aerodynamically dominated mode and the 'collective flap mode' for the model obtained by balanced truncation.

The components of the input matrix corresponding to the states of the rigid body rotor mode obtained by balanced truncation, see Figures 3.21a-c, are nearly identical for the two sets of models except above 20 m/s, where the rigid body rotor mode becomes a 2nd order mode. The components of $\mathbf{B}_{r,i}$ for both the rigid body rotor mode and the aerodynamically dominated mode (black asterisks) varies smoothly with wind speed, except at around rated wind speed, and at 20 m/s where the two 1st order poles of these two modes couples to become a 2nd order pole.

The red points and circles in Figures 3.21d-f show the components of $\mathbf{B}_{r,i}$ related to the 1st collective flap mode included by modal truncation. The 1st collective flap mode is a 2nd order mode below 16 m/s and above 16 m/s the 1st collective flap mode consist of two 1st order modes, when quasi-steady aerodynamics is assumed as explained previously. The trend is that these components are low at low wind speeds for all three inputs, showing that the influence of the 1st collective flap mode on the generator speed response is low.

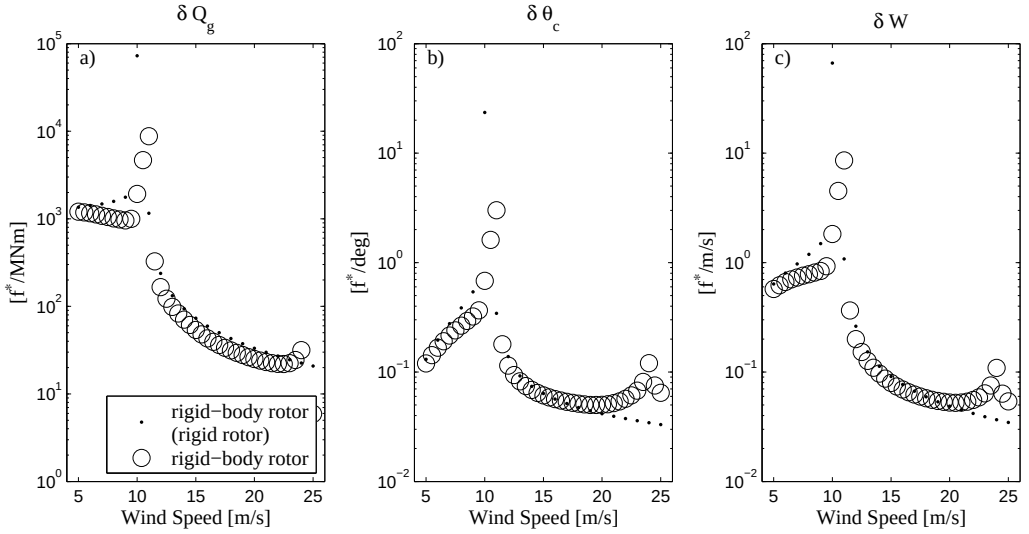

Figure 3.20: Magnitudes of the components of the reduced-order input matrix $\mathbf{B}_r$ corresponding to the state of the rigid body rotor mode for a set of reduced-order aeroelastic models of the NREL 5 MW wind turbine in normal operation at various wind speeds obtained by modal truncation with quasi-steady aerodynamics (◯). Comparison with predictions for a model with rigid rotor, drivetrain and rigid lateral tower and quasi-steady aerodynamics (•)

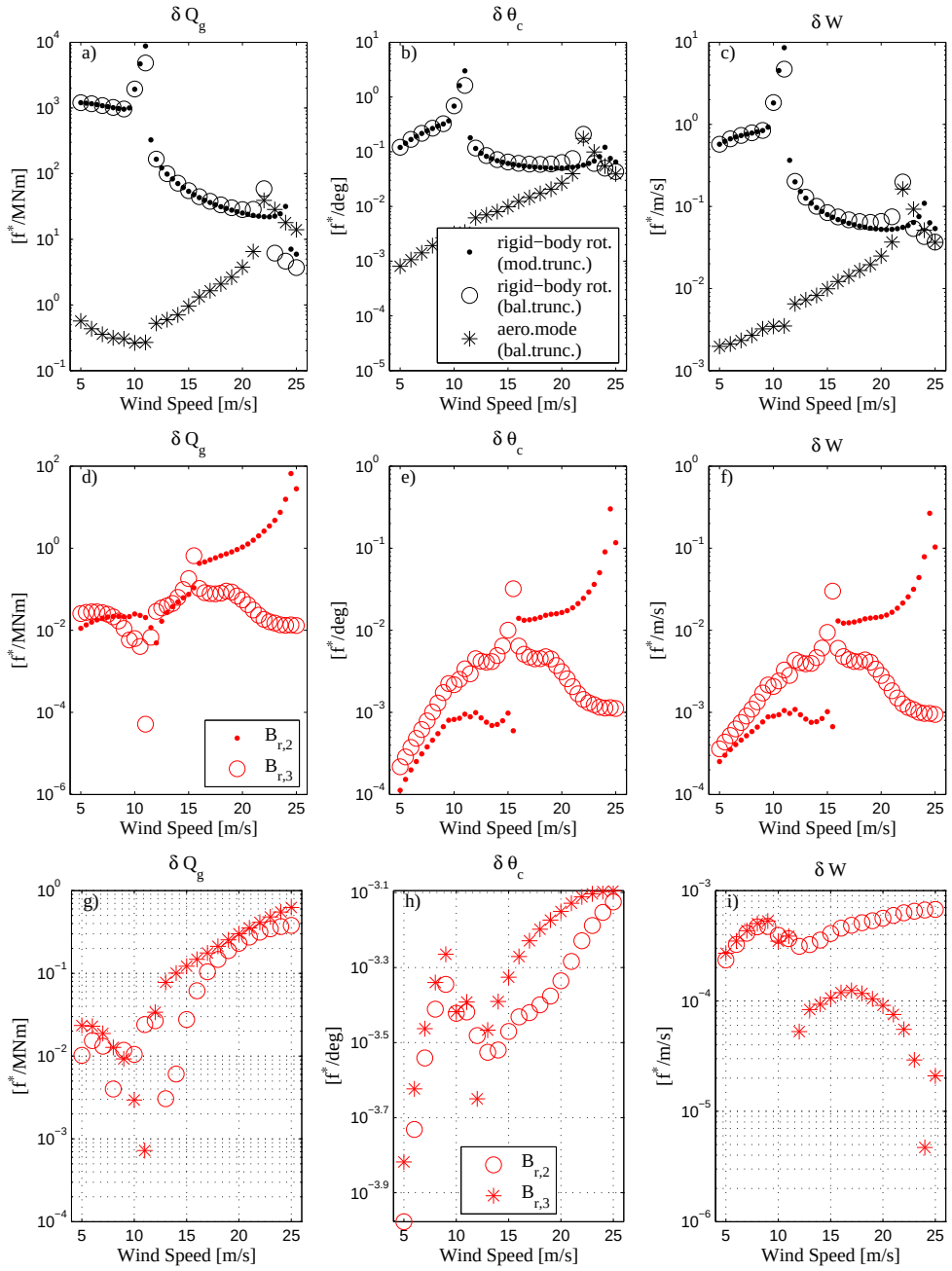

Figure 3.21: Magnitudes of the components of the reduced-order input matrix $\mathbf{B}_r$ for a set of reduced-order aeroelastic models of the NREL 5 MW wind turbine in normal operation at various wind speeds. Figures a-c shows the components corresponding to the states of the rigid body rotor mode predicted by modal truncation and balanced truncation including 14 balanced states, and shows the components corresponding to the state of an aerodynamically dominated mode predicted by balanced truncation. Figures d-f shows the components related to the states of the 1$^{\text{st}}$ collective flap mode obtained by modal truncation with quasi-steady aerodynamics and Figures g-i shows the components corresponding to the states of a 'collective flap' mode predicted by balanced truncation.

Some discontinuity with wind speed is seen at 16 m/s for all three inputs, because here the flap mode turns from being one 2$^{\text{nd}}$ order mode to two 1$^{\text{st}}$ order modes. Above 16 m/s the amount of excitation of the 1$^{\text{st}}$ collective flap mode increase and becomes equally important in the generator speed response as the rigid body rotor mode, because of the coupling between rigid body rotor mode and collective flap motion at high pitch angles. Above 16 m/s the sign of $\mathbf{B}_{r,i}$ (not shown) for the rigid body rotor mode and the 1$^{\text{st}}$ collective flap mode are opposite, showing that the effect of the 1$^{\text{st}}$ collective flap mode counteracts the effect of the rigid body rotor mode on the generator speed signal at 0 Hz, as previously explained.

The red circles and red asterisks in Figures 3.21g-i shows the components of $\mathbf{B}_r$ related to the 'collective flap' mode predicted by balanced truncation. It is observed that these components vary smoothly with wind speed except for some abrupt changes at around rated wind speed, where the poles of this model change.

Figure 3.22 shows the two components of the input matrices $\mathbf{B}_{r,i}$ corresponding to the states of the 1$^{\text{st}}$ lateral tower mode (row a), the 1$^{\text{st}}$ longitudinal tower mode (row b) and the 1$^{\text{st}}$ drivetrain mode (row c) for the NREL 5 MW wind turbine in normal operation at wind speeds from 5 m/s to 25 m/s for the reduced-order models obtained by modal truncation ($\bullet$) and balanced truncation ($\bigcirc$). The figure shows a comparison with the components of the input matrix corresponding to the 1$^{\text{st}}$ longitudinal tower mode for a turbine with rigid lateral tower, rigid drivetrain and rotor and quasi-steady aerodynamics (dashed lines in row b).

The two components corresponding to the 1$^{\text{st}}$ lateral tower mode are shown in row a in Figure 3.22. Below 11 m/s both these components are almost constant for generator torque input, because the lateral tower mode here is excited mainly by the generator torque reaction forces on the tower. Above 11 m/s, both components increase slighly with wind speed, which can be explained by the influence of longitudinal tower motion in this mode, that causes the 1$^{\text{st}}$ lateral tower mode also to be excited by variations in thrust forces. For the two other inputs: changes in collective pitch angles and mean wind speed, row a in Figure 3.22, the two components increase with wind speed, showing that the lateral tower mode has increasing influence on the generator speed response in response to excitation with these inputs. This observation can be explained by the fact that there are higher variations in the thrust forces in response to collective pitching and changes in mean wind speed as the wind speed increases. This observation can also be explained by the longitudinal tower motion in the 1$^{\text{st}}$ lateral tower modes at high wind speed, causing higher excitation of the lateral tower mode. The components of the input matrix corresponding to the 1$^{\text{st}}$ lateral tower mode of the model obtained by modal and balanced truncation are similar.

Figure 3.22 row b shows the variation of the two components in $\mathbf{B}_{r,i}$ corresponding to the states of the 1$^{\text{st}}$ longitudinal tower mode. For generator torque inputs the two components are close to zero below 11 m/s, whereas above 11 m/s the components increase with wind speed. The generator torque input excites the longitudinal tower mode mainly through changes in thrust forces caused by changes in the inflow at the blades when the rotor speed changes. The increasing pitch angles from 11 m/s cause these changes in thrust to increase with wind speed. For collective pitch and mean wind speed inputs, the two components increase with wind speed, because of the higher changes in thrust associated with collective pitching and changes in mean wind speed. The dashed black and red curves in row b in Figure 3.22 shows the components for a turbine with rigid lateral tower, rigid drivetrain and rotor and quasi-steady aerodynamics. For this simplified model the

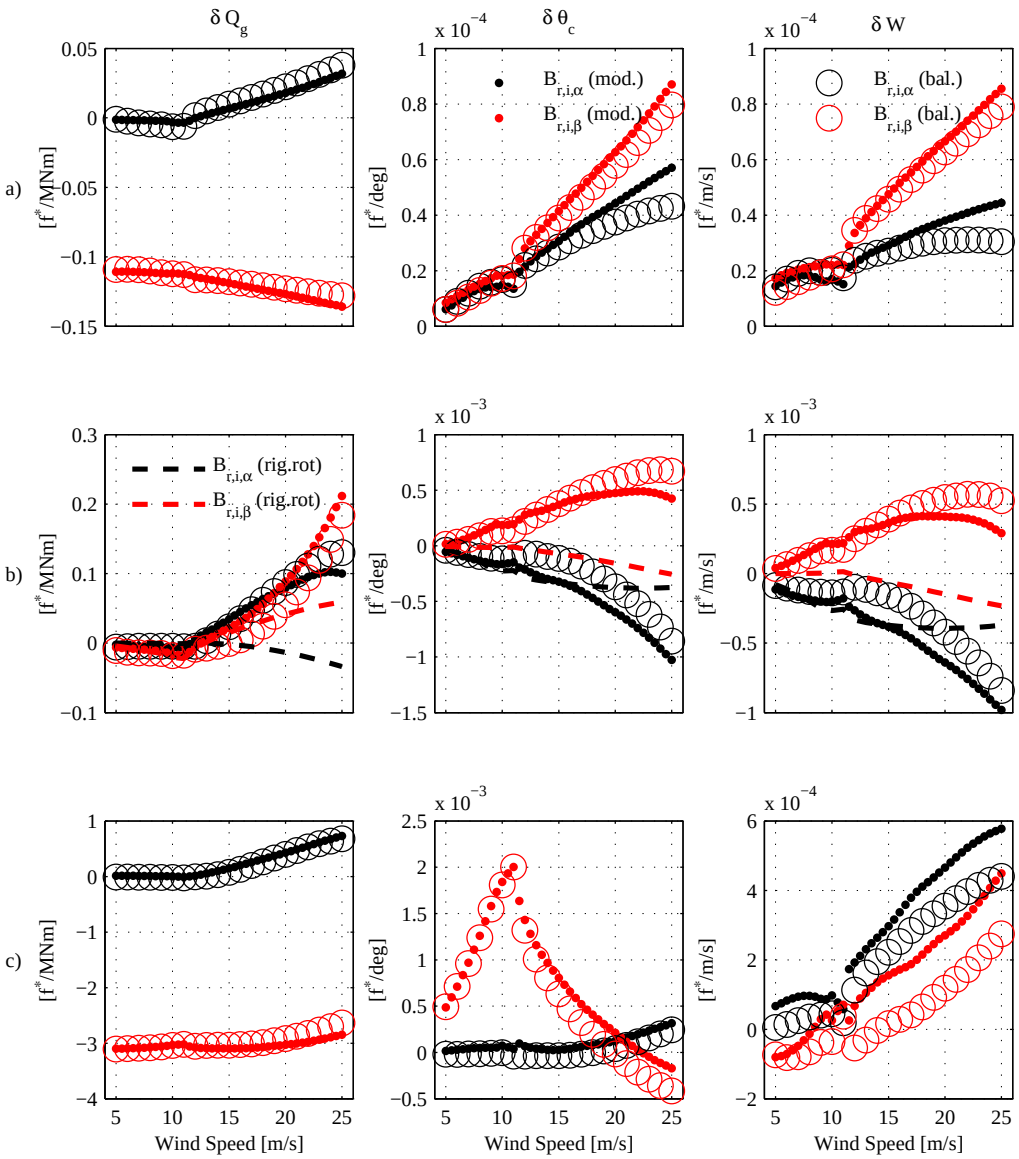

Figure 3.22: Components of the reduced-order input matrix $\mathbf{B}_r$ for a set of reduced-order aeroelastic models of the NREL 5 MW wind turbine in normal operation at various wind speeds, corresponding to the states of the 1st lateral tower mode (row a), the 1st longitudinal tower mode (row b) and the 1st drivetrain torsion mode (row c). Comparison between components of models obtained by balanced truncation with unsteady aerodynamics (○) with models obtained by modal truncation with quasi-steady aerodynamics (●) and with components for a turbine with rigid rotor, drivetrain and rigid lateral tower and quasi-steady aerodynamics (dashed lines).

inputs are smaller than for a fully flexible turbine, especially at high wind speeds. This observation can be explained by the fact that the 1st longitudinal tower mode couples with collective flap motion such that the aerodynamic damping of the longitudinal tower mode is lower than for a rigid rotor. This lower aerodynamic damping of the 1st longitudinal tower mode cause the tower vibrations to be larger and thereby cause larger changes in the rotor speed, through the changes in aerodynamic rotor torque associated with the longitudinal tower vibration.

Figure 3.22 row c shows the two components of $\mathbf{B}_{r,i}$ corresponding to the states of the 1st torsional drivetrain mode. For generator torque inputs, both of the components are see to vary smoothly with wind speed. For collective pitch inputs, the magnitude increase similar to the static flap deflection of the blades, because the 1st drivetrain mode is excited by pitching inertia forces as described in Chapter 2. For wind speed inputs, both components increase with wind speed, which can be explained by the larger pitch angles causing larger variations in the aerodynamic rotor torque in response to changes in the mean wind speed. The components found by balanced truncation are similar to those obtained by modal truncation, except for wind speed inputs where the components found by balanced truncation are lower than those obtained by modal truncation, which can be explained by the lack of unsteady aerodynamics in the latter model, causing too high changes in the aerodynamic rotor torque, as explained previously in Figure 2.7.

3.4 Chapter summary

In this chapter, linear aeroelastic low-order models of wind turbines are designed by order reduction of a high-order model of a wind turbine of MW size. The high-order model is a linearization of a structurally nonlinear finite beam element model of tower, drivetrain and blades coupled with an unsteady Blade Element Momentum model of aerodynamic forces including effects of shed vorticity and dynamic stall. Linearization is performed around a deflected state of the blades determined by the static aerodynamic forces due to an assumed uniform inflow to the rotor. Order reduction is done by modal truncation using aeroelastic mode shapes predicted by the high-order model and by balanced truncation using balanced states.

The main findings are that a relatively large number of aerodynamically dominated modes are required in the modal truncation technique to provide good approximation of the low-frequency response of the wind turbine. A large number of these aerodynamically dominated modes are required due to the assumption in the BEM model of no spanwise aerodynamic coupling of unsteady aerodynamic forces on the blades. Each of these aerodynamically dominated modes thereby mainly describes changes in aerodynamic forces at local sections along the blade span. The aerodynamically dominated modes, that describes the unsteady aerodynamic forces at sections at the blade mid-span, are found to couple to the rigid body rotor rotation mode and thereby influence the generator speed response. The aerodynamically dominated modes describing the variations in aerodynamic forces at sections closer to the blade tip contributes mainly to changes in the thrust due to lower inflow angles, and are therefore found to couple to the 1st longitudinal tower mode through the collective flap motion of this mode.

Reduced-order models are subsequently designed by modal truncation under assumption of quasi-steady aerodynamics, which provides accurate predictions of the investigated frequency response functions from generator torque, collective pitch angle and mean wind speed changes to the generator speed output, except at around the 1st torsional drivetrain mode under collective pitching, as described in Chapter 2. It is shown how the frequency

response functions predicted with the high-order model with quasi-steady aerodynamics are gradually approximated by increasing the number of modes in the reduced-order model. Good approximation is achieved up to the frequency of the 2^{nd} drivetrain torsional mode from a 13^{th} order state space model including the rigid body rotor mode, the 1^{st} longitudinal and lateral tower modes, the 1^{st} and 2^{nd} collective flap modes and the 1^{st} and 2^{nd} drivetrain torsion modes.

Order reduction of the high-order aeroelastic model of the wind turbine is subsequently done by balanced truncation. A total of 14 balanced states are required to capture each of the frequency response functions from generator torque, collective pitch angle demands and mean wind speed to generator speed. The modal and balanced truncation technique are found to be equally effective in capturing the effect of the structurally dominated modes. A comparison is made of the poles and some of the corresponding mode shapes predicted by the full-order and the balanced reduced-order models and the main finding is, that although the poles predicted by the balanced reduced-order models are accurate, the mode shapes of e.g. the collective flap mode does not resemble those of the full-order models. It is found that models obtained by balanced truncation can accurately capture the effect of the large number of aerodynamically dominated modes on the generator speed response by a single time constant and the balanced reduction technique is therefore suited to reduce the number of aerodynamic states in the models.

A set of reduced-order models are designed by both modal truncation and balanced truncation for a modern wind turbine in normal operation at wind speeds in the interval from 5 m/s to 25 m/s. The reduced-order models are put on the eigenvalue decomposed form using a specific normalization of the eigenvectors. In the eigenvalue decomposed form, the components of the system matrices each relate to the dynamics of a specific pole of the reduced-order model, which facilitates that the system matrices can be interpolated or parameterized with wind speed suited for design of gain-scheduling controllers. The reduced-order system matrices obtained by modal and balanced truncation realized on the eigenvalue decomposed form are shown to be suited for interpolation with a scheduling variable. However, some abrupt changes in the system matrices occurs at operation points where two 1^{st} order modes collapse into a single 2^{nd} order mode and vice versa. The components related to the structurally dominated modes predicted by these models are similar, except for the collective flap modes, showing that the two reduction techniques agrees on how to include the influence of these modes.

Chapter 4

Order reduction of aeroelastic models using structural and aerodynamic basis functions

The purpose of this chapter is to describe and test another method to reduce the order of aeroelastic models. The order reduction method use projection with structural and aerodynamic basis functions to separately reduce the number of structural degrees of freedom and aerodynamic states.

As an example, the order reduction method is tested on a high-order linear aeroelastic model of a wind turbine blade. The model is similar to the model described in Chapter 2 and used throughout the thesis, however only the states of one blade is used here, including a degree of freedom describing blade pitching around a pitch bearing. The high-order model is a geometrically nonlinear finite beam element model of a modern wind turbine blade, linearized around a deflected state of the blade and coupled with a model of unsteady aerodynamics describing effects of shed vorticity and dynamic stall. Reduced-order aeroelastic models are designed for the wind turbine blade including a simplified model of a pitch actuator, which is assumed to provide almost no lag on the actual pitch to a demanded pitch angle input. The purely structural blade modes predicted by the high-order model are used to reduce the number of structural degrees of freedom. Reduction of the number of aerodynamic states is done using aerodynamic basis functions that are slaves of these structural mode shapes. Prior to reduction, the aerodynamic states in the model are transformed such that they describe the lag on the aerodynamic forces caused by the shed vorticity and dynamic stall and such that the quasi-steady aerodynamic forces are a function of only the structural degrees of freedom.

The main findings are that for accurate prediction of the aeroelastic damping of the 1^{st} flap mode above rated, it is important to include the 1^{st} structural flap mode and the 1^{st} structural torsional blade mode due to an aeroelastic coupling between flap and torsion. It is found, that the aeroelastic frequency response from mean wind speed changes to blade root flap bending moment is strongly influenced by both the 1^{st} and 2^{nd} flap modes and accurate approximation close to 0 Hz is obtained by residualization of aeroelastic modes with frequency higher than the 2^{nd} aeroelastic flap mode. It is found that the four aerodynamic slave modes of the 1^{st} and 2^{nd} structural flap modes can correctly capture the effect of unsteady aerodynamic forces caused by shed vorticity and dynamic stall on the aeroelastic frequencies and damping of the low-frequency blade modes and on the frequency response from mean wind speed to blade root flap bending moment.

Section 4.1 contains a description of the proposed order reduction scheme in a general form. In Section 4.2 the order reduction technique is used to reduce the order of the aeroelastic wind turbine blade model, where Section 4.2.1 contains a short description of the high-order blade model and Section 4.2.2 describes the low-frequency aeroelastic blade modes. In Section 4.2.3 the specific reduced-order system of equations are derived which are subsequently used in Sections 4.2.4 and 4.2.5 to analyze the necessary complexity of the reduced-order models. A summary of the chapter is given in Section 4.3.

4.1 Order reduction method

The governing equations of many aeroelastic systems are described by a high-order set of ordinary differential equations in the general nonlinear form:

$$\mathbf{M}(t, \mathbf{x}_s, \mathbf{p})\ddot{\mathbf{x}}_s = \mathbf{f_s}(t, \mathbf{x}_s, \dot{\mathbf{x}}_s, \mathbf{x}_a, \mathbf{p}, \mathbf{u}) \tag{4.1a}$$

$$\dot{\mathbf{x}}_a = \mathbf{f_a}(t, \mathbf{x}_a, \mathbf{x}_s, \dot{\mathbf{x}}_s, \ddot{\mathbf{x}}_s, \mathbf{p}, \mathbf{u}) \tag{4.1b}$$

where Equation (4.1a) describes structural dynamics under influence of aerodynamic forces and Equation (4.1b) describes the lag of unsteady aerodynamic forces. The variable $\mathbf{x}_s$ denotes the structural degrees of freedom, $\mathbf{x}_a$ is the aerodynamic state-vector, $\mathbf{u}$ is a vector of inputs, $\mathbf{p}$ is an array of parameters and $\mathbf{M}$ is the mass matrix. The function $\mathbf{f_s}$ represents the resulting forces on the structure from e.g. elastic stiffness forces, structural viscous damping, aerodynamic forces and external forces such as gravity forces and actuator forces. The function $\mathbf{f}_a$ in Equation (4.1b) represents structural and external excitation of the aerodynamic state.

The set of ordinary differential equations (4.1a) describing the structural degrees of freedom can be obtained by converting a set of partial differential equations using spatial discretization by a finite element or finite difference discretization scheme [59, 60]. Most aerodynamic models can be described as a set of first order ordinary differential equations [21]. An example could be the unsteady panel code [11], where the aerodynamic states $\mathbf{x}_a$ represents discrete vortex strengths. Current engineering type models used to describe the effect of unsteady aerodynamics of wind turbines, such as the ONERA model of dynamic stall [16], Øye's dynamic stall model [15], models of shed vorticity and dynamic stall proposed by Beddoes & Leishman [10] and dynamic inflow models [7] are all formulated as a set of ordinary differential equations.

In the present work, it is proposed to reduce separately the structural degrees of freedom and the number of aerodynamic state-variable by using a low number of structural and aerodynamic basis functions, respectively, in the following projections:

$$\mathbf{x}_s \approx \mathbf{\Phi}_s \mathbf{q}_s \quad , \quad \mathbf{x}_a^* \approx \mathbf{\Phi}_a \mathbf{q}_a \tag{4.2}$$

where $\mathbf{\Phi}_s = \mathbf{\Phi}_s(t, \mathbf{p})$ is an $N_s \times N_s^r$ matrix consisting of N_s^r structural basis functions in the columns, where N_s is the number of degrees of freedom. The matrix $\mathbf{\Phi}_a = \mathbf{\Phi}_a(t, \mathbf{p})$ is an $N_a \times N_a^r$ matrix with N_a^r aerodynamic basis functions in columns where N_a is the number of aerodynamic states in the full-order model. The variables $\mathbf{q}_a$ and $\mathbf{q}_s$ in Equation (4.2) are the new generalized aerodynamic and structural states.

Assuming that a set of structural and aerodynamic basis functions can be found, the reduced-order system of equations are found by inserting the projections from Equation (4.2) into the system of equations (4.1) and pre-multiply with $\mathbf{\Phi}_a^T$ and $\mathbf{\Phi}_s^T$ in Equation (4.1a) and (4.1b), respectively. Since the matrices $\mathbf{\Phi}_s$ and $\mathbf{\Phi}_a$ are not necessarily composed of orthogonal vectors, the reduction scheme is a so-called Petrov-Galerkin projection [38]. The reduced-order system of equations can then be written in similar form as the full-order system:

$$\mathbf{M}_{pj}(t, \mathbf{q}_s, \mathbf{p})\ddot{\mathbf{q}}_s = \mathbf{\Phi}_s^T \mathbf{f_s}(t, \mathbf{\Phi}_s \mathbf{q}_s, \mathbf{\Phi}_s \dot{\mathbf{q}}_s, \mathbf{\Phi}_a \mathbf{q}_a, \mathbf{p}, \mathbf{u}) \tag{4.3a}$$

$$\dot{\mathbf{q}}_a = (\mathbf{\Phi}_a^T \mathbf{\Phi}_a)^{-1} \mathbf{\Phi}_a^T \mathbf{f_a}(t, \mathbf{\Phi}_s \mathbf{q}_s, \mathbf{\Phi}_s \dot{\mathbf{q}}_s, \mathbf{\Phi}_s \ddot{\mathbf{q}}_s, \mathbf{\Phi}_a \mathbf{q}_a, \mathbf{p}, \mathbf{u}) \tag{4.3b}$$

where $\mathbf{M}_{pj} = \mathbf{\Phi}_s^T \mathbf{M} \mathbf{\Phi}_s$ is the reduced-order projected mass matrix.

Typically, the structural mode shapes of the low-frequency dynamic vibration modes are used to approximate the structural degrees of freedom. Depending on the spatial distribution of the loading on the structure, the low-frequency modes may not fully be able to approximate the low-frequency response of some external load. Better approximation of the low-frequency response, without increasing the order of the model, can be achieved by *static* or *dynamic residualization*. In static residualization [30] the external loading on the high-frequency modes are included under the assumption that the vibration of these modes does not lag the external loading, such that the inertia and damping forces of the high-frequency modes are neglected. For accurate approximation of flutter, Karpel [37] propose to do dynamic residualization in which the effect of damping forces of high-frequency modes is retained, without increasing the order of the model.

Residualization is performed here by using a combined set of both low- and high-frequency mode shapes in $\mathbf{\Phi}_s$ and subsequently partition the system of equations into components corresponding to the low- and the high-frequency modes, such that the projected structural equations of motion (4.3a) can be written:

$$\begin{bmatrix} \mathbf{M}_{tt} & \mathbf{M}_{tr} \\ \mathbf{M}_{rt} & \mathbf{M}_{rr} \end{bmatrix} \begin{Bmatrix} \ddot{\mathbf{q}}_{s,t} \\ \ddot{\mathbf{q}}_{s,r} \end{Bmatrix} = \begin{Bmatrix} \mathbf{\Phi}_{s,t}^T \\ \mathbf{\Phi}_{s,r}^T \end{Bmatrix} \mathbf{f_s}(t, \mathbf{q}_s, \dot{\mathbf{q}}_s, \mathbf{q}_a, \mathbf{p}, \mathbf{u}) \tag{4.4}$$

where index t denotes low-frequency modes to be retained ('t' for *truncated*) and index r denotes high-frequency modes to be residualized. By neglecting inertia forces of high-frequency modes ($\mathbf{M}_{rr} = \mathbf{0}$) the bottom partition in Equation (4.4) can be written as:

$$\mathbf{0} = \mathbf{\Phi}_{s,r}^T \mathbf{f}_s(t, \mathbf{q}_{s,t}, \mathbf{q}_{s,r}^*, \dot{\mathbf{q}}_{s,t}, \dot{\mathbf{q}}_{s,r}^*, \ddot{\mathbf{q}}_{s,t}, \mathbf{q}_a, \mathbf{p}, \mathbf{u}) \tag{4.5}$$

from which the states describing the high-frequency modes: $\mathbf{q}_{s,r}^*$, $\dot{\mathbf{q}}_{s,r}^*$ can be written as a function of the states of the retained, low-frequency modes;

$$(\mathbf{q}_{s,r}^*, \dot{\mathbf{q}}_{s,r}^*) = \mathbf{f}(t, \mathbf{q}_{s,t}, \dot{\mathbf{q}}_{s,t}, \ddot{\mathbf{q}}_{s,t}, \mathbf{q}_a, \mathbf{p}, \mathbf{u}) \tag{4.6}$$

The states of the high-frequency modes can thereby be removed from the system of equations which in the residualized version becomes:

$$\mathbf{M}_{tt} \ddot{\mathbf{q}}_{s,t} = \mathbf{\Phi}_{s,t} \mathbf{f}_s^*(t, \mathbf{q}_{s,t}, \dot{\mathbf{q}}_{s,t}, \ddot{\mathbf{q}}_{s,t}, \mathbf{p}, \mathbf{u}) \tag{4.7}$$

4.2 Example

The order reduction scheme is now used to design reduced-order aeroelastic models of a modern wind turbine blade based on a high-order linear aeroelastic model. The following section gives a short description of this high-order aeroelastic blade model.

4.2.1 High-order linear aeroelastic blade model

Reduced-order models are designed based on the high-order aeroelastic wind turbine model described in Chapter 2, in which only the aerodynamic and structural states of a single blade are used. The high-order model is a linearization of a geometrically nonlinear finite beam element model coupled with an unsteady Blade Element Momentum model of aerodynamic forces including the effects of shed vorticity and dynamic stall. Linearization is performed around an assumed steady state of a blade operating at various operating points defined by a mean wind speed, rotor speed and pitch angle in which the blade is stationary deflected by the static aerodynamic forces from assumed uniform inflow.

The aeroelastic model is described by the following system of equations:

$$\dot{\mathbf{x}}_a + \mathbf{A}_d\mathbf{x}_a + \mathbf{C}_{sa}\dot{\mathbf{z}}_s + \mathbf{K}_{sa}\mathbf{z}_s = \mathbf{B}_{ua}\mathbf{u} \tag{4.8a}$$

$$\mathbf{M}\ddot{\mathbf{z}}_s + (\mathbf{C}_s + \mathbf{G} + \mathbf{C}_a)\dot{\mathbf{z}}_s + (\mathbf{K} + \mathbf{K}_{cf} + \mathbf{K}_a + \mathbf{K}_{sf})\mathbf{z}_s + \mathbf{A}_f\mathbf{x}_a = \mathbf{B}_{us}\mathbf{u} \tag{4.8b}$$

where $\mathbf{z}_s$ contains the structural degrees of freedom, where one degree of freedom describes pitching around the pitch-bearing and in total 114 degrees of freedom describes the nodal deflections along three axes and rotations around three axes of 19 nodes along the blade. The aerodynamic state equation (4.8a), where $\mathbf{x}_a$ is the aerodynamic state vector, describe the time lag of the unsteady aerodynamic forces. Aerodynamic forces are calculated in 28 calculation points along the blade, giving in total 112 aerodynamic states. The matrix $\mathbf{M}$ is the mass matrix, $\mathbf{K}$ the elastic stiffness matrix, $\mathbf{K}_{cf}$ the centrifugal stiffness matrix, $\mathbf{C}_s$ the structural damping matrix, $\mathbf{G}$ the gyroscopic matrix, $\mathbf{C}_a$ the aerodynamic damping matrix and $\mathbf{K}_a$ the aerodynamic stiffness matrix and $\mathbf{K}_{sf}$ is the geometric stiffness matrix due to the movement of the steady state aerodynamic force vector. The matrix $\mathbf{A}_f$ represents coupling from aerodynamic states to structural states and matrices $\mathbf{C}_{sa}$ and $\mathbf{K}_{sa}$ describes coupling between structural velocities and displacements to aerodynamic states and $\mathbf{A}_d$ describes the lag on the aerodynamic forces. The matrices $\mathbf{B}_{ua}$ and $\mathbf{B}_{us}$ in Equation (4.8) represent the small changes in aerodynamic and structural forces from changes in chosen inputs $\mathbf{u}$, e.g. changes in the mean wind speed and pitch torque from a pitch actuator around the state, which has been linearized around.

Two versions are used of this high-order blade model. In one model, the blade is allowed to perform frictionless, rigid body rotation around the pitch bearing and no assumptions are made on pitch actuator dynamics to study the pure aeroelastic blade response. The model with no actuator is used prior to order reduction in a description of the aeroelastic frequencies and damping of the low-frequency blade modes. In the second model, a simplified pitch actuator model is included. The pitch actuator is modeled such that the actual blade pitch angle respond as a second order filter in response to a demanded pitch input angle. The pitch actuator model is implemented as a second order filter with unit gain and a very high filter frequency, such that the blade responds almost immediately to a demanded pitch angle, whereby the dynamic effects of the pitch actuator is neglected in the present study and the pitch actuator is denoted as *quasi-static*. The pitch actuator stabilizes the rigid body pitching mode and allows to study the frequency response of the blade.

Prior to order reduction, a convenient transformation of the aerodynamic states $\mathbf{x}_a$ is applied to cast the system of equations on a form, where the quasi-steady aerodynamic forces are a function of only the structural states, such that the aerodynamic states are used to represent the lag due to shed vorticity and dynamic stall. The idea by using this form of the system of equations is to use the structural basis functions in $\mathbf{\Phi}_s$ to represent the quasi-steady aeroelastic response, and then use the aerodynamic basis functions in $\mathbf{\Phi}_a$ solely to describe the effect of lag on aerodynamic forces. The idea is illustrated in Figure 4.1 that shows the typical variations in the normalized lift forces at a blade section in response to a step in angle of attack predicted by the unsteady and quasi-steady aerodynamic models used to characterize the effect of shed vorticity in attached flow [11]. With a quasi-steady aerodynamic model, there is by definition no lag in the aerodynamic forces acting on the blade section in response to a change in the inflow and the aerodynamic forces instantly reach the level that occurs only after a while. In the unsteady aerodynamics model the memory effect of the shed vorticity cause a lower change in lift in fast changes of the inflow. The quasi-steady aerodynamic model predicts by definition

the exact same aerodynamic forces as the unsteady aerodynamic model in the frequency response at 0 Hz. The following section describes how to perform this transformation.

The aerodynamic state vector corresponding to quasi-steady aerodynamics: $\mathbf{x}_a(t) = \mathbf{x}_a^{QS}(t)$ is defined as the aerodynamic state vector where the time derivative of $\mathbf{x}_a$ is zero. If we define $\dot{\mathbf{x}}_a = \mathbf{f}(t, \mathbf{x}_a, \mathbf{z}_s, \dot{\mathbf{z}}_s)$ then $\mathbf{x}_a^{QS}$ is defined from:

$$\mathbf{f}(t, \mathbf{x}_a^{QS}, \mathbf{z}_s, \dot{\mathbf{z}}_s) = \mathbf{0} \tag{4.9}$$

and is found from (4.8a) to be:

$$\mathbf{x}_a^{QS} = -\mathbf{A}_d^{-1}\mathbf{C}_{sa}\dot{\mathbf{z}}_s - \mathbf{A}_d^{-1}\mathbf{K}_{sa}\mathbf{z}_s + \mathbf{A}_d^{-1}\mathbf{B}_{ua}\mathbf{u} \tag{4.10}$$

The right-hand-side terms in (4.10) describe the changes in inflow and angle of attack at the blades due to structural velocities, displacements and from changes in the inputs, respectively. The aerodynamic state vector in Equation (4.8) is transformed using a coordinate shift into a new aerodynamic state vector $\mathbf{x}_a^*$ defined from:

$$\mathbf{x}_a(t) = \mathbf{x}_a^{QS}(t) + \mathbf{x}_a^*(t) \tag{4.11}$$

such that a zero aerodynamic state vector $\mathbf{x}_a^*(t) = \mathbf{0}$ in the new coordinates corresponds to quasi-steady aerodynamics. A new transformed system of equations in which $\mathbf{x}_a^*$ is the aerodynamic state vector, is obtained by inserting $\mathbf{x}_a$ from Equations (4.11) and (4.10) into the system of equations (4.8) and is found to be:

$$\dot{\mathbf{x}}_a^* + \mathbf{A}_d\mathbf{x}_a^* - \mathbf{A}_d^{-1}\mathbf{C}_{sa}\ddot{\mathbf{z}}_s - \mathbf{A}_d^{-1}\mathbf{K}_{sa}\dot{\mathbf{z}}_s = \mathbf{0} \tag{4.12a}$$

$$\mathbf{M}\ddot{\mathbf{z}}_s + \mathbf{C}_{QS}\dot{\mathbf{z}}_s + \mathbf{K}_{QS}\mathbf{z}_s + \mathbf{A}_f\mathbf{x}_a^* = \left[\mathbf{B}_{us} - \mathbf{A}_f\mathbf{A}_d^{-1}\mathbf{B}_{ua}\right]\mathbf{u} \tag{4.12b}$$

where the new total aeroelastic stiffness and damping matrices are defined as

$$\mathbf{K}_{QS} = \mathbf{K} + \mathbf{K}_{cf} + \mathbf{K}_a + \mathbf{K}_{sf} - \mathbf{A}_f\mathbf{A}_d^{-1}\mathbf{K}_{sa} \tag{4.13}$$

$$\mathbf{C}_{QS} = \mathbf{C} + \mathbf{G} + \mathbf{C}_a - \mathbf{A}_f\mathbf{A}_d^{-1}\mathbf{C}_{sa} \tag{4.14}$$

In the derivation of the transformed aerodynamic state equation (4.12a), the time derivative of the inputs are set to zero: $\dot{\mathbf{u}} = \mathbf{0}$, thereby assuming instant changes in the inputs. Instead of the original terms in the aerodynamic state equation: $\mathbf{C}_{sa}\dot{\mathbf{z}}_s$ and $\mathbf{K}_{sa}\mathbf{z}_s$, there

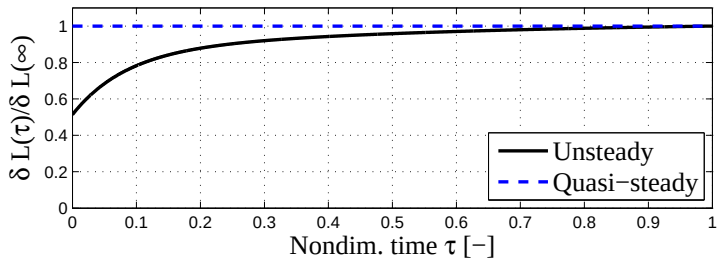

Figure 4.1: Typical variations in lift at a blade section in response to a step in angle of attack predicted by unsteady and quasi-steady aerodynamic models of shed vorticity in attached flow [11].

are now two new terms $-\mathbf{A}_d^{-1}\mathbf{C}_{sa}\ddot{\mathbf{z}}_s$ and $-\mathbf{A}_d^{-1}\mathbf{K}_{sa}\dot{\mathbf{z}}_s$ in which the order of the time derivative has increased.

The transformed system of equations (4.12) can be written in the first order form:

$$\dot{\mathbf{x}}_n = \mathbf{A}_n\mathbf{x}_n + \mathbf{B}_n\mathbf{u} \tag{4.15a}$$

$$\mathbf{y} = \mathbf{C}_n\mathbf{x}_n \tag{4.15b}$$

where $\mathbf{y}$ are a set of chosen outputs and $\mathbf{C}_n$ is the corresponding output matrix, and where:

$$\mathbf{x}_n = \left\{ \begin{array}{ccc} \mathbf{x}_a^* & \mathbf{z}_s & \dot{\mathbf{z}}_s \end{array} \right\}^T \tag{4.16}$$

$$\mathbf{A}_n = \left[\begin{array}{ccc} \mathbf{I} & -\mathbf{A}_d^{-1}\mathbf{K}_{ux} & -\mathbf{A}_d^{-1}\mathbf{C}_{ux} \\ \mathbf{0} & \mathbf{I} & \mathbf{0} \\ \mathbf{0} & \mathbf{0} & \mathbf{M} \end{array} \right]^{-1} \left[\begin{array}{ccc} -\mathbf{A}_d & \mathbf{0} & \mathbf{0} \\ \mathbf{0} & \mathbf{0} & \mathbf{I} \\ -\mathbf{A}_f & -\mathbf{K}_{QS} & -\mathbf{C}_{QS} \end{array} \right] \tag{4.17}$$

$$\mathbf{B}_n = \left[\begin{array}{c} \mathbf{0} \\ \mathbf{0} \\ \mathbf{B}_{us} - \mathbf{A}_f\mathbf{A}_d^{-1}\mathbf{B}_{ua} \end{array} \right] \tag{4.18}$$

$$\mathbf{C}_n = \left[\begin{array}{ccc} \mathbf{C}_{n1} & \mathbf{C}_{n2} & \mathbf{C}_{n3} \end{array} \right] \tag{4.19}$$

and where the components of the output matrix are found as:

$$\mathbf{C}_{n1} = \mathbf{C}_1 \tag{4.20}$$

$$\mathbf{C}_{n2} = \mathbf{C}_2 - \mathbf{C}_1\mathbf{A}_d^{-1}\mathbf{K}_{sa} \tag{4.21}$$

$$\mathbf{C}_{n3} = \mathbf{C}_3 - \mathbf{C}_1\mathbf{A}_d^{-1}\mathbf{C}_{sa} \tag{4.22}$$

where matrices $\mathbf{C}_1$, $\mathbf{C}_2$, $\mathbf{C}_3$ are components of the original output matrix related to $\mathbf{x}_a$, $\mathbf{z}_s$ and $\dot{\mathbf{z}}_s$, respectively.

4.2.2 Low-frequency aeroelastic blade modes

A short description is now given of the aeroelastic frequencies and damping of the low-frequency blade modes predicted by the full-order model with unsteady aerodynamics. The ability to correctly predict the aeroelastic frequencies and damping of the low-frequency blade modes of the full-order model is used to evaluate the reduced-order models in Sections 4.2.4 and 4.2.5. The aeroelastic frequencies and damping are found from the eigenvalues λ of the matrix $\mathbf{A}$, i.e. from the algebraic eigenvalue problem: $\mathbf{A}\mathbf{v} = \lambda\mathbf{v}$, where $\mathbf{v}$ is the eigenvector.

Figures 4.2a-c show the aeroelastic frequencies and damping of the low-frequency blade modes for the NREL 5 MW wind turbine blade in normal operation at wind speeds from 5 m/s to 25 m/s predicted by the full-order models. The blue and black markers in Figure 4.2 show the frequency and damping of the blade modes for the blade model with and without the quasi-static pitch actuator, respectively. The results of the model without the quasi-static pitch actuator is shown to describe the purely aeroelastic blade response.

The aeroelastic frequencies of the 1st blade flap mode without pitch actuator is found to decrease with wind speed up to rated and to increase with wind speed above rated (see bottom Figure 4.2a). The low aeroelastic frequencies of the 1st flap mode around rated wind speed can be explained by a structural coupling between the flap mode and the rigid body pitching mode, because of negative aerodynamic stiffness forces trying to

pitch the blade. The aeroelastic frequency of the 1st flap mode increase when the pitch actuator model is included and the coupling to the rigid body pitching mode vanish. The aeroelastic damping of the 1st flap mode is found to increase up to rated wind speed both with and without pitch actuator, because the relative wind speeds increase [55]. Above rated, the damping ratio of the 1st flap mode without pitch actuator is found to decrease with wind speed, whereas the model including the quasi-static pitch actuator predicts nearly constant damping. The decreasing damping ratio of the 1st flap mode above rated can be explained by the structural coupling to the rigid body pitching mode causing the blade to perform rigid body pitching motion instead of flapping motion.

The aeroelastic frequency of the 2nd blade flap mode is nearly constant with wind speed and is not largely affected by the presence of the quasi-static pitch actuator. The aeroelastic damping of this mode increases up to rated wind speed, because of increasing relative inflow velocities.

The aeroelastic frequency of the 1st edge blade mode with no pitch actuator (see mid Figure 4.2a) is found to increase up to rated wind speed and to decrease above rated

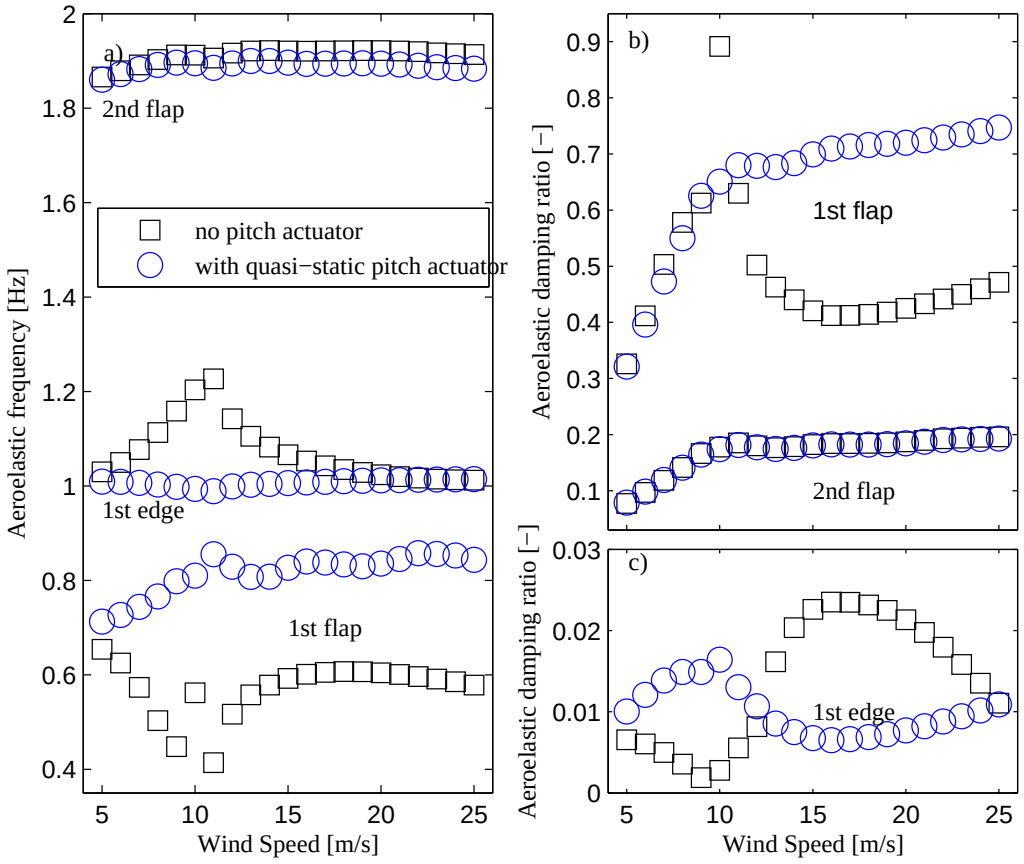

Figure 4.2: Aeroelastic frequencies and damping of the low-frequency blade modes for the NREL 5 MW wind turbine blade in normal operation at wind speeds from 5 m/s to 25 m/s predicted by high-order models with unsteady aerodynamics with and without 'quasi-static' pitch actuator model.

wind speed. This variation in the frequency of the 1st edge mode can be explained from a structural coupling with free-free torsional blade mode, that cause the blade to perform torsional deflection when it deflects in the edgewise direction at wind speeds where the static flap deflection is high. The model including pitch actuator predicts a nearly constant frequency of the edge wise blade mode, because of the lack of coupling to torsion in this mode. The 1st edgewise mode is very lowly damped by aerodynamics, because the edgewise blade motion cause only little change in the angle of attack.

4.2.3 Reduced-order system matrices

In this section, the reduced-order system of equations for the aeroelastic blade model is derived. The reduced-order system of equations are found by inserting the projections from Equation (4.2) into the system of equations (4.12) and pre-multiply with $\mathbf{\Phi}_a^T$ and $\mathbf{\Phi}_s^T$ in Equation (4.12a) and (4.12b), respectively. The reduced-order equations can then be written in similar form as the full-order system:

$$\dot{\mathbf{q}}_a + \underbrace{(\mathbf{\Phi}_a^T\mathbf{\Phi}_a)^{-1}\mathbf{\Phi}_a^T\mathbf{A}_d\mathbf{\Phi}_a}_{\mathbf{A}_{d,\Phi}}\mathbf{q}_a - \underbrace{(\mathbf{\Phi}_a^T\mathbf{\Phi}_a)^{-1}\mathbf{\Phi}_a^T\mathbf{A}_d^{-1}\mathbf{C}_{sa}\mathbf{\Phi}_s}_{\mathbf{C}_{sa,\Phi}}\ddot{\mathbf{q}}_s - \underbrace{(\mathbf{\Phi}_a^T\mathbf{\Phi}_a)^{-1}\mathbf{\Phi}_a^T\mathbf{A}_d^{-1}\mathbf{K}_{sa}\mathbf{\Phi}_s}_{\mathbf{K}_{sa,\Phi}}\dot{\mathbf{q}}_s = \mathbf{0} \tag{4.23a}$$

$$\underbrace{\mathbf{\Phi}_s^T\mathbf{M}\mathbf{\Phi}_s}_{\mathbf{M}_\Phi}\ddot{\mathbf{q}}_s + \underbrace{\mathbf{\Phi}_s^T\mathbf{C}_{QS}\mathbf{\Phi}_s}_{\mathbf{C}_\Phi}\dot{\mathbf{q}}_s + \underbrace{\mathbf{\Phi}_s^T\mathbf{K}_{QS}\mathbf{\Phi}_s}_{\mathbf{K}_\Phi}\mathbf{q}_s + \underbrace{\mathbf{\Phi}_s^T\mathbf{A}_f\mathbf{\Phi}_a}_{\mathbf{A}_{f,\Phi}}\mathbf{q}_a = \mathbf{\Phi}_s^T\left[\mathbf{B}_{us} - \mathbf{A}_f\mathbf{A}_d^{-1}\mathbf{B}_{ua}\right]\mathbf{u} \tag{4.23b}$$

where the matrices $\mathbf{M}_\Phi$, $\mathbf{C}_\Phi$ and $\mathbf{K}_\Phi$ are the reduced-order mass, aeroelastic damping and aeroelastic stiffness matrices and where $\mathbf{A}_{f,\Phi}$ is the new coupling from the aerodynamic states to the structural states, $\mathbf{A}_{d,\Phi}$ is the reduced-order aerodynamic lag matrix and $\mathbf{C}_{sa,\Phi}$ and $\mathbf{K}_{sa,\Phi}$ are the reduced-order coupling matrices from structural deflections and rotations to the aerodynamic states.

In the present work, the structural blade mode shapes are used to reduce the number of structural degrees of freedom. To achieve better approximation at low frequencies, a static residualization step is performed in which the low-frequency effect of high-frequency blade modes are included without increasing the order of the model. In the static residualization step, the effect of high-frequency blade modes are included by neglecting the inertia forces and damping forces of the high-frequency modes. By expansion with the purely structural mode shapes of both low- and high-frequency modes, the projected system of equations (4.23b) can be partitioned as:

$$\begin{bmatrix} \mathbf{M}_{\Phi,tt} & \mathbf{M}_{\Phi,tr} \\ \mathbf{M}_{\Phi,rt} & \mathbf{M}_{\Phi,rr} \end{bmatrix}\begin{Bmatrix} \ddot{\mathbf{q}}_{s,t} \\ \ddot{\mathbf{q}}_{s,r} \end{Bmatrix} + \begin{bmatrix} \mathbf{C}_{\Phi,tt} & \mathbf{C}_{\Phi,tr} \\ \mathbf{C}_{\Phi,rt} & \mathbf{C}_{\Phi,rr} \end{bmatrix}\begin{Bmatrix} \dot{\mathbf{q}}_{s,t} \\ \dot{\mathbf{q}}_{s,r} \end{Bmatrix} + \begin{bmatrix} \mathbf{K}_{\Phi,tt} & \mathbf{K}_{\Phi,tr} \\ \mathbf{K}_{\Phi,rt} & \mathbf{K}_{\Phi,rr} \end{bmatrix}\begin{Bmatrix} \mathbf{q}_{s,t} \\ \mathbf{q}_{s,r} \end{Bmatrix} + \begin{bmatrix} \mathbf{A}_{f,\Phi,t} \\ \mathbf{A}_{f,\Phi,r} \end{bmatrix}\mathbf{q}_a = \begin{bmatrix} \mathbf{\Phi}_t^T \\ \mathbf{\Phi}_r^T \end{bmatrix}\left[\mathbf{B}_{us} - \mathbf{A}_f\mathbf{A}_d^{-1}\mathbf{B}_{ua}\right]\mathbf{u} \tag{4.24}$$

where index t denotes the index of modes that are retained in the model and r denotes the index of high-frequency modes that are residualized. By neglecting inertia and damping forces of the high-frequency modes ($\mathbf{M}_{\Phi,rr} = \mathbf{C}_{\Phi,rr} = \mathbf{0}$) and the cross-coupling inertia

and damping terms from high-frequency modes on the low-frequency modes ($\mathbf{M}_{\Phi,tr} = \mathbf{C}_{\Phi,tr} = \mathbf{0}$), the generalized states describing the high-frequency modes can be written as a function of $\mathbf{q}_{s,t}$, $\dot{\mathbf{q}}_{s,t}$, $\ddot{\mathbf{q}}_{s,t}$, $\mathbf{u}$ and the aerodynamic states $\mathbf{q}_a$:

$$\begin{aligned}\mathbf{q}_{s,r} = \mathbf{K}_{\Phi,rr}^{-1}\Big[\boldsymbol{\Phi}_r^T\big[\mathbf{B}_{us} - \mathbf{A}_f\mathbf{A}_d^{-1}\mathbf{B}_{ua}\big]\mathbf{u} - \mathbf{M}_{\Phi,rt}\ddot{\mathbf{q}}_{s,t} - \\ \mathbf{C}_{\Phi,rt}\dot{\mathbf{q}}_{s,t} - \mathbf{K}_{\Phi,rt}\mathbf{q}_{s,t} - \mathbf{A}_{f,\Phi,r}\mathbf{q}_a\Big]\end{aligned} \tag{4.25}$$

The reduced-order system of equations, including the static residualization, is obtained from the top-partition of (4.24) by inserting $\mathbf{q}_{s,r}$ from (4.25). The reduced-order system of equations on first order form is then found as:

$$\dot{\mathbf{q}} = \mathbf{A}_r\mathbf{q} + \mathbf{B}_r\mathbf{u} \tag{4.26a}$$

$$\mathbf{y} = \mathbf{C}_r\mathbf{q} + \mathbf{D}_r\mathbf{u} \tag{4.26b}$$

with the reduced-order system matrices:

$$\mathbf{q} = \left\{ \begin{array}{cccc} \mathbf{q}_a & \mathbf{q}_{s,t} & \dot{\mathbf{q}}_{s,t} \end{array} \right\}^T$$

$$\mathbf{A}_r = \begin{bmatrix} \mathbf{A}_\Phi & -\mathbf{K}_{sa,\Phi} & -\mathbf{C}_{sa,\Phi} \\ \mathbf{0} & \mathbf{I} & \mathbf{0} \\ \mathbf{0} & \mathbf{0} & \mathbf{M}_\Phi \end{bmatrix}^{-1} \begin{bmatrix} -\mathbf{A}_{d,\Phi} & \mathbf{0} & \mathbf{0} \\ \mathbf{0} & \mathbf{0} & \mathbf{I} \\ -\mathbf{A}_{f,\Phi} & -\mathbf{K}_\Phi & -\mathbf{C}_\Phi \end{bmatrix}$$

$$\mathbf{B}_r = \begin{bmatrix} \mathbf{0} \\ \mathbf{0} \\ \left(\boldsymbol{\Phi}_t^T - \mathbf{K}_{\Phi,tr}\mathbf{K}_{\Phi,rr}^{-1}\boldsymbol{\Phi}_r^T\right)\left[\mathbf{B}_{us} - \mathbf{A}_f\mathbf{A}_d^{-1}\mathbf{B}_{ua}\right] \end{bmatrix}$$

$$\mathbf{C}_r = \begin{bmatrix} \mathbf{C}_{n1}\boldsymbol{\Phi}_a - \mathbf{C}_{n2}\boldsymbol{\Phi}_r\mathbf{K}_{rr}^{-1}\mathbf{A}_{f,r} \\ \mathbf{C}_{n2}\boldsymbol{\Phi}_t - \mathbf{C}_{n2}\boldsymbol{\Phi}_r\mathbf{K}_{rr}^{-1}\mathbf{K}_{rt} \\ \mathbf{C}_{n3}\boldsymbol{\Phi}_t - \mathbf{C}_{n2}\boldsymbol{\Phi}_r\mathbf{K}_{rr}^{-1}\mathbf{C}_{rt} \end{bmatrix}^T$$

$$\mathbf{D}_r = \mathbf{C}_{n2}\boldsymbol{\Phi}_r\mathbf{K}_{\Phi,rr}^{-1}\boldsymbol{\Phi}_r^T\big[\mathbf{B}_{us} - \mathbf{A}_f\mathbf{A}_d^{-1}\mathbf{B}_{ua}\big]$$

and with the new reduced-order matrices:

$$\mathbf{M}_\Phi = \Big[\mathbf{M}_{\Phi,tt} - \mathbf{K}_{\Phi,tr}\mathbf{K}_{\Phi,rr}^{-1}\mathbf{M}_{\Phi,rt}\Big]$$

$$\mathbf{C}_\Phi = \Big[\mathbf{C}_{\Phi,tt} - \mathbf{K}_{\Phi,tr}\mathbf{K}_{\Phi,rr}^{-1}\mathbf{C}_{\Phi,rt}\Big]$$

$$\mathbf{K}_\Phi = \Big[\mathbf{K}_{\Phi,tt} - \mathbf{K}_{\Phi,tr}\mathbf{K}_{\Phi,rr}^{-1}\mathbf{K}_{\Phi,rt}\Big]$$

$$\mathbf{A}_{f,\Phi} = \Big[\mathbf{A}_{f,\Phi,t} - \mathbf{K}_{\Phi,tr}\mathbf{K}_{\Phi,rr}^{-1}\mathbf{A}_{f,\Phi,r}\Big]$$

The static residualization step is responsible for additional terms in the reduced-order aeroelastic mass, stiffness and damping matrices through the coupling terms from low-frequency modes on the high-frequency modes and gives additional terms also in the reduced-order input matrix, output matrix and in the direct transfer matrix.

4.2.4 Reduction of structural order

In the present work, the matrix $\boldsymbol{\Phi}_s$ is represented by the low-frequency structural, undamped mode shapes of the blade. Reduction is done using the pure rigid body pitching mode governed only by the pitching inertia forces. Reduction is further done using the

structural mode shapes found by fixing the blade at the root (cantilevered) and these mode shapes are determined from the following eigenvalue problem

$$-\omega_{s,i}^2 \mathbf{M}\phi_{s,i} + \mathbf{K}\phi_{s,i} = \mathbf{0} \tag{4.27}$$

where $\omega_{s,i}$ is the natural frequency and $\phi_{s,i}$ is the eigenvector corresponding to mode i. Reduced-order models of varying complexity are analyzed in this and following sections. The content on these models is listed in Table 4.1, where the first column describes what structural blade modes are used and the second column describes how the aerodynamic part is reduced. This section analyze the effect of using purely structural modes to reduce the number of structural degrees of freedom by models no.1-6, that includes up to six structural modes. In models no.1-6 all aerodynamic states are retained in the model to focus on reducing only the number of structural states. Reduced-order models no.7-9 listed in Table 4.1 have varying complexity of the aerodynamic model and these models are discussed in the next sections.

Figures 4.3a-c show the aeroelastic frequencies and damping of the low-frequency structurally dominated blade modes for the NREL 5 MW wind turbine blade in normal operation at wind speeds from 5 m/s to 25 m/s predicted by high-order models with unsteady aerodynamics (black squares) and with reduced-order models no.1-5.

The model no.1 includes all aerodynamic states and the rigid body pitching mode, the 1$^{\text{st}}$ flap and 1$^{\text{st}}$ edge structural blade modes. This model predicts correctly the aeroelastic frequency and damping of the 1$^{\text{st}}$ aeroelastic flap mode at low wind speeds, whereas above rated both the frequencies and the damping ratios of the 1$^{\text{st}}$ flap mode are predicted

Model	**Structural modes**	**Aerodynamic basis functions**
1	rigid body pitching, 1$^{\text{st}}$ flap and 1$^{\text{st}}$ edge	all aerodynamic states
2	rigid body pitching, 1$^{\text{st}}$ flap, 1$^{\text{st}}$ edge and 2$^{\text{nd}}$ flap	all aerodynamic states
3	rigid body pitching, 1$^{\text{st}}$ flap, 1$^{\text{st}}$ edge, 2$^{\text{nd}}$ flap and 1$^{\text{st}}$ torsion	all aerodynamic states
4	rigid body pitching, 1$^{\text{st}}$ flap, 1$^{\text{st}}$ edge, and 2$^{\text{nd}}$ flap (w.res.)	all aerodynamic states
5	rigid body pitching, 1$^{\text{st}}$ flap, 1$^{\text{st}}$ edge, 2$^{\text{nd}}$ flap and 1$^{\text{st}}$ torsion (w.res.)	all aerodynamic states
6	rigid body pitching, 1$^{\text{st}}$ flap, 1$^{\text{st}}$ edge, 1$^{\text{st}}$ torsion, 2$^{\text{nd}}$ flap and 3$^{\text{rd}}$ flap (w.res.)	all aerodynamic states
7	rigid body pitching, 1$^{\text{st}}$ flap, 1$^{\text{st}}$ edge, and 2$^{\text{nd}}$ flap (w.res.)	none
8	rigid body pitching, 1$^{\text{st}}$ flap, 1$^{\text{st}}$ edge, and 2$^{\text{nd}}$ flap (w.res.)	slaves of 1$^{\text{st}}$ flap
9	rigid body pitching, 1$^{\text{st}}$ flap, 1$^{\text{st}}$ edge, and 2$^{\text{nd}}$ flap (w.res.)	slaves of 1$^{\text{st}}$ and 2$^{\text{nd}}$ flap modes

Table 4.1: Description of the content of reduced-order models in terms of what structural mode shapes and aerodynamic shape functions are included. All mode shapes used to represent the structural degrees of freedom and used to make aerodynamic slave modes are the purely structural mode shapes.

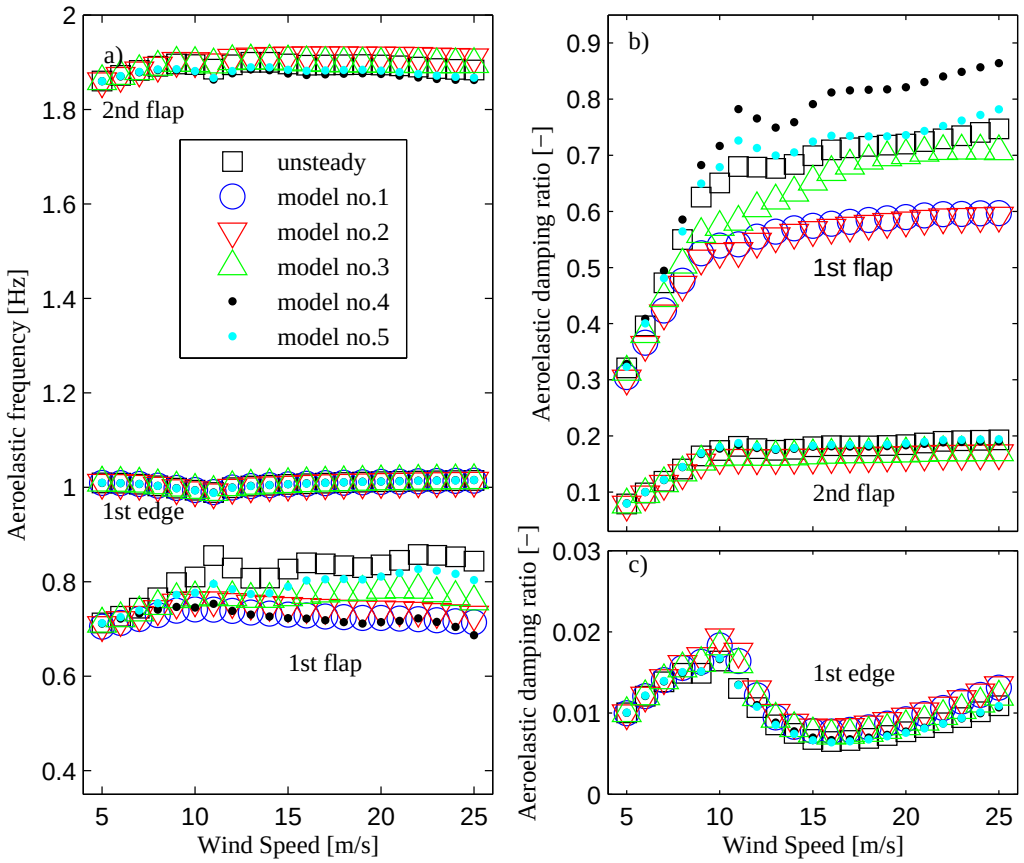

Figure 4.3: Aeroelastic frequencies and damping of the low-frequency blade modes for the NREL 5 MW wind turbine blade in normal operation at wind speeds from 5 m/s to 25 m/s predicted by high-order models with unsteady aerodynamics (black) and by reduced-order models no.1-5 with the content listed in Table 4.1.

too low with this model. The model no.1 predicts correctly the aeroelastic damping and frequency of the 1st edge mode at all wind speeds.

The red markers in Figure 4.3 show the aeroelastic frequencies and damping ratios predicted with model no.2 including also the 2nd structural flap mode. By including the 2nd flap mode the aeroelastic frequency and damping of the 2nd flap mode is captured accurately, whereas the pole of the 1st flap mode above rated is still not correct at above rated wind speeds.

The model no.3, including also the 1st torsional blade mode with a natural frequency at standstill of 5.80 Hz, is seen to give a clearly better approximation of the aeroelastic frequency and damping of the 1st flap mode above rated than previous models. This observation can be explained by the lack of blade torsion in the 1st structural flap mode, caused by coupling with aerodynamic forces. Blade vibration in the 1st aeroelastic flap mode couples to torsional blade vibration through the changes in the aerodynamic torque around the elastic center at the blade sections, due to the changes in inflow from the blade vibration. Figure 4.3 shows that the aeroelastic damping of the 1st flap mode predicted

by the reduced-order model increases when the torsional mode is included. The blade torsion in the 1st aeroelastic flap mode cause higher aerodynamic damping because torsional blade deflection towards feathering is in phase with the downwind flap deflection velocity, as reported previously in a stability analysis performed by Hansen [54]. In model no.4 the effect of all aeroelastic modes with frequency above the 2nd flap mode, and thereby also the effect of the 1st torsional blade mode, is included by static residualization. The main effect of static residualization is a shift in the aeroelastic frequency and damping of the 1st flap mode relative to model no.3, which may be due to the effect of the 1st torsional mode not being correctly captured by residualization. The cyan curves in Figure 4.3 show the results of model no.5 including the 1st torsional blade mode and the static effect of all modes above the 1st torsional blade model, showing better approximation of the aeroelastic frequency and damping of the 1st flap mode above rated. Thus, it is seen to be important for correct approximation of the aeroelastic frequency and damping of the 1st flap mode above rated, to include the dynamic (opposed to the static) effect of the 1st torsional blade mode.

The reduced-order models are now evaluated on how they approximate the aeroelastic frequency response from mean wind speed changes to blade root bending moments in the flap direction. Figure 4.4 shows the aeroelastic blade frequency response of the NREL 5 MW wind turbine blade in normal operation at 14 m/s and 20 m/s predicted by the full-order model including unsteady aerodynamics (black) and predicted by reduced-order models no.1,2,4 and 6 listed in Table 4.1. Three vertical lines in Figure 4.4 are used to mark disturbances from e.g. sampling of turbulence at the rotational frequency (1P) and

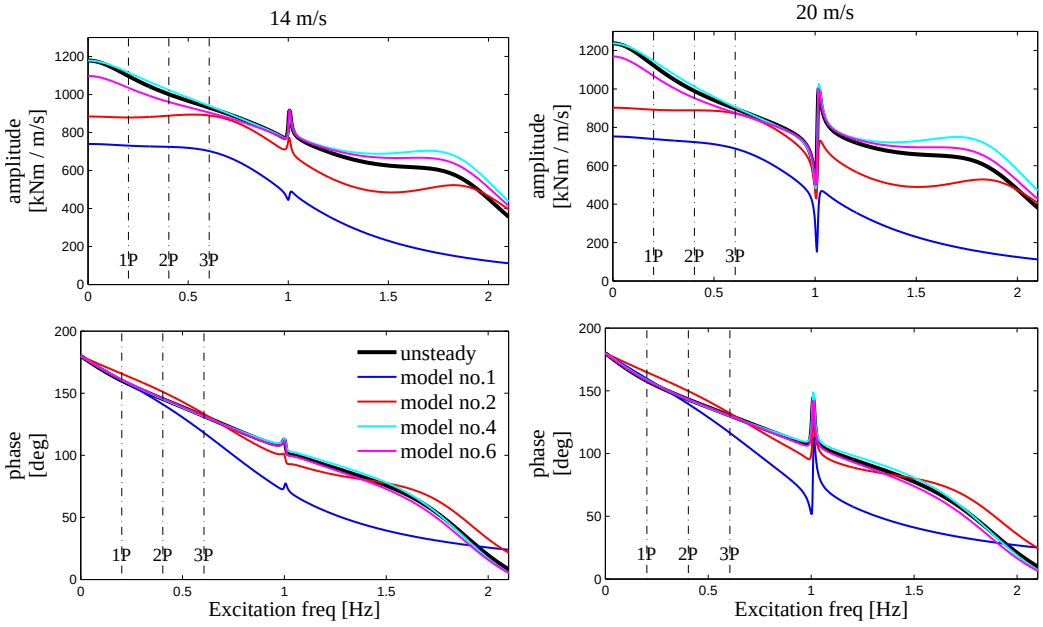

Figure 4.4: Aeroelastic blade frequency response from mean wind speed changes to blade root flap bending moment for the NREL 5MW blade in normal operation at 14 m/s and 20 m/s. Comparison between predictions of full-order model with unsteady aerodynamics (black) and reduced-order models no.1, 2, 4 and 6 of varying structural complexity.

multiples thereof, to show at what frequencies good accuracy is required (assuming that the blades samples turbulence similarly at all blade sections).

The aeroelastic frequency response from mean wind speed to blade root flap bending moment predicted by the full-order model with unsteady aerodynamics, is characterized by an amplitude at 0 Hz of around 1200 kNm/(m/s) at both 14 m/s and 20 m/s and a phase of 180 deg at 0 Hz, because the positive direction of the flap bending moment is defined positive towards the rotational direction, using the right-hand rule. The frequency response predicted by model no.1 including the pure rigid body pitching mode, the 1st structural flap mode and the 1st structural edge mode is shown with blue curves in Figure 4.4 and is generally governed by the highly damped second order response of the 1st flap mode, that cause the decreasing amplitude beginning at around 0.7 Hz. at both wind speeds. At 0 Hz, the model no.1 predicts too low amplitude compared to the high-order model.

The model no.2 which also includes the 2nd flap mode (red curves) predicts a more accurate - but still not a correct - amplitude a low frequencies, showing that the 2nd flap mode contributes largely at low frequencies. Especially at 1P the model no.2 predicts a frequency response amplitude that deviates largely from the full-order model. Better approximation of the frequency response close to 0 Hz is achieved at both wind speeds by including the static contribution from structural modes with natural frequency above the 2nd flap mode (model no.4 - cyan curves). The model no.4 gives a slight offset at the response around the aeroelastic frequency of the 2nd flap mode, which can be avoided by further including the 1st torsional mode (magenta curves) in model no.6, that also includes the 3rd flap mode, because this mode contributes to the response at 0 Hz.

4.2.5 Reduction of aerodynamic states

It is now analyzed, what aerodynamic basis functions that should be used in the Petrov-Galerkin projection of the aerodynamic states in Equation (4.2). In the present work, the aerodynamic basis functions are defined to be slaves of some of the structural mode shapes.

The aerodynamic basis functions are defined as the stationary response of the aerodynamic state $\mathbf{x}_a^*$ due to a harmonic vibration of a structural mode shape $\mathbf{z}_s = \phi_{s,i} e^{j\omega_{s,i}t}$ at the natural frequency of mode i, where $j = \sqrt{-1}$. From Equation (4.12a) it is seen, that the stationary response is given by $\mathbf{x}_a^* = \phi_a e^{j\omega_{s,i}t}$ where ϕ_a is determined from:

$$\left[j\omega_{s,i}\mathbf{I} + \mathbf{A}_d\right]\phi_a = \left[-\omega_{s,i}^2 \mathbf{A}_d^{-1}\mathbf{C}_{sa} + j\omega_{s,i}\mathbf{A}_d^{-1}\mathbf{K}_{sa}\right]\phi_{s,i} \tag{4.28}$$

These aerodynamic basis functions are complex-valued and the projection of the aerodynamic states in Equation (4.2) is done by approximation with the real part of $\phi_a \mathbf{q}_a$ by using

$$\mathbf{x}_a^* \approx \mathrm{Re}\{\phi_a \mathbf{q}_a\} = \phi_{a,\alpha}\mathbf{q}_{a,\alpha} - \phi_{a,\beta}\mathbf{q}_{a,\beta} = \begin{bmatrix} \phi_{a,\alpha} & -\phi_{a,\beta} \end{bmatrix} \begin{Bmatrix} \mathbf{q}_{a,\alpha} \\ \mathbf{q}_{a,\beta} \end{Bmatrix} \tag{4.29}$$

to ensure that $\mathbf{x}_a^*$ remains real-valued, where indices α and β denote real and imaginary parts, respectively. Equation (4.29) shows that two aerodynamic basis functions: the real-part $\phi_{a,\alpha}$ and the imaginary part $\phi_{a,\beta}$ are used to represent $\mathbf{x}_a^*$ for each of the chosen structural modes.

Order reduction using aerodynamic basis functions is studied from models no.7-9 listed in Table 4.1. Figure 4.5 shows a comparison of the aeroelastic frequencies and damping of low-frequency blade modes of the NREL 5 MW blade in normal operation at wind speeds

from 5 m/s to 25 m/s predicted by full-order models with unsteady aerodynamics (black), full-order models with quasi-steady aerodynamics (blue) and predicted by reduced-order models no.7-9.

The model with quasi-steady aerodynamics (blue markers in Figure 4.5) is a model that includes all structural degrees of freedom and no aerodynamic states, due to the chosen realization of the system of equations in (4.12). The model with quasi-steady aerodynamics is seen to predict an aeroelastic frequency of the 1st flap mode that drops to zero and a damping ratio that increase to unity at 15 m/s, i.e. the mode becomes overdamped above 15 m/s, which can be explained by a prediction of too large aerodynamic damping compared to that of unsteady aerodynamics. The higher aerodynamic damping predicted with quasi-steady aerodynamics also explains the higher damping ratios and lower aeroelastic frequencies of the 2nd blade flap mode predicted with quasi-steady aerodynamics.

The model no.7 (red markers) includes the four structural modes used previously in model no.4 and no aerodynamic states and is seen to predict aeroelastic frequencies and

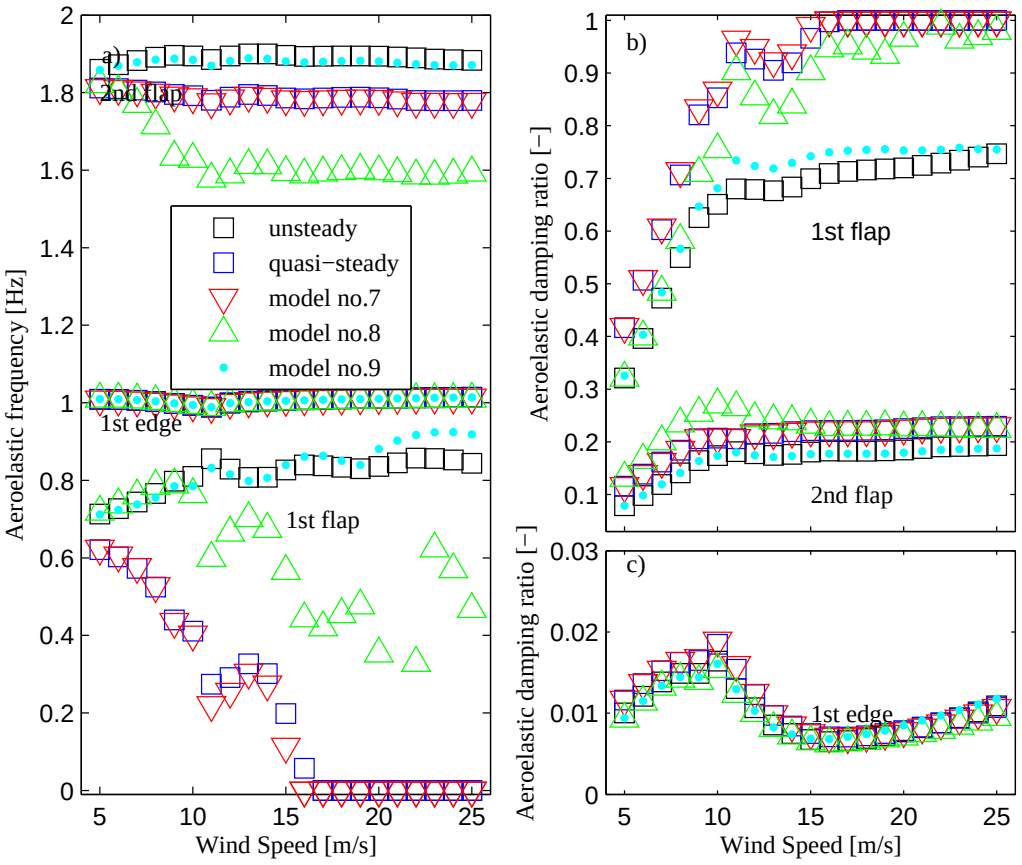

Figure 4.5: Aeroelastic frequencies and damping of the low-frequency blade modes for the NREL 5 MW wind turbine blade in normal operation at wind speeds from 5 m/s to 25 m/s predicted by high-order models with unsteady aerodynamics (black), full-order models with quasi-steady aerodynamics (blue) and by reduced-order models no.7-9 listed in Table 4.1.

damping of the low-frequency modes that is very similar to that predicted with quasi-steady aerodynamics, showing that the chosen structural modes, that can capture the unsteady aerodynamic response can also capture the quasi-steady aerodynamic response.

In model no.8 (green markers), the two aerodynamic basis functions that are slaves of the 1st structural flap mode are included in the model, such that the model includes a total of ten states. The two aerodynamic basis functions that are slaves of the 1st flap mode is seen to capture the aeroelastic frequency and damping of the 1st flap mode below rated wind speeds, whereas above rated the model no.8 still predicts too high damping of the 1st flap mode compared to the full-order model with unsteady aerodynamics. Model no.9 (cyan markers) further includes the two aerodynamic basis functions that are slaves of the 2nd structural flap mode, and the reduced-order model is now seen to predict accurately the aeroelastic frequency and damping of both the 1st and 2nd flap modes.

Figure 4.6 shows the aeroelastic frequency response from mean wind speed to blade root flap bending moment for the NREL 5 MW wind turbine blade in normal operation at 14 m/s and 20 m/s, predicted by the full-order blade model with unsteady aerodynamics (black) and with reduced-order models no.7 and 9.

The blue curves in Figure 4.6 show the frequency response predicted by model no.7 in which no aerodynamic states are included, such that the aerodynamic model corresponds to quasi-steady aerodynamics. The frequency response predicted with model no.7 is very

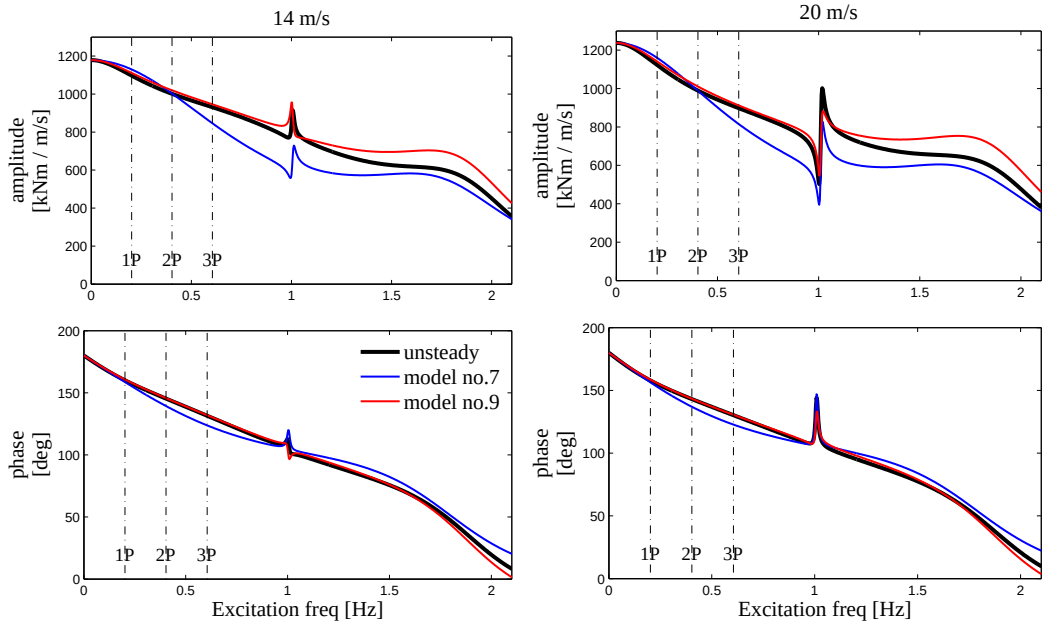

Figure 4.6: Aeroelastic frequency response from mean wind speed to blade root flap bending moment for the NREL 5 MW wind turbine blade in normal operation at 14 m/s and 20 m/s predicted by the full-order blade model with unsteady aerodynamics (black) and reduced-order models no.7 and no.9 including ten generalized structural states and respectively zero and four generalized aerodynamic states.

similar to the frequency response of the quasi-steady aerodynamic model containing all structural degrees of freedom, which is not shown for the same reason. From model no.7 it is seen, that the frequency response predicted with a model assuming quasi-steady aerodynamics has a slightly higher amplitude at frequencies around 1P than the full-order model with unsteady aerodynamics. Also, at frequencies around 3P the quasi-steady model predicts a clearly lower amplitude than the model including unsteady aerodynamics. The lower amplitudes in the frequency response predicted with quasi-steady aerodynamics can be explained by a larger aerodynamic damping at the 1st flap mode predicted with this model.

The red curves in Figure 4.6 show the frequency response predicted by model no.9 where the four aerodynamic slave modes of the 1st and 2nd structural flap modes are used to approximate the effect of shed vorticity and dynamic stall. These four aerodynamic basis functions are seen to capture nicely the effect of the unsteady aerodynamics on the frequency response from mean wind speed to the blade root flap bending moments. The deviations in the frequency response predicted by model no.9 around 1.5 Hz and 2.0 Hz is caused by too low order of the structural part, see results of model no.4 in Figure 4.4.

4.3 Chapter summary

In this chapter it is analyzed how to reduce separately the number of structural and aerodynamic states in high-order aeroelastic models. It is proposed to reduce the order of such high-order aeroelastic models by projection of the structural vector of degrees of freedom and the aerodynamic state vector separately onto a reduced set of structural and aerodynamic basis functions, respectively.

As an example, the order reduction method is used to design reduced-order aeroelastic models of the NREL 5 MW reference wind turbine blade in normal operation at various wind speeds based on a high-order linear aeroelastic model. The high-order model is a linearized finite beam element model coupled with an unsteady Blade Element Momentum model of aerodynamic forces including the effects of shed vorticity and dynamic stall. In the example, reduction of the number of structural degrees of freedom is done by Petrov-Galerkin projection with structural blade mode shapes and the number of aerodynamic states are reduced by projection using aerodynamic basis functions, that are defined as slaves of these structural mode shapes.

The accuracy of the reduced-order models are evaluated by how they approximate the aeroelastic frequency and damping ratios of the low-frequency blade modes. Prior to reducing the order, the effect of adding a 'quasi-static' pitch actuator is analyzed, assumed to provide an actual pitch angle in response to a demanded pitch angle with almost no lag. The pitch actuator stabilizes the rigid body pitching mode and affects the 1st blade flap mode at all wind speeds, explained by lack of coupling to the rigid body pitching mode, and affects the 1st edge blade mode mainly at around rated, explained by lack of coupling to free-free torsional blade mode in the presence of the actuator.

Main findings are that the aeroelastic frequencies and damping of the low-frequency blade modes can be accurately approximated by using the low-frequency purely structural blade mode shapes. The 1st structural torsional mode is found to be important to include for accurate prediction of the aeroelastic frequency and damping of the 1st flap mode above rated. For accurate approximation of the aeroelastic frequency response from mean wind speed to blade root flap bending moment at low frequencies it is found to be important to include the static effect of high-frequency structurally dominated modes, which can be done using static residualization.

Accurate approximation of the effect of unsteady aerodynamic forces on the low-frequency blade modes and on the aeroelastic blade frequency response is obtained using four aerodynamic basis functions that are slaves of the 1^{st} and 2^{nd} structural flap modes. Thus, the idea of reducing the order of aerodynamic states by projection with aerodynamic basis functions is seen to work using basis functions that are slaves of structural mode shapes.

Chapter 5

Conclusions and future work

The main purposes of this thesis are to analyze the necessary model complexity of aeroelastic models used for design of wind turbine controllers and to design low-order models that accurately captures the aeroelastic wind turbine response and are suited for design of modern model-based controllers and estimators.

5.1 Conclusions

The thesis provides a detailed analysis of the open-loop aeroelastic frequency response of a modern wind turbine, that serves as a benchmark for validation of low-order aeroelastic wind turbine models used for control design. The analysis describes the necessary model complexity of control design models of wind turbines by gradually increasing the complexities of the structural and aerodynamic models in a high-order linear aeroelastic model. The high-order model is a linearization of a structurally nonlinear finite beam element model of tower, drivetrain and blades coupled with an unsteady Blade Element Momentum (BEM) model of aerodynamic forces including effects of shed vorticity and dynamic stall. Linearization is performed around a deflected state of the blades determined by the static aerodynamic forces due to an assumed uniform inflow to the rotor.

The generator speed response is already known to be affected by the longitudinal tower flexibility that cause a non-minimum phase zero in the open-loop frequency response from collective pitch to generator speed. Lateral tower motion is found to be important in correct modelling of the non-minimum phase zeros due to the nacelle roll associated with lateral tower vibration. The frequency response from collective pitch to generator speed is found to be affected by another non-minimum phase zero at the aeroelastic frequency of the 1^{st} collective flap mode. To accurately approximate this non-minimum phase zero, it is found to be important to include the collective blade flap degrees of freedom. The effect of neglecting the effects of shed vorticity and dynamic stall and assume quasi-steady aerodynamics has been discussed. An assumption of quasi-steady airfoil aerodynamics is seen to affect the frequency response from collective pitch angle demand to generator speed not below the frequency of the 1^{st} drivetrain mode, where the lag on aerodynamic forces affects the predictions of a single-input single-output transfer function zero.

Linear aeroelastic models of low order are designed for a modern wind turbine by order reduction of high-order aeroelastic models. The low-order models are designed using two order reduction techniques: modal truncation and balanced truncation. Order reduction by modal truncation is done using the full-turbine, aeroelastic mode shapes. It is found that in the modal truncation technique, a relatively large number of aerodynamically dominated modes are required in the reduced-order model for good approximation, due to the assumption of independent flow tubes in the BEM model. The aeroelastic model assumes that the unsteady aerodynamic forces at local sections along the blades does not couple with each other spanwise through aerodynamics, but only through structural displace-

ment, thereby increasing the required order of the model. A set of reduced-order models designed by modal truncation under assumption of quasi-steady aerodynamics was found to provide good approximation of the frequency response from generator torque, collective pitch and mean wind speed inputs to the generator speed output by using the rigid body rotor rotation mode, the 1st lateral and longitudinal tower modes, the 1st and 2nd collective flap modes and the 1st and 2nd drivetrain torsional modes.

Reduced-order models were subsequently designed by balanced truncation, using a set of basis functions that most efficiently describes the signal energy in the transfer functions from chosen inputs to outputs. Good approximation was obtained using 14 balanced states. Compared to the modal truncation technique, the balanced truncation technique was found to capture the effect of shed vorticity and dynamic stall with only few states, however the mode shapes predicted by balanced truncation does not necessarily resemble the aeroelastic mode shapes of the wind turbine. The reduced-order system matrices obtained by modal and balanced truncation are shown to be suited for parametrization with a parameter that defines the optimal stationary operation with wind speed, by using a unique eigenvalue decomposed form of the system of equations. The reduced-order models obtained by both methods are therefore suited for design of gain-scheduling wind turbine controllers.

Another order reduction method is proposed to reduce the order of aeroelastic models, that use projection of the vector of structural degrees of freedom and aerodynamic state vector onto a reduced set of structural and aerodynamic basis functions, respectively. The order reduction method is tested on the high-order linear aeroelastic model used previously for frequency response analysis, by retaining only the degrees of freedom and aerodynamic states of a single blade. Prior to order reduction it is proposed to transform the aerodynamic states used in the system of equations into new states, that solely describe the lag of unsteady aerodynamic forces, such that the quasi-steady aerodynamic forces are slaves of the structural states. The effect of gradually increasing the structural and aerodynamic complexities in the reduced-order models is evaluated from how the reduced-order models approximate the aeroelastic frequencies and damping of the low-frequency blade modes and on the aeroelastic frequency response from mean wind speed variations to the flap blade root bending moments.

The main findings are that to describe the aeroelastic frequencies and damping of the 1st aeroelastic flap mode it is important to include the 1st structural, torsional blade mode, because of an aeroelastic coupling between flap and torsion, also reported in literature. Accurate approximation of the low-frequency aeroelastic blade frequency response from mean wind speed variations to the flap blade root bending moments is obtained when the effect of high-frequency modes is included by static residualization. It is found, that four aerodynamic basis functions that are slaves of the 1st and 2nd structural blade flap modes can efficiently describe the effect of more than a hundred aerodynamic states used to describe the effects of shed vorticity and dynamic stall along the blade.

5.2 Future work

Some suggestions are now given into relevant future work within the topics treated in the thesis.

Improvements of the reduced-order models

Reduced-order models are designed in the thesis based on a high-order linear aeroelastic model in which linearization is performed around an operational state of the wind turbine defined by e.g. the static forces from an assumed uniform wind speed over the rotor and under assumption of frozen wake.

Previous studies has shown the importance of including dynamic inflow in the control design models, i.e. to describe the time-lag of the induction when the aerodynamic loading on the rotor changes. The typical engineering type models describes the effect of dynamic inflow as a time-lag on the induced velocities using one or more time constants at each aerodynamic calculation point. These engineering type models of dynamic inflow uses too many states in order for the models to be suited for control design. Henriksen [9] has proposed a simplified model of dynamic inflow that includes only a single state to describe the mean changes in the induced velocities over the rotor.

The methodologies described in Chapter 4 may be used to design low-order models of dynamic inflow, by projection with a set of aerodynamic basis functions. One possibility could be to include the effect of dynamic inflow by the aerodynamic shape functions that are slaves of the rigid body pitching motion or found as the distribution of changes in the induction along the blade caused by a harmonic change in the mean wind speed over the rotor.

The proposed methodology in Chapter 4 to use projection with aerodynamic basis functions may also be used to create reduced-order models that captures the aerodynamic loading on the rotor in response to rotor yawing. Previous studies show that the dynamic loading on the rotor when yawing can be accurately predicted by a vortex-lattice model [10]. To capture the aerodynamics of yawing the rotor, one could possibly use either the eigenmodes of the rotor wake or the aerodynamic modes that are slaves of e.g. rigid yawing of the rotor.

Another topic for future work is to design reduced-order linear aeroelastic models for operation around an anisotropic condition. Anisotropy may be caused e.g. by wind shear or blades that are pitched differently. In the thesis, the Coleman transformation is used together with an assumption of isotropy to ensure that the system matrices contains non-periodic terms, which ensures that the models are linear time-invariant. However, the system matrices can also be realized as linear time-invariant models when operating around an anisotropic condition, by using a Lyapunov-Floquet transformation, as described by Skjoldan [61]. The ability to design linear time-invariant models in the case of anisotropy enables, that reduced-order models can be designed using the methods presented and used in the thesis.

Controller and estimator design using reduced-order models

The thesis analyses the effect of model complexity on the open-loop aeroelastic frequency response of a wind turbine and a set of reduced-order models has been design that accurately approximates the wind turbine response of a set of control and disturbance inputs. The thesis describes how to obtain a set of reduced-order models that can be used to design gain-scheduling controllers.

The next step is to use the set of reduced-order models for wind turbine control and estimator design. The set of reduced-order models may be used to design a set of controllers at each local operation point along one or more scheduling variables, and then subsequently make a table look-up on the controller gains at the specific operational point encountered under operation. Such a set of models may also be suited for the fast update of controllers

that use online re-linearization, such as Model Predictive Controllers [9]. It should be analyzed how the closed-loop performance of a wind turbine is improved by changing the complexity of the controller and observer design models.

Bibliography

[1] P.-O. Nissen. *Wind Power - the Danish Way: From Poul la Cour to Modern Wind Turbines*. Poul la Cour Foundation, 2009.

[2] T. Burton, D. Sharpe, N. Jenkins, and E. Bossanyi. *Wind Energy Handbook*. Wiley-Blackwell, September 2001.

[3] European Wind Energy Association. *UpWind - Design limits and solutions for very large turbines*. EWEA, March 2011.

[4] M. O. L. Hansen. *Aerodynamics of Wind Turbines*. Earthscan, August 2012.

[5] H. Snel and J. G. Schepers. Joint investigation of dynamic inflow effects and implementation of an engineering method. Technical Report ECN-C-94-107, Netherlands Energy Research Foundation ECN, Petten, The Netherlands, 1995.

[6] M. O. L. Hansen, J. N. Sørensen, S. Voutsinas, N. Sørensen, and H. Aa. Madsen. State of the art in wind turbine aerodynamics and aeroelasticity. *Progress in Aerospace Sciences*, 42(4):285–330, June 2006.

[7] S. Øye. Unsteady wake effects caused by pitch-angle changes. In *Proceedings of the First IEA Symposium on the aerodynamics of wind turbines*, London, UK, 1986.

[8] N. N. Sørensen and H. Aa. Madsen. Modelling of transient wind turbine loads during pitch motion. In *Proceedings (online)*, Athens, Greece, 2006. European Wind Energy Association.

[9] L. C. Henriksen, M. H. Hansen, and N. K. Poulsen. A simplified dynamic inflow model and its effect on the performance of free mean wind speed estimation. *Wind Energy*, 2012.

[10] J. G. Leishman. Challenges in modelling the unsteady aerodynamics of wind turbines. *Wind energy*, 5(2-3):85–132, 2002.

[11] J. Katz and A. Plotkin. *Low-Speed Aerodynamics*. Cambridge University Press, February 2001.

[12] M. H. Hansen, M. Gaunaa, and H. Aa. Madsen. A Beddoes-Leishman type dynamic stall model in state-space and indicial formulations. Technical Report Risø-R-1354(EN), Risø, National Laboratory, 2004.

[13] W. Mccroskey. Unsteady airfoils. *Annual Review of Fluid Mechanics*, 14:285–311, 1982.

[14] F. Rasmussen, J. T. Petersen, and H. Aa. Madsen. Dynamic stall and aerodynamic damping. *ASME Journal of Solar Energy Engineering*, 121(3):150–155, August 1999.

[15] S. Øye. Dynamic stall simulated as time lag of separation. In *Proceedings of the European Wind Energy Conference*, Thessaloniki, Greece, 1994.

[16] C. Tran and D. Petot. Semi-empirical model for the dynamic stall of airfoils in view of the application to the calculation of responses of a helicopter blade in forward flight. *Vertica*, 5(1):35–53, 1981.

[17] H. Aa. Madsen and F. Rasmussen. A near wake model for trailing vorticity compared with the blade element momentum theory. *Wind Energy*, 7(4):325–341, 2004.

[18] K. C. Hall. Eigenanalysis of unsteady flows about airfoils, cascades, and wings. *AIAA Journal*, 32(12):2426–2432, December 1994.

[19] E. H. Dowell. Eigenmode analysis in unsteady aerodynamics: Reduced-order models. *Aiaa Journal*, 34(8):1578–1583, August 1996.

[20] J. P. Thomas, E. H. Dowell, and K. C. Hall. Static/dynamic correction approach for reduced-order modeling of unsteady aerodynamics. *Journal of Aircraft*, 43(4):865–878, August 2006.

[21] E. H. Dowell, E. F. Crawley, H. C. C. Jr, D. A. Peters, R. H. Scanlan, and F. Sisto, editors. *A Modern Course in Aeroelasticity*. Springer, 3rd edition, June 1995.

[22] K. Saranyasoontorn and L. Manuel. Low-dimensional representations of inflow turbulence and wind turbine response using proper orthogonal decomposition. *Journal of Solar Energy Engineering*, 127(4):553–562, July 2005.

[23] M. H. Hansen, A. Hansen, T. J. Larsen, S. Øye, P. Sørensen, and P. Fuglsang. Control design for a pitch-regulated, variable speed wind turbine. Technical Report Risø-R-1500(EN), Risø National Laboratory, Denmark, January 2005.

[24] M. H. Hansen and F. Zahle. Aeroelastic optimization of MW wind turbines. Technical Report Risø-R-1803(EN), DTU Wind Energy, 2011.

[25] E. A. Bossanyi. Wind turbine control for load reduction. *Wind Energy*, 6(3):229–244, 2003.

[26] W. E. Leithead and S. Dominguez. Coordinated control design for wind turbine control systems. In *Scientific proceedings of the EWEC 2006*, volume 2006, pages 56–59, Athens, Greece, 2006.

[27] B. Fischer. Reducing rotor speed variations of floating wind turbines by compensation of non-minimum phase zeros. In *Scientific proceedings of the EWEA 2012*, pages 144–147, Copenhagen, 2012.

[28] A. D. Wright and M. J. Balas. Design of state-space-based control algorithms for wind turbine speed regulation. *Journal of Solar Energy Engineering*, 125(4):386–395, 2003.

[29] R. R. Craig and M. C. Bampton. Coupling of substructures for dynamic analysis. *AIAA journal*, 6(7):1313–1319, 1968.

[30] R. D. Cook, D. S. Malkus, M. E. Plesha, and R. J. Witt. *Concepts and Applications of Finite Element Analysis*. Wiley, 4 edition, October 2001.

[31] T. van Engelen. Control design based on aero-hydro-servo-elastic linear models from TURBU (ECN). In *Proceedings of the European Wind Energy Conference*, 2007.

[32] E. A. Bossanyi. GH bladed theory manual. Technical Report 282/BR/009, Garrad Hassan and Partners Ltd, 2007.

[33] J. Jonkman and M. Buhl Jr. FAST user's guide. Technical report, NREL, 2005.

[34] S. Kanev and T. van Engelen. Wind turbine extreme gust control. *Wind Energy*, 13(1):18–35, 2010.

[35] K. Selvam, S. Kanev, J. W. van Wingerden, T. van Engelen, and M. Verhaegen. Feedback-feedforward individual pitch control for wind turbine load reduction. *International Journal of Robust and Nonlinear Control*, 19(1):72–91, 2009.

[36] M. Karpel. Design for active flutter suppression and gust alleviation using state-space aeroelastic modeling. *Journal of Aircraft*, 19(3):221–227, 1982.

[37] M. Karpel. Reduced-order aeroelastic models via dynamic residualization. *Journal of Aircraft*, 27(5):449–455, May 1990.

[38] A. C. Antoulas. *Approximation of Large-Scale Dynamical Systems*. Society for Industrial Mathematics, January 2005.

[39] T. Ersal, H. K. Fathy, D. G. Rideout, L. S. Louca, and J. L. Stein. A review of proper modeling techniques. *Journal of Dynamic Systems, Measurement, and Control*, 130(6):1–13, 2008.

[40] B. Moore. Principal component analysis in linear systems: Controllability, observability, and model reduction. *Automatic Control, IEEE Transactions on*, 26(1):17–32, 1981.

[41] E. A. Jonckheere. Principal component analysis of flexible systemsOpen-loop case. *IEEE Transactions on Automatic Control*, 29(12):1095–1097, 1984.

[42] B. S. Kallesøe. Effect of steady deflections on the aeroelastic stability of a turbine blade. *Wind Energy*, 14(2):209–224, 2011.

[43] C. L. Bottasso, A. Croce, Y. Nam, and C. E. D. Riboldi. Power curve tracking in the presence of a tip speed constraint. *Renewable Energy*, 40(1):1–12, April 2012.

[44] F. D. Bianchi, R. J. Mantz, and C. F. Christiansen. Control of variable-speed wind turbines by LPV gain scheduling. *Wind Energy*, 7(1):1–8, 2004.

[45] K. Z. Østergaard, J. Stoustrup, and P. Brath. Linear parameter varying control of wind turbines covering both partial load and full load conditions. *International Journal of Robust and Nonlinear Control*, 19(1):92–116, 2009.

[46] C. L. Lawson and R. J. Hanson. *Solving Least Squares Problems*. Society for Industrial and Applied Mathematics, January 1987.

[47] J. Jonkman, S. Butterfield, W. Musial, and G. Scott. Definition of a 5-MW reference wind turbine for offshore system development. Technical report, NREL, 2009.

[48] Department of Wind Energy, The Technical University of Denmark. Welcome to HAWC2! http://www.hawc2.dk/, Accessed date: 27. April 2012.

[49] P. F. Skjoldan and M. H. Hansen. On the similarity of the Coleman and Lyapunov-Floquet transformations for modal analysis of bladed rotor structures. *Journal of Sound and Vibration*, 327(3-5):424–439, November 2009.

[50] T. J. Larsen. How 2 HAWC2 , the user's manual (ver. 3-9)(EN). Technical Report Risø-R-1597, Risø, DTU, 2010.

[51] A. Kretz, H. Aa. Madsen, and J. T. Petersen. Measured and simulated turbulence - compared at a section of a rotating wind turbine blade. Technical Report Risø-R-672(EN), Risø, National Laboratory, March 1994.

[52] S. Øye. FLEX4 simulation of wind turbine dynamics. In *Proceedings of the 28th IEA Meeting of Experts*, volume Annex XI, pages 71–77, 1996.

[53] K. Holm-Jørgensen and S. R. K. Nielsen. System reduction in multibody dynamics ofwindturbines. *Multibody System Dynamics*, 21(2):147–165, October 2008.

[54] M. H. Hansen. Aeroelastic properties of backward swept blades. In *Proceedings of the 49th AIAA Aerospace Sciences Meeting Including the New Horizons Forum and Aerospace Exposition*, Orlando, Florida, 2011.

[55] M. H. Hansen. Aeroelastic instability problems for wind turbines. *Wind Energy*, 10(6):551–577, 2007.

[56] F. W. Fairman. *Linear Control Theory: The State Space Approach*. Wiley-Blackwell, April 1998.

[57] A. J. Laub, M. T. Heath, C. C. Paige, and R. C. Ward. Computation of system balancing transformations and other applications. *Ieee Transactions on Automatic Control*, 32(2):115–122, February 1987.

[58] G. Obinata and B. D. O. Anderson. *Model Reduction for Control System Design*. Springer, 1 edition, December 2000.

[59] J. J. Thomsen. *Vibrations and stability: Advanced theory, analysis, and tools*. Springer, Berlin; New York, 2003.

[60] B. S. Kallesøe, J. J. Thomsen, and M. H. Hansen. *Aeroservoelasticity of Wind Turbines*. PhD thesis, Technical University of Denmark, Department of Mechanical Engineering, 2007.

[61] P. F. Skjoldan, M. H. Hansen, R. Rubak, and K. Thomsen. *Aeroelastic modal dynamics of wind turbines including anisotropic effects*. Risø-PhD-66(EN). Danmarks Tekniske Universitet, Risø National laboratoriet for Bæredygtig Energi, 2011.

Publications P1-P3

P1

Open-loop frequency response analysis of a wind turbine using a high-order linear aeroelastic model

Wind Energy, (accepted in revised form, March 2013)

WIND ENERGY
Wind Energ. 2012; **00**:1–**??**
DOI: 10.1002/we

RESEARCH ARTICLE

Open-loop frequency response analysis of a wind turbine using a high-order linear aeroelastic model

Ivan Sønderby and Morten H. Hansen

Department of Wind Energy, Technical University of Denmark, Roskilde, Denmark

ABSTRACT

Wind turbine controllers are commonly designed based on low-order linear models to capture the aeroelastic wind turbine response due to control actions and disturbances. This paper characterize the aeroelastic wind turbine dynamics that influence the open-loop frequency response from generator torque and collective pitch control actions of a modern non-floating wind turbine based on a high-order linear model. The model is a linearization of a geometrically nonlinear finite beam element model coupled with an unsteady Blade Element Momentum model of aerodynamic forces including effects of shed vorticity and dynamic stall. The main findings are that the lowest collective flap modes have limited influence on the response from generator torque to generator speed, due to large aerodynamic damping. The transfer function from collective pitch to generator speed is affected by two non-minimum phase zeros below the frequency of the 1st drivetrain mode. To correctly predict the non-minimum phase zeros, it is essential to include lateral tower and blade flap degrees of freedom.

KEYWORDS

wind turbine control design, linear control design models, wind turbine aeroelasticity, modal analysis

Correspondence

I. Sønderby, Technical University of Denmark, Department of Wind Energy, DTU Risø Campus, DK-4000 Roskilde, Denmark. E-mail: ivsq@dtu.dk

Received . . .

1. INTRODUCTION

Most modern wind turbines operate with variable rotor speed and are controlled by generator torque and collective pitch control. The primary task of the wind turbine controller is to optimize the generated power below rated wind speed and to reduce the aerodynamic loading and maintain the rated rotor speed above rated wind speed. Below rated wind speed, the generator torque is usually used to control the rotor speed for optimal energy extraction. Above rated collective pitch and generator torque are used in combination to keep constant rotor speed and generated power. Proper design of a wind turbine controller can reduce power variations, fatigue and extreme loads on components and prevent instabilities to occur. The controller must be designed on a model that correctly predicts the aero-servo-elastic response of the wind turbine to meet the objectives of the controller. This article seeks to answer the question: What is important to include in a model for wind turbine control design?

Bossanyi [1] has investigated the necessary model complexity used for control design of a pitch-regulated, variable-speed non-floating wind turbine. When operating in generator torque control, he suggests to use a model that contains at least rigid-body rotation of the drivetrain and rotor and the first torsional drivetrain mode by coupling of the rotor inertia to a generator inertia by a torsional spring. For above rated operation using collective pitch control, he suggests also to model at least the inertia of the rotor and generator, the pitch actuator and the longitudinal tower vibration, because the pitch controller can excite the longitudinal tower vibration and therefore must be included in the model.

Wright & Balas [2] investigate how the complexity of the control design model influence collective pitch control of a two-bladed turbine. They find that it is important to include rigid-body rotor rotation, drivetrain flexibility, the first collective flap modes and longitudinal tower bending mode. To ensure stable closed-loop behavior the controller model must include the free-free drivetrain mode.

Linear wind turbine models for control design are provided by the TURBU tool [3]. The control design models are found by retaining the low-frequency aeroelastic modes of the tower and blade components by order reduction of a high-order linear wind turbine model. The control design models predicts the open- and closed-loop frequency responses from collective pitch to rotor speed among others [3]. However, the effect of modeled aerodynamics and structural dynamics on the aeroelastic frequency response is not directly addressed. There are examples of use of linearized models provided by TURBU for extreme gust control [4] and individual pitch control [5].

Leithead et.al. [6] analyze the frequency response from collective pitch demand to generator speed and show existence of a non-minimum phase zero at the 1st tower modes and show how to compensate for them in closed-loop operation. The non-minimum phase zero is a limitation on the bandwidth of the pitch to speed controller because of the large negative change in phase occurring at the zero which is not cancelled by the poles of the tower motion. The change in phase associated with the non-minimum phase zero makes the speed respond opposite to that of a minimum phase zero and must therefore be correctly predicted. The non-minimum phase zeros is a problem for large turbines and especially for offshore turbines, because of the low tower frequencies. Fischer [7] clarifies under what conditions that the non-minimum phase zero exists from a simplified model including a longitudinal tower degree of freedom and one state to describe rigid-body rotor rotation. Changes in the aerodynamic forces are modeled with quasi-steady gradients of rotor torque and thrust from changes in pitch and in the relative wind speed seen by the rotor.

The purpose of this article is to characterize the aeroelastic wind turbine dynamics that affects the frequency response of a modern, three-bladed, landbased wind turbine in open-loop. The open-loop response is analyzed based on a high-order linear model and serves as a benchmark for validation of predictions of low-order models used in control design for wind turbines. The aeroelastic wind turbine response is analyzed using a linear aeroelastic wind turbine model recently developed in house called HAWCStab2 that is similar to an older model [8] except for a new nonlinear kinematic formulation. The model is a linearization of a nonlinear co-rotational finite beam element model coupled with an unsteady Blade Element Momentum model of aerodynamic forces including effects of shed vorticity and dynamic stall [9]. The paper analyze the aeroelastic wind turbine frequency response of generator speed under generator torque and collective pitch demand control inputs for small vibrations about steady state for operation at various wind speeds and with varying model complexity. The main findings are that the frequency response from generator torque to speed is affected by the lateral tower modes close to their aeroelastic frequencies due to nacelle roll, whereas the lowest collective flap modes are not important to include because of their high aerodynamic damping. Both longitudinal and lateral tower motion are found to affect predictions of the non-minimum phase zero at the 1st tower modes in the transfer function from collective pitch to speed, opposed to previous investigations [7] that only include the longitudinal tower motion. It is found, that collective flap vibration introduces another non-minimum phase zero below the frequency of the 1st drivetrain mode if pitch actuator dynamics is neglected.

This paper contains first a description of the high-order linear aeroelastic model of the NREL 5 MW wind turbine used in the subsequent analysis. The linear aeroelastic model is then validated with a nonlinear aeroelastic model by comparing the aeroelastic frequency response functions from collective pitch angle demands and generator torque control actions for small amplitude inputs for normal operation at 8 m/s and 20 m/s. The complexity of the linear model is then varied to clarify what must be included to capture the aeroelastic frequency response from generator torque to generator speed for operation at 8 m/s and 20 m/s and from collective pitch inputs to generator speed for operation at 14 m/s and 20 m/s to exemplify operation at all wind speeds.

2. HIGH-ORDER LINEAR AEROELASTIC MODEL

This section contains a description of the linear aeroelastic model of the NREL 5 MW onshore wind turbine defined by Jonkman et.al.[10] and used for subsequent frequency response analysis. The model is identical to the available HAWC2 model [11] except that the static tilt is set to 0 deg to ensure uniform inflow. The structural damping of the drivetrain is lowered, by changing the Rayleigh parameter for stiffness proportional damping of torsional motion from 0.0184 Nm·s/Nm to 0.0120 Nm·s/Nm.

2.1. Model description

The high-order model used for frequency response analysis is the recent linear aeroelastic model HAWCStab2 developed in house. A more complete description of the linear aeroelastic model is provided by Hansen [9] for an isolated blade. The model is a linearization of a geometrically nonlinear finite beam element model coupled with an unsteady Blade Element Momentum model of aerodynamic loads on the blades including effects of shed vorticity and dynamic stall. So far, the model assumes frozen wake and does not include a model of dynamic inflow. A comparison is made using nonlinear time-simulations to clarify the effect of dynamic inflow.

Wind Energ. 2012; **00**:1–?? © 2012 John Wiley & Sons, Ltd.
DOI: 10.1002/we
Prepared using weauth.cls

Linearization is performed analytically around a stationary deflected state of the blades obtained from an equilibrium between elastic and centrifugal forces and the static aerodynamic forces due to an assumed uniform inflow to the rotor plane. Gravity forces are neglected to obtain this stationary steady operational state for any operational point given by a mean wind speed, pitch angle and rotor speed.

The discretization used in the finite beam element model is illustrated in Figure 1. The number of elements used to model the tower, drivetrain and each blade are eight, four and 19 Timoshenko beam elements, respectively. Four elements are used for the drivetrain to ensure correct modeling of bending and torsion of the drivetrain. Each element has two nodes and six degrees of freedom (DOFs) per node to describe rotation and translation in all three axis. The generator and pitch bearings are modeled as frictionless bearings. Pitch actuators are modeled by second order response of actual pitch to demanded input. The aeroelastic turbine dynamics is investigated without effect of actuators, and the frequency of the actuator model is therefore set so high that the demanded pitch angle is reached almost instantly for the frequency range analyzed. Aerodynamic forces on the blades are modeled by using 30 aerodynamic calculation points distributed such that they are closely spaced at the blade root and tip. The model of unsteady aerodynamics includes at each aerodynamic calculation point, two states to approximate the frequency response of the Theodorsen theory and two states are used to describe trailing edge separation and dynamic stall as described in Hansen et.al. [12].

All degrees of freedom describing blade and hub motion and all aerodynamic states are transformed into multiblade coordinates by the Coleman transformation to remove dependency of the rotor azimuth angle in the system matrices. The state vector $\mathbf{z}_k$ that describes the structural and aerodynamical states for blade k in blade-fixed coordinates, is transformed into multiblade coordinates by the Coleman transformation:

$$\mathbf{z}_k = \mathbf{a}_o + \mathbf{a}_1 \cos\left(\Omega t + \tfrac{2\pi}{3}(k-1)\right) + \mathbf{b}_1 \sin\left(\Omega t + \tfrac{2\pi}{3}(k-1)\right),\ k = 1,2,3 \tag{1}$$

where $\mathbf{a}_0$, $\mathbf{a}_1$ and $\mathbf{b}_1$ are the collective and the two cyclic components of $\mathbf{z}$, respectively. When the blades are identical and identically mounted (isotropic rotor) and the wind speed is uniform over the rotor and perpendicular to the rotor, then the Coleman transformation removes dependency of the azimuth angle in the system matrices of the linearized aeroelastic model [13].

2.2. Equations of motion

The linear high-order aeroelastic model is described by the system of equations

$$\mathbf{M}\ddot{\mathbf{z}}_s + (\mathbf{C}_s + \mathbf{G} + \mathbf{C}_a)\dot{\mathbf{z}}_s + (\mathbf{K} + \mathbf{K}_a + \mathbf{K}_{sf})\mathbf{z}_s + \mathbf{A}_f\mathbf{x}_a = \mathbf{F}_s \tag{2a}$$

$$\dot{\mathbf{x}}_a + \mathbf{A}_d\mathbf{x}_a + \mathbf{C}_{sa}\dot{\mathbf{z}}_s + \mathbf{K}_{sa}\mathbf{z}_s = \mathbf{F}_a \tag{2b}$$

where Equation (2a) governs structural vibration and Equation (2b) describes the aerodynamic states used to model unsteady aerodynamics on the blades. The matrices $\mathbf{M}$, $\mathbf{K}$ and $\mathbf{C}_s$ are the mass, stiffness and structural damping matrix, respectively. The stiffness matrix models both elastic stiffness and centrifugal blade stiffness. The matrix $\mathbf{G}$ models gyroscopic forces on the blades and $\mathbf{C}_a$ and $\mathbf{K}_a$ are the aerodynamic damping and stiffness matrices, respectively. The aerodynamic states couples to the structural states through the term $\mathbf{A}_f\mathbf{x}_a$ and the structural dynamics excites the aerodynamic states through both a velocity dependent term $\mathbf{C}_{sa}\dot{\mathbf{z}}_s$ and a translation/rotation dependent term $\mathbf{K}_{sa}\mathbf{z}_s$. The matrix $\mathbf{A}_d$ describes the lag on the aerodynamic loads. The terms $\mathbf{F}_s$ and $\mathbf{F}_a$ represents structural and aerodynamical forces due to actuators and changes in the wind speed.

An eigenvalue problem can be set up directly on the first order form of Equations (2) but to improve its conditioning the structural vector of DOFs is transformed using a reduced set of structural undamped eigenvectors and leaving bearing DOF untransformed. Transformation is done using half the number of elastic modes for each substructure of the turbine model corresponding to the modes with lowest frequency. The modes are determined for each substructure by assuming that the given substructure is fixed in one end and that all other substructures are rigid. The transformation is $\mathbf{z}_s = \mathbf{\Phi}_{sr}\mathbf{q}_{sr}$, where $\mathbf{\Phi}_{sr}$ is the projection matrix with eigenvectors in columns and $\mathbf{q}_{sr}$ is the new reduced vector of generalized coordinates. The applied transformation cause no visible error on the frequency responses analyzed in later sections. After transformation of the vector of structural DOF, the system in Equations (2) can be written as

$$\mathbf{M}\mathbf{\Phi}_{sr}\ddot{\mathbf{q}}_{sr} + (\mathbf{C}_s + \mathbf{G} + \mathbf{C}_a)\mathbf{\Phi}_{sr}\dot{\mathbf{q}}_{sr} + (\mathbf{K} + \mathbf{K}_a + \mathbf{K}_{sf})\mathbf{\Phi}_{sr}\mathbf{q}_{sr} + \mathbf{A}_f\mathbf{x}_a = \mathbf{F}_s \tag{3a}$$

$$\dot{\mathbf{x}}_a + \mathbf{A}_d\mathbf{x}_a + \mathbf{C}_{sa}\mathbf{\Phi}_{sr}\dot{\mathbf{q}}_{sr} + \mathbf{K}_{sa}\mathbf{\Phi}_{sr}\mathbf{q}_{sr} = \mathbf{F}_a \tag{3b}$$

The system in Equations (3) is put on first order form:

$$\dot{\mathbf{x}} = \mathbf{A}\mathbf{x} + \mathbf{B}\mathbf{u} \tag{4a}$$

$$y = \mathbf{C}\mathbf{x} \tag{4b}$$

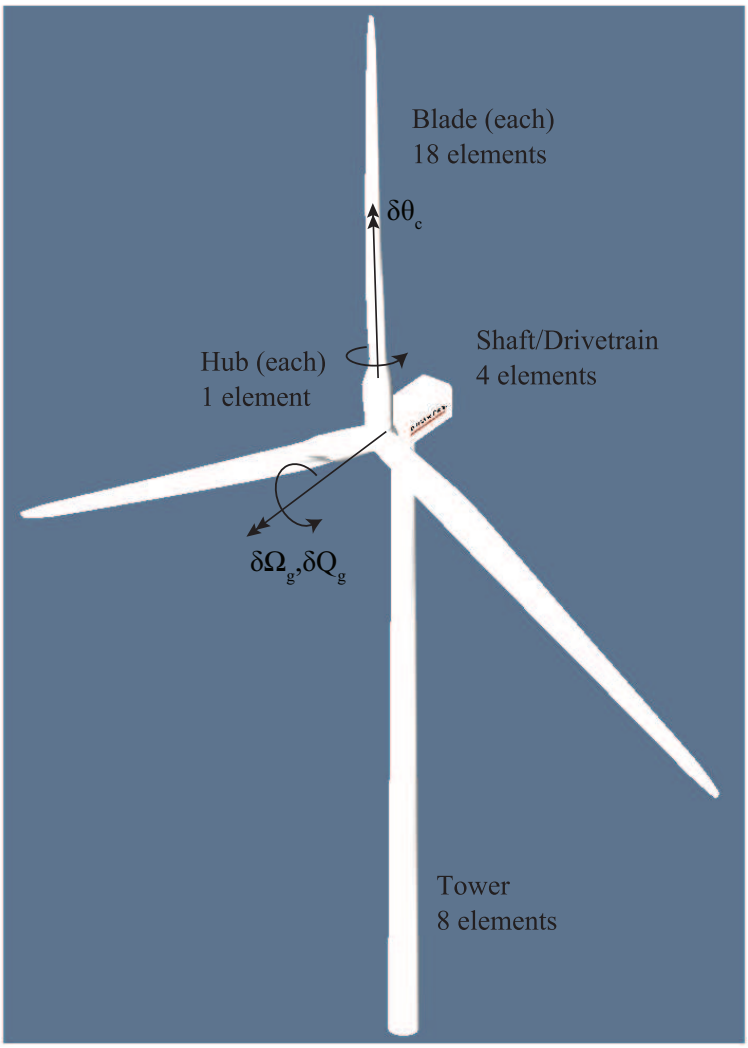

Figure 1. Snap shots from HAWCStab2 animation of NREL wind turbine listing the number of elements and showing the definitions of positive directions of inputs and outputs.

where in the present analysis:

$$\mathbf{x} = \begin{Bmatrix} \mathbf{x}_a \\ \mathbf{q}_{sr} \\ \dot{\mathbf{q}}_{sr} \end{Bmatrix} \quad ; \quad \mathbf{u} = \begin{Bmatrix} \delta Q_g \\ \delta\theta_c \end{Bmatrix} \quad ; \quad y = \{ \ \delta\Omega_g \ \} \tag{5}$$

$$\mathbf{A} = \begin{bmatrix} -\mathbf{A}_d & -\mathbf{K}_{sa}\mathbf{\Phi}_{sr} & -\mathbf{C}_{sa}\mathbf{\Phi}_{sr} \\ \mathbf{0} & \mathbf{0} & \mathbf{I} \\ -\mathbf{M}_{pj}^{-1}\mathbf{\Phi}_{sr}^T\mathbf{A}_f & -\mathbf{M}_{pj}^{-1}\mathbf{\Phi}_{sr}^T(\mathbf{K}+\mathbf{K}_a+\mathbf{K}_{sf})\mathbf{\Phi}_{sr} & -\mathbf{M}_{pj}^{-1}\mathbf{\Phi}_{sr}^T(\mathbf{C}+\mathbf{G}+\mathbf{C}_a)\mathbf{\Phi}_{sr} \end{bmatrix} \tag{6}$$

$$\mathbf{B} = \begin{bmatrix} \mathbf{0} \\ \mathbf{0} \\ \mathbf{M}_{pj}^{-1}\mathbf{\Phi}_{sr}^T\mathbf{B}_{us} \end{bmatrix} \quad ; \quad \mathbf{C} = \begin{bmatrix} \mathbf{0} & \mathbf{0} & 0...1...0 \end{bmatrix} \tag{7}$$

where $\mathbf{M}_{pj} = \mathbf{\Phi}_{sr}^T\mathbf{M}\mathbf{\Phi}_{sr}$ is the projected mass matrix and $\mathbf{B}_{us}$ is defined from

$$\mathbf{F}_s = \mathbf{B}_{us} \begin{Bmatrix} \delta Q_g \\ \delta\theta_c \end{Bmatrix} \tag{8}$$

Focus here is on the response of generator torque and collective pitch demand inputs which means that there are no forces on the aerodynamic equation such that $\mathbf{F}_a = \mathbf{0}$. Forces due to actuators $\mathbf{F}_s$ are linearized with respect to the inputs, by

Wind Energ. 2012; **00**:1–?? © 2012 John Wiley & Sons, Ltd.
DOI: 10.1002/we
Prepared using weauth.cls

retaining the linear term in the Taylor expansions of variations in the inputs around static generator torque and static pitch torque at each operation point. The output matrix $\mathbf{C}$ extracts the generator speed variations $\delta\Omega_g$. Figure 1 shows the definitions of positive inputs and outputs. There is no gearbox model, i.e., the low speed shaft (LSS) speed of the generator is used in the analysis.

In Section 4, the linear model is used to analyze the frequency response functions between each input and each output. To investigate the effects of model complexity, different versions of the linear model is used: Substructures may be made rigid by removing the DOFs in the projection matrix $\mathbf{\Phi}_{sr}$. In cases referred to as *purely structural*, the mean aerodynamic forces are included to find the static blade deflection, but the variation of aerodynamic forces are removed in the linear system of equations. In cases referred to as *'unst.aerodyn.'*, the model includes unsteady airfoil aerodynamics, whereas quasi-steady airfoil aerodynamics is referred to as *'qs.aerodyn.'*. The assumption of quasi-steady airfoil aerodynamics is achieved by setting $\dot{\mathbf{x}}_a = \mathbf{0}$ in Equation (3b), solving for $\mathbf{x}_a$ and inserting the solution in (3a).

If all substructures are made rigid, only the generator bearing is retained, and quasi-steady aerodynamics is assumed, the linear model reduces to the simple 1st order model proposed by Bossanyi [1] and often used in control design models:

$$I_r \delta\dot{\Omega}_g = \delta Q_g + \left.\frac{\partial Q}{\partial \Omega}\right|_0 \delta\Omega_g + \left.\frac{\partial Q}{\partial \theta}\right|_0 \delta\theta_c \tag{9}$$

where I_r is the total rotational inertia of the drivetrain and rotor and Q is the aerodynamic torque on the rotor. The frequency responses predicted with the high-order linear model are compared with the predictions using this 1st order model. In this analysis the gradients of the aerodynamic torque assumes that the wake is frozen such that there is no change in the induction for changes away from the operation point. Bossanyi [1] does not say whether frozen-wake or quasi-steady gradients are used in his analysis, but in Burton et.al. [14] it is suggested to use the quasi-steady gradients.

3. VALIDATION WITH TIME-SIMULATIONS USING NONLINEAR MODEL

This section presents a validation of the aeroelastic frequency response predicted by the linear model with the response predicted by the nonlinear aeroelastic model HAWC2 [15]. Validation is done on the frequency response from generator torque and collective pitch to generator speed for the NREL 5 MW wind turbine operating at 8 and 20 m/s for small amplitude input signals. The effects of dynamic inflow are clarified by validation with the nonlinear model. The linear aeroelastic model is then used to perform aeroelastic modal analysis to explain the sources of resonances in the frequency responses.

3.1. Frequency response

The frequency response functions predicted by the linear model given by Equation (4) is found from the transfer function matrix $\mathbf{G}(s)$, which is the ratio of the Laplace transform of the output $Y(s)$ to the Laplace transform of the inputs $\mathbf{U}(s)$:

$$\mathbf{G}(s) = \frac{Y(s)}{\mathbf{U}(s)} = \mathbf{C}(s\mathbf{I} - \mathbf{A})^{-1}\mathbf{B} \tag{10}$$

where s is the complex Laplace variable. The steady amplitude and phase shift relative to the input is found by matrix inversion as the modulus and phase of $\mathbf{G}(i\omega)$, where $i = \sqrt{-1}$ and ω is the excitation frequency.

The nonlinear aeroelastic model used in the simulations includes geometrical nonlinearities due to large deflections, nonlinear unsteady and wake aerodynamics and nonlinear couplings between structural degrees of freedom and aerodynamic states. Structural damping is modeled as Rayleigh type damping where damping is assumed proportional to structural stiffness and inertia. Spectral damping is used in the linear model, where a damping matrix is deduced that gives a specific damping ratio to each structural mode. Structural damping in the linear model is tuned to approximate the structural damping in the nonlinear model at standstill. The nonlinear aeroelastic model includes dynamic inflow modeled as two 1st order filters with radial dependent time constants. The two filters models the dynamic contribution to the induction from the far wake and the near wake, respectively [15, 16].

Figure 2 shows a typical time-series of variations in generator LSS speed used for the extraction of the frequency response function from HAWC2. The left diagram shows the time-series at start up and until reaching close to steady state. The large overshoot on the speed during the initial transients has no influence on the present analysis. Excitation from gravity forces, wind shear, tower shadow and wind turbulence are removed to reach close to stationary state. The rotor accelerates until generator torque and collective pitch control actions limits the rotational speed to around 12.1 rpm. At $t = 200$ s, the pitch angles are fixed to the desired value which is slightly different than that set by the controller, thereby causing a slight disturbance on the speed signal which is dampened by the generator torque control. At $t = 295$ s, generator torque is fixed and harmonic signal is overlayed at $t = 300$ s on static generator torque and collective pitch separately, until

the end of the simulation. The overlayed harmonic changes in generator torque and collective pitch has amplitudes of 48.5 kNm on the low speed shaft and 0.5 deg, respectively. A total of 205 simulations has been performed for each operation point and input type using harmonic excitation at different frequencies, such that the frequency response can be obtained in an interval $]0;3]$ Hz.

After transients have dampened out a Fourier transformation is done on a time signal spanning one period at the excitation frequency. In simulations where the generator torque and collective pitch angles are varied at frequencies below 0.1 Hz, the signal is extracted from $t = 1300$ s. For excitation frequencies above 0.1 Hz, the signal is extracted from $t = 800$ s. Figure 2d shows the time-series used for Fourier transformation. The time step size is set such that one period at the excitation frequency includes 2^N samples, where $N \in [6;14]$ depending on the excitation frequency. It is ensured that the sampling frequency is always higher than 50 Hz for excitation frequencies below 0.1 Hz and always higher than 100 Hz for excitation frequencies above 0.1 Hz, to avoid damping and frequency shifts introduced by the Newmark time-integration scheme used in HAWC2.

Estimates of the linear frequency response are achieved by taking the Fourier amplitude and phase at the excitation frequency, whereby remaining nonlinear and transient effects are minimized. Figures 3 and 4 show comparisons of the frequency response from generator torque and collective pitch demand to generator speed, respectively, predicted by the linear and nonlinear models at 8 m/s and 20 m/s. The response predicted by the linear model is similar to the response obtained from nonlinear time-simulations for small excitation amplitudes. The responses deviates around 1.6 Hz and 2.7 Hz, which can be explained by differences in the models of structural damping of the 1st and 2st drivetrain modes, because the responses can be made to fit, separately at 8 m/s and 20 m/s, by applying small changes in the structural drivetrain damping in the linear model. Note the large phase drop at the tower frequency in Figure 4 which is 720 deg and 360 deg for operation at 8 m/s and 20 m/s, respectively, due to the non-minimum phase zeros as discussed later.

The time-simulations with the nonlinear model include effects of dynamic inflow whereas the linear model assumes frozen wake. Dynamic inflow has no significant effect on the frequency response from generator torque to speed at both 8 m/s and 20 m/s, but it affects the frequency response from collective pitch to speed for operation at lower wind speeds. At 8 m/s, Figure 4a shows that dynamic inflow affects the response around the 1st tower modes at 0.32 Hz and below by decreasing the amplitude and increasing the phase relative to frozen wake response. The reason is that the axial induction increases when pitching to stall such that the inflow velocity decreases. Thus, the influence of dynamic inflow is to give a negative change in aerodynamic rotor torque, which counteracts the positive change in torque due to higher angles of attack. As a result, a lower change in rotor speed is needed at 0 Hz to establish zero net variations in the aerodynamic torque on the rotor. At high wind speeds the axial induction factors are small and therefore the effect of the wake dynamics is small already at 14 m/s (not shown).

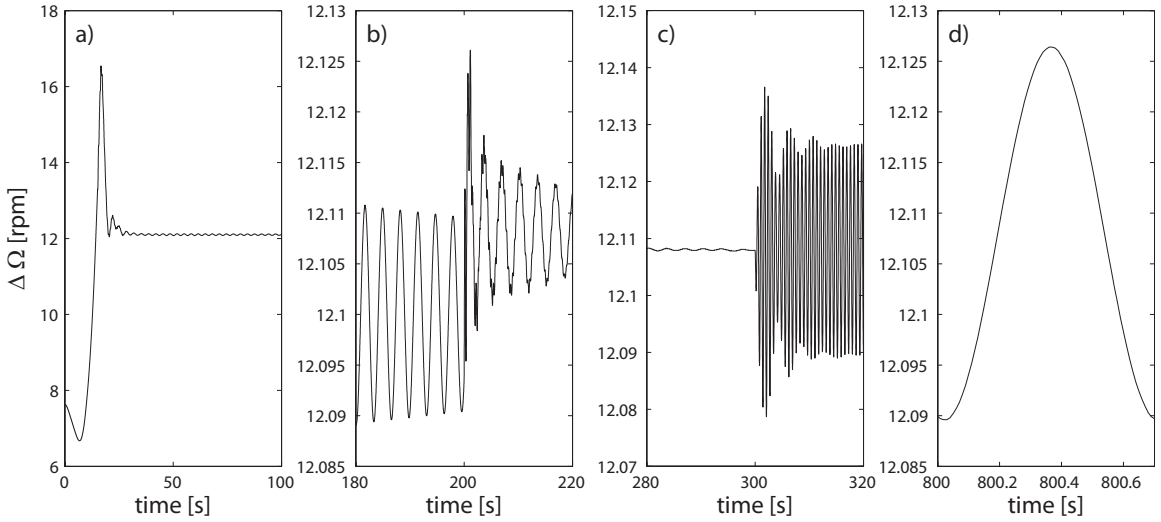

Figure 2. Typical time-series of generator speed from simulations using nonlinear aeroelastic model by subsequent FFT analysis a) at start up, b) before and after pitch angle is fixed, c) before and after harmonic excitation is initiated and d) of the assumed stationary variation.

Wind Energ. 2012; **00**:1–?? © 2012 John Wiley & Sons, Ltd.
DOI: 10.1002/we
Prepared using weauth.cls

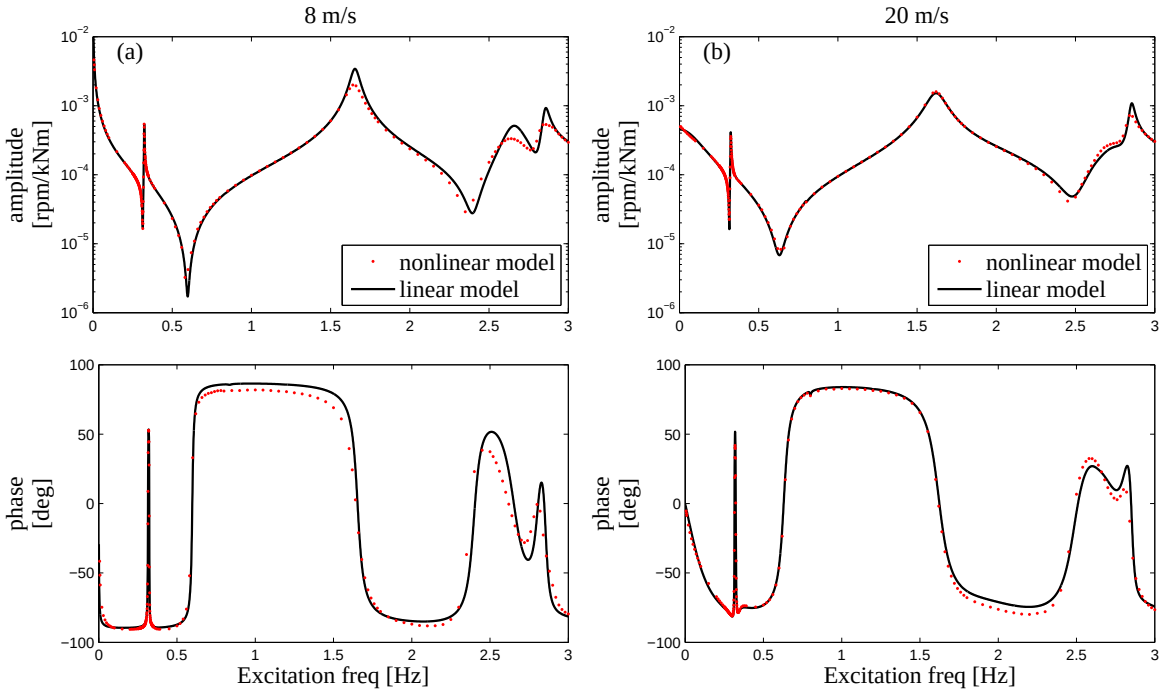

Figure 3. Aeroelastic frequency response from generator torque δQ_g to generator speed $\delta\Omega_g$ for NREL 5 MW wind turbine in operation at 8 and 20 m/s. Validation of aeroelastic frequency response predicted by linear model with time-simulations using nonlinear aeroelastic model.

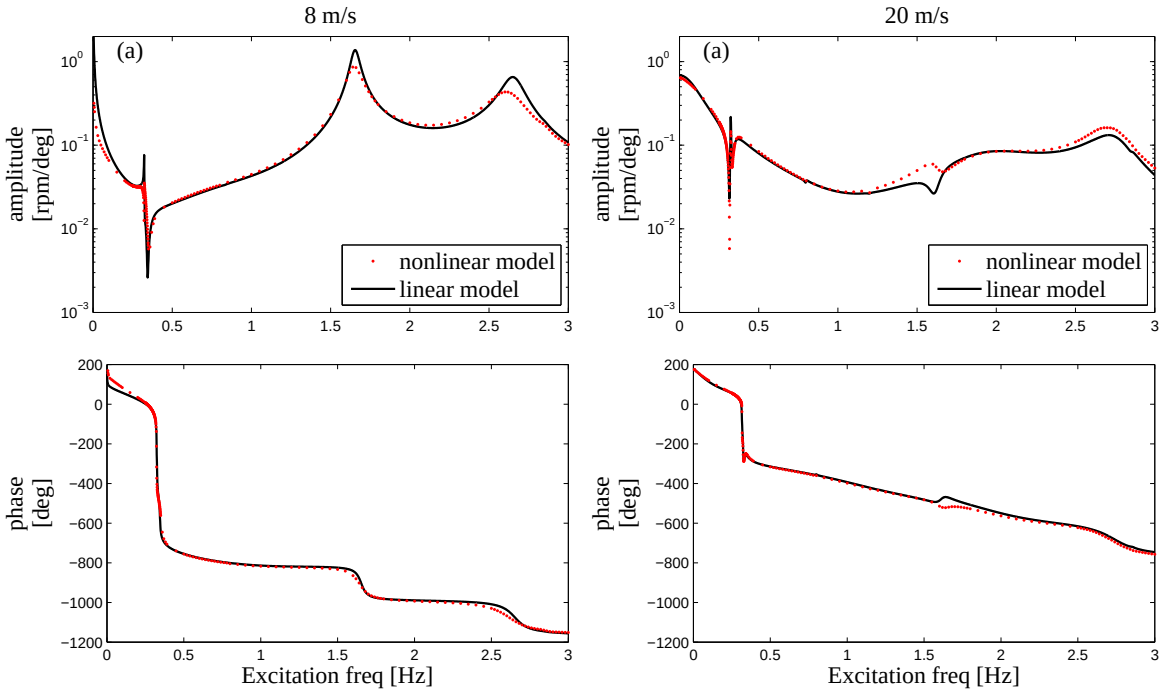

Figure 4. Aeroelastic frequency response from collective pitch angle $\delta\theta_c$ to generator speed $\delta\Omega_g$ for NREL 5 MW wind turbine in operation at 8 and 20 m/s. Validation of aeroelastic frequency response predicted by linear model with time-simulations using nonlinear aeroelastic model.

3.2. Aeroelastic modal analysis

The linear aeroelastic model is used to determine the aeroelastic modes responsible for the dynamics in the frequency response shown in Figures 3 and 4. The homogenous solution to Eq. (4a) is:

$$\mathbf{x} = \mathbf{v}e^{\lambda t} = \mathbf{v}e^{\alpha t}(\cos\omega t + i\sin\omega t) \tag{11}$$

where $\mathbf{v}$ and λ are solutions to the algebraic eigenvalue problem:

$$(\mathbf{A} - \lambda\mathbf{I})\mathbf{v} = \mathbf{0} \tag{12}$$

and $\mathbf{v}$ is an eigenvector and $\lambda = \alpha + i\beta$ the corresponding eigenvalue.

The solution to the eigenvalue problem (12) consists of structurally and aerodynamically dominated modes. The structurally dominated modes consist mainly of pairs of complex conjugated eigenvectors and eigenvalues and are characterized by the aeroelastic damping ratio ξ and aeroelastic frequency ω given by:

$$\omega = \mathrm{Im}\{\lambda\} \qquad \xi = -\mathrm{Re}\{\lambda\}/|\lambda| \tag{13}$$

Table I lists the aeroelastic frequencies and damping of structurally dominated modes ordered according to the aeroelastic frequency for operation at 8 m/s, 14 m/s and 20 m/s. Due to the free generator bearing, there is a mode, that describes rigid-body rotation of the drivetrain and rotor in the generator bearing. This rigid-body rotation mode is a 1st order mode at 8 m/s and 14 m/s and a highly damped 2nd order mode at 20 m/s. In operational points where the blades are pitched, rigid-body rotation of drivetrain and rotor couple structurally with collective flap motion, such that vibrational energy in the rotor rotation is transferred to collective flap vibration, which is not entirely limited by aerodynamic damping, whereby the rigid-body rotation mode becomes a 2nd order mode. Most modern wind turbines have the same order of some of the structurally dominated modes. The 1st tower modes will typically have lower frequency than the 1st collective flap mode, because of large rotor inertia in the tower motion.

The aerodynamic modes (not listed in Table I) describe dynamics in the local aerodynamic forces in each radial section of the rotor. In the model of unsteady airfoil aerodynamics it is assumed that aerodynamic forces at one radial section is uncoupled from aerodynamic forces in the other sections along the blade, except for coupling through the structural motion. The aerodynamic modes are either cyclic aerodynamic modes that vibrates at the frequency of the rotor speed, or collective modes that has real eigenvalue and are characterized by their time constant $\tau = -1/\lambda$. The collective aerodynamic modes has cut-off frequencies from 0.07 Hz up to 17.0 Hz depending on the relative inflow velocity. Aerodynamic modes with low cut-off frequencies represent dynamics of shed vorticity and dynamic stall in blade sections close to the blade root, because the relative inflow velocity is smaller here and the time constants therefore larger [12].

Table I. Open-loop aeroelastic frequencies and damping of structurally dominated modeshapes with low aeroelastic frequency for NREL 5 MW turbine operating at 8, 14 and 20 m/s.

nr.	ω [Hz]	ξ [%]	ω [Hz]	ξ [%]	ω [Hz]	ξ [%]	Description
	8 m/s		14 m/s		20 m/s		
1	λ = -0.0112 rad/s		λ = -0.0184 rad/s		0.035	95.9	Rigid-body rotation of shaft and rotor
2	0.32	0.38	0.32	0.44	0.32	0.61	1st lateral tower
3	0.33	6.19	0.33	7.30	0.33	7.98	1st longitudinal tower
4	0.57	64.1	0.60	77.3	0.63	80.0	1st backward whirling blade flap
5	0.84	54.8	0.80	0.69	0.80	0.56	1st backward whirling blade edge
6	0.78	1.45	0.81	68.1	0.84	71.4	1st collective blade flap
7	0.91	47.9	0.99	60.8	1.01	65.2	1st forward whirling blade flap
8	1.18	1.76	1.20	1.11	1.20	0.81	1st forward whirling blade edge
9	1.55	16.4	1.52	20.9	1.53	21.7	2nd backward whirling blade flap
10	1.65	2.4	1.65	2.43	1.62	3.14	1st collective blade edge/drive train torsion
11	1.92	12.5	1.93	17.0	1.93	16.6	2nd collective blade flap
12	1.89	13.7	1.93	15.3	1.94	16.3	2nd forward whirling blade flap
13	2.63	1.92	2.64	2.04	2.62	2.10	2nd longitudinal tower
14	2.65	3.62	2.68	3.76	2.73	3.89	2nd collective edge/drive train torsion
15	2.76	3.34	2.77	3.77	2.75	3.65	1st tower torsion (yaw)
16	2.85	0.71	2.85	0.70	2.85	0.62	2nd lateral tower

Wind Energ. 2012; **00**:1–?? © 2012 John Wiley & Sons, Ltd.
DOI: 10.1002/we
Prepared using weauth.cls

4. FREQUENCY RESPONSE ANALYSIS USING HIGH-ORDER LINEAR MODEL

The last section showed that the linear aeroelastic model accurately predicts the frequency response from generator torque and collective pitch actions to generator speed compared to a nonlinear model. In this section, the complexity of the linear model is varied by changing the number of state variables to clarify what must be included in a model to capture these responses. In each case, the purely structural response due to the actuator input is investigated before the aeroelastic response, to see the effect of structural dynamics. A separate section is in each case used to analyze the response at the 1st tower modes.

It is desirable that the speed/power controller can handle effects of fluctuations in the inflow due to e.g. wind shear, which is responsible for mainly 1P and 2P loads on the blades and 3P and 6P loads on the tower, where 1P is the rotational frequency of the rotor, equal to 0.2 Hz at above rated wind speeds. Wind speed fluctuations due to turbulence are generally more low-frequent [14]. Thus, it is desirable that a controller model can correctly predict the response of generator torque and collective pitch actuation at least up to 6P, which is around 1.2 Hz at above rated operation.

4.1. Generator torque to generator speed

Figure 5 shows the purely structural frequency response from generator torque to speed for various cases of model complexity for the NREL 5 MW turbine in normal operation at 8 m/s and 20 m/s. The only difference in the conditions at 8 m/s and 20 m/s is the blade pitch, the mean rotational speed of the drivetrain and rotor, and the static blade deformation about which the geometrically nonlinear structural model has been linearized. The green curves in Figure 5 show the structural frequency response for a fully rigid turbine. Rigid-body rotation of the drivetrain and rotor can explain the response up to around the natural frequency of the 1st lateral tower mode at 0.32 Hz. The response of a rigid turbine equals the response of the 1st order model: $I_r \delta\dot{\Omega}_g = \delta Q_g$ and the rotational inertia causes a phase of 90 deg at all frequencies and a drop in amplitude with frequency.

When the tower is made flexible (red curves), the generator torque is in resonance with the 1st and 2nd lateral tower modes at 0.32 Hz and 2.9 Hz at both wind speeds. The lateral tower modes are excited by the generator reaction torque and are observable on the speed signal because of nacelle roll relative to the tower top. The 1st and 2nd lateral tower modes cause two zeros to appear very close to these modes at 0.315 Hz and 1.8 Hz. At the zero at 0.315 Hz, the change in rotor speed caused by the nacelle roll associated with the lateral tower motion counteracts the rigid-body rotation caused by the

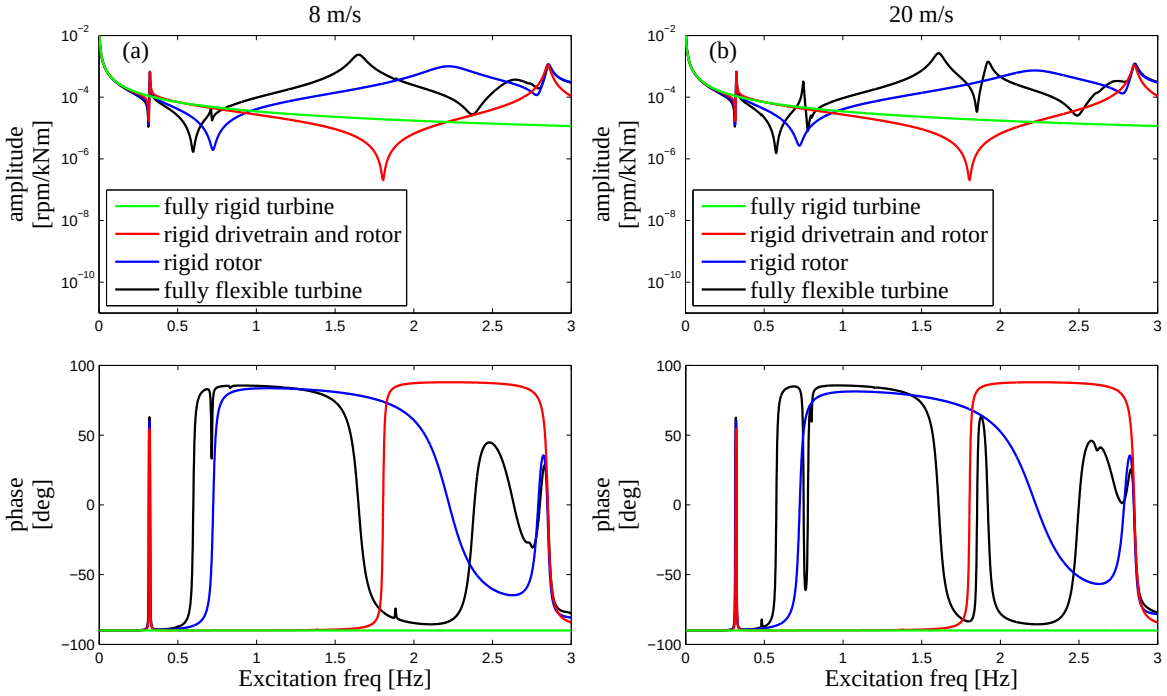

Figure 5. Purely structural frequency response from generator torque to generator speed for NREL 5 MW wind turbine operating at 8 and 20 m/s. Comparisons of frequency response predicted with models with no aerodynamic forces and with a fully rigid turbine (green), rigid drivetrain and rotor (red), rigid rotor (blue) and fully flexible turbine (black).

generator action torque. The zero nearly cancels the pole at 0.32 Hz creating a zero net phase shift across the 1st tower modes. After resonance of the 1st lateral tower mode, the response is again governed by rigid-body rotation of the drivetrain and rotor. The similar phenomena occurs at the zero located at 1.8 Hz where it is nacelle roll associated with the 2nd lateral tower mode that cancels the rigid-body rotor rotation in the generator speed output.

The blue curves in Figure 5 show the structural frequency response when the tower and drivetrain are flexible and the rotor is rigid. The 1st torsional mode of the drivetrain leads to resonance at 2.2 Hz and a zero at 0.72 Hz at both 8 m/s and 20 m/s. At the zero at 0.72 Hz, the rotor is moving while the generator end of the drivetrain is stationary, because the generator torque is counterbalanced by rotor inertia forces.

The black curves in Figure 5 show the purely structural frequency response for a fully flexible turbine. Due to the added blade flexibility, the 1st drivetrain mode now couples with the 1st collective edge blade mode, whereby the resonance frequency is decreased from 2.2 Hz to 1.6 Hz. The zero at 0.59 Hz at both wind speeds is also shifted from 0.72 Hz due to blade flexibility. At 20 m/s, the 1st and 2nd collective flap modes influence the frequency response close to their modal frequencies of 0.75 Hz and 1.92 Hz due to the static blade pitch and are accompanied by two zeros very close to these frequencies at 0.78 Hz and 1.86 Hz. The zeros and poles related to each of the 1st and 2nd collective flap modes make phase shifts that cancels each other. At the zero at 0.78 Hz, the generator torque excites both the 1st drivetrain mode and the 1st collective flap mode in a motion where edgewise blade bending relative to the hub in clockwise rotor direction is in phase with flapwise bending downstreams and in phase with the applied generator torque. The inertia forces from blade vibration in both the 1st drivetrain mode and the 1st collective flap mode counteracts the applied generator torque. Similarly, at the zero at 1.86 Hz, the generator torque excites the 1st drivetrain mode and the 2nd collective flap mode, and the inertia forces from this motion counteracts the generator torque to form a zero in the generator speed output.

Figure 6 shows a comparison between the purely structural response (magenta curves) and the aeroelastic response (black curves) for a fully flexible turbine. The main effects of including aerodynamic forces is seen at 20 m/s below the 1st tower modes and around the 1st and 2nd collective flap modes.

The response predicted by the simple 1st order model in Equation (9) with rigid structure and quasi-steady aerodynamics (blue curves) predicts the correct tendencies below the 1st tower modes. At 20 m/s aerodynamic forces decrease the amplitude at low frequencies and create a positive phase shift of 90 deg at 0 Hz compared to the purely structural response, because aerodynamic damping forces dominate the inertia forces that vanish at 0 Hz. At 8 m/s, the aerodynamic damping of the rotor is low and the response is dominated by inertia until very close to 0 Hz. Although not seen for the present

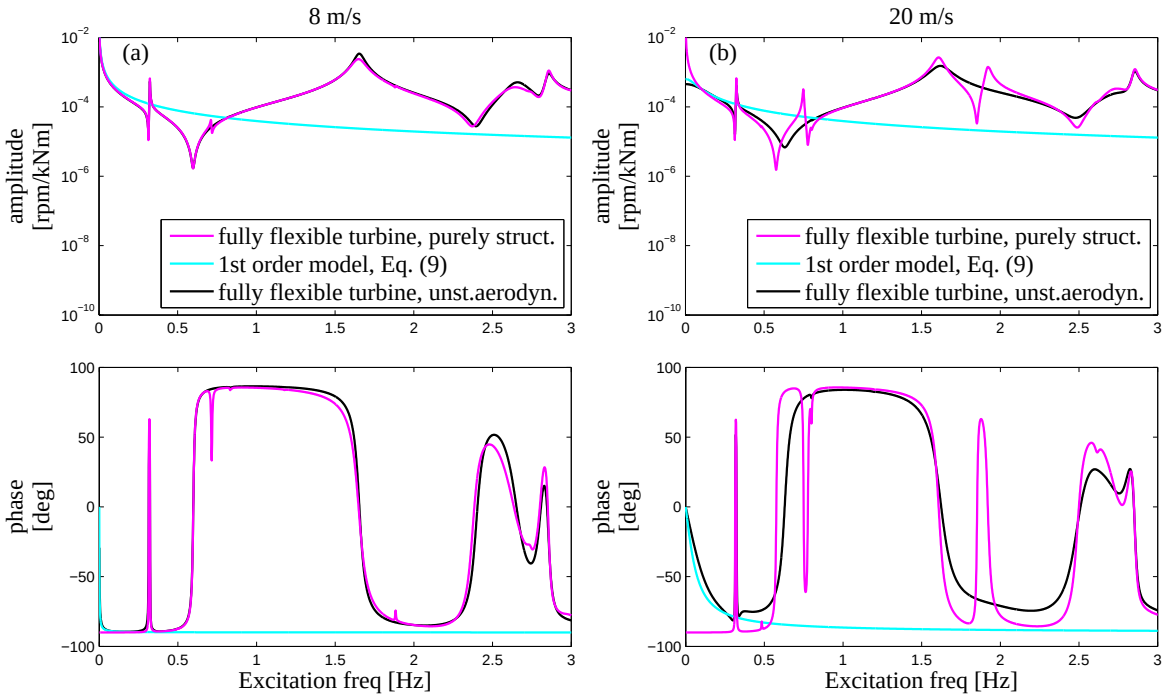

Figure 6. Aeroelastic frequency response from generator torque to generator speed for NREL 5 MW wind turbine operating at 8 m/s and 20 m/s. Comparisons of frequency response predicted with fully flexible structure and no aerodynamic forces (magenta), with the 1st order model in Equation (9) (cyan) and with fully flexible turbine with unsteady aerodynamic forces (black).

Wind Energ. 2012; **00**:1–?? © 2012 John Wiley & Sons, Ltd.
DOI: 10.1002/we
Prepared using weauth.cls

turbine, the static change in blade deflection caused by static changes in aerodynamic forces at 0 Hz, could cause that the aerodynamic gradients predicted for a rigid rotor are wrong. The aerodynamic gradients could in particular be predicted wrongly by a rigid-rotor assumption for a swept blade, because changes in steady state aerodynamic forces from a change in e.g. generator torque could cause high blade torsion.

Around the 1st and 2nd collective flap modes, the amplitude is reduced, due to large aerodynamic damping of flap vibration. The influence of the collective flap modes is seen from Figure 7 that shows a pole-zero map of the transfer functions in Figure 6. The figure shows poles and zeros that influence the frequency response and that does not cancel out in the transfer function. There are zero-pole cancelations of all asymmetric flap and edgewise modes. There are no zero-pole cancelations of the 1st and 2nd drivetrain modes at all wind speeds because the generator torque excites the drivetrain modes. There is zero-pole cancelation of the 1st collective flap mode at both 8 m/s and 20 m/s. The 2nd collective flap mode is canceled by a zero at 8 m/s and is nearly canceled at 20 m/s indicating that aerodynamic damping does not entirely limit vibration of the 2nd collective flap mode and is responsible for the phase difference of 10 deg seen around 2.2 Hz in Figure 6. Generally, it can be concluded, that the collective flap modes are not essential to include to model the transfer function from generator torque to speed because of aerodynamic damping. For excitation frequencies below 3 Hz, there is no significant difference between using unsteady and quasi-steady aerodynamics (not shown) on the response from generator torque to generator speed because the modes that influence the response are mainly modes characterized by vibration in the rotor plane where the effect of aerodynamic forces is small, except on the rigid-body rotor mode. There is no effect of lag on lift and drag on the rigid-body rotor mode because the frequency of vibration is so low, that lag only occurs at blade sections close to the blade root, where the components to the overall changes in aerodynamic rotor torque are small compared to sections closer to the blade tip.

The results shown above are for the NREL 5 MW turbine in onshore operation. For another turbine the ordering of the aeroelastic frequencies of the 1st and 2nd collective flap modes are likely to change relative to the zero at 0.72 Hz and the 1st drivetrain mode at 1.6 Hz, respectively, but without any significant effect on the response due to large aerodynamic damping of these modes.

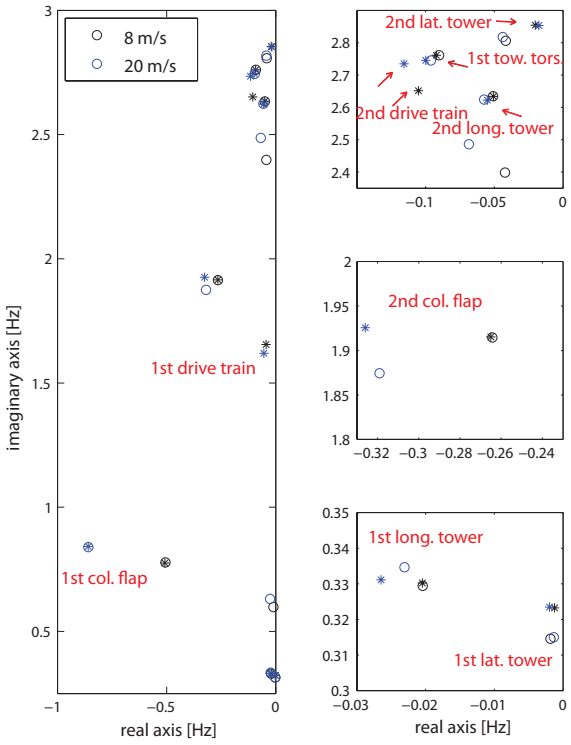

Figure 7. Aeroelastic poles and zeros of minimal realization of transfer function from generator torque to generator speed for NREL 5 MW wind turbine operating at 8 m/s and 20 m/s. (∗ poles, ○ zeros).

4.1.1. Effect of longitudinal tower vibration

The influence of longitudinal tower motion on the response from generator torque to generator speed is illustrated in Figure 8. The figure shows the aeroelastic frequency response close to the 1st tower modes for a turbine with a tower that is very stiff in longitudinal direction (blue curves) and for a fully flexible turbine (black curves) operating at 8 m/s and 20 m/s. The vertical lines show the aeroelastic frequencies of the 1st tower modes for a fully flexible turbine. For a fully flexible turbine, there is a zero at 0.315 Hz and a pole at 0.323 Hz due to nacelle roll associated with the 1st **lateral** tower mode. There are no changes in amplitude or any phase shifts occurring across the frequency of the 1st **longitudinal** mode at 0.33 Hz which shows that the 1st longitudinal tower mode has no influence. Thus, any deviations between the blue and black curves arise due to longitudinal tower motion in the 1st lateral tower mode. It can be seen that longitudinal tower vibration has a small influence only at 20 m/s, which is seen as larger phase shifts across the zero at 0.315 Hz and at the 1st lateral tower mode.

The small changes due to the increased longitudinal tower stiffness occurring at 20 m/s are caused by removal of longitudinal tower motion in the 1st lateral tower mode. Figure 9 shows the tower top motion in the 1st longitudinal and lateral tower modes for a fully flexible turbine with no aerodynamic forces (a), a turbine with rigid drivetrain and rotor and quasi-steady aerodynamics (b) and for a fully flexible turbine with unsteady aerodynamic forces (c) for the NREL turbine in normal operation at 8 m/s, 14 m/s and 20 m/s. Without aerodynamic forces, the 1st lateral and longitudinal tower modes consist of purely lateral and longitudinal tower motion, respectively. Thus, gyroscopic forces due to rotor tilting in the 1st longitudinal tower mode does not provide large coupling between lateral and longitudinal tower motion. For a turbine with a rigid drivetrain and rotor with aerodynamic forces (b), the 1st lateral tower mode has a component in the longitudinal direction that changes with operation point. The similar trend is seen for a fully flexible turbine (c). Thus, the coupling of the 1st lateral tower mode to longitudinal tower motion must be through aerodynamics, indicating that lateral tower vibration changes the aerodynamic thrust.

4.2. Collective pitch demand to generator speed

Figure 10 shows the purely structural frequency response from collective pitch to generator speed for various cases of model complexity for the NREL 5 MW turbine operating at the above rated wind speeds 14 m/s and 20 m/s. The green curves show the structural response for a fully rigid turbine, where the pitching inertia forces of the flapwise bent blades, makes the amplitude increase with the square of frequency and gives a phase of -90 deg except very close to 0 Hz. Because the blades are bent downwind, the pitching inertia forces have a positive torque creating component in the positive direction

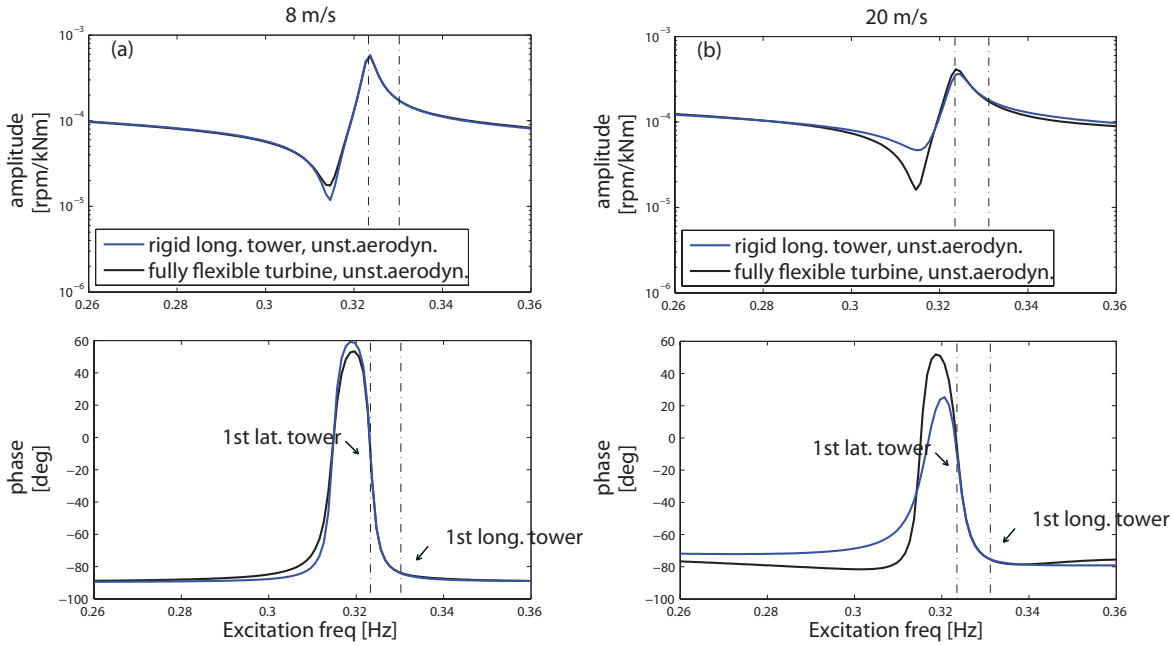

Figure 8. Aeroelastic frequency response at frequencies close to the 1st tower modes from generator torque to generator speed for NREL 5 MW wind turbine operating at 8 m/s and 20 m/s. Comparisons of frequency response predicted for a turbine with a tower that is very stiff in longitudinal direction (blue) and for a fully flexible turbine (black).

Wind Energ. 2012; **00**:1–?? © 2012 John Wiley & Sons, Ltd.
DOI: 10.1002/we
Prepared using weauth.cls

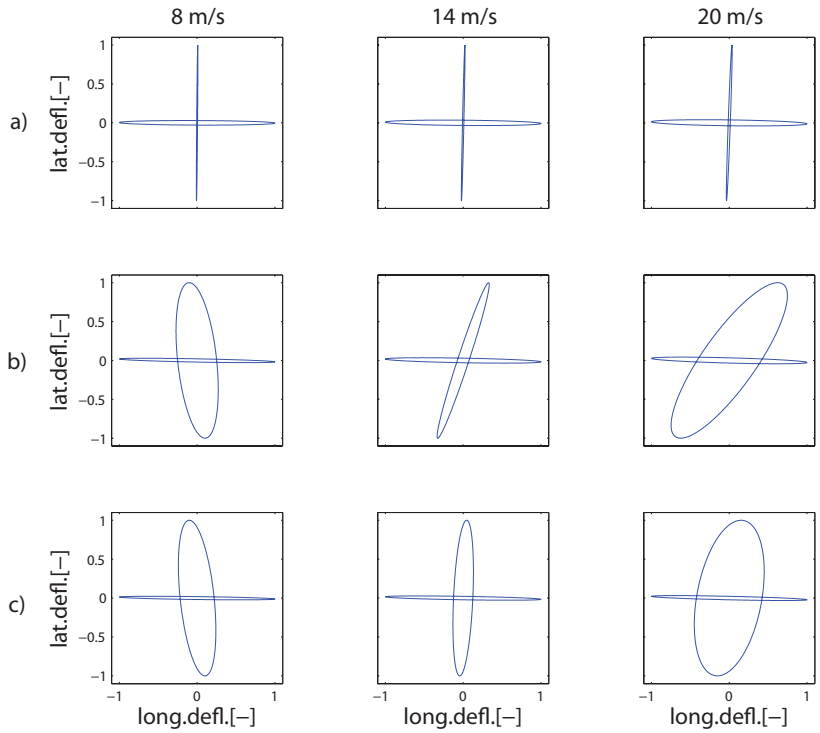

Figure 9. Tower top motion of the 1st lateral and longitudinal modes for a) a fully flexible turbine without aerodynamic forces, b) a fully flexible turbine and unsteady aerodynamics and for c) a turbine with rigid drivetrain and rotor and unsteady aerodynamics in normal operation at 8 m/s, 14 m/s and 20 m/s. Tower is seen from above and positive longitudinal tower deflection is defined to be upstreams, i.e. the wind is coming from the right of the plots.

of δQ_g for a positive pitch towards stall leading to a phase of -90 deg. The amplitude is slightly higher at 14 m/s than at 20 m/s, because of the larger static flap deflection.

The blue curves in Figure 10 shows the purely structural frequency response when the drivetrain is flexible and tower and rotor are rigid. Drivetrain flexibility causes a resonance with the 1st drivetrain mode at 2.2 Hz. The drivetrain mode is excited by the pitch actuator due to misalignment between the center of gravity and the pitching axis. The phase shifts -180 deg across the frequency of the 1st drivetrain mode at 14 m/s and 20 m/s.

The black curves in Figure 10 shows the structural response for a fully flexible turbine. The pitch actuator excites the 1st collective flap mode at 0.74 Hz, because the centers of gravity along the blade are not aligned with the pitch axis. The 1st collective flap mode is accompanied by a minimum-phase zero at 0.73 Hz, where collective pitching excites both the 1st drivetrain mode and the 1st collective flap mode. At this zero, the vibration of the 1st collective flap mode causes a torque to act on the rotor in the negative direction of δQ_g for a change in pitch towards stall, that counteracts the pitching inertia forces such that the net torque variations are zero. The zero nearly cancels the phase shift due to the 1st collective flap mode. The 1st drivetrain mode is in resonance at 1.6 Hz, shifted from 2.2 Hz due to added blade flexibility and is accompanied again by a phase shift of -180 deg. The 2nd collective flap mode at 1.9 Hz highly influence the response at both 14 m/s and 20 m/s. The amplitude at the 2nd collective flap mode is much higher than at the 1st collective flap mode, because the pitching inertia forces are larger at higher excitation frequencies, and because the 2nd collective flap mode lies close to the 1st drivetrain mode, where rotor speed variations are larger, which provides larger excitation of the 2nd collective flap mode. Resonance of the 2nd collective flap mode is accompanied by a zero at 1.89 Hz and 1.80 Hz at 14 m/s and 20 m/s, respectively. At these zeros, collective pitching excites both the 1st drivetrain mode and the 2nd collective flap mode. The 2nd collective flap mode couples to rotor rotation when the blades are pitched and is excited such that it creates a torque in the negative direction of δQ_g for a change in pitch towards stall and thereby counteracts the torque created due to vibration of the 1st drivetrain mode, such that there are no net generator speed variations. This coupling is more significant at 20 m/s where the blades are more pitched.

A comparison has been made of the pitching inertia forces for a rigid blade undergoing harmonic pitch angle variations around the undeformed state and statically deflected state of the NREL blade in normal operation at various wind speeds to clarify the effect of static blade deflection. The pitching inertia forces are measured as the amplitude of forces in the

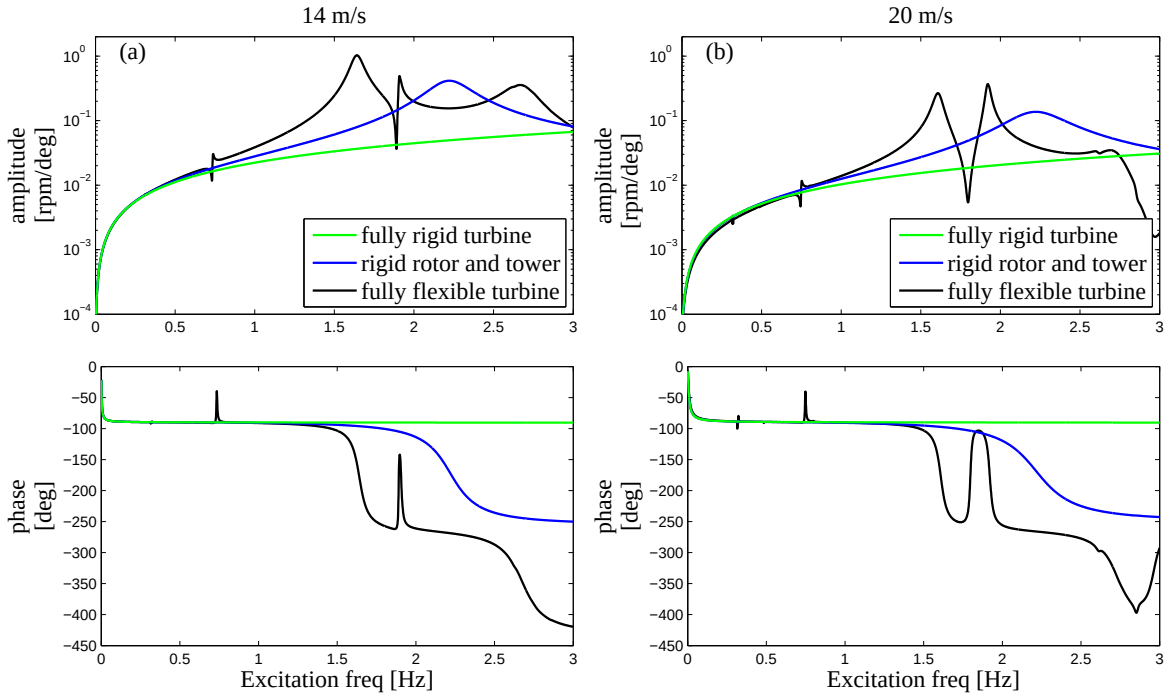

Figure 10. Purely structural frequency response from collective pitch to generator speed for NREL 5 MW wind turbine operating at 14 and 20 m/s. Comparisons of frequency response predicted from models assuming no aerodynamic forces and fully rigid turbine (green), rigid rotor and tower (blue) and a fully flexible turbine (black).

rotational direction of the rotor arising from harmonic variations in pitch angle at frequency ω_θ and amplitude A_θ. The total pitching inertia forces for the blade are found by summing up over the number of blade elements assuming constant structural properties over each element. The amplitude of pitching inertia forces $A_{p,i}$ for element i can be written

$$A_{p,i} = \omega_\theta^2 m_i l_i \sin\phi_{0,i} A_\theta \tag{14}$$

where $\phi_{0,i}$ and l_i are the polar coordinates of the element centre of gravity in the blade system, m_i is the element mass and $A_{p,i}$ is the amplitude of pitching inertia forces.

Figure 11 shows the total amplitude A_p of pitching inertia forces versus wind speed for the NREL 5 MW turbine blade in the undeformed and statically deformed state in response to harmonic pitching with an amplitude of 1 deg at a frequency of 1 Hz together with the static position of the centre of gravity at the blade tip in the rotor coordinate system. The pitching inertia forces are larger than of the undeflected blade at wind speeds below 22 m/s because the blades are highly deflected downstreams in the flap direction and peaks at 11 m/s where the thrust forces are highest. For blades with a significant prebend upstreams, the pitching inertia forces are expected to be lower, because the static position of the centre of gravity in the flap direction is further upstreams than for a non-prebended blade.

The influence of aerodynamic forces on the frequency response is now analyzed. Figure 12 shows a comparison of the response for a fully rigid turbine without and with quasi-steady aerodynamic forces and the response predicted by the simplified model in Equation (9). At 0 Hz, the effect of including aerodynamic forces is to increase the amplitude and shift the phase with 180 deg because of changes in aerodynamic torque caused by pitching. The steady state effect of a constant change in collective pitch is that the generator speed settles at a new equilibrium between the steady state generator torque and the aerodynamic torque on the rotor. Pitching towards feather gives less aerodynamic torque because of lower angles of attack, whereby the rotor speed decreases. The decrease in rotor speed gives an additional inflow velocity component, that increases the angle of attack and thereby the aerodynamic torque, such that the net variation in aerodynamic rotor torque is zero at 0 Hz.

The response predicted with a fully rigid turbine with quasi-steady aerodynamics (cyan curves) has a minimum-phase zero at 1.1 Hz and 2.1 Hz at 14 m/s and 20 m/s, respectively, where there is a positive phase shift of around 180 deg, due to pitching inertia forces. Under harmonic collective pitch angle variations, the pitching inertia forces gives a torque on the rotor in positive direction of δQ_g for a change in pitch towards stall, whereas the aerodynamic torque gives a higher torque in the negative direction and thus excites the rotor in the opposite direction as the pitching inertia forces. The pitching

Wind Energ. 2012; **00**:1–?? © 2012 John Wiley & Sons, Ltd.
DOI: 10.1002/we
Prepared using weauth.cls

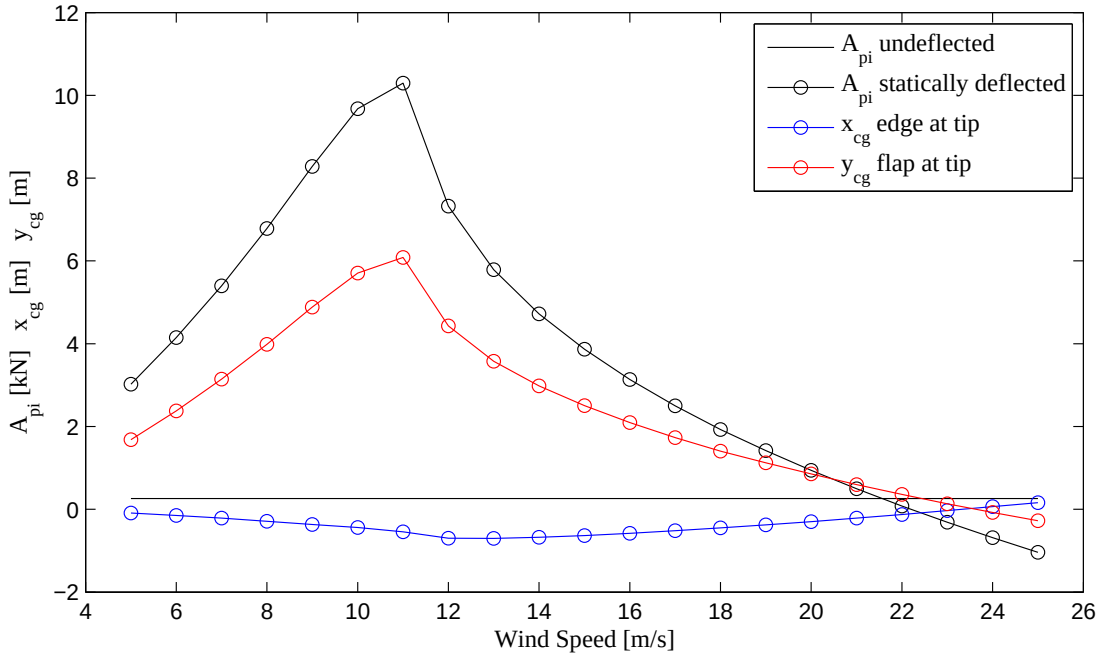

Figure 11. Amplitude of pitching inertia forces in the forward rotational direction of the rotor for a rigid NREL 5 MW blade undergoing harmonic pitch angle variations with amplitude of 1 deg and frequency of 1 Hz. Comparison of pitching inertia forces for undeflected blade and statically deflected blade for normal operation at various wind speeds. Static position of the centre of gravity at the blade tip in the blade coordinate system (x:positive towards rotational direction,y:positive downstreams).

inertia forces grows with excitation frequency and above the zeros at 1.1 Hz and 2.1 Hz at 14 m/s and 20 m/s, respectively, they are large enough to dominate the response over variations in aerodynamic torque.

The black curves in Figure 12 show the frequency response for a turbine with rigid blades in the flap direction. At 0.32 Hz, collective pitching now couples with the 1st tower modes to create a minimum phase and a non-minimum phase zero at 14 m/s and 20 m/s that causes the phase to shift approximately 360 deg crossing the frequencies of the 1st tower modes, because of 180 deg phase shift over the non-minimum phase zero and -180 deg over the lateral tower mode. The longitudinal tower mode introduce a zero and a pole with phase shifts that cancels each other. The minimum-phase zero at 0.71 Hz and 0.84 Hz for 14 m/s and 20 m/s, respectively, are shifted from 1.1 Hz and 2.1 Hz. To illustrate why the added drivetrain and edge flexibility causes these zeros to shift to a lower frequency, the purely structural response for a turbine with rigid flap is shown in Figure 12 (magenta curves). Collective pitching excites the 1st drivetrain mode structurally and vibration of this mode excites the rotor in phase with the pitching inertia forces, such that the variations in aerodynamic torque are suppressed at lower excitation frequencies.

Figure 14 shows a map of poles and zeros that does not cancel out of the transfer function from collective pitch to generator speed for the turbine where the blades are made rigid in the flap direction. There are pole-zero cancelations of all asymmetric flap and edgewise modes (not shown), no zero-pole cancelations of the 1st and 2nd collective flap modes, and a lowly damped zero exist at 0.71 Hz and 0.84 Hz for 14 m/s and 20 m/s, respectively. At 14 m/s the zero is non-minimum phase and causes a -180 deg phase shift in the black curves in Figure 12, and at 20 m/s it is a minimum phase zero causing a positive phase shift of 180 deg.

Figure 13 shows a comparison of the response for a fully flexible turbine without aerodynamic forces (blue curves) and with quasi-steady aerodynamic forces (cyan curves). The response predicted by the simplified model in Equation (9) is also included (green curves) to show that it captures the steady state response well at 0 Hz at both 14 m/s and 20 m/s.

Compared to the response of a turbine where blades are rigid in the flap direction (black curves in Figure 12), there is a large change in phase between the 1st tower modes and the 1st drivetrain mode, which must be due to the added flapwise blade flexibility. To explain this observation, the aeroelastic poles and zeros for the fully flexible turbine has been plotted in Figure 14. The pole-zero map shows that the lowly damped zeros at 0.71 Hz and 0.84 Hz at 14 m/s and 20 m/s, respectively, which are predicted for a turbine with rigid flap, are replaced by two highly damped non-minimum phase zeros at 0.67 Hz and 1.1 Hz. These non-minimum phase zeros creates a phase shift of -180 deg in the cyan curves in Figure 13 which occurs over a large frequency interval. It can be concluded that collective flap DOFs must be included to correctly predict existence of the non-minimum phase zeros at 0.67 Hz and 1.1 Hz for 14 m/s and 20 m/s, respectively.

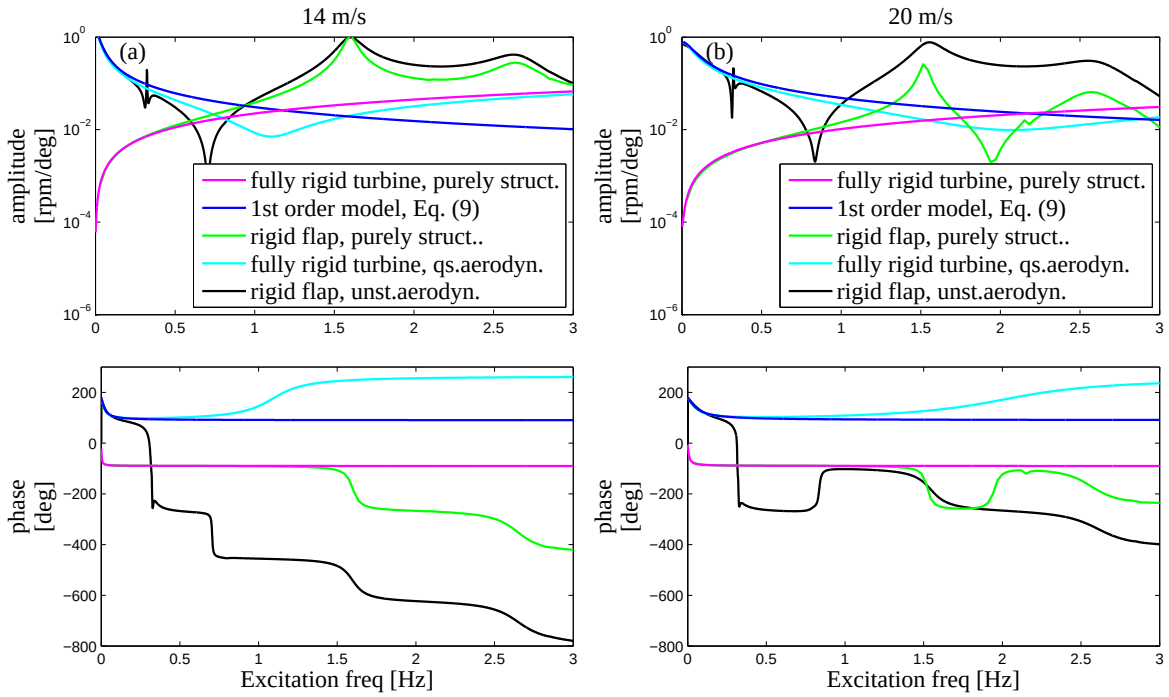

Figure 12. Purely structural and aeroelastic frequency response from collective pitch to generator speed for NREL 5 MW wind turbine operating at 14 m/s and 20 m/s. Comparisons of frequency response with models including a fully rigid turbine with no aerodynamic forces (magenta), the 1st order model in Equation (9) (blue), turbine with rigid flap and no aerodynamic forces (green), a fully rigid turbine with quasi-steady aerodynamics (cyan) and a turbine with blades rigid in flap direction and unsteady aerodynamics (black).

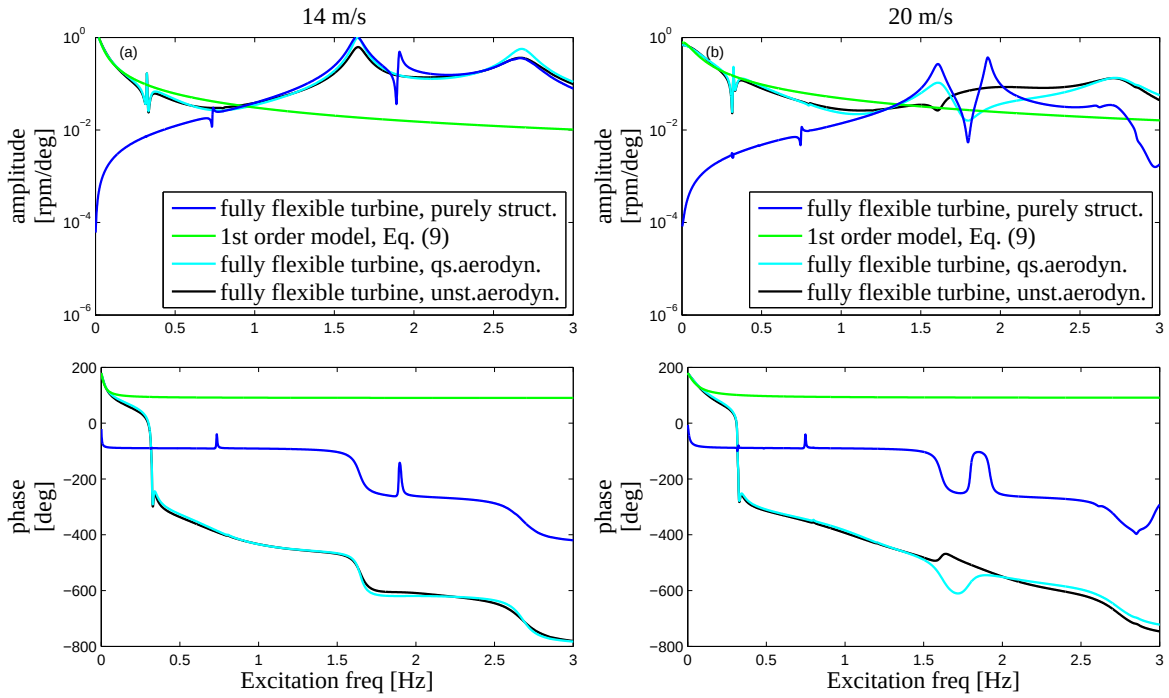

Figure 13. Aeroelastic frequency response from collective pitch to generator speed for NREL 5 MW wind turbine operating at 14 m/s and 20 m/s. Comparisons of frequency response with models including a fully flexible turbine with no aerodynamic forces (blue), the 1st order model in Equation (9) (green), a fully flexible turbine with quasi-steady aerodynamics (cyan) and a fully flexible turbine with unsteady aerodynamics (black).

Wind Energ. 2012; **00**:1–?? © 2012 John Wiley & Sons, Ltd.
DOI: 10.1002/we
Prepared using weauth.cls

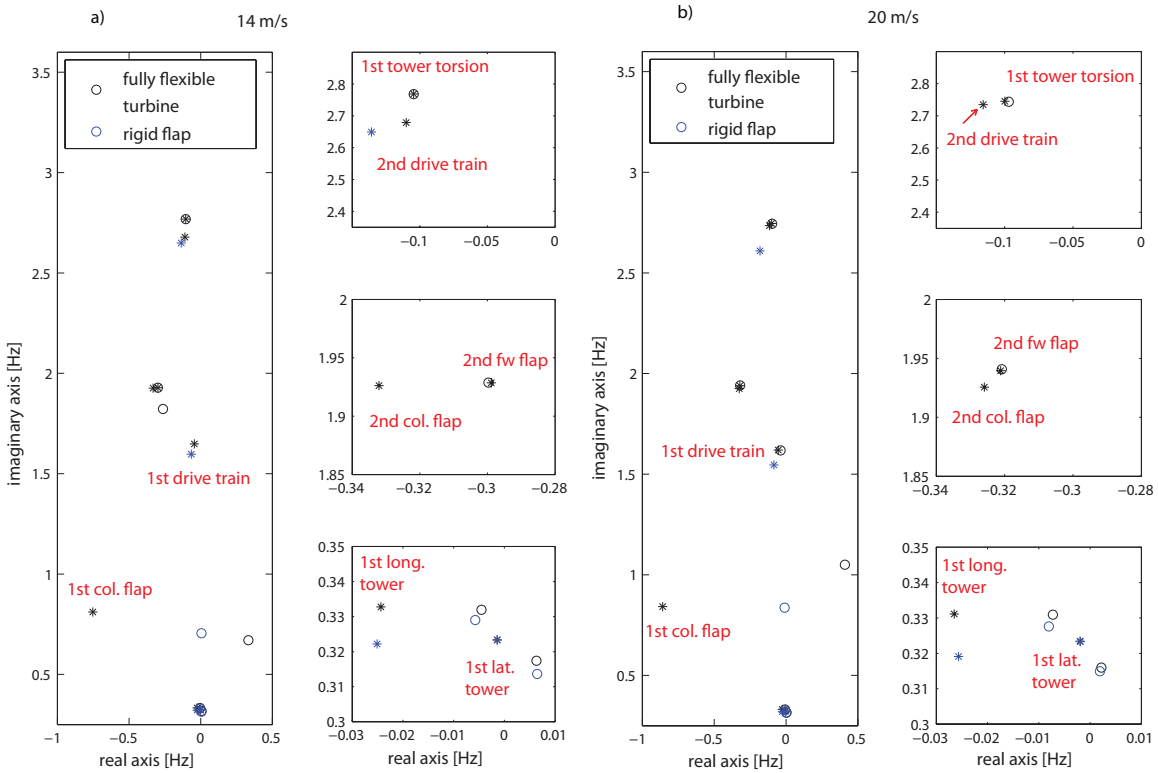

Figure 14. Aeroelastic poles and zeros of minimal realization of transfer function from collective pitch demand to generator speed for NREL 5 MW wind turbine operating at 14 m/s and 20 m/s. Comparison between pole-zero map for fully flexible turbine with unsteady aerodynamics (black) and turbine with blades rigid in flap direction with unsteady aerodynamics (blue) (∗ poles, ∘ zeros).

The cyan curves in Figure 13 shows, that quasi-steady aerodynamic forces changes the structural response at the 1st drivetrain mode and the 2nd collective flap modes by adding damping that lowers the response at these modes. The 1st drivetrain mode is mainly damped by aerodynamics at 20 m/s, because at larger pitch angles, the 1st drivetrain mode couples more with collective flap vibration. The zero located in between at 1.89 Hz and 1.80 Hz at 14 m/s and 20 m/s, respectively, is also damped by aerodynamic forces and the effect of the zero on the frequency response is not visible at 14 m/s, but can still be seen at 1.80 Hz at 20 m/s.

The effect of using unsteady aerodynamics instead of quasi-steady aerodynamics is seen by comparing the magenta and black curves in Figure 13. At 14 m/s there is no clear difference, whereas at 20 m/s a clear difference is observed at the 1st drivetrain mode and the 2nd collective flap mode. To explain this change, a pole-zero map has been plotted in Figure 15 for a fully flexible turbine with quasi-steady aerodynamics (blue points) and with unsteady aerodynamics (black points), that shows the poles of the 1st drivetrain mode and the 2nd collective flap mode at various wind speeds together with the zero with a frequency between these poles. The quasi-steady aerodynamic model predicts correct location of the poles of the 1st drivetrain mode, but estimates a too low aeroelastic frequency of the 2nd collective flap mode. At 10 m/s the 2nd collective flap mode tends to cancel with a zero, such that there is no influence of 2nd collective flap mode at this wind speed, because of lower pitch angles. With increasing wind speed the zero moves and does not cancel the pole. With unsteady aerodynamics a similar trend is seen, but at 20 m/s the zero has moved close to the 1st drivetrain mode, thereby almost cancelling the pole of the 1st drivetrain mode and creating a drop in amplitude at the frequency of the 1st drivetrain mode at 20 m/s in the black curves in Figure 13.

4.2.1. Non-minimum phase zero at the 1st tower modes

Controllability of generator speed with collective pitch is affected by a non-minimum phase zero close to the frequency of the 1st tower bending modes. Figure 16 shows the real part of zeros with frequency close to the 1st tower modes for normal operation at below rated wind speed up to 25 m/s. The zeros are calculated for three different models including only longitudinal tower flexibility and quasi-steady aerodynamics (as Fischer [7]), both longitudinal and lateral tower flexibility, rigid drivetrain and rotor and quasi-steady airfoil aerodynamics and for a fully flexible turbine and unsteady aerodynamics. The figure shows that a model that only includes longitudinal tower flexibility and rigid-body rotation of the rotor predicts

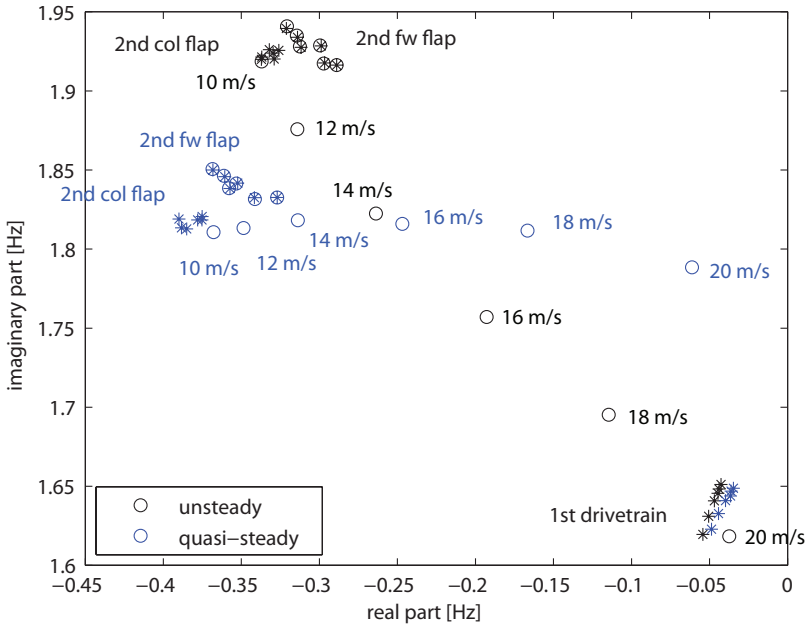

Figure 15. Aeroelastic poles and zeros of transfer function from collective pitch demand to generator speed for NREL 5 MW wind turbine operating at 14 m/s and 20 m/s with frequencies close to the 1st drivetrain mode. Comparison between pole-zero map for fully flexible turbine with quasi-steady aerodynamics (blue) and unsteady aerodynamics (black) (∗ poles, ○ zeros).

that there are non-minimum phase zeros below 15 m/s and the non-minimum phase zeros turns into minimum phase zeros above 15 m/s. Collective pitching excites the longitudinal tower vibrations through changes in thrust forces. At the 1st longitudinal tower mode, the thrust forces are in resonance with the longitudinal tower mode and the tower top deflection and velocity in the longitudinal direction shift with a phase of -180 deg across the 1st longitudinal tower mode. The longitudinal tower motion change the inflow and below 15 m/s the resulting change in aerodynamic torque is large enough to counterbalance the effect on the aerodynamic torque from the change in angle of attack caused by pitching the blades. The change in inflow caused by longitudinal tower vibration, cause the aerodynamic torque to experience a phase shift of -180 deg across the 1st longitudinal tower mode, following the phase shift of the longitudinal tower velocity and causing the non-minimum phase zero at the generator speed output. Above 15 m/s, the steady state relative velocities increase such that the effect on the aerodynamic torque of longitudinal tower vibration decrease. The changes in aerodynamic torque from a change in collective pitch angle is thereby mainly determined by the change in angle of attack caused by pitching the blades. As a results, the non-minimum phase zero change to a minimum-phase zero, that nearly cancels the effect of the 1st longitudinal tower mode.

When lateral tower flexibility is included (blue curves in Figure 16, the single zero becomes two zeros and one of them is a non-minimum phase zero for all wind speeds. It can be concluded that it is important to include lateral tower degree of freedom to predict correctly that there are non-minimum phase zeros. Below rated wind speed, the model with fully flexible turbine and unsteady aerodynamics predicts existence of up to three non-minimum phase zeros at the 1st tower modes. At 8 m/s, the pole of the 1st longitudinal mode and three non-minimum phase zeros gives a total phase drop of -720 deg, as seen previously in Figure 3a.

Under collective pitch angle variations, the tower vibrates in both lateral and longitudinal directions, which is illustrated in Figure 17 that shows the aeroelastic frequency response from collective pitch demand to tower top lateral and longitudinal deflections for the NREL 5 MW turbine with rigid drivetrain and rotor in normal operation at 14 m/s and 20 m/s. The figure shows a comparison of lateral tower top deflection predicted for a turbine with rigid drivetrain and rotor and for a turbine with rigid drivetrain and rotor where the tower is made very stiff in the longitudinal direction, to analyze the effect of longitudinal vibration on forces in the lateral direction. For a positive change in pitch angle (towards stall) the thrust forces increase and results in fore-aft deflection in phase with the change in pitch angle, except close to 0 Hz where rigid-body rotor rotation results in small phase differences. Lateral tower deflection hugely increase at the 1st tower modes, along with longitudinal tower vibration and results in lateral tower deflection equal in size to longitudinal deflection at 0.3 Hz. At the 1st tower modes the lateral tower deflection is shifted with a phase of approximately -90 deg relative to the longitudinal deflection, showing that forces acting on the tower in the sideways direction are in phase with

Wind Energ. 2012; **00**:1–?? © 2012 John Wiley & Sons, Ltd.
DOI: 10.1002/we
Prepared using weauth.cls

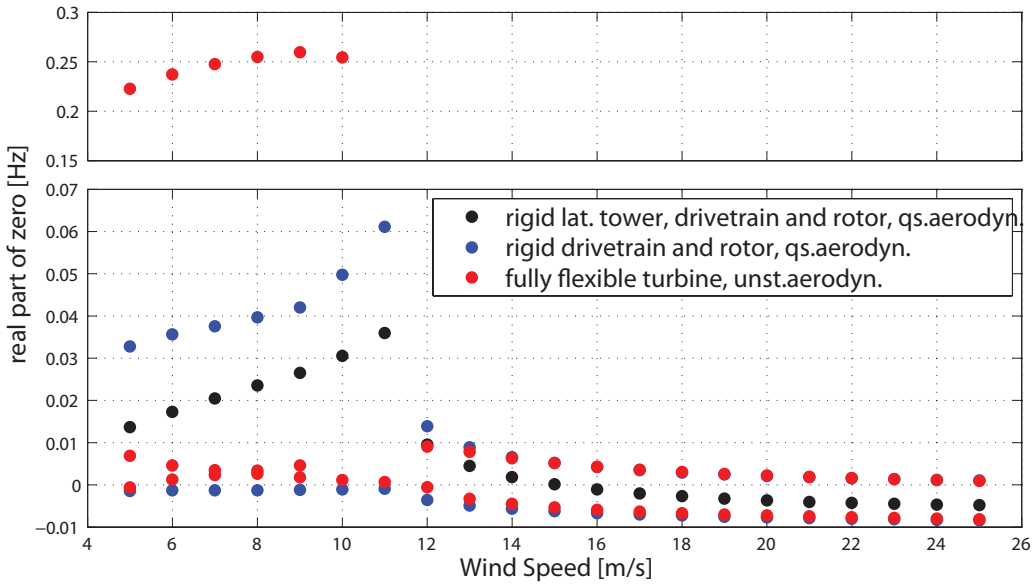

Figure 16. Variation of real part of zeros close to the 1st tower modes in transfer function from collective pitch to generator speed for NREL 5 MW wind turbine in normal operation at various wind speeds. Comparisons between transfer function zeros predicted by linear models assuming rigid tower in lateral direction and rigid drivetrain and rotor and quasi-steady aerodynamics (black), rigid drivetrain and rotor and quasi-steady aerodynamics (blue) and for fully flexible turbine with unsteady aerodynamics (red).

the longitudinal tower velocity. The dotted lines show that the lateral tower top deflection is order of magnitudes smaller if the tower is made stiff in the longitudinal direction, showing that sideways tower forces mainly arise due to asymmetry from rotor tilting associated with longitudinal tower deflection.

Figure 18 shows the frequency response from collective pitch to generator speed close to the 1st tower modes for operation at 14 m/s and 20 m/s as predicted by three different linear models including 1) only tower longitudinal tower flexibility and quasi-steady aerodynamics, 2) lateral and longitudinal tower flexibility and quasi-steady aerodynamics and 3) for a fully flexible turbine with unsteady aerodynamics. The figure also shows the response of generator speed measured at the generator bearing and at the generator end of the shaft found by the nonlinear time-simulations using HAWC2 for a fully flexible turbine. At 14 m/s, the model that only includes longitudinal tower flexibility (red curves) predicts that there is a non-minimum phase zero at 0.32 Hz where phase drops almost -360 deg over the shown narrow frequency range. At 20 m/s, the same model predicts a minimum-phase zero at 0.32 Hz, giving a net phase shift of approximately 0 deg across the shown frequency interval, because of 180 deg phase shift of the minimum-phase zero and -180 deg phase shift of the 1st longitudinal tower mode. With lateral tower flexibility included, the frequency response is affected by a non-minimum phase zero at 0.32 Hz resulting in a phase drop of approximately -360 deg at both 14 m/s and 20 m/s.

The dotted black and magenta curves in Figure 18 compares the generator speed response measured at the generator bearing and at the generator end of the shaft found from the nonlinear time-simulations using HAWC2. There is no non-minimum phase zero at the speed measured on the shaft at 20 m/s, showing that the detected influence of lateral tower motion is caused by nacelle roll associated with lateral tower vibration. The nacelle roll cause a change in the generator speed output that counteracts the increased speed due to the larger aerodynamic rotor torque arising from blade pitching, and the nacelle roll thereby promotes existence of the non-minimum phase zeros.

So, it has been shown to be essential to include lateral tower dynamics besides what is included in the model suggested by Fischer [7]. It is important for correct prediction of non-minimum phase zeros, to include static blade torsion when predicting the gradients of thrust and torque, because blade torsion directly changes the angle of attack. Correct predictions of structural damping of both lateral and longitudinal tower motion may influence predictions of non-minimum phase behavior, because damping influence the amount of vibration of these modes.

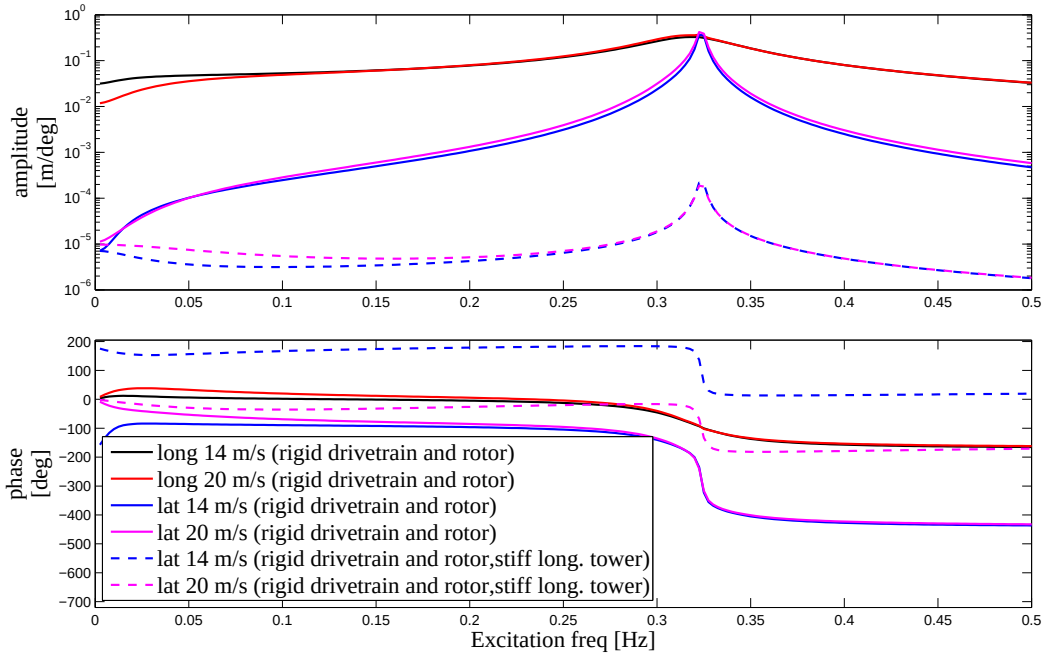

Figure 17. Aeroelastic frequency response from collective pitch demand to longitudinal and lateral tower top displacement for the NREL 5 MW turbine in normal operation at 14 m/s and 20 m/s. Comparison between the response for a turbine with a rigid drivetrain and rotor and a turbine with rigid drivetrain and rotor where the tower is made very stiff in the longitudinal direction.

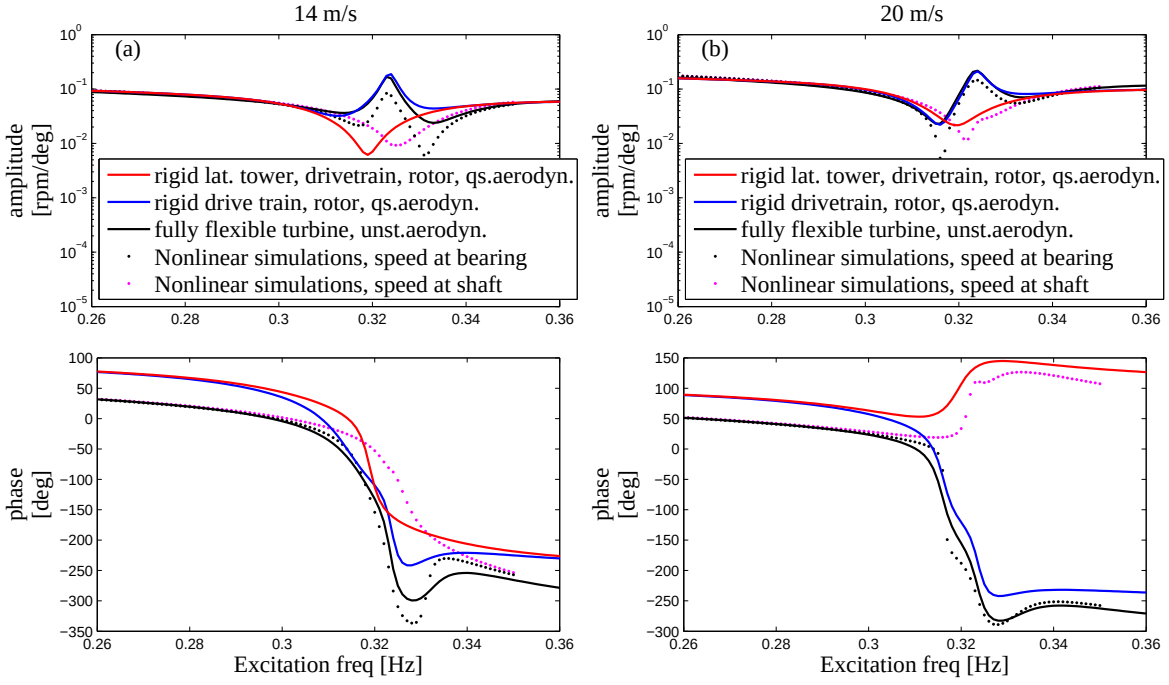

Figure 18. Aeroelastic frequency response from collective pitch demand to generator speed at the frequency of the 1st tower mode for NREL 5 MW wind turbine operating at 14 m/s and 20 m/s. Comparisons of frequency response predicted by linear models assuming rigid tower in lateral direction, rigid drivetrain and rotor and quasi-steady aerodynamics (red), rigid drivetrain and rotor and quasi-steady aerodynamics (blue) and for a fully flexible turbine with unsteady aerodynamics (black curve). Comparison between generator speed response measured at bearing output and at shaft end from nonlinear time-simulations with a fully flexible turbine.

Wind Energ. 2012; **00**:1–?? © 2012 John Wiley & Sons, Ltd.
DOI: 10.1002/we
Prepared using weauth.cls

5. CONCLUSIONS

The open-loop aeroelastic frequency response of a wind turbine from generator torque and collective pitch control actions to generator speed is analyzed based on a recently developed high-order linear aeroelastic model. The frequency response is analyzed for the onshore NREL 5 MW wind turbine in normal operation at various wind speeds. The analysis examplifies the aeroelastic frequency response of most non-floating, three-bladed, upwind wind turbines, because the ordering of the 1st tower, collective flap and drivetrain/collective edge modes is the same. The linear aeroelastic model is shown to be valid for small amplitude inputs compared to the response of generator speed predicted by time-simulations with the nonlinear aeroelastic model HAWC2.

The aeroelastic frequency response from generator torque to variations in generator speed is shown to be affected by mainly rigid-body rotor rotation and by resonance of the 1st drivetrain torsional mode, which is coupled with collective edgewise blade vibration. The lateral tower modes affects the response close to their aeroelastic frequencies due to nacelle roll, whereas the effect of longitudinal tower vibration is insignificant. Inertia forces acting on the blades due to variations in the rotational speed excites the collective flap modes, mostly at high wind speeds where the blades are pitched. However, due to large aerodynamic damping the influence of the collective flap modes on the transfer function from generator torque to generator speed is insignificant.

The aeroelastic response from collective pitch demand to generator speed is determined by rigid-body rotation of drivetrain and rotor below the frequencies of the 1st tower modes. At the 1st tower modes there are up to three non-minimum phase zeros below rated wind speed and one non-minimum phase zero above rated. For correct prediction of the non-minimum phase zero above rated, it is shown to be important to include both the 1st lateral and longitudinal tower modes. Between the 1st tower modes and the 1st drivetrain mode, the frequency response is affected by a highly damped non-minimum phase zero at above rated wind speeds. To correctly predict existence of this zero it is shown to be necessary to model correctly the influence of pitching inertia forces due to flapwise bent blades and to include the 1st drivetrain mode, and collective flap degrees of freedom. It is important to include aerodynamic damping of the 1st drivetrain mode mainly at high pitch angles. At 14 m/s, there is no difference in the response predicted with a quasi-steady and an unsteady model of airfoil aerodynamics. At 20 m/s, the quasi-steady response deviates at the 1st drivetrain mode, where it fails to predict the correctly influence of a minimum-phase zero, that nearly cancels the pole of the 1st drivetrain mode.

REFERENCES

1. Bossanyi EA. Wind turbine control for load reduction. *Wind Energy* 2003; **6**(3):229–244.
2. Wright AD, Balas MJ. Design of State-Space-Based control algorithms for wind turbine speed regulation. *Journal of Solar Energy Engineering* 2003; **125**(4):386–395.
3. van Engelen T. Control design based on aero-hydro-servo-elastic linear models from TURBU (ECN). *Proceedings of the European Wind Energy Conference*, 2007.
4. Kanev S, van Engelen T. Wind turbine extreme gust control. *Wind Energy* 2010; **13**(1):1835.
5. Selvam K, Kanev S, Wingerden JWv, Engelen Tv, Verhaegen M. Feedback-feedforward individual pitch control for wind turbine load reduction. *International Journal of Robust and Nonlinear Control* 2009; **19**(1):72–91.
6. Leithead W, Dominguez S. Coordinated control design for wind turbine control systems. *Scientific proceedings of the EWEC 2006*, vol. 2006, Athens, Greece, 2006; 56–59.
7. Fischer B. Reducing rotor speed variations of floating wind turbines by compensation of non-minimum phase zeros. *Scientific proceedings of the EWEA 2012*, Copenhagen, 2012; 144–147.
8. Hansen MH. Aeroelastic stability analysis of wind turbines using an eigenvalue approach. *Wind Energy* 2004; **7**(2):133–143.
9. Hansen MH. Aeroelastic properties of backward swept blades. *Proceedings of the 49th AIAA Aerospace Sciences Meeting Including the New Horizons Forum and Aerospace Exposition*, Orlando, Florida, 2011.
10. Jonkman J, Butterfield S, Musial W, Scott G. Definition of a 5-MW reference wind turbine for offshore system development. *Technical Report*, NREL 2009.
11. Department of Wind Energy, The Technical University of Denmark. Welcome to HAWC2! http://www.hawc2.dk/.
12. Hansen MH, Gaunaa M, Madsen H. A Beddoes-Leishman type dynamic stall model in state-space and indicial formulations. *Technical Report Risø-R-1354(EN)*, Risø,National Laboratory 2004.
13. Skjoldan P, Hansen M. On the similarity of the coleman and Lyapunov-Floquet transformations for modal analysis of bladed rotor structures. *Journal of Sound and Vibration* Nov 2009; **327**(3-5):424–439.
14. Burton T, Sharpe D, Jenkins N, Bossanyi E. *Wind Energy Handbook*. Wiley-Blackwell, 2001.
15. Larsen TJ. How 2 HAWC2 , the user's manual (ver. 3-9)(EN). *Technical Report Risø-R-1597*, Risø,DTU 2010.
16. Sørensen NN, Madsen H. Modelling of transient wind turbine loads during pitch motion. *Proceedings (online)*, European Wind Energy Association: Athens, Greece, 2006.

DOI: 10.1002/we
Prepared using weauth.cls

P2

On order reduction of high-order linear aeroelastic models for wind turbine control design

manuscript for journal paper, submitted to *Wind Energy*, 2013

WIND ENERGY
Wind Energ. 2012; **00**:1–**??**
DOI: 10.1002/we

RESEARCH ARTICLE

On order reduction of high-order linear aeroelastic models for wind turbine control design

Ivan Sønderby and Morten H. Hansen

Department of Wind Energy, Technical University of Denmark, Roskilde, Denmark

ABSTRACT

Linear models of low order describing the aeroelastic response of wind turbines are required in the design of modern model-based controllers. In this paper low-order aeroelastic models of wind turbines are designed by order reduction of a high-order linear aeroelastic model using modal truncation. The high-order model is a linearization of a geometrically nonlinear finite beam element model of wind turbine substructures coupled with an unsteady Blade Element Momentum (BEM) model including effects of shed vorticity and dynamic stall. Low-order models are designed to approximate the open-loop aeroelastic frequency response from generator torque, collective pitch angle demand and mean wind speed inputs to generator speed output in open-loop. It is shown to be necessary to include a relatively large number of aerodynamically dominated modes, which are uncoupled due to the assumption of independent annular flow tubes in the BEM theory. Reduced-order models are subsequently designed based on an assumption of quasi-steady aerodynamics followed by modal truncation. To approximate the transfer function from generator torque, collective pitch angle demand and mean wind speed to generator speed, it is shown to be essential to include the rigid-body rotor mode, the 1st longitudinal and lateral tower modes and the 1st drivetrain mode. The 1st collective flap mode must be included because the rigid-body rotor mode couples to this mode at high wind speeds due to the increased collective pitch angle. Reduced-order models are deduced for all operational wind speeds and they can easily be connected by interpolation due to the modal truncation approach that retains the state space. This set of reduced-order models are therefore suited fr subsequent gain-scheduling control design. Copyright © 2012 John Wiley & Sons, Ltd.

KEYWORDS

wind turbine, model-based control design, aeroelasticity, order reduction

Correspondence

I. Sønderby, Technical University of Denmark, Department of Wind Energy, DTU Risø Campus, DK-4000 Roskilde, Denmark. E-mail: ivsq@dtu.dk

Received . . .

1. INTRODUCTION

Modern model-based control design requires linear models of low order that provides good approximation of the aeroelastic response of wind turbines in response to control signals and disturbances. Low-order models are used to tune controller gains for optimal closed-loop response and to estimate the wind speed and turbine states based on measurements [1]. The purpose of this paper is to design low-order models by order reduction of a high-order linear aeroelastic model to be used for model-based wind turbine control design.

The TURBU tool [2] can provide reduced-order models by order reduction of a high-order linear wind turbine model, which couples a finite beam element model of tower, drivetrain and three blades with an unsteady Blade Element Momentum (BEM) model including aerodynamic states to describe dynamic stall. Reduced-order models provided by the TURBU tool are utilized for extreme gust control [3] and individual pitch control [4]. Order reduction of structural states is done using the Component Mode Synthesis method [5, 6], by reducing the order of the models of each substructure and subsequently assemble these models, whereas order reduction is not applied of the equations describing lag on aerodynamic forces. In the TURBU tool, one can reduce the order of the model from 600 to 100 states and conserve the frequency

response up to 5 Hz as stated in [2]. To conserve the frequency response at low frequencies it was required to "*include the quasi-steady behavior of the high-frequency modes*" in the blade and tower substructures.

In Finite Element analysis of structural mechanics, other methods are proposed for order reduction, which are reviewed by Cook [6]. One approach is to do modal expansion, where the basis is shifted and a set of generalized state variables are used to describe vibration of a reduced set of structural mode shapes. To achieve better approximation at low frequencies, a static correction can be applied whereby the static deflection under external excitation of the structure is ensured to be exact.

Design of linear low-order aeroelastic models for model-based control design has been extensively studied for aircrafts [7, 8]. Traditionally, the structure is assumed to vibrate in prescribed structural mode shapes and order reduction techniques are developed to represent unsteady aerodynamic forces cast in the frequency domain by rational transfer function matrices of low order for each structural mode shape, such that the aeroelastic model can be realized in a state space formulation and be used in model-based control design.

Moore [9] propose order reduction by *balanced truncation* where the state space model is transformed into a basis such that the state variables most effectively describe the 'energy' transmitted from multi-inputs to multi-outputs. Balanced *residualization* is a variant of balanced reduction proposed by Fernando & Nicholson [10] aiming at good approximation at low frequencies. A common approach is to apply frequency weighting on both in- and outputs before the balanced states are found for better approximation in the chosen frequency interval [11].

Recent advances in design of gain-scheduling controllers for wind turbines are designs of a linear parameter-varying (LPV) state space model of the wind turbine that covers specific regions of the operating curve and models nonlinear changes with operation point by parameter-varying matrices in the state space model. LPV controllers are designed by Bianchi et al. [12] based on a model that includes nonlinear variations in aerodynamic torque. Østergaard et al. [13] also parameterizes aerodynamic thrust variations and includes drivetrain torsional flexibility and longitudinal tower flexibility and shows improvements in performance relative to classical controllers.

Adegas et al. [14] propose an order reduction scheme to design reduced-order LPV wind turbine models using balanced truncation in combination with modal truncation. It is proposed to realize the reduced-order state space model on a canonical companion form, because this form is unique. Control design on the set of low-order models can be done by designing a controller for each of the frozen values of the scheduling variable and interpolate the controller gain as done by Bottasso et al. [15]. For LPV-control design the set of reduced-order system matrices must be parameterized, e.g. by assuming polynomial dependency with respect to the scheduling variable, which can be done by using linear least squares optimization [16].

Sønderby & Hansen [17] analyze the open-loop aeroelastic frequency response of a modern wind turbine. The low-frequency response from generator torque to generator speed is affected by resonance of the rigid-body rotor mode, the 1^{st} lateral tower mode and the 1^{st} drivetrain mode. The non-minimum phase zero in the response from collective pitch angle demand to generator speed mainly caused by longitudinal tower motion is shown to be affected also by lateral tower motion. Vibration of the blades in the flap direction showed to affect existence of another non-minimum phase zero below the 1^{st} drivetrain mode. A common approximation in aeroelasticity is to assume quasi-steady aerodynamics [18] where the time constants related to unsteady lift and drag are assumed to be much smaller than the time constants of structural dynamics. The quasi-steady assumption means, that under changes in the inflow due to structural motion or changes in wind speed, the aerodynamic forces moves on the static lift, drag and moment curves. The time constants that characterize unsteady aerodynamics due to shed vorticity and dynamic stall for a wind turbine are very high, leading to low cut-off frequencies and influence on the low frequency response [17]. An assumption of quasi-steady sectional aerodynamics has no significant influence on the response from generator torque to speed, but affects the speed in response to collective pitch inputs at around the 1^{st} drivetrain and 2^{nd} collective flap modes.

In this paper low-order models are designed for model-based wind turbine control design using order reduction by modal truncation with aeroelastic wind turbine mode shapes predicted by a high-order linear aeroelastic wind turbine model called HAWCStab2 [19]. The model is a linearization of a nonlinear co-rotational finite beam element model coupled with an unsteady BEM model of aerodynamic forces including effects of shed vorticity and dynamic stall. Reduced-order models are designed to approximate the open-loop aeroelastic frequency response from changes in generator torque, collective pitch demands and mean wind speed to generator speed of the reference NREL 5 MW reference turbine [20] for small vibrations about steady state operation at various wind speeds. The paper shows that the reduced-order models are suited for parametrization along an operation point trajectory when realized on modal form.

The main findings are that a relatively large number of aerodynamically dominated modes affect the low-frequency response, because the BEM model assumes that there is no aerodynamic coupling between unsteady aerodynamic forces in sections along the blades. Reduced-order models are subsequently designed based on an assumption of quasi-steady aerodynamics followed by modal truncation. A reduced-order model that contains the rigid-body rotor mode, the 1^{st} lateral and longitudinal tower modes, the 1^{st} and 2^{nd} collective flap modes and the 1^{st} and 2^{nd} drivetrain mode predicted with quasi-steady aerodynamics is seen to correctly approximate the low frequency response from generator torque, collective

Wind Energ. 2012; **00**:1–?? © 2012 John Wiley & Sons, Ltd.
DOI: 10.1002/we
Prepared using weauth.cls

pitch angle demands and harmonic variations in mean wind speed to generator speed output. The reduced-order system matrices are shown to be suited for parametrization.

The paper contains first a short description of the high-order linear aeroelastic model used for subsequent model reduction and a description of the influence of assuming quasi-steady aerodynamics on e.g. the aeroelastic frequencies and damping of wind turbine modes. Then, a mathematical description of the modal truncation method is given and it is shown how some of the aerodynamically dominated modes influence the frequency response through coupling with rigid-body rotor rotation and longitudinal tower vibration. Results are then shown of modal truncation with aeroelastic mode shapes using quasi-steady aerodynamics. The last section describes how the components of the reduced-order system matrices are connected at various wind speeds.

2. HIGH-ORDER LINEAR AEROELASTIC MODEL

A brief description is now given of the linear aeroelastic model used for order reduction. A more complete description of the model is provided by Hansen [19] for an isolated blade. The model of the NREL 5 MW turbine is identical to the HAWC2 model used for frequency response analysis in [17].

2.1. Model description

The model used for order reduction is a linearization of a finite beam element model of tower, drivetrain, hub and blades including geometrical nonlinearities, which is coupled with an unsteady BEM model including effects of shed vorticity and dynamic stall. So far, the model assumes frozen wake, whereby it is assumed that the induction is static.

Linearization is performed analytically around an operational state defined by a mean wind speed, pitch angle and rotor speed in which the blades are stationary deflected. The stationary deflected state of the blades is obtained from a nonlinear equilibrium between elastic and centrifugal forces and the static aerodynamic forces from an assumed uniform inflow to the rotor plane. The stationary steady operational state is obtained by neglecting gravity forces, wind shear, turbulence and other causes of a skew inflow to the rotor e.g. tilt and yaw angles.

In the particular model of the NREL reference turbine the tower, drivetrain and each blade are modeled by eight, four and 19 Timoshenko beam elements, respectively. Each element has two nodes and six degrees of freedom (DOF) per node describe rotation and translation in all three axis. Pitch actuators are modeled as second order low-pass filters between reference and actual pitch angle as described by Hansen [21]. In the present analysis the filter frequency is set so high that there is practically no phase lag between demanded and actual pitch angles. Aerodynamic forces are evaluated at 30 aerodynamic calculation points along each blade. Unsteady sectional aerodynamics is described using two states for shed-vorticity effects and two states to model dynamic stall at each aerodynamic calculation point as described in Hansen et al. [22].

Structural DOF describing blade and hub motion and all aerodynamic states are described in multiblade coordinates using the Coleman transformation. Linearization is performed around a state where isotropic rotor and isotropic external conditions are assumed, to remove dependency of the azimuth angle in the system matrices [23].

2.2. Equations of motion

The linear aeroelastic model is described by the following system of equations

$$\mathbf{M}\ddot{\mathbf{z}}_s + (\mathbf{C}_s + \mathbf{G} + \mathbf{C}_a)\dot{\mathbf{z}}_s + (\mathbf{K} + \mathbf{K}_a + \mathbf{K}_{sf})\mathbf{z}_s + \mathbf{A}_f\mathbf{x}_a = \mathbf{F}_s \tag{1a}$$

$$\dot{\mathbf{x}}_a + \mathbf{A}_d\mathbf{x}_a + \mathbf{C}_{sa}\dot{\mathbf{z}}_s + \mathbf{K}_{sa}\mathbf{z}_s = \mathbf{F}_a \tag{1b}$$

where $\mathbf{z}_s$ contains the structural DOF and $\mathbf{x}_a$ contains aerodynamic states used to describe time-lags due to unsteady aerodynamics and where $\mathbf{M}$ is the mass matrix, $\mathbf{K}$ the stiffness matrix, $\mathbf{C}_s$ the structural damping matrix, $\mathbf{G}$ the gyroscopic matrix, $\mathbf{C}_a$ the aerodynamic damping matrix, $\mathbf{K}_a$ the aerodynamic stiffness matrix and $\mathbf{K}_{sf}$ the geometric stiffness matrix due to the movement of the steady state aerodynamic force vector. The matrix $\mathbf{A}_f$ represents coupling from aerodynamic states to structural states and matrices $\mathbf{C}_{sa}$ and $\mathbf{K}_{sa}$ describes coupling between structural velocities and displacements to aerodynamic states and $\mathbf{A}_d$ describes the lag on the aerodynamic forces. The right-hand side terms $\mathbf{F}_s$ and $\mathbf{F}_a$ represent structural and aerodynamical forces due to actuators and changes in the wind speed, respectively. To improve the conditioning of the eigenvalue problem set up directly on the first order form of Equation (1), a reduced state transformation is applied using structurally undamped eigenvectors as described in [17] but omitted here for brevity.

The system in Equation (1) is put on first order form:

$$\dot{\mathbf{x}} = \mathbf{A}\mathbf{x} + \mathbf{B}\mathbf{u} \tag{2a}$$

$$y = \mathbf{C}\mathbf{x} \tag{2b}$$

where, by definition:

$$\mathbf{x} = \left\{ \begin{array}{c} \mathbf{x}_a \\ \mathbf{q}_{sr} \\ \dot{\mathbf{q}}_{sr} \end{array} \right\} \quad ; \quad \mathbf{u} = \left\{ \begin{array}{c} \delta Q_g \\ \delta\theta_c \\ \delta W \end{array} \right\} \quad ; \quad y = \delta\Omega_g \tag{3}$$

$$\mathbf{A} = \left[\begin{array}{ccc} -\mathbf{A}_d & -\mathbf{K}_{sa} & -\mathbf{C}_{sa} \\ \mathbf{0} & \mathbf{0} & \mathbf{I} \\ -\mathbf{M}^{-1}\mathbf{A}_f & -\mathbf{M}^{-1}(\mathbf{K}+\mathbf{K}_a+\mathbf{K}_{sf}) & -\mathbf{M}^{-1}(\mathbf{C}+\mathbf{G}+\mathbf{C}_a) \end{array} \right] \tag{4}$$

$$\mathbf{B} = \left[\begin{array}{cc} \mathbf{0} & \mathbf{B}_{da} \\ \mathbf{0} & \mathbf{0} \\ \mathbf{M}^{-1}\mathbf{B}_{us} & \mathbf{M}^{-1}\mathbf{B}_{ds} \end{array} \right] \quad ; \quad \mathbf{C} = \left[\begin{array}{ccc} \mathbf{0} & \mathbf{0} & 0...1...0 \end{array} \right] \tag{5}$$

where $\mathbf{B}_{us}$, $\mathbf{B}_{ds}$ and $\mathbf{B}_{da}$ have been linearized with respect to the inputs and are defined from:

$$\mathbf{F}_s = \mathbf{B}_{us} \left\{ \begin{array}{c} \delta Q_g \\ \delta\theta_c \end{array} \right\} + \mathbf{B}_{ds}\delta W \quad ; \quad \mathbf{F}_a = \mathbf{B}_{da}\delta W \tag{6}$$

and where $\mathbf{C}$ extracts the generator speed variations $\delta\Omega_g$. Changes in generator torque δQ_g and generator speed $\delta\Omega_g$ are defined positive in the opposite direction as the rotor rotates and $\delta\theta_c$ is defined positive towards stall. The low speed shaft (LSS) speed of the generator is used in the analysis, whereby it is assumed that there is no gearbox.

2.3. Low-frequency aeroelastic modes and aerodynamic delays

The aeroelastic modes predicted by the linear wind turbine model consist of structurally and aerodynamically dominated modes. Table I lists the aeroelastic frequencies ω_d and damping ratios ξ of the structurally dominated modes ordered according to the aeroelastic frequencies for the NREL 5 MW turbine in normal operation at 8 m/s, 14 m/s and 20 m/s where:

$$\omega_d = \mathrm{Im}\{\lambda_i\} \qquad \xi = -\mathrm{Re}\{\lambda_i\}/|\lambda_i| \tag{7}$$

and λ_i is the i'th eigenvalue of $\mathbf{A}$. Each of the aerodynamically dominated modes (**not** listed in Table I) describe variations in aerodynamic forces in local sections along the blade span due to the four by four block diagonal form of the $\mathbf{A}_d$ matrix. The BEM model assumes that changes in aerodynamic forces at one aerodynamic calculation point does not couple with changes in aerodynamic forces at neighboring calculation points, except weakly through structural motion, whereby the eigenvectors of the aerodynamically dominated modes are only weakly coupling in the aerodynamic state variables across the calculation points. Only the collective aerodynamically dominated modes are shown to influence the low frequency response and are characterized by their cut-off frequencies $\omega_c = -\lambda_i$ where λ_i are the purely real eigenvalues corresponding to these modes. Figure 1 shows the variations of cut-off frequencies with blade radius of time delays modeling shed vorticity and dynamic stall for NREL 5 MW turbine in normal operation at 8 m/s, 14 m/s and 20 m/s found under assumption of no coupling of the delays with structural states. The cut-off frequencies in Figure 1 are the eigenvalues of the 4×4 diagonal blocks of the $\mathbf{A}_d$ matrix obtained directly from the steady state BEM solution. The dashed horizontal line shows the aeroelastic frequency of the 1$^{\mathrm{st}}$ longitudinal tower mode for comparison. The figure shows cut-off frequencies of two of the four time delays at each blade section; one that characterizes the effect of shed-vorticity below stall and one characterizing the pressure lag in the boundary layer in stalled flow [22]. The cut-off frequencies increase with blade radius, because the relative inflow velocities increase, causing a faster update of the aerodynamic forces because the shed vorticity is faster convected away from the airfoil and the movement of the separation point of the dynamic stall becomes faster. The cut-off frequencies have an order of magnitude similar to the aeroelastic frequency of the 1$^{\mathrm{st}}$ tower modes at some sections, and the delays may couple to the rigid-body rotor rotation mode and the 1$^{\mathrm{st}}$ tower modes.

Wind Energ. 2012; **00**:1–?? © 2012 John Wiley & Sons, Ltd.
DOI: 10.1002/we
Prepared using weauth.cls

Table I. Open-loop aeroelastic frequencies and damping of structurally dominated mode shapes with low aeroelastic frequency for NREL 5 MW turbine operating at 8 m/s, 14 m/s and 20 m/s.

nr.	ω_d **[Hz]**	ξ **[%]**	ω_d **[Hz]**	ξ **[%]**	ω_d **[Hz]**	ξ **[%]**	**Description**
	8 m/s		14 m/s		20 m/s		
1	λ_1 = -0.0112 rad/s		λ_1 = -0.0184 rad/s		0.035	95.9	Rigid-body rotation of shaft and rotor
2	0.32	0.38	0.32	0.44	0.32	0.61	1^{st} lateral tower
3	0.33	6.19	0.33	7.30	0.33	7.98	1^{st} longitudinal tower
4	0.57	64.1	0.60	77.3	0.63	80.0	1^{st} backward whirling blade flap
5	0.84	54.8	0.80	0.69	0.80	0.56	1^{st} backward whirling blade edge
6	0.78	1.45	0.81	68.1	0.84	71.4	1^{st} collective blade flap
7	0.91	47.9	0.99	60.8	1.01	65.2	1^{st} forward whirling blade flap
8	1.18	1.76	1.20	1.11	1.20	0.81	1^{st} forward whirling blade edge
9	1.55	16.4	1.52	20.9	1.53	21.7	2^{nd} backward whirling blade flap
10	1.65	2.4	1.65	2.43	1.62	3.14	1^{st} collective blade edge/drive train torsion
11	1.92	12.5	1.93	17.0	1.93	16.6	2^{nd} collective blade flap
12	1.89	13.7	1.93	15.3	1.94	16.3	2^{nd} forward whirling blade flap
13	2.63	1.92	2.64	2.04	2.62	2.10	2^{nd} longitudinal tower
14	2.65	3.62	2.68	3.76	2.73	3.89	2^{nd} collective edge/drive train torsion
15	2.76	3.34	2.77	3.77	2.75	3.65	1^{st} tower torsion (yaw)
16	2.85	0.71	2.85	0.70	2.85	0.62	2^{nd} lateral tower

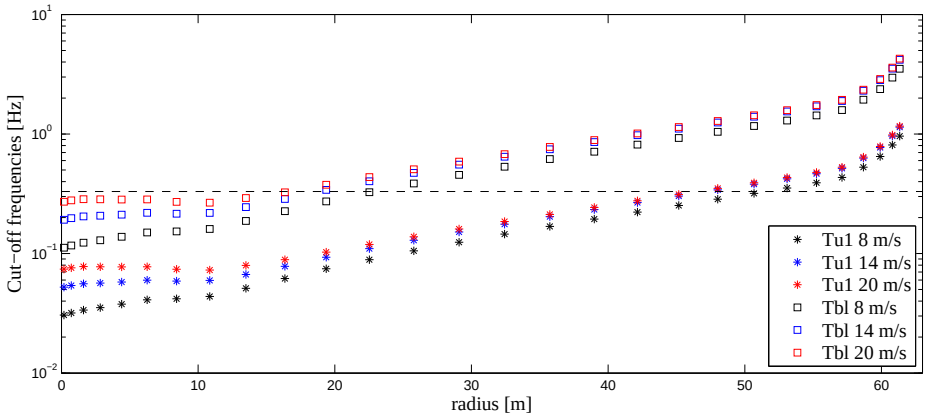

Figure 1. Variation of cut-off frequencies with blade radius of time delays modeling lag on aerodynamic forces due to shed vorticity and dynamic stall in separate blade sections for NREL 5 MW blade in normal operation at 8 m/s, 14 m/s and 20 m/s, where T_{u1} denotes one of two time delays describing shed vorticity below stall and T_{bl} denotes pressure lag in the boundary layer in stalled flow [22]. Cut-off frequencies are found under the assumption that there is no coupling to structural states. The dashed horizontal line shows the aeroelastic frequency of the 1^{st} longitudinal tower mode for comparison.

3. QUASI-STEADY AERODYNAMICS

Quasi-steady aerodynamics is assumed by setting $\dot{\mathbf{x}}_a = \mathbf{0}$ in the aerodynamic state equation (1b), isolate for $\mathbf{x}_a$ and then substitute $\mathbf{x}_a$ in Equation (1a). An analysis of the effect of assuming quasi-steady aerodynamics on the aeroelastic frequency response of two of the three transfer functions studied here, i.e. from generator torque and collective pitch angle demand to generator speed, can be found in previous studies [17], and is not repeated here. Figure 2 shows the aeroelastic frequency response from mean wind speed harmonic variations to generator speed at 14 m/s and 20 m/s predicted using unsteady aerodynamics (filled line) and quasi-steady aerodynamics (dotted line). Note, that in the frequency response we assume instant change in the mean wind speed; the unsteady aerodynamic model does not describe dynamics related to how fast the mean wind speed changes in for example a gust. The full-order response of generator speed of harmonic variations in mean wind speed is similar to that of collective pitch excitation below 1.0 Hz; a change in mean wind speed changes the angle of attack and thereby the aerodynamic forces similar to a change in pitch angle.

At both 14 m/s and 20 m/s, there are two non-minimum phase zeros at 1.2 Hz and 2.0 Hz causing negative phase shifts of -180 deg. At the zero at 1.2 Hz, the changes in mean wind speed excites the 1st torsional drivetrain mode, which couples with the 1st edgewise blade bending mode. An increase in mean wind speed gives a positive change in lift forces at the blade sections which forces the blade to bend relative to the hub positive clockwise. The edgewise blade vibration in the 1st drivetrain torsion mode changes the relative velocities at the blade sections, causing decreasing angle of attack and lift, that counteracts the change in lift from the mean wind speed increase, such that there is little net change in aerodynamic torque. The zero at 2.0 Hz exist due to coupling between collective blade vibration in the 1st drivetrain mode and in the 2nd drivetrain mode, such that the net change in aerodynamic rotor torque is close to zero.

The effect of assuming quasi-steady aerodynamics (dotted lines in Figure 2) is to increase the amplitude of the generator speed signal at the 1st drivetrain mode, because the model predicts too large changes in aerodynamic torque for a change in wind speed in attached flow due to the neglected effect of shed vorticity. The aeroelastic frequency response from generator torque, collective pitch and mean wind speed inputs to generator speed output all show little effect of assuming quasi-steady aerodynamics at excitation frequencies below the 1st drivetrain mode, cf. [17], because at these low frequencies lag on aerodynamic forces appears only at the inner blade sections that have no large contribution to the overall changes in aerodynamic rotor torque and thrust.

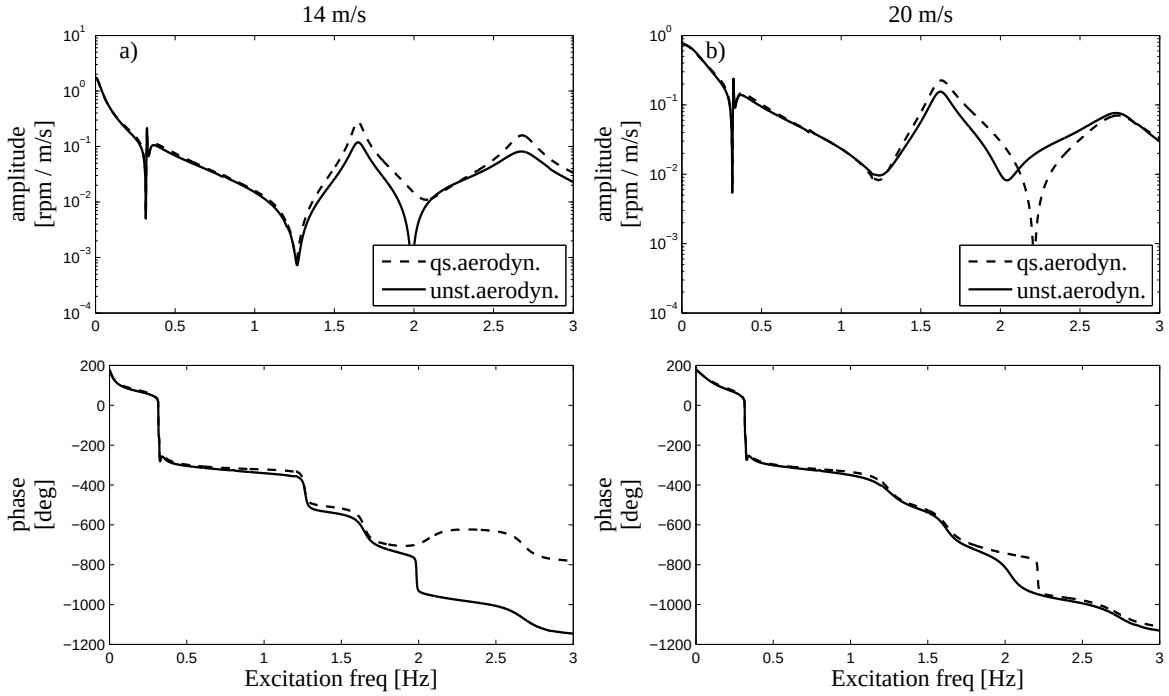

Figure 2. Aeroelastic frequency response from changes in mean wind speed to generator speed for NREL 5 MW turbine at normal operation at 14 m/s and 20 m/s. Comparison between the response predicted by the full-order model with unsteady aerodynamics (filled lines) and with quasi-steady aerodynamics (dashed lines).

Wind Energ. 2012; **00**:1–?? © 2012 John Wiley & Sons, Ltd.
DOI: 10.1002/we
Prepared using weauth.cls

Figure 3 shows the eigenvalues corresponding to aeroelastic modes with low frequency predicted with quasi-steady aerodynamics. Figure 3a shows the real part of the eigenvalues and Figure 3b the positive imaginary part of the eigenvalues. The black curves in Figure 3 show the real and imaginary parts of the pole of the rigid-body rotor mode, where the dashed black line is for the rigid-body rotor mode predicted by a simplified model assuming rigid lateral tower, rigid drivetrain and rotor and quasi-steady aerodynamics. This simplified model is used for comparison to study the effects of flexibility of the rotor and drivetrain and the effects of lateral tower flexibility.

Below 15 m/s there is no significant difference between the pole of the rigid-body rotor mode predicted from the high-order model with quasi-steady aerodynamics and from that predicted using the simplified model, whereas above 15 m/s the eigenvalue of the rigid-body rotor mode becomes more negative than that predicted with a model assuming rigid rotor, because the rigid-body rotor mode couples with the 1st collective flap mode. Above 24 m/s the rigid-body mode couples with the 1st collective flap mode to form a 2nd order mode with real value of approximately -0.25 Hz and non-zero imaginary value.

The red curves in Figure 3 show the real and imaginary parts of the eigenvalues of the 1st collective flap mode. Both the dotted red curves (●) and red curves marked with circles (○) are associated with the 1st collective flap mode. Below 16 m/s, the 1st collective flap mode consists of a set of complex-conjugate poles. Up to 16 m/s, the real part of the pole of the 1st collective flap mode decrease and the aeroelastic frequency decrease, because the aerodynamic damping of this mode increase with wind speed due to higher relative inflow velocities [24]. Above 16 m/s the 1st collective flap mode becomes overdamped and the set of complex-conjugated eigenvalues of the 1st collective flap mode shift to become two poles with purely real and distinct eigenvalues. The assumption of quasi-steady aerodynamics causes that the aerodynamic damping of the 1st collective flap mode is larger than when unsteady aerodynamics is included, see Table I. The green, blue and cyan curves in Figure 3 show the poles of the 1st lateral and longitudinal tower modes and the 1st drivetrain torsional mode.

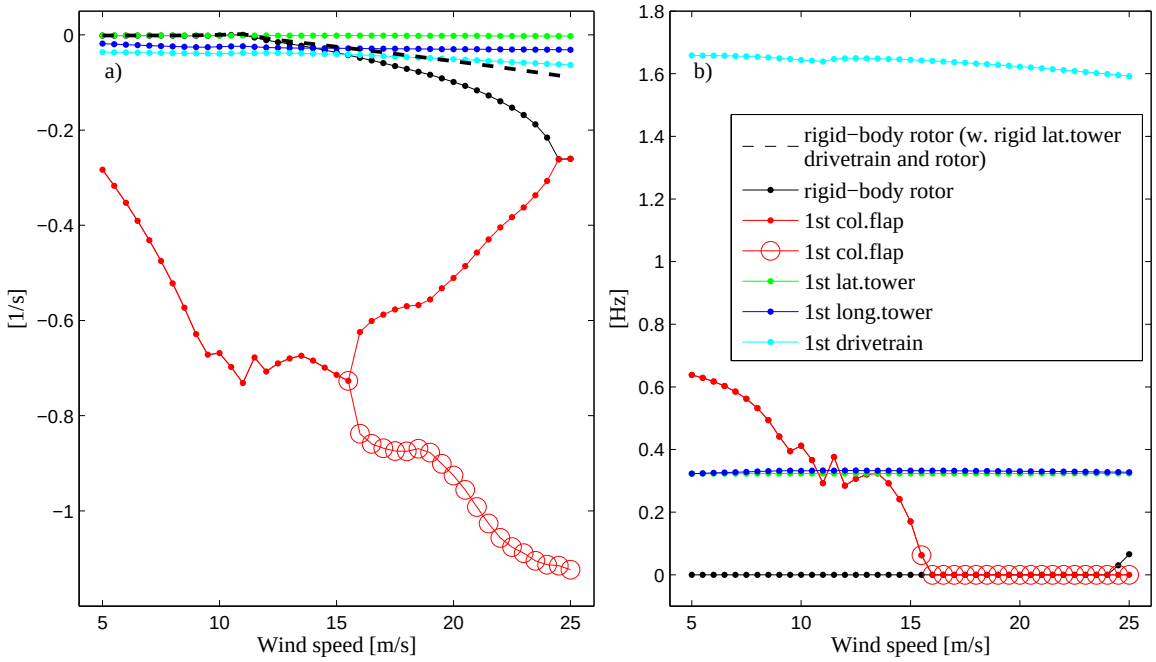

Figure 3. Poles of low-frequency aeroelastic mode shapes for the NREL 5 MW wind turbine in normal operation at wind speeds from 5 m/s to 25 m/s equidistant with 0.5 m/s under assumption of quasi-steady aerodynamics. Figure (a) shows the real part of the eigenvalues and Figure (b) the imaginary part, which is equal to the aeroelastic frequency.

4. ORDER REDUCTION

This section shows how the transfer functions from generator torque, collective pitch angle demands and mean wind speed to generator speed can be approximated by modal truncation.

4.1. Reduction by modal truncation

Order reduction by modal truncation [11] is done by first applying a full-order state transformation: $\mathbf{x} = \mathbf{\Phi q}$ where $\mathbf{\Phi}$ is denoted the *modal matrix* and contains all the eigenvectors of $\mathbf{A}$ in columns. By this state transformation, the system of equations (2) can be written:

$$\dot{\mathbf{q}} = \mathbf{\Lambda q} + \mathbf{\Phi}^{-1}\mathbf{B u} \tag{8a}$$

$$y = \mathbf{C\Phi q} \tag{8b}$$

where $\mathbf{q}$ is the new state vector with generalized states that each describes the motion of a mode shape and $\mathbf{\Lambda}$ is the Jordan form of $\mathbf{A}$. For any square matrix $\mathbf{A}$, the Jordan form is a block diagonal matrix that consist of Jordan blocks. If all eigenvectors of $\mathbf{A}$ are linearly independent, then the Jordan form is a diagonal matrix with the eigenvalues of $\mathbf{A}$ in the diagonal such that each Jordan block is of size 1×1. For all systems used in the present analysis, the modal matrix $\mathbf{\Phi}$ has full rank and thus $\mathbf{A}$ has a diagonal Jordan form.

The eigenvalue decomposed form (8) is then partitioned:

$$\begin{Bmatrix} \dot{\mathbf{q}}_1 \\ \dot{\mathbf{q}}_2 \end{Bmatrix} = \begin{bmatrix} \mathbf{\Lambda}_1 & \mathbf{0} \\ \mathbf{0} & \mathbf{\Lambda}_2 \end{bmatrix} \begin{Bmatrix} \mathbf{q}_1 \\ \mathbf{q}_2 \end{Bmatrix} + \begin{bmatrix} \left[\mathbf{\Phi}^{-1}\right]_1 \\ \left[\mathbf{\Phi}^{-1}\right]_2 \end{bmatrix} \mathbf{B u} \tag{9a}$$

$$y = \mathbf{C} \begin{bmatrix} \mathbf{\Phi}_1 & \mathbf{\Phi}_2 \end{bmatrix} \begin{Bmatrix} \mathbf{q}_1 \\ \mathbf{q}_2 \end{Bmatrix} \tag{9b}$$

where indices 1 and 2 denote subcomponents of the matrices. Order reduction by modal truncation is done by representing the full-order model by the subcomponents of the system matrices with index 1, that corresponds to low-frequency aeroelastic modes and by neglecting all other subcomponents denoted with index 2, such that the reduced-order system of equations are given by:

$$\dot{\mathbf{q}}_1 = \mathbf{\Lambda}_1\mathbf{q}_1 + \left[\mathbf{\Phi}^{-1}\right]_1 \mathbf{B u} \tag{10a}$$

$$y = \mathbf{C\Phi}_1\mathbf{q}_1 \tag{10b}$$

This scheme of a full-order state transformation followed by reduction is applied instead of using a classical modal expansion $\mathbf{x} \approx \Phi_r\mathbf{q}_r$ to get the diagonal structure of $\mathbf{\Lambda}$, which ensures that only the chosen subset of modes are excited by the inputs and measured at the outputs. The modal matrix $\mathbf{\Phi}$ is not orthonormal, regardless of normalization of the eigenvectors, i.e. $\mathbf{\Phi}^{-1} \neq \mathbf{\Phi}^*$, where $*$ denotes the conjugate transpose.

The components of the reduced-order system matrices in Equation (10) are complex but are made real by using a coordinate transformation into the real and imaginary parts of the generalized states $\mathbf{q}_1$. For each set i of complex-conjugated eigenvalues and eigenvectors, the transformed system is written:

$$\dot{\mathbf{q}}_{r,i} = \mathbf{A}_{r,i}\mathbf{q}_{r,i} + \mathbf{B}_{r,i}\mathbf{u} \quad ; \quad y = \mathbf{C}_{r,i}\mathbf{q}_{r,i} \tag{11a}$$

$$\mathbf{A}_{r,i} = \begin{bmatrix} -\xi\omega_n & -\omega_d \\ \omega_d & -\xi\omega_n \end{bmatrix} ; \mathbf{B}_{r,i} = \begin{bmatrix} \mathbf{B}_{r,i,\alpha} \\ \mathbf{B}_{r,i,\beta} \end{bmatrix} = \begin{bmatrix} \left[\mathbf{\Phi}^{-1}\right]_{i,\alpha}\mathbf{B} \\ \left[\mathbf{\Phi}^{-1}\right]_{i,\beta}\mathbf{B} \end{bmatrix} \tag{11b}$$

$$\mathbf{C}_{r,i} = \begin{bmatrix} \mathbf{C}_{r,i,\alpha} \\ \mathbf{C}_{r,i,\beta} \end{bmatrix}^T = 2\mathbf{C} \begin{bmatrix} \mathbf{\Phi}_{i,\alpha} \\ -\mathbf{\Phi}_{i,\beta} \end{bmatrix}^T \tag{11c}$$

where $\mathbf{q}_{r,i} = \begin{Bmatrix} \mathrm{Re}(\mathbf{q}_{1,i}) & \mathrm{Im}(\mathbf{q}_{1,i}) \end{Bmatrix}^T$ and where ω_n is the undamped frequency of mode i found as $\omega_n = |\lambda_i|$, where λ_i is the i'th eigenvalue of $\mathbf{A}$. In Equations (11) ω_d and ξ are the damped frequency and the damping ratio of mode i, respectively, as defined previously in Equation (7). The indices α and β denote the real and imaginary parts, respectively. The factor $2\mathbf{C}$ in the output matrix in (11c) arise because the total output equals twice the real part of the output for one of the complex-conjugated poles.

4.2. Modal truncation including unsteady aerodynamics

In this section, two examples are used to describe the influence of aerodynamically dominated modes on the aeroelastic frequency response of a wind turbine. Because the BEM model assumes that there is no spanwise aerodynamical coupling of unsteady aerodynamic forces on the blades, a relatively large number of aerodynamically dominated modes must be included for good approximation.

Wind Energ. 2012; **00**:1–?? © 2012 John Wiley & Sons, Ltd.
DOI: 10.1002/we
Prepared using weauth.cls

4.2.1. Influence of aerodynamically dominated modes on steady state responses

Figure 4 shows a comparison between the aeroelastic frequency response from generator torque to generator speed predicted by the high-order model (black) and by a reduced-order model obtained by modal truncation including the rigid-body rotor rotation mode (blue) at 8 m/s and 20 m/s. The reduced-order model is seen to accurately approximate the response below the 1st tower modes at 8 m/s but not at 20 m/s, where it predicts too large amplitude at 0 Hz. The red curves in Figure 4 are obtained when including five aerodynamically dominated modes as discussed later.

To find out what modes might cause that the rigid-body rotor mode predicts an offset at 0 Hz, the influence of each mode on the frequency response has been determined. For each of the transfer functions, the importance of each mode is evaluated by the maximum amplification in the frequency response predicted by each modal subsystem in Equation (8), denoted the modal H_∞ norm. Figure 5 shows the modal H_∞ norms versus aeroelastic frequencies and cut-off frequencies of purely real eigenvalues for the transfer function from generator torque to generator speed of all structurally dominated modes (black) and all collective aerodynamically dominated modes (red) at 8 m/s, 14 m/s and 20 m/s.

At 20 m/s in Figure 5c, five to ten collective aerodynamically dominated modes with cut-off frequencies below 0.3 Hz have modal norms close to that of the rigid-body mode, which is located at $\omega_d = 0.035$ Hz at 20 m/s, and are therefore expected to significantly change the frequency response. At lower wind speeds, the modal norms of the collective aerodynamically dominated modes decrease and therefore also the influence of these modes. A similar influence of the aerodynamically dominated modes is seen in the frequency response from collective pitch angle demand and mean wind speed to generator speed (not shown). A reduced-order model that includes the rigid-body rotor mode and the five most important aerodynamically dominated modes which are highlighted by red squares in Figure 5c, predicts the frequency response in the red curves in Figure 4. The inclusion of these modes in the reduced-order model significantly improves the approximation to the steady state generator speed response to generator torque variations.

To evaluate how many aerodynamically dominated modes are needed, reduced-order models has been designed that includes the rigid-body rotor mode and from zero to ten of the most important aerodynamically dominated modes. Figure 6 shows the relative error on the amplitude at 0 Hz predicted by the eleven reduced-order models at 20 m/s for the transfer functions from generator torque, collective pitch angle demand and mean wind speed to generator speed. Without any aerodynamically dominated modes the amplitude at 0 Hz deviates with up to 100% relative to the high-order response. A static error below 20% in the response from collective pitch demand to generator speed is achieved by including at least five aerodynamically dominated modes.

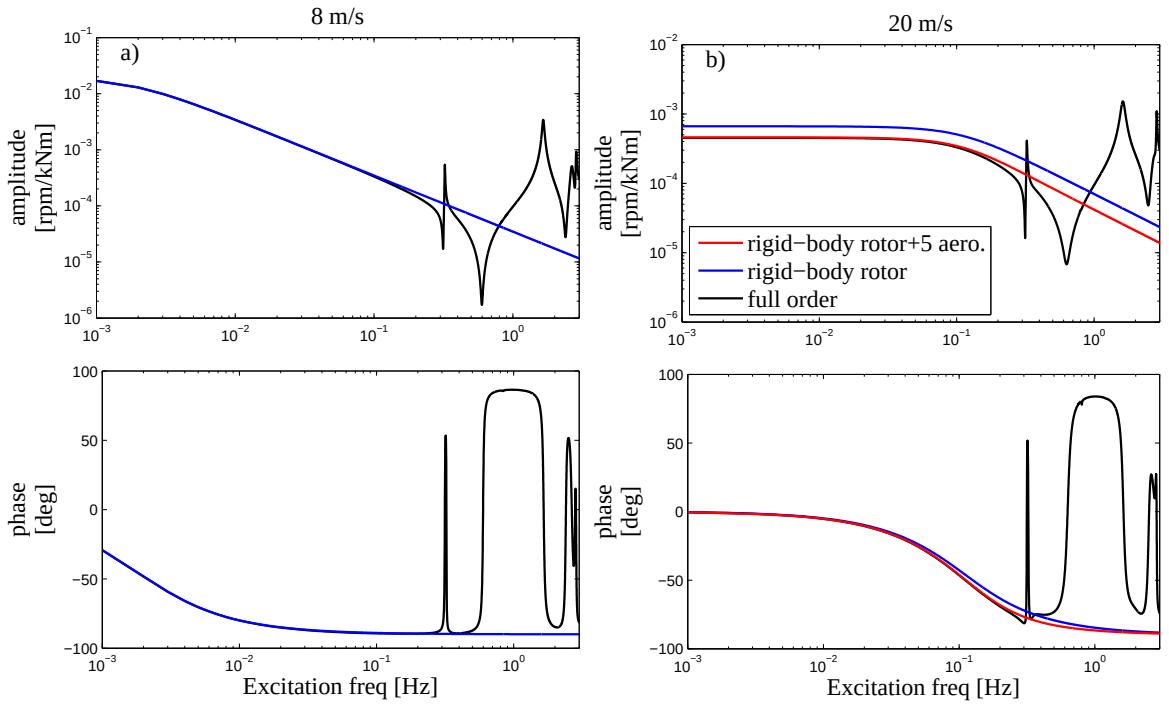

Figure 4. Aeroelastic frequency response from generator torque to generator speed for NREL 5 MW wind turbine in normal operation at 8 m/s and 20 m/s predicted by the full-order model (black) and a reduced-order model including the rigid-body rotor mode (blue) and a model including the rigid-body rotor mode and five collective aerodynamically dominated modes (red).

To explain the effect of the collective aerodynamically dominated modes, Figure 7 shows the variations in aerodynamic forces along a blade in the direction perpendicular to the chord axis, denoted δF_c^*, for the most important aerodynamically dominated mode at 8 m/s, 14 m/s and 20 m/s, respectively. The force variations are determined from the eigenvectors of these modes, which are normalized such that the generator speed components are positive and such that the maximum absolute value is unity. At 8 m/s and 14 m/s the most important aerodynamic modes characterize changes in aerodynamic forces only in one calculation point, whereas the mode at 20 m/s shows variation in aerodynamic forces at many sections along the blade because of coupling with rigid-body rotor rotation, as explained in the following.

The aerodynamically dominated modes are excited by a change in the angle of attack, caused e.g. by blade pitching, flapwise bending, or change of wind speed. At low wind speed a change in angle of attack will cause only small changes in aerodynamic forces because of low relative velocities. For increasing wind speeds, a change in angle of attack will cause large variations in the aerodynamic rotor torque and thrust and the aerodynamically dominated modes will therefore couple with rigid-body rotation of the rotor and the flapwise blade bending modes, causing a change in aerodynamic forces at all sections along the blade. Figure 7 shows that at 20 m/s the structural coupling with rigid-body rotor rotation and flapwise blade bending modes gives a change in relative velocities that decrease the angle of attack - giving higher lift forces - in the inner part of the blade because of stall, and giving lower lift at mid- and outer part where the blades operate in attached flow.

The aerodynamically dominated modes that influence the generator speed variations at 0 Hz at high wind speeds are all characterized by a large variation in aerodynamic forces at the blade mid-span. This observation can be explained by the facts, that the aerodynamically dominated modes at the blade mid-span contributes more to the aerodynamic rotor torque than modes close to the blade root and close to the blade tip, because of low relative velocities and thereby low changes in lift at the blade root and because of low inflow angles at the blade tip causing that changes in lift mainly changes the thrust forces.

It has now been shown that some aerodynamically dominated modes couple with rigid-body rotor rotation and thereby are important in predicting the response of generator speed variations at 0 Hz. Vice versa, the rigid-body rotor mode will couple to some of the aerodynamically dominated modes at above rated wind speeds. Figure 4 showed that approximation with the rigid-body rotor mode alone predicts too high amplitude at 0 Hz in the transfer function from generator torque to speed at 20 m/s, which is because the rigid-body rotor mode couples with some of the aerodynamically dominated modes. The rigid-body rotor mode approximates the changes in rotor speed at 0 Hz too high, because the effective changes in lift when the rotor speed changes are predicted too small in this mode.

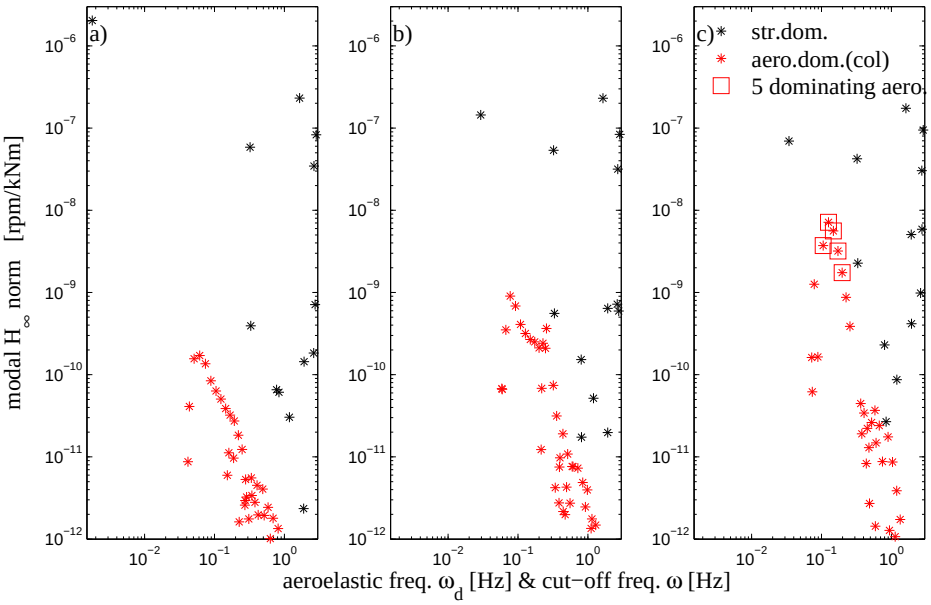

Figure 5. H_∞ norms of each aeroelastic modal subsystem of the system of equations (8) of each structurally dominated modes (black) and collective aerodynamically dominated modes (red) in the transfer function from generator torque to generator speed for the NREL 5 MW wind turbine in normal operation at a) 8 m/s, b) 14 m/s and c) 20 m/s. The red squares in c) show the five most dominating aerodynamically dominated modes at 20 m/s.

Wind Energ. 2012; **00**:1–?? © 2012 John Wiley & Sons, Ltd.
DOI: 10.1002/we
Prepared using weauth.cls

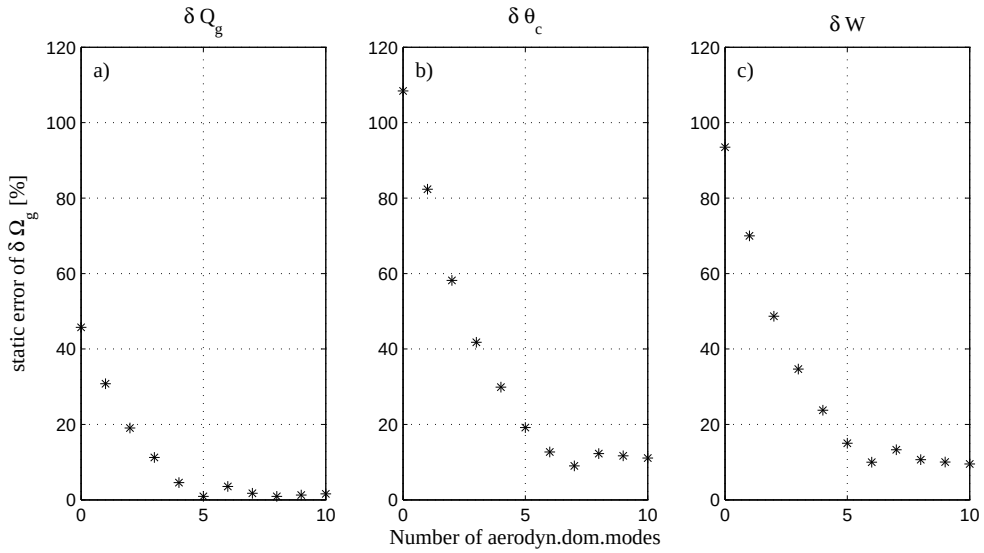

Figure 6. Relative error on the amplitude at 0 Hz in the transfer functions from generator torque, collective pitch angle demand and mean wind speed to generator speed versus number of collective aerodynamically dominated modes included in reduced-order model. The reduced-order model includes the rigid-body rotor mode and from zero to ten aerodynamically dominated modes for the NREL 5 MW wind turbine in normal operation at 20 m/s.

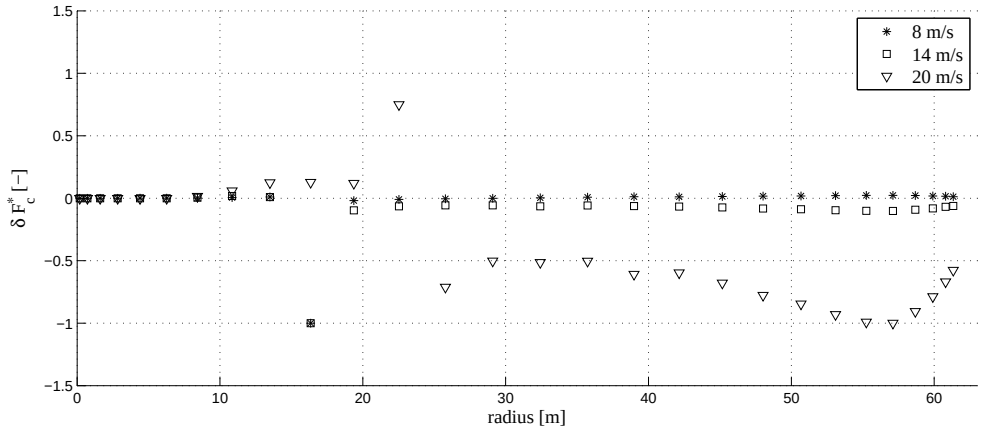

Figure 7. Normalized changes in aerodynamic forces perpendicular to local chord direction versus blade radius of three aerodynamically dominated modes with cut-off frequencies of 0.062 Hz, 0.077 Hz and 0.13 Hz for NREL 5 MW wind turbine in normal operation at 8 m/s, 14 m/s and 20 m/s, respectively. Each of the three modes has the highest influence on rotor speed output of all aerodynamically dominated modes at the specific wind speeds.

4.2.2. Influence of aerodynamically dominated modes on dynamic responses

The last section showed that five to ten aerodynamically dominated modes must be included to achieve good approximation of the response at frequencies below the 1st tower modes. This section shows that other aerodynamically dominated modes affect accurate prediction of the non-minimum phase zeros at the 1st longitudinal tower mode in the response from collective pitch to generator speed [25]. These aerodynamically dominated modes are necessary to include in modal truncation, because the 1st longitudinal tower mode couples to these modes. However, it has previously been shown, that a model assuming rigid drivetrain and rotor, and quasi-steady aerodynamics can correctly predict the existence of non-minimum phase zeros at above rated wind speeds in the transfer function from collective pitch to generator speed [17].

Figure 8 shows the aeroelastic frequency response from collective pitch angle demand to generator speed for the NREL 5 MW wind turbine in normal operation at 14 m/s and 20 m/s as predicted by the high-order model (black) and by reduced-order models designed by modal truncation including different aeroelastic modes. All reduced-order models in this section include the rigid-body rotor mode and the ten most dominating aerodynamically dominated modes to ensure accurate prediction of changes in aerodynamic torque at 0 Hz.

The red curves in Figure 8 show that a model including also the 1st longitudinal and lateral tower modes predicts existence of a minimum phase zero at 0.31 Hz at both 14 m/s and 20 m/s at the aeroelastic frequency of the 1st longitudinal tower mode. The green curves in Figure 8 shows, that when furthermore the 1st collective flap mode is included, the model predicts a non-minimum phase zero at 0.32 Hz at 14 m/s but not at 20 m/s.

The reason why the 1st collective flap mode must be included, when it is previously shown that a rigid rotor can predict the non-minimum phase zero [17], is because the 1st longitudinal tower mode couples with the 1st collective flap mode. In the forced response of collective pitching at the 1st tower mode, the flap motion is however somewhat limited by the changes in thrust forces associated with the variation in collective pitch. The 1st longitudinal tower mode couples with the 1st collective flap mode, because of the changes in aerodynamic forces at the blades due to changes in relative velocities caused by the longitudinal tower motion. The 1st longitudinal tower mode is characterized by a motion where a positive tower velocity in the downwind direction is in phase with a collective flapwise deflection velocity relative to the hub in the upwind direction, due to the changes in aerodynamic forces on the blades associated with the longitudinal tower motion. The reason why the model without the 1st collective flap mode cannot correctly predict the non-minimum phase zero at the 1st tower modes is because of too small changes in aerodynamic torque and thrust predicted with these modes, due to the collective flap vibration in the 1st longitudinal tower mode.

The cyan curves in Figure 8b show, that the non-minimum phase can be correctly predicted at 20 m/s by including four collective aerodynamically dominated modes with cut-off frequencies of $\omega_c = 0.41$ Hz, 0.45 Hz, 0.60 Hz and 0.75 Hz. The cut-off frequencies are slightly higher than of those aerodynamically dominated modes already included, because these modes are characterized by changes in aerodynamic forces at the blade tip where the inflow velocities are higher and the cut-off frequencies therefore higher. Figure 9 shows snap shots of variation in aerodynamic forces of the aerodynamically dominated mode with a cut-off frequency of 0.75 Hz. The chosen mode is characterized by high changes in thrust forces at the blade tip, which can be explained by the relative small inflow angles at the blade tip. The changes in thrust forces associated with the aerodynamically dominated modes at the blade tip, makes these modes important for correct prediction of the non-minimum phase zero at the 1st longitudinal tower mode.

Wind Energ. 2012; **00**:1–?? © 2012 John Wiley & Sons, Ltd.
DOI: 10.1002/we
Prepared using weauth.cls

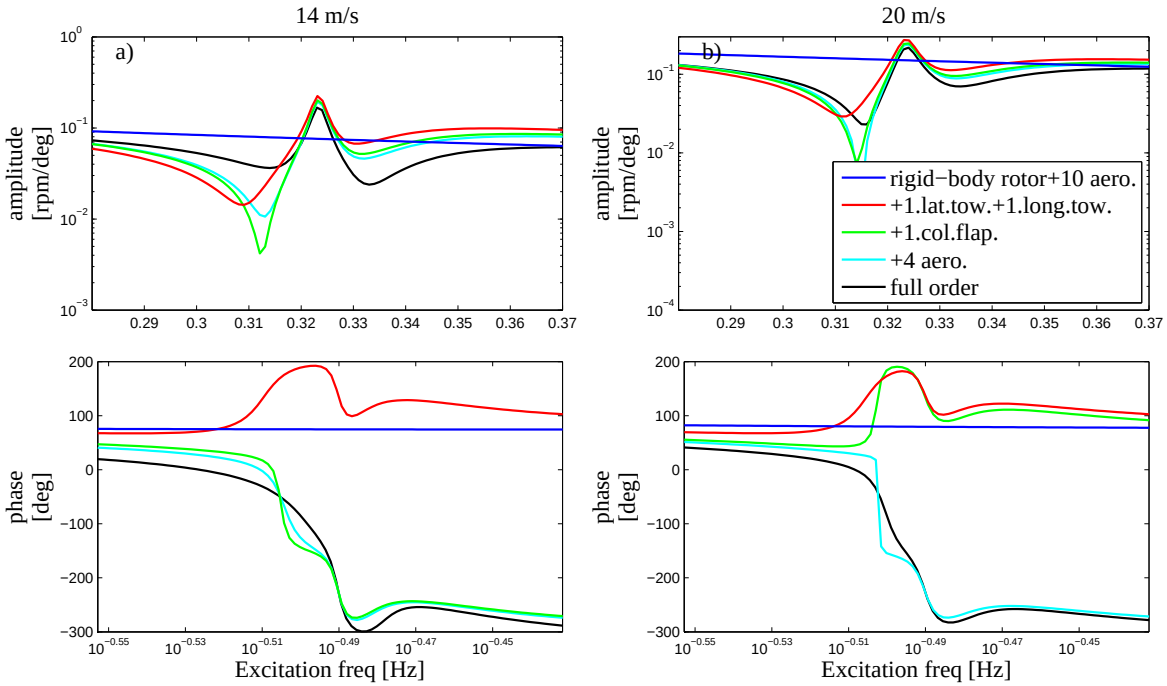

Figure 8. Aeroelastic frequency response from collective pitch angle demand to generator speed predicted by the full-order model with unsteady aerodynamics (black) and predicted by a reduced-order model including the rigid-body mode and ten collective aerodynamically dominated modes (blue), and by reduced-order models including **also** the 1^{st} lateral and longitudinal tower modes (red), including **also** the 1^{st} collective flap mode (green) and including **also** four collective aerodynamically dominated modes characterizing unsteady aerodynamics at the blade tip (cyan).

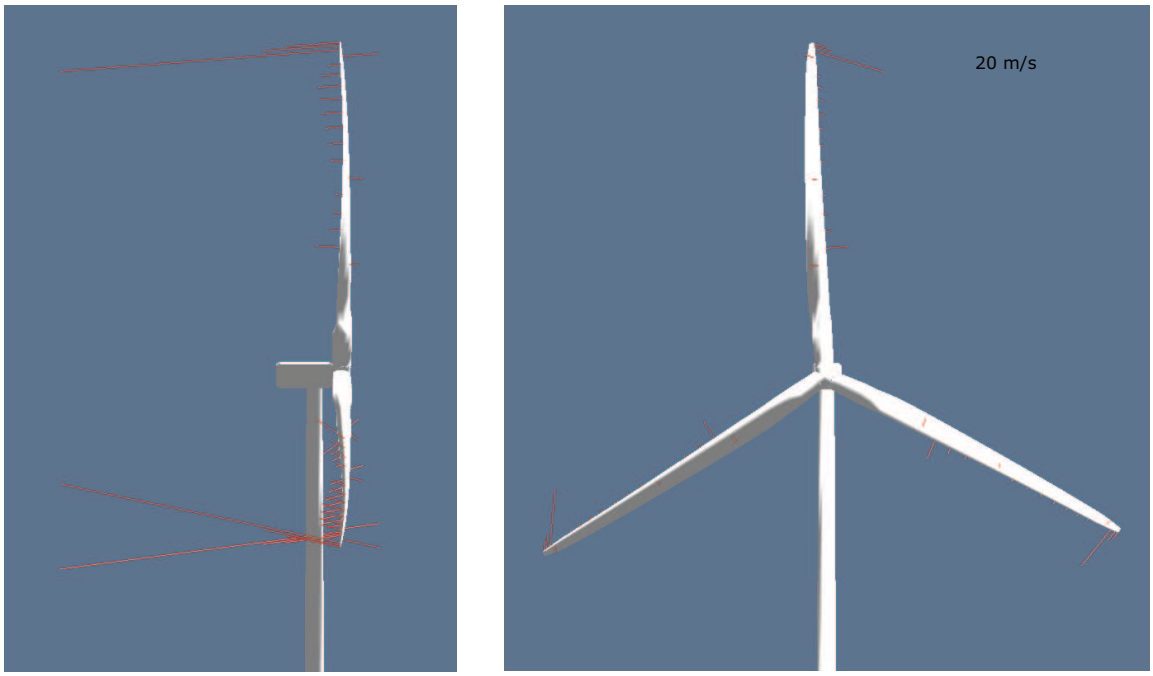

Figure 9. Snap shots of variations in aerodynamic forces of one collective aerodynamically dominated mode with cut-off frequency of $\omega_c = 0.75$ Hz for the NREL 5 MW in normal operation at 20 m/s. This mode is characterized by unsteady aerodynamics in a blade section close to the tip, where a change in angle of attack produces high changes in thrust.

4.3. Modal truncation including quasi-steady aerodynamics

An assumption of quasi-steady aerodynamics has been found to give accurate predictions of the aeroelastic frequency response from changes in generator torque, collective pitch angles and in mean wind speed, except at around the 1st drivetrain torsion mode in the response from collective pitch to speed, where a quasi-steady aerodynamic model fails to correctly predict a zero located close to pole of this mode [17]. Limitations of the pitch actuator may limit the changes in actual pitch angles at variations in the pitch angle demands at the frequencies of the 1st drivetrain mode and thereby also the influence of the unsteady aerodynamics at these frequencies.

Order reduction is now performed by modal truncation using aeroelastic mode shapes in which quasi-steady aerodynamics is assumed. It is shown how each of the transfer functions from generator torque, collective pitch angle demands and mean wind speed to generator speed can be approximated by gradually increasing the number of aeroelastic modes in the reduced-order model. Table II list the content of the various reduced-order models.

4.3.1. Frequency response from generator torque to generator speed

Figure 10 shows the aeroelastic frequency response from generator torque to generator speed predicted by a full-order model with quasi-steady aerodynamics (black) and by four different reduced-order models denoted by model no. 1 to 4 defined in Table II.

The reduced-order model no. 1, that includes the rigid-body rotor mode and the 1st lateral tower mode estimates correctly the high gain at 0 Hz, see blue curves in Figure 10. The model correctly predicts the zero at 0.315 Hz and the resonance peak at 0.32 Hz at both 8 m/s and 20 m/s, because they exist due to nacelle roll associated with the 1st lateral tower mode.

The red curves in Figure 10 show the response predicted by the reduced-order model no. 2 including also the 1st drivetrain mode. At 8 m/s, the model captures correctly the presence of the minimum-phase zero at 0.72 Hz and the resonance peak at the 1st drivetrain mode. At 20 m/s, the model 2 predicts a non-minimum phase zero at 0.72 Hz that causes a negative phase shift of -180 deg. By including also the 2nd collective flap mode (model no. 3), the zero at 0.72 Hz becomes a minimum-phase zero at 20 m/s, whereas at 8 m/s there is no visible change in the response. The prediction of a non-minimum phase zero of the reduced-order model no. 2 at 0.72 Hz, can be explained by a coupling of the 1st drivetrain mode with the 2nd collective flap mode at high wind speeds due to the larger pitch angles. The 2nd collective flap mode (model no. 3) compensates for the flap motion already included with the 1st drivetrain mode. By additionally including the 2nd drivetrain and the 2nd lateral tower modes (model no. 4), the reduced-order model can correctly predict the response up to 3 Hz.

4.3.2. Frequency response from collective pitch and mean wind speed to generator speed

Figures 11 and 12 show the aeroelastic frequency response from collective pitch angle demand and mean wind speed, respectively, to generator speed for the NREL 5 MW turbine in normal operation at 14 m/s and 20 m/s, predicted by the full-order model with unsteady airfoil aerodynamics (black), under assumption of instant update in the mean wind speed, and with quasi-steady aerodynamics (dashed black) and by five different reduced-order models that includes the aeroelastic modes given in model no. 5 to 9 in Table II.

The blue curves in Figures 11 and 12 show the responses predicted by the model no. 5 that includes the rigid-body rotor mode. At 14 m/s, the model correctly predicts the response at 0 Hz whereas at higher wind speeds , e.g. 20 m/s, it predicts too high amplitude for both pitch and wind speed inputs, as already described in Section 4.2.1 for the model including unsteady aerodynamics. A correct amplitude and phase is achieved at up to the aeroelastic frequency of the 1st tower modes by including also the 1st collective flap mode in model no. 6, shown with red curves. The rigid-body rotor mode couples with the 1st collective flap mode at high wind speed when quasi-steady aerodynamics is assumed, such that

Table II. Description of the aeroelastic modes included in the various reduced-order models used to approximate the aeroelastic frequency response of the NREL 5 MW turbine. The aeroelastic modes are determined using quasi-steady aerodynamics.

Model no.	Aeroelastic modes included in model
1	rigid-body rotor, 1st lateral tower
2	rigid-body rotor, 1st lateral tower, 1st drivetrain
3	rigid-body rotor, 1st lateral tower, 1st drivetrain, 2nd collective flap
4	rigid-body rotor, 1st lateral tower, 1st drivetrain, 2nd collective flap, 2nd drivetrain, 2nd lateral tower
5	rigid-body rotor
6	rigid-body rotor, 1st collective flap
7	rigid-body rotor, 1st lateral tower, 1st longitudinal tower, 1st collective flap
8	rigid-body rotor, 1st lateral tower, 1st longitudinal tower, 1st collective flap, 1st drivetrain
9	rigid-body rotor, 1st lateral tower, 1st longitudinal tower, 1st collective flap, 1st drivetrain, 2nd collective flap, 2nd drivetrain

Wind Energ. 2012; **00**:1–?? © 2012 John Wiley & Sons, Ltd.
DOI: 10.1002/we
Prepared using weauth.cls

the rigid-body rotor mode alone predicts too high gain at 0 Hz because flap vibration lowers the aerodynamic damping of this mode due to the effect of the flapwise blade motion on the angle of attack in the velocity triangle.

The dashed red curves in Figures 11 and 12 show the aeroelastic response predicted by the model no. 7 that includes also the 1st tower modes. At both 14 m/s and 20 m/s and for both inputs, the negative phase shift of -360 deg caused by the non-minimum phase zero at the 1st longitudinal tower mode is captured by the model.

The green curves in Figures 11 and 12 show the response of the reduced-order model no. 8, where also the 1st drivetrain mode is included. For collective pitch inputs, the model approximates well both amplitude and phase up to the frequency of the 1st drivetrain mode, except that it predicts too low amplitude at frequencies in between the 1st tower modes and the 1st drivetrain mode mainly at 20 m/s. For mean wind speed inputs, the model no. 8 (green curves in Figure 12) does not capture correctly the non-minimum phase zero at the 1st longitudinal tower mode, which can be explained by the collective flap motion introduced by the 1st drivetrain mode.

The cyan curves in Figures 11 and 12 show the response predicted by model no. 9 including the 2nd collective flap mode and the 2nd drivetrain mode and a total of thirteen states. The combined effect of adding the 2nd collective flap mode and the 2nd drivetrain mode leads to a good approximation of the full order response with quasi-steady aerodynamics up to 3 Hz at both 14 m/s and 20 m/s for both inputs.

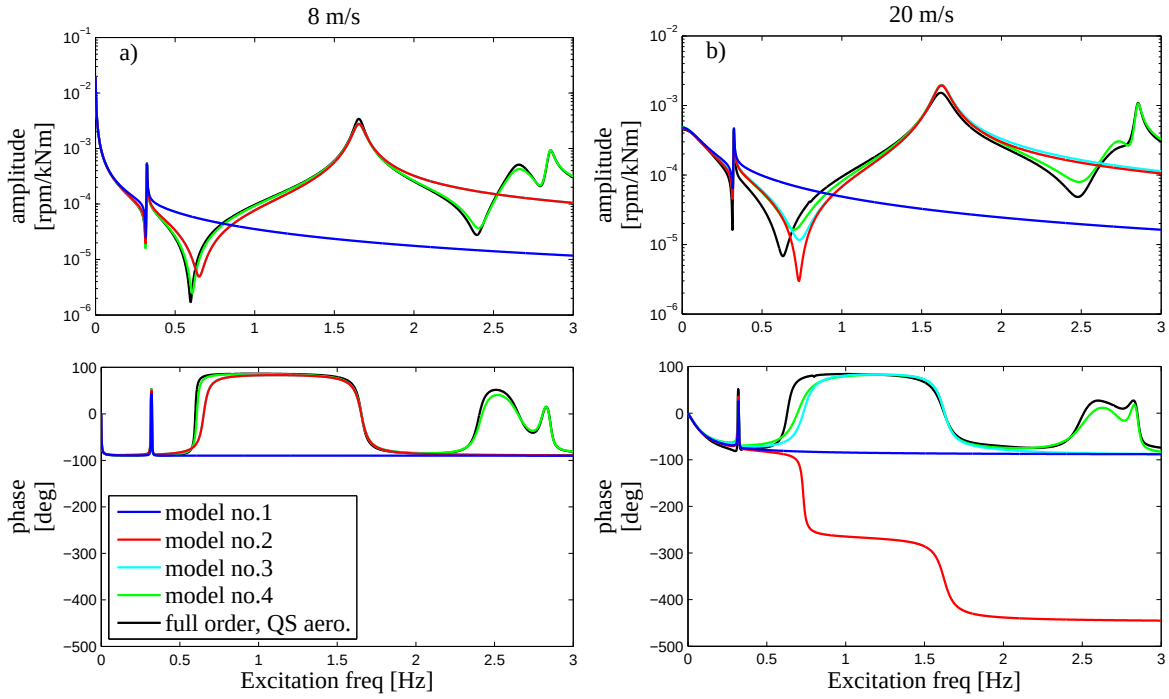

Figure 10. Aeroelastic frequency response from generator torque to generator speed for NREL 5 MW turbine in normal operation at 8 m/s and 20 m/s. Comparison between responses predicted by a model assuming quasi-steady aerodynamics (black) and predicted by reduced-order models obtained by modal truncation including the aeroelastic modes in model no. 1 to 4 defined in Table II.

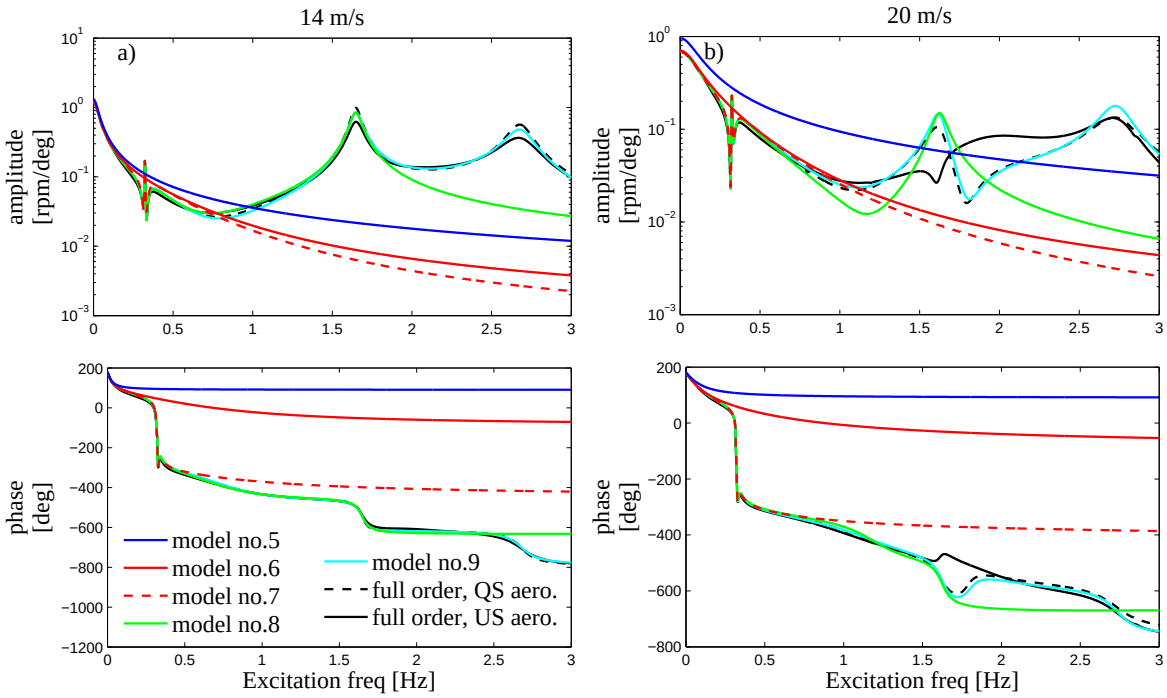

Figure 11. Aeroelastic frequency response from collective pitch demand to generator speed for NREL 5 MW turbine in normal operation at 14 m/s and 20 m/s. Comparison between responses predicted by a model assuming quasi-steady aerodynamics (black curves) and predicted by reduced-order models obtained by modal truncation including the aeroelastic modes in model no. 5 to 9 listed in Table II.

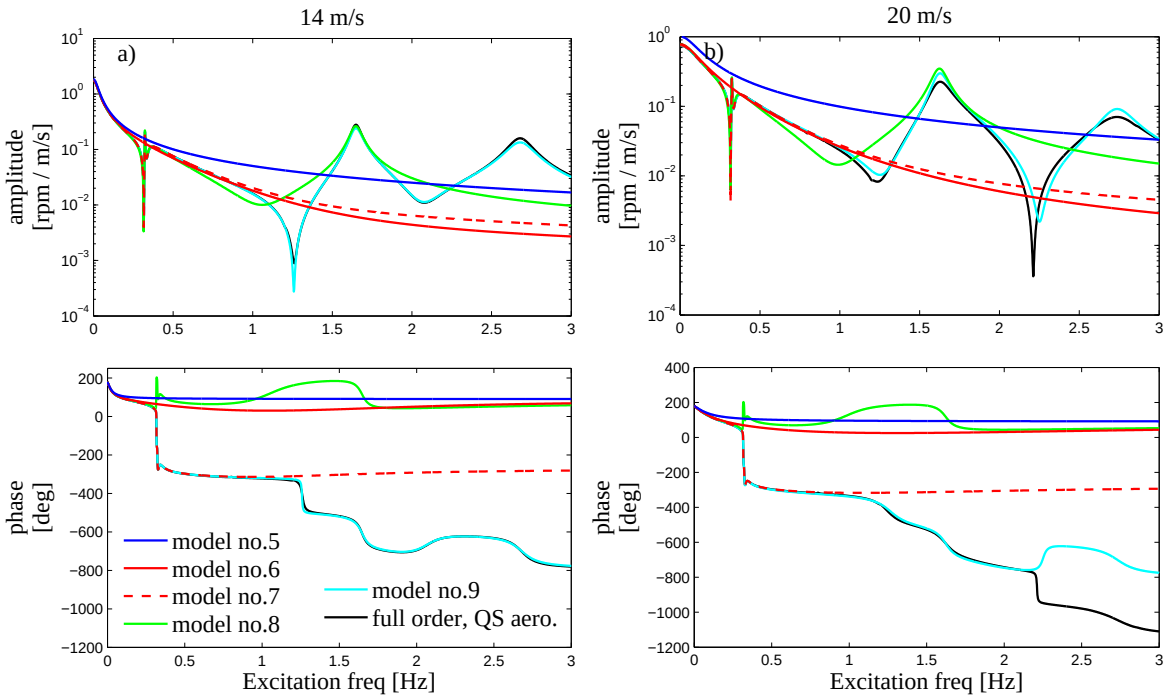

Figure 12. Aeroelastic frequency response from changes in mean wind speed to generator speed for NREL 5 MW turbine in normal operation at 14 m/s and 20 m/s. Comparison between responses predicted by a model assuming quasi-steady aerodynamics (black curves) and predicted by reduced-order models obtained by modal truncation including the aeroelastic modes in model no. 5 to 9 listed in Table II.

Wind Energ. 2012; **00**:1–?? © 2012 John Wiley & Sons, Ltd.
DOI: 10.1002/we
Prepared using weauth.cls

4.4. Reduced-order models for controller design

A set of reduced-order models of the type no. 8 using quasi-steady aerodynamics and including the rigid-body rotor mode, the 1st lateral and longitudinal tower modes, the 1st drivetrain mode and the 1st collective flap mode, i.e. five modes in total, has been designed for the NREL 5 MW turbine in normal operation at wind speeds from 5 m/s to 25 m/s, equidistant with 0.5 m/s. The model no.8 is used here for brevity, although this model not accurately predicts the phase of the response of mean wind speed changes, see Figure 12. The results however still apply for models of higher complexity, because the subset of the matrices corresponding to the state-variables of the modes in model no.8 remains unchanged in model no.9. The modes included in the reduced-order models are ordered according to their mode shape to make the models suited for parametrization.

The reduced-order dynamic matrix $\mathbf{A}_r$ is on block diagonal form and consists of matrices $\mathbf{A}_{r,i}$ of the five modes that are used in the reduced-order models, see Equation (11). The components of $\mathbf{A}_{r,i}$ are the real and imaginary parts of the eigenvalues of mode i and are shown previously in Figure 3. The real and imaginary parts of the eigenvalues of the rigid-body rotor mode, the 1st lateral and longitudinal tower modes and the 1st drivetrain mode all vary smoothly with wind speed, whereas the components for the 1st collective flap mode show some discontinuities at 11 m/s, where the mean blade pitch changes from negative to positive pitch angles. The 1st collective flap mode was seen to shift from a 2nd order mode up to 16 m/s into two 1st order modes above 16 m/s. Above 16 m/s both 1st order modes are included in the model to ensure that the order of the reduced-order model is the same at all wind speeds.

The components of the reduced-order input matrix $\mathbf{B}_r$ and of the reduced-order output matrix $\mathbf{C}_r$ depends on how the eigenvectors of $\mathbf{A}$ are normalized prior to the eigenvalue decomposition. Here, the eigenvectors are normalized such that their generator speed component becomes

$$\phi_{i,\Omega} = \omega_d\big(\frac{\xi}{\sqrt{1-\xi^2}} + j2\big) \qquad \text{and} \qquad \bar{\phi}_{i,\Omega} = \omega_d\big(\frac{\xi}{\sqrt{1-\xi^2}} - j2\big) \tag{12}$$

where $\phi_{i,\Omega}$ and $\bar{\phi}_{i,\Omega}$ are the generator speed components of the two eigenvectors related to each 2nd order mode and where $j = \sqrt{-1}$ and ω_d and ξ are the aeroelastic frequency and damping ratio of the corresponding mode, respectively. This specific normalization of the eigenvectors is convenient, because it ensures that the components of the reduced-order input and output matrices can be given a physical interpretation. When the eigenvectors of $\mathbf{A}$ are normalized such that their generator speed components are given by those in Equation (12), then the reduced-order output matrix for this mode is found from Equations (5) and (11c) to be:

$$\mathbf{C}_{r,i} = \begin{bmatrix} 2\text{Re}(\phi_{i,\Omega}) & -2\text{Im}(\phi_{i,\Omega}) \end{bmatrix} = \begin{bmatrix} 2\omega_n\xi & -4\omega_d \end{bmatrix} \qquad \text{(for 2nd order modes)} \tag{13}$$

where ω_n is the undamped frequency of this mode found as $\omega_n = |\lambda_i|$, where λ_i is the i'th eigenvalue of $\mathbf{A}$. Similarly, the eigenvectors of the 1st order modes are normalized prior to order reduction, such that their generator speed component equals: $\phi_{i,\Omega} = -2\lambda_i$. The component of the output matrix $\mathbf{C}_{r,i}$ for the 1st order modes is then:

$$\mathbf{C}_{r,i} = -2\lambda_i \qquad \text{(for 1st order modes)} \tag{14}$$

The components of $\mathbf{C}_{r,i}$ given in Equations (13) and (14) are the scaled real and imaginary parts of the eigenvalues related to the corresponding mode, which makes the output matrix suited for parametrization, as shown in the following. Figure 13 shows the components of the reduced-order output matrix $\mathbf{C}_r$ extracting the generator speed output from the generalized state-variables of the rigid-body rotor mode, the 1st collective flap mode, the 1st lateral and longitudinal tower modes and the 1st drivetrain mode for the NREL 5 MW wind turbine in normal operation at wind speeds from 5 m/s to 25 m/s. For comparison, the output matrix for a fully flexible turbine including unsteady aerodynamics are compared to the output matrix corresponding to the 1st longitudinal tower mode and the rigid-body rotor mode for a turbine with rigid lateral tower, drivetrain and rotor including quasi-steady aerodynamics, as introduced previously.

The black points and black dashed curves in Figure 13 show the components of the output matrix corresponding to the generalized state-variable of the rigid-body rotor mode, denoted $\mathbf{C}_{r,1}$. Both for a fully flexible turbine and a turbine with rigid rotor, the components increase with wind speed above rated, because the aerodynamic damping of the rigid-body rotor motion - and thereby the magnitude of the eigenvalue λ of this mode - increase with wind speed, due to the increased blade pitch angles. The component $\mathbf{C}_{r,1}$ for a fully flexible turbine are higher than for a turbine with rigid rotor which can be explained by decreasing inertia in the rigid-body rotor mode due to coupling with collective flap blade vibration, causing the magnitude of the eigenvalue to increase.

The red points and red circles in Figure 13 show the components of the output matrix corresponding to the 1st collective flap mode which are denoted $\mathbf{C}_{r,2}$ and $\mathbf{C}_{r,3}$. Up to 16 m/s, the 1st collective flap mode is a 2nd order mode, as previously explained, and the two components $\mathbf{C}_{r,2}$ and $\mathbf{C}_{r,3}$ are equal to the first and second components of $\mathbf{C}_{r,i}$ in Equation (13), respectively. Both components increase up to 16 m/s, because the aerodynamic damping of the flap mode increase. The

component $\mathbf{C}_{r,2}$ is continuous across 16 m/s, where the flap mode change into two 1st order modes, because the specific normalization of the eigenvectors ensures this; i.e. $\mathbf{C}_{r,2}$ can be written as $2\omega_n\xi = -2\mathrm{Re}(\lambda)$, which is identical to the output component for the 1st order mode: -2λ when the eigenvalue becomes purely real at 16 m/s. Above 16 m/s the two components $\mathbf{C}_{r,2}$ and $\mathbf{C}_{r,3}$ vary similarly to the eigenvalues of the two 1st order modes shown previously in Figure 3.

The green points in Figure 13 show the components of the output matrix corresponding to the state-variables of the 1st lateral tower mode, which are denoted $\mathbf{C}_{r,4}$ and $\mathbf{C}_{r,5}$ and corresponds to the first and second component of $\mathbf{C}_{r,i}$ in (13). The component $\mathbf{C}_{r,4}$ increase slightly with wind speed due to the increasing aeroelastic damping of the 1st lateral tower mode, which can be explained by coupling to longitudinal tower motion, as explained previously in [17]. The other component $\mathbf{C}_{r,5}$ is almost constant with wind speed.

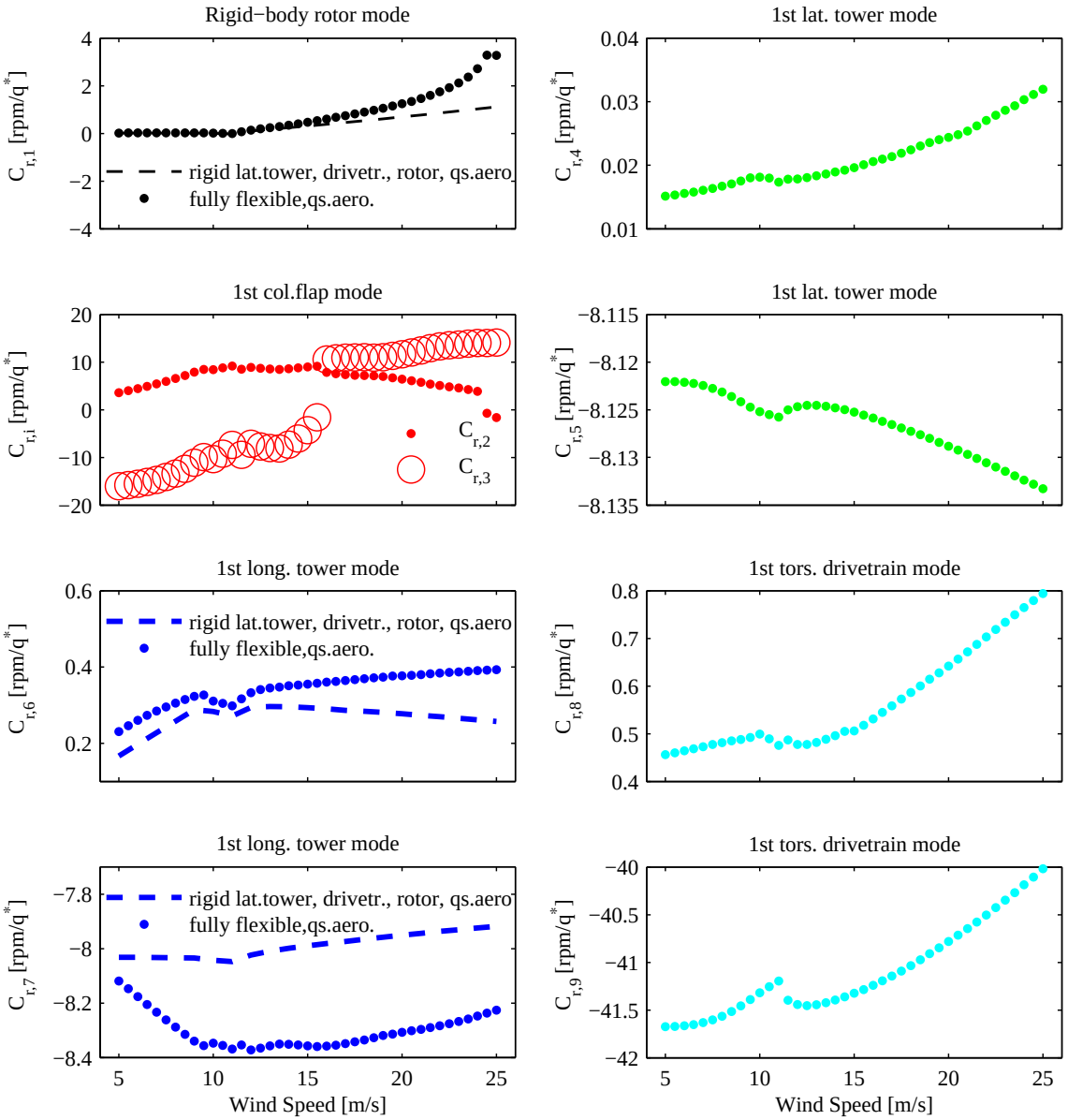

Figure 13. Components of the reduced-order output matrices $\mathbf{C}_{r,i}$ extracting the generator speed output from the generalized state-variables of the rigid-body rotor mode, the 1st collective flap mode, the 1st lateral and longitudinal tower modes and the 1st drivetrain mode for the NREL 5 MW wind turbine in normal operation at wind speeds from 5 m/s to 25 m/s and found under assumption of quasi-steady aerodynamics. The dashed curves show the output matrices predicted with a model with rigid lateral tower, rigid rotor and drivetrain including quasi-steady aerodynamics. The unit q^* denotes the unit of the generalized state-variables $\mathbf{q}_i$.

Wind Energ. 2012; **00**:1–?? © 2012 John Wiley & Sons, Ltd.
DOI: 10.1002/we
Prepared using weauth.cls

The blue points and blue dashed lines in Figure 13 show the two components of the output matrix corresponding to the 1st longitudinal tower mode which are denoted $\mathbf{C}_{r,6}$ and $\mathbf{C}_{r,7}$ and which equals the first and second components of $\mathbf{C}_{r,i}$ in (13), respectively. The figure shows a comparison between $\mathbf{C}_{r,6}$ and $\mathbf{C}_{r,7}$ for a fully flexible turbine and a turbine with rigid lateral tower, drivetrain and rotor. The model with a rigid rotor predicts components with magnitudes below that for a fully flexible turbine, which can be explained by the lack of collective flap vibration in the longitudinal mode. The aeroelastic damping of the 1st longitudinal tower mode is higher for a rigid rotor than for a flexible because of collective flap vibration out of phase with longitudinal tower top vibration, which explains the lower magnitudes of $\mathbf{C}_{r,7}$.

The cyan points in Figure 13 show the components of $\mathbf{C}_{r,i}$ for the 1st torsional drivetrain mode, which are denoted $\mathbf{C}_{r,8}$ and $\mathbf{C}_{r,9}$ and correspond to the first and second components of $\mathbf{C}_{i,i}$ in (13), respectively. The component $\mathbf{C}_{r,8}$ increase gradually with wind speed, which can be explained by larger aerodynamic damping of the rotor rotation motion in the 1st longitudinal tower mode, due to higher pitch angles, which also explains the increasing values of the other component $\mathbf{C}_{r,9}$ with wind speed.

The reduced-order input matrix $\mathbf{B}_r$ consist of modal blocks of $\mathbf{B}_{r,i}$, defined in Equation (11), that each describes the external excitation of the i'th mode. With the specific normalization of the eigenvectors of $\mathbf{A}$ in Equations (13) and (14), the components of $\mathbf{B}_{r,i}$ can be given a physical interpretation from the transfer function matrix from the three inputs to the generator speed output of the i'th modal subsystem of the system of equations in (10). The modal transfer function matrix is denoted $\mathbf{G}_{r,i}(s)$ and is found from Equation (11) to be

$$\mathbf{G}_{r,i}(s) = \mathbf{C}_{r,i}(s\mathbf{I} - \mathbf{A}_{r,i})^{-1}\mathbf{B}_{r,i} \tag{15}$$

for both 1st and 2nd order modes, where s is the Laplace variable and the matrices $\mathbf{A}_{r,i}$, $\mathbf{B}_{r,i}$ and $\mathbf{C}_{r,i}$ are the system matrices of the i'th modal subsystem. A physical interpretation of the components of $\mathbf{B}_r$ is found from the amplitude of the frequency response of $\mathbf{G}_{r,i}(s)$ at 0 Hz for 1st order modes and at the aeroelastic frequency ω_d for 2nd order modes, which are found to be:

$$|\mathbf{G}_{r,i}(0)| = -2\mathbf{B}_{r,i} \qquad \text{(for 1st order modes)} \tag{16}$$

$$|\mathbf{G}_{r,i}(j\omega_d)|^2 = \frac{4}{\xi^2}\left(\mathbf{B}_{r,i,\alpha}^2 + (1-\xi^2)\mathbf{B}_{r,i,\beta}^2 - 2\xi\sqrt{1-\xi^2}\mathbf{B}_{r,i,\alpha}\mathbf{B}_{r,i,\beta}\right) \qquad \text{(for 2nd order modes)} \tag{17}$$

where $\mathbf{B}_{r,i,\alpha}$ and $\mathbf{B}_{r,i,\beta}$ are the components of the modal input matrix for 2nd order modes.

Equation (16) shows that for 1st order modes, we can understand the components of the input matrix $\mathbf{B}_{r,i}$ as the amplitude at 0 Hz in the aeroelastic frequency response of this mode scaled with a factor of $1/2$; i.e. $\mathbf{B}_{r,i}$ denotes how much the i'th mode contributes to the amplitude at 0 Hz in the aeroelastic frequency response from the generator torque, collective pitch and mean wind speed inputs to the generator speed output.

Equation (17) shows that for 2nd order modes, we can understand both components $\mathbf{B}_{r,i,\alpha}$ and $\mathbf{B}_{r,i,\beta}$ of the input matrix as the amplitude in the frequency response of this modal subsystem evaluated at the resonance peak, i.e. at $\omega = \omega_d$. For modes that are lowly damped, the last term in (17) can be neglected, showing that whenever the magnitudes of $\mathbf{B}_{r,i,\alpha}$ and $\mathbf{B}_{r,i,\beta}$ either decrease or increase, so does the amplitude at the aeroelastic frequency of this mode: $|\mathbf{G}_{r,i}(j\omega_d)|$.

Figure 14 shows the magnitude of the components of the reduced-order input matrix $\mathbf{B}_{r,i}$ from the three inputs: a) generator torque, b) collective pitch angle and c) mean wind speed to the generalized state-variables of the rigid-body rotor mode (black points) and the 1st collective flap mode (red points and circles). The figure shows a comparison with the input matrix corresponding to the rigid-body rotor mode predicted with a model with rigid lateral tower, rigid rotor and drivetrain and quasi-steady aerodynamics, which are shown with black crosses.

Up to around 15 m/s, the black points and black crosses in Figure 14 are close to each other, showing that the assumption of rigid rotor has no effect on the response of the rigid-body rotor mode. For collective pitch and mean wind speed inputs above 15 m/s, the input $\mathbf{B}_{r,i}$ increase relative to that of a turbine with rigid rotor because the rigid-body rotor mode couples with the 1st collective flap mode at high wind speeds, causing the aerodynamic damping of this mode to decrease and thereby the amplitude of the generator speed output at 0 Hz to increase, as shown previously in Figures 11 and 12.

The red points and circles in Figure 14 show the components of $\mathbf{B}_{r,i}$ for the 1st collective flap mode. The 1st collective flap mode is a 2nd order mode below 16 m/s and above 16 m/s the 1st collective flap mode consist of two 1st order modes, as explained previously. The trend is that the components of $\mathbf{B}_{r,i}$ for the 1st collective flap mode are very low at low wind speeds for all three inputs, showing that the influence of the 1st collective flap mode on the generator speed response is low. Some discontinuity with wind speed is seen at 16 m/s for all three inputs, because here the flap mode turns from being one 2nd order mode to two 1st order modes. Above 16 m/s the amount of excitation of the 1st collective flap mode increase and becomes equally important in the generator speed response as the rigid-body rotor mode, because of the coupling between

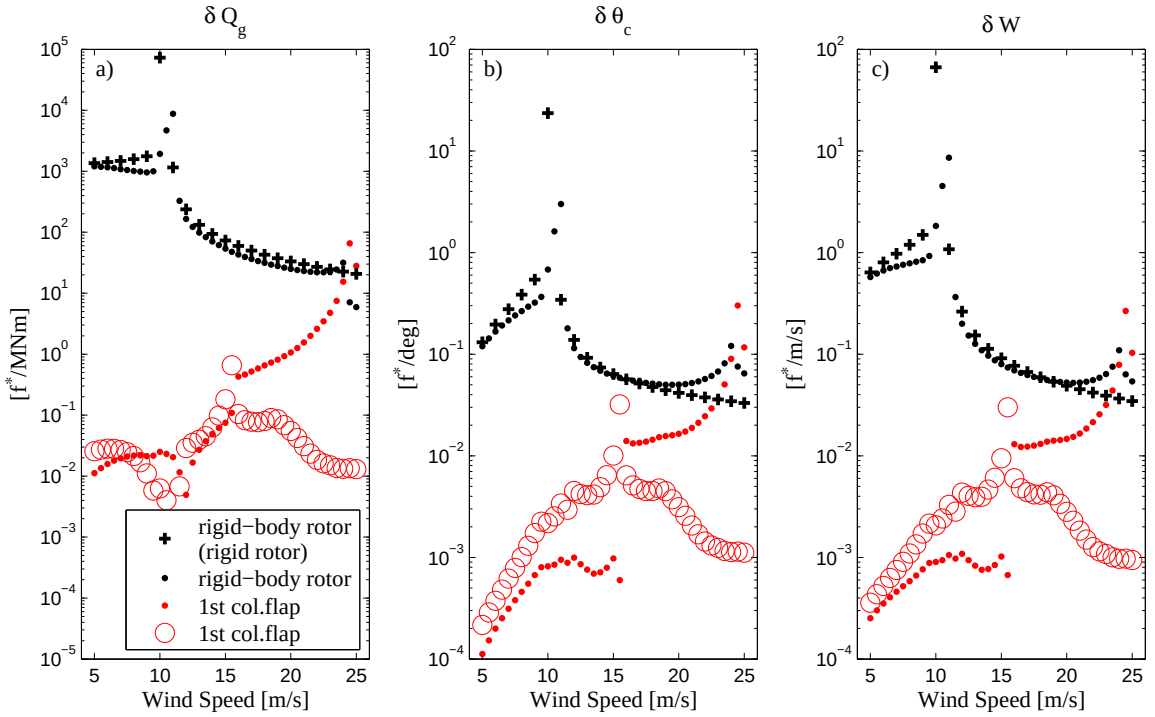

Figure 14. Magnitude of the components of the reduced-order input matrix $\mathbf{B}_r$ corresponding to the rigid-body rotor mode and the 1st collective flap mode for NREL 5 MW wind turbine in normal operation at wind speeds from 5 m/s to 25 m/s equidistant with 0.5 m/s for generator torque, collective pitch and mean wind speed inputs. Comparison between components of $\mathbf{B}_r$ for a fully flexible turbine with quasi-steady aerodynamics and a turbine with rigid lateral tower, rigid rotor and drivetrain with quasi-steady aerodynamics. The unit f^* represents the unit of the generalized force acting on each mode shape.

rigid-body rotor mode and collective flap motion at high pitch angles. Above 16 m/s the sign of $\mathbf{B}_{r,i}$ (not shown) for the rigid-body rotor mode and the 1st collective flap mode are opposite, showing that the effect of the 1st collective flap mode counteracts the effect of rigid-body rotor mode on the generator speed signal at 0 Hz, as previously explained.

Figure 15 shows the two components $\mathbf{B}_{r,i,\alpha}$ and $\mathbf{B}_{r,i,\beta}$ of the input matrices $\mathbf{B}_{r,i}$ to the 1st lateral tower mode (row a), the 1st longitudinal tower mode (row b) and the 1st drivetrain mode (row c) for the NREL 5 MW wind turbine in normal operation at wind speeds from 5 m/s to 25 m/s. The figure shows a comparison of the components of the input matrix corresponding to the 1st longitudinal tower mode for a fully flexible turbine including quasi-steady aerodynamics and a turbine with rigid lateral tower, rigid drivetrain and rotor and quasi-steady aerodynamics (dashed lines).

The components $\mathbf{B}_{r,i,\alpha}$ and $\mathbf{B}_{r,i,\beta}$ corresponding to the 1st lateral tower mode are shown in row a) in Figure 15. Below 11 m/s both these components are almost constant for generator torque input, because the lateral tower mode here is excited mainly by the generator torque reaction forces on the tower. Above 11 m/s, both components increase slighly with wind speed, which can be explained by the influence of longitudinal tower motion in this mode, as reported in [17], that causes the 1st lateral tower also to be excited by variations in thrust forces. For the two other inputs: changes in collective pitch angles and mean wind speed, the components $\mathbf{B}_{r,i,\alpha}$ and $\mathbf{B}_{r,i,\beta}$ both increase with wind speed, showing that the lateral tower mode has increasing influence on the generator speed response in response to excitation with these inputs. This observation can be explained by higher variations in thrust forces from collective pitching and changes in mean wind speed as the wind speed increases, due to higher relative velocities and can also be explained by the longitudinal tower motion in the 1st lateral tower modes at high wind speed, causing higher excitation of the lateral tower mode.

Figure 15 row b) shows the variation of the components $\mathbf{B}_{r,i,\alpha}$ and $\mathbf{B}_{r,i,\beta}$ for the 1st longitudinal tower mode. For generator torque inputs these two components are close to zero below 11 m/s, whereas above 11 m/s the components increase with wind speed. The generator torque input excites the longitudinal tower mode mainly through changes in thrust forces caused by changes in relative velocities at the blades when the rotor speed changes. The increasing pitch angles from 11 m/s cause these changes in thrust to increase with wind speed. Also for collective pitch and mean wind speed inputs, the components $\mathbf{B}_{r,i,\alpha}$ and $\mathbf{B}_{r,i,\beta}$ increase with wind speed, because of the higher changes in thrust associated with collective pitching and changes in mean wind speed. The dashed black and red curves in row b) in Figure 15 shows the input to the 1st longitudinal tower mode for a turbine with rigid lateral tower, rigid drivetrain and rotor and quasi-steady aerodynamics.

DOI: 10.1002/we
Prepared using weauth.cls

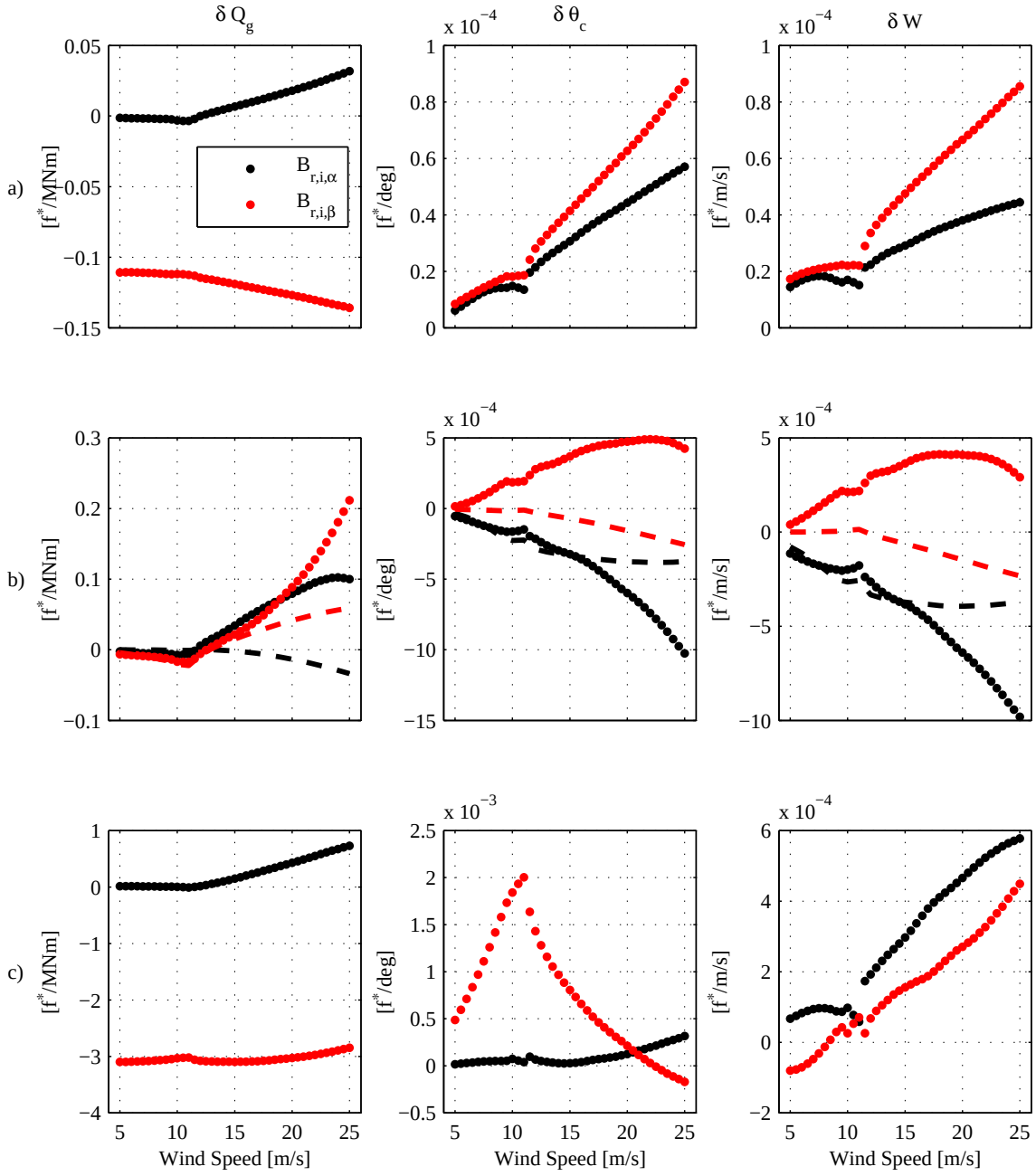

Figure 15. Components of the reduced-order input matrix $\mathbf{B}_{r,i}$ corresponding to excitation of the 1^{st} lateral tower mode (row a), the 1^{st} longitudinal tower mode (row b) and the 1^{st} drivetrain mode (row c) for the NREL 5 MW wind turbine in normal operation at wind speeds from 5 m/s to 25 m/s equidistant with 0.5 m/s. Comparison between $\mathbf{B}_{r,i}$ for a fully flexible turbine including quasi-steady aerodynamics and a turbine with rigid lateral tower, drivetrain and rotor and quasi-steady aerodynamics (dashed curves). The three columns shows components for generator torque, collective pitch and mean wind speed inputs.

For this simplified model the inputs are smaller than for a fully flexible turbine, especially at high wind speeds. This observation can be explained by the fact that the 1^{st} longitudinal tower mode couples with collective flap motion such that the aerodynamic damping of the longitudinal tower mode is lower than for a rigid rotor. This lower aerodynamic damping of the 1^{st} longitudinal tower mode cause the tower vibrations to be larger and thereby cause larger changes in the rotor speed, through the aeroelastic coupling between longitudinal tower vibration and the rotor speed through changes in the aerodynamic rotor torque.

Figure 15 row c) shows $\mathbf{B}_{r,i,\alpha}$ and $\mathbf{B}_{r,i,\beta}$ corresponding to the 1st torsional drivetrain mode. For generator torque inputs, both of the components are see to vary smoothly with wind speed. For collective pitch inputs, the magnitude increase similar to the static flap deflection of the blades, because the 1st drivetrain mode is excited by pitching inertia forces as described in [17]. For wind speed inputs, both components increase with wind speed, which can be explained by the larger pitch angles causing larger variations in the aerodynamic rotor torque when the mean wind speed changes.

5. CONCLUSIONS

In this paper, linear aeroelastic low-order wind turbine models are designed by order reduction of a high-order model of a modern pitch-regulated wind turbine. Order reduction is done by modal truncation using aeroelastic mode shapes predicted by a high-order model, which is a linearization of a geometrically nonlinear finite beam element model of tower, drivetrain and blades coupled with an unsteady Blade Element Momentum (BEM) model of aerodynamic forces including effects of shed vorticity and dynamic stall.

The main findings are that a relatively large number of aerodynamically dominated modes must be included to provide good approximation of the frequency response of e.g. the rigid-body rotor rotation mode and the 1st longitudinal tower mode, which is due to the assumption in the BEM model of no spanwise aerodynamic coupling of unsteady aerodynamic forces on the blades. Reduced-order models are subsequently designed under assumption of quasi-steady aerodynamics and it is shown how the frequency response functions predicted with the high-order model with quasi-steady aerodynamics are gradually approximated by increasing the number of modes in the reduced-order model. Good approximation is achieved up to the frequency of the 2nd drivetrain torsional mode from a 13th order state-space model including the rigid-body rotor mode, the 1st longitudinal and lateral tower modes, the 1st and 2nd collective flap modes and the 1st and 2nd drivetrain modes. By using a convenient normalization of the eigenvectors of the modes used in the model, the system matrices of the reduced-order models are shown to be suited for parametrization with operating point and therefore suited for design of gain-scheduling controllers.

Wind Energ. 2012; **00**:1–?? © 2012 John Wiley & Sons, Ltd.
DOI: 10.1002/we
Prepared using weauth.cls

REFERENCES

1. Bossanyi EA. Wind turbine control for load reduction. *Wind Energy* 2003; **6**(3):229–244.
2. van Engelen T. Control design based on aero-hydro-servo-elastic linear models from TURBU (ECN). *Proceedings of the European Wind Energy Conference*, 2007.
3. Kanev S, van Engelen T. Wind turbine extreme gust control. *Wind Energy* 2010; **13**(1):18–35.
4. Selvam K, Kanev S, Wingerden JWv, Engelen Tv, Verhaegen M. Feedback-feedforward individual pitch control for wind turbine load reduction. *International Journal of Robust and Nonlinear Control* 2009; **19**(1):72–91.
5. Craig RR, Bampton MC. Coupling of substructures for dynamic analysis. *AIAA journal* 1968; **6**(7):1313–1319.
6. Cook RD, Malkus DS, Plesha ME, Witt RJ. *Concepts and Applications of Finite Element Analysis*. 4 edn., Wiley, 2001.
7. Dowell EH ((ed.)). *A Modern Course in Aeroelasticity*. 3rd edn., Springer, 1995.
8. Karpel M. Design for active flutter suppression and gust alleviation using state-space aeroelastic modeling. *Journal of Aircraft* 1982; **19**(3):221–227.
9. Moore B. Principal component analysis in linear systems: Controllability, observability, and model reduction. *Automatic Control, IEEE Transactions on* 1981; **26**(1):17–32.
10. Fernando K, Nicholson H. Singular perturbational model reduction of balanced systems. *IEEE Transactions on Automatic Control* Apr 1982; **27**(2):466 – 468.
11. Antoulas AC. *Approximation of Large-Scale Dynamical Systems*. Society for Industrial Mathematics, 2005.
12. Bianchi FD, Mantz RJ, Christiansen CF. Control of variable-speed wind turbines by LPV gain scheduling. *Wind Energy* 2004; **7**(1):1–8.
13. Østergaard KZ, Stoustrup J, Brath P. Linear parameter varying control of wind turbines covering both partial load and full load conditions. *International Journal of Robust and Nonlinear Control* 2009; **19**(1):92–116.
14. Adegas FD, Sønderby I, Hansen MH, Stoustrup J. Reduced-order LPV model of flexible wind turbines from high fidelity aeroelastic codes. *IEEE Systems and Control Conference*, 2013. (submitted).
15. Bottasso C, Croce A, Nam Y, Riboldi C. Power curve tracking in the presence of a tip speed constraint. *Renewable Energy* Apr 2012; **40**(1):1–12.
16. Lawson CL, Hanson RJ. *Solving Least Squares Problems*. Society for Industrial and Applied Mathematics, 1987.
17. Sønderby I, Hansen MH. Open-loop frequency response analysis of a wind turbine using a high-order linear aeroelastic model. *Wind Energy* 2013; (accepted).
18. Bisplinghoff RL, Ashley H, Halfman RL. *Aeroelasticity*. Dover Publications: New York, 1996.
19. Hansen MH. Aeroelastic properties of backward swept blades. *Proceedings of the 49th AIAA Aerospace Sciences Meeting Including the New Horizons Forum and Aerospace Exposition*, Orlando, Florida, 2011.
20. Jonkman J, Butterfield S, Musial W, Scott G. Definition of a 5-MW reference wind turbine for offshore system development. *Technical Report*, NREL 2009.
21. Hansen MH, Zahle F. Aeroelastic optimization of MW wind turbines. *Technical Report Risø-R-1803(EN)*, DTU Wind Energy 2011.
22. Hansen MH, Gaunaa M, Madsen H. A Beddoes-Leishman type dynamic stall model in state-space and indicial formulations. *Technical Report Risø-R-1354(EN)*, Risø, National Laboratory 2004.
23. Skjoldan P, Hansen M. On the similarity of the Coleman and Lyapunov-Floquet transformations for modal analysis of bladed rotor structures. *Journal of Sound and Vibration* Nov 2009; **327**(3-5):424–439.
24. Hansen MH. Aeroelastic instability problems for wind turbines. *Wind Energy* 2007; **10**(6):551–577.
25. Leithead W, Dominguez S. Coordinated control design for wind turbine control systems. *Scientific proceedings of the EWEC 2006*, vol. 2006, Athens, Greece, 2006; 56–59.

P3

Reduced-order LPV Model of Flexible Wind Turbines from High Fidelity Aeroelastic Codes

manuscript submitted for 2013 IEEE Multi-conference on Systems and Control

Reduced-Order LPV Model of Flexible Wind Turbines from High Fidelity Aeroelastic Codes

Fabiano D. Adegas[1], Ivan B. Sønderby[2], Morten H. Hansen[2], Jakob Stoustrup[1]

Abstract— **Linear aeroelastic models used for stability analysis of wind turbines are commonly of very high order. These high-order models are generally not suitable for control analysis and synthesis. This paper presents a methodology to obtain a reduced-order linear parameter varying (LPV) model from a set of high-order linear time invariant (LTI) models. Firstly, the high-order LTI models are locally approximated using modal and balanced truncation and residualization. Then, an appropriate coordinate transformation is applied to allow interpolation of the model matrices between points on the parameter space. The obtained LPV model is of suitable size for designing modern gain-scheduling controllers based on recently developed LPV control design techniques. Results are thoroughly assessed on a set of industrial wind turbine models generated by the recently developed aeroelastic code HAWCStab2.**

I. Introduction

Linear aeroelastic models used for stability analysis of wind turbines are commonly of very high order. Multibody dynamics coupled with unsteady aerodynamics (e.g. dynamic stall) are among the recently developments in wind turbine aeroelasticity [1]. The resulting models contains hundreds or even thousands of flexible modes and aerodynamic delays. In order to synthesize wind turbine controllers, a common practice is to obtain linear time-invariant (LTI) models from a nonlinear model for different operating points. Modern control analysis and synthesis tools are inefficient for such high-order dynamical systems; reducing the model size is crucial to analyze and synthesize model-based controllers.

Model-based control of wind turbines has been extensively researched during the last decade [2]. The linear parameter varying (LPV) framework shown to be suitable to cope, in a systematic manner, with the inherent varying dynamics of a wind turbine over the operating envelope [3], [4], [5]. Wind turbine LPV models are usually simple, first-principles based, often neglecting dynamics related to aerodynamic phenomena and some structural modes. This in turn restricted LPV control of wind turbines to the academic environment only. A procedure to encapsulate high-fidelity dynamics of wind turbines as an LPV system would be beneficial to facilitate industrial use of LPV control.

This paper presents a procedure to obtain a reduced-order LPV wind turbine model from a set of high-order LTI models. Firstly, the high-order LTI models are locally approximated using modal and balanced truncation and residualization. Then, an appropriate manipulation of the coordinate system is applied to allow interpolation of the model matrices between points of the parameter space. The obtained LPV model is of suitable size for synthesizing modern gain-scheduling controllers based on the recent advances on LPV control design. Time propagation of the varying parameter is not explicitly utilized. Therefore, the procedure assumes that the varying parameter do not vary excessively fast in time, in line with common practices in gain-scheduling control [6]. Results are thoroughly assessed on a set of industrial wind turbine models derived by the recently developed aeroelastic code HAWCStab2.

This paper is organized as follows. The modeling principles of the high-order LTI wind turbine models are exposed in Section II. Section III is devoted to present the proposed method. Section IV brings a numerical example along with results. Conclusions and future work are discussed in Section V.

II. Wind Turbine Model

A nonlinear high-fidelity aeroelastic model is the starting point of the modeling procedure. The wind turbine structure is modeled with nonlinear kinematics based on co-rotational Timoshenko elements. Aerodynamics are modeled with Blade Element Momentum (BEM) coupled with unsteady aerodynamics based of shed-vorticity and dynamic stall. Linearization is performed analytically around a steady operational state for a given mean wind speed, rotor speed and collective pitch angle. Hansen [7] gives a more complete description of the linear aeroelastic model for an isolated blade. Two main equations of motion, one related to structural dynamics and another related to aerodynamics contitutes the LTI model

$$\begin{aligned} M\ddot{q}_s(t) + (C+G+C_a)\,\dot{q}_s(t) + (K+K_{sf}+K_a)u_s(t) \\ +A_f x_a(t) = F_s(t) \\ \dot{x}_a(t) + A_d x_a(t) + C_{sa}\dot{q}_s(t) + K_{sa} q_s(t) = F_a(t) \end{aligned} \quad (1)$$

where q_s are the elastic and bearing degrees of freedom, x_a are aerodynamic state variables, M is the structural mass matrix, C the structural damping matrix (Rayleigh), G the gyroscopic matrix, C_a is the aerodynamic damping matrix, K the elastic stiffness matrix, K_{sf} the geometric stiffness matrix, K_a the aerodynamic stiffness matrix, A_f is the coupling of the structure to aerodynamic states, A_d represents aerodynamic time lags, C_{sa} and K_{sa} are coupling matrices to

*This work is supported by Vestas Wind Systems A/S under the scope of Vestas Control Programme at Aalborg University.

[1]Dept. of Electronic Systems, Aalborg University, 9220-DK Aalborg, Denmark fda,jakob at es.aau.dk

[2]Dept. of Wind Energy, Technical University of Denmark, 2000-DK, Roskilde, Denmark ivsq,mhha at dtu.dk

structural states. F_s and F_a represent forces due to actuators and wind disturbance. The equations in first order form are

$$\begin{aligned} \dot{x}(t) &= Ax(t) + Bu(t) \\ y(t) &= Cx(t) + Du(t) \end{aligned} \tag{2a}$$

$$x(t) = \begin{bmatrix} x_a(t) & q_s(t) & \dot{q}_s(t) \end{bmatrix}^T \quad u(t) = \begin{bmatrix} Q_g(t) & \beta(t) & V(t) \end{bmatrix}^T \tag{2b}$$

where the controllable inputs are the generator torque Q_g and collective pitch angle β, and V is the uniform wind speed disturbance input. The model outputs considered here are the generator angular velocity Ω and tower top lateral displacement q. The first output is usually measured and feed to a speed controller that manipulates the pitch angle β. The second output can be utilized for lateral tower load mitigation by generator torque control [**?**]. The aeroelastic tool offers the possibility to select other inputs and ouputs, but we limit to the ones just mentioned to clearly expose the results.

III. Reduced Order LPV Model

Consider N_s stable multiple-input multiple-output (MIMO) LTI dynamical systems (2) of order n corresponding to parameter values $\theta^{(i)}$, $i = 1, 2, \ldots, N_s$,

$$S_i : \begin{cases} \dot{x}_i(t) = A_i x_i(t) + B_i u(t) \\ y(t) = C_i x_i(t) + D_i u(t) \end{cases}, \quad i = 1, \ldots, N_s. \tag{3}$$

where $A_i \in \mathbb{R}^{n \times n}$, $B_i \in \mathbb{R}^{n \times n_u}$, $C_i \in \mathbb{R}^{n_y \times n}$, $D_i \in \mathbb{R}^{n_y \times n_u}$. We seek a reduced-order parameterized model $S(\theta)$ of order $r < n$ which approximates S_i,

$$S(\theta) : \begin{cases} \dot{x} = A(\theta)x(t) + B(\theta)u(t) \\ y(t) = C(\theta)x(t) + D(\theta)u(t) \end{cases} \tag{4}$$

where $A(\theta) \in \mathbb{R}^{r \times r}$, $B(\theta) \in \mathbb{R}^{r \times n_u}$, $C(\theta) \in \mathbb{R}^{n_y \times r}$, $D(\theta) \in \mathbb{R}^{n_y \times n_u}$ are continuous functions of a vector of varying parameters $\theta := \begin{bmatrix} \theta_1, \theta_2, \ldots, \theta_{N_\theta} \end{bmatrix}^T$. The dynamics of the original system S_i and the approximated system $S(\theta)$ are assumed to evolve smoothly with respect to $\theta^{(i)}$ and θ, respectively. The parameter θ may represent the current operating point. It also may describe deviations on aerodynamics and structural properties for the sake of parametric model uncertainties. Plant parameters to be designed under an integrated plant-controller synthesis scheme could also be parameterized.

Variation in aerodynamic forces under structural vibration contributes significantly to changes in natural frequencies and damping of some structural modes. A specific procedure that takes these particularities into account is proposed here. A flowchart containing the required steps is depicted in Fig. 1.

Known methods for model reduction constitutes the proposed scheme and are briefly explained in the sequel, in the context of our application. Consult the survey of [8] for a more comprehensive exposure on model reduction.

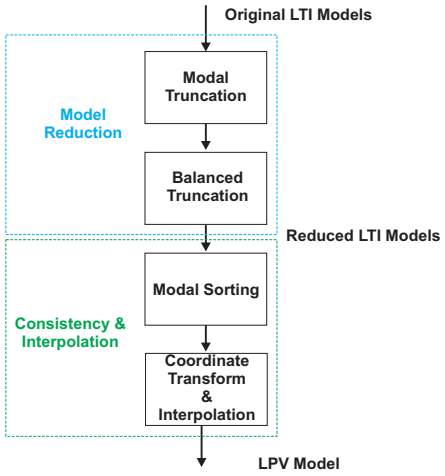

Fig. 1. Scheme overview.

A. Model Reduction

A reduced order model is commonly obtained by truncation of appropriate states. Let the state vector x_i be partitioned into $x_i := [x_{r,i} \quad x_{t,i}]^T$ where $x_{r,i}$ is the vector of retained states and $x_{t,i}$ is the vector of truncated states. The original system is partitioned accordingly

$$\begin{aligned} \begin{bmatrix} \dot{x}_{r,i}(t) \\ \dot{x}_{r,i}(t) \end{bmatrix} &= \begin{bmatrix} A_{rr,i} & A_{rt,i} \\ A_{tr,i} & A_{tt,i} \end{bmatrix} \begin{bmatrix} x_{r,i}(t) \\ x_{t,i}(t) \end{bmatrix} + \begin{bmatrix} B_{r,i} \\ B_{t,i} \end{bmatrix} u(t) \\ y &= \begin{bmatrix} C_{r,i} & C_{t,i} \end{bmatrix} \begin{bmatrix} x_{r,i}(t) \\ x_{t,i}(t) \end{bmatrix} + Du(t) \end{aligned} \tag{5}$$

and the reduced model is simply given by the state-space equation of the retained states

$$\begin{aligned} \dot{x}_{r,i} &= A_{rr,i}x_i(t) + B_{r,i}u(t), \\ y &= C_{r,i}x_{r,i} + Du(t) \end{aligned} \tag{6}$$

If the original model is a stable system so is its truncated counterpart. While truncation tends to produce a good approximation in the frequency domain, the zero frequency gains (DC gains) are not guaranteed to match. This can be of particular importance in a wind turbine model because some aerodynamic states may not influence the transient behaviour but can contribute significantly to low frequency gains. Matching DC gains can be enforced by a model residualization method by setting the derivative of $x_{t,i}$ to zero in (5) and solving the resulting equation for $x_{r,i}$. After trivial manipulations, the reduced model is given by

$$\begin{aligned} \dot{x}_{r,i} &= \left[A_{rr} - A_{rt}A_{tt}^{-1}A_{tr}\right]_i x_{r,i} + \left[B_r - A_{rt}A_{tt}^{-1}B_t\right]_i u(t) \\ y &= \left[C_r - C_t A_{tt}^{-1}A_{tr}\right]_i x_{r,i} + \left[D - C_t A_{tt}^{-1}B_t\right]_i u(t) \end{aligned} \tag{7}$$

Note that $A_{tt,i}$ is assumed invertible for (7) to hold. Residualization is performed in both modal and balanced reduction steps.

1) Modal Truncation: Due to size and numerical properties associated with large size systems and low damped dynamics, most model reduction algorithms based on Hankel singular values fail to produce a good reduced model. In

order to start the reduction process, the original model is truncated to an intermediate size for subsequent reduction in a more accurate way. In modal form the system is put into a modal realization before states are truncated [9]. The modal form realization has the state matrix A is in block diagonal form with either 1×1 or 2×2 blocks when the eigenvalue is real or complex, respectively. Let system S_i be represented in modal form,

$$S_{m,i}: \begin{cases} \dot{x}_i(t) = A_{m,i}x_{m,i}(t) + B_{m,i}u(t) \\ y(t) = C_{m,i}x_{m,i}(t) + D_{m,i}u(t) \end{cases} \tag{8a}$$

$$\begin{aligned} &A_{m,i} = \mathrm{diag}(A_{m,k,i}), \\ &A_{m,k,i} = -e_{k,i} \quad \text{for real eigenvalues,} \\ &A_{m,k,i} = \begin{bmatrix} -\xi_{k,i}\omega_{k,i} & \omega_{k,i}\sqrt{1-\xi^2} \\ \omega_{k,i}\sqrt{1-\xi^2} & -\xi_{k,i}\omega_{k,i} \end{bmatrix} \quad \text{for complex eigen.} \\ &B_{m,i} = \begin{bmatrix} B_{m,1,i} \\ B_{m,2,i} \\ \vdots \\ B_{m,k,i} \end{bmatrix}, \quad C_{m,i} = \begin{bmatrix} C_{m,1,i} & C_{m,2,i} & \dots & C_{m,k,i} \end{bmatrix} \\ &i = 1,\dots,N_s, \quad k = 1,\dots,N_m. \end{aligned} \tag{8b}$$

where N_m is the number of modes, $\xi_{k,i}$ and $\omega_{k,i}$ are the damping ratio and natural frequency of mode k and model i. The diagonal blocks are usually arranged in ascending order according to their eigenvalue magnitudes. The magnitude of a complex eigenvalue is $\omega_{k,i}$ while for a purely real eigenvalue is $e_{k,i}$. The retained states are then the ones with magnitudes smaller than a chosen treshhold $\bar{\omega}$. The intermediate model must contain all modes within the frequencies of interest for control design. A large number of states (300 to 450) is expected at this stage since many modes are of low frequency.

2) Balanced Truncation: The order of the intermediate system is further reduced by balanced truncation. In balanced truncation [**?**] the system is transformed to a balanced realization. A MIMO LTI system of the form (3) is said to be balanced if, and only if, its controllability and observability grammians are equal and diagonal, i.e. $P_i = Q_i = \mathrm{diag}\,(\sigma_1,\dots,\sigma_n)$, where $\sigma_1,\dots,\sigma_n$ denotes the Hankel singular values sorted in decreasing order and matrices P_i, Q_i are the controllability and the observability Gramians. The gramians are solutions of the following Lyapunov equations

$$\begin{aligned} A_iP_i + P_iA_i^T + B_iB_i^T &= 0 \\ A_i^TQ_i + Q_iA_i + C_i^TC_i &= 0 \end{aligned} \tag{9}$$

If this holds, the balanced system is given by

$$S_{b,i}: \begin{cases} \dot{x}_{b,i} = W_i^TA_iV_ix_{b,i}(t) + W_i^TB_iu_i(t) \\ y(t) = C_iV_ix_{b,i}(t) + D_iu_i(t) \end{cases} \tag{10}$$
$$i = 1,\dots,N_s.$$

where $x_b \in \mathbb{R}^n$, $V = UZ\Sigma^{-1/2}$ and $W = LY\Sigma^{-1/2}$, together with the factorizations $P = UU^T$, $Q = LL^T$ and the singular value decomposition $U^TL = Z\Sigma Y^T$ [10]. This state coordinate equalizes the input-to-state and state-to-output energy transfers, making the Hankel singular values a measure of the contribution of each state to the input/output behavior.

Denote $V_{i(r)}$ and $W_{i(r)}$ the first r columns of V_i and W_i. The reduced-order systems $\hat{S}_i$

$$\hat{S}_i: \begin{cases} \dot{\hat{x}}_i = \hat{A}_i\hat{x}_i(t) + \hat{B}_iu_i(t) \\ \hat{y}(t) = \hat{C}_i\hat{x}_i(t) + \hat{D}_i\hat{u}_i(t) \end{cases} \qquad i = 1,\dots,N_s. \tag{11}$$

are obtained by truncation when the projectors $V_{i(r)}$ and $W_{i(r)}$ are applied to the intermediate sized model. In words, the balanced truncation removes the states with low Hankel singular values, thus not much information about the system will be lost. When applied to a stable system, balanced truncation preserves stability and guarantes and an upper bound on the approximation error in an H_∞ sense [11]. Expected order of the final reduced system is 7 to 20 states. The choice of the final order depends on the required model complexity and admissible error between the full and reduced model.

B. State-Space Consistency & Interpolation

Consider the balanced reduced models $\hat{S}_i$ and put them in modal form. The first step towards a consistent state-space representation is to assure that all modes keep their positions in the state matrix throughout the parameter space. The second step to a consistent state-space is to ensure that values of the entries of the system matrices change smoothly between each LTI system. At this point, the system matrices cannot be readily interpolated because the modal and balanced similarity transformations applied to the original system are not unique. One could think of interpolating the system in modal form. Indeed, the state matrix A is unique up to a permutation of the location of the modes and could easily be interpolated, but the similarity transformation that puts the system in modal form is not unique. Therefore, matrices $\hat{B}$ and $\hat{C}$ may have entries with abrupt value changes. The balanced realization is unique up to a sign change and consequently abrubt sign changes in the system matrices may occur from one LTI system to another. As suggested by [12], these issues can be corrected by properly changing the sign of the correspondent eigenvectors.

Istead of correcting the eigenvectors before similarity transformations, we propose to transform the reduced order LTI systems into a representation based on the companion canonical form. No unique canonical form for multivariable systems is known to exist [13]. However, there exist algorithms which, for a system under arbitrary similarity transformation, find a unique companion form [14]. One algorithm with such properties is implemented in the function *canon* of MATLAB. The companion form is poorly conditioned for most state-space computations [15]. In order to avoid numerical issues, each mode k of the reduced system in modal coordinates is transformed into a companion realization. The system matrices of this particular realization

are

$$A_{c,i} = \text{diag}(A_{c,k,i}), \quad B_{c,i} = \begin{bmatrix} B_{c,1,i} \\ B_{c,2,i} \\ \vdots \\ B_{c,k,i} \end{bmatrix},$$
$$C_{c,i} = \begin{bmatrix} C_{c,1,i} & C_{c,2,i} & \dots & C_{c,k,i} \end{bmatrix},$$
$$\begin{cases} A_{c,k,i} = -a_{k,i} \\ B_{c,k,i} = \begin{bmatrix} 1 & b_{1,k,i} & \dots & b_{n_u-1,k,i} \end{bmatrix} \\ C_{c,k,i} = \begin{bmatrix} c_{1,k,i} \\ \dots \\ c_{n_y-1,k,i} \\ 0 \end{bmatrix} \end{cases} \text{for real eigenvalues,}$$
$$\begin{cases} A_{c,k,i} = \begin{bmatrix} 0 & -a_{k,i,1} \\ 1 & -a_{k,i,2} \end{bmatrix}, \\ B_{c,k,i} = \begin{bmatrix} 0 & b_{11,k,i} & \dots & b_{1n_u-1,k,i} \\ 1 & b_{21,k,i} & \dots & b_{2n_u,k,i} \end{bmatrix} \\ C_{c,k,i} = \begin{bmatrix} c_{11,k,i} & \dots & c_{1r,k,i} \\ \vdots & \ddots & \vdots \\ c_{n_y1,k,i} & \dots & c_{n_yr,k,i} \end{bmatrix} \end{cases} \text{for complex eigen.}$$
$$i = 1, \dots, N_s, \quad k = 1, \dots, N_m. \tag{12}$$

The characteristic polynomial of each mode appears in the rightmost column of the matrix $A_{c,k,i}$. The entries of $A_{c,k,i}$, $B_{c,k,i}$ and $C_{c,k,i}$ may be easily checked for possible inconsistencies of a particular mode, by detecting abrupt value changes between LTI systems. The state-space matrices are now at a realization suitable for interpolation. Let $z(\theta)$ be one matrix entry, function of θ. We focus on the polynomial dependence

$$z(\theta) = \sum_{k=1}^{N_p} \eta_k p_k(\theta) \tag{13}$$

where p_k is a set of multivariate polynomials on the parameters $\theta_1, \dots, \theta_{N_\theta}$ and η_k are coefficients to be determined. Let z_i be the values of a matrix element for $i = 1, \dots, N_s$. Define the following matrices

$$H = \begin{bmatrix} p_1(\theta^{(1)}) & \dots & p_{N_p}(\theta^{(1)}) \\ \vdots & \ddots & \vdots \\ p_1(\theta^{(N_s)}) & \dots & p_{N_p}(\theta^{(N_s)}) \end{bmatrix} = \begin{bmatrix} P_1 & \dots & P_{n_p} \end{bmatrix}$$
$$Z^T = \begin{bmatrix} z_1 & \dots & z_{N_s} \end{bmatrix}, \quad \Gamma^T = \begin{bmatrix} \eta_1 \dots \eta_{N_p} \end{bmatrix}. \tag{14}$$

A linear least squares fit minimizes the quadratic error between $z(\theta^{(i)})$ and z_i, $i = 1, \dots, N_s$

$$\Gamma^* = \arg\min_{\Gamma} (Z - H\Gamma)^T (Z - H\Gamma) \tag{15}$$

The optimal Γ^* is determined by initialy computing a singular value decomposition of H

$$\Upsilon \Xi \Psi^T = \text{svd}(H) \tag{16}$$

With the decomposition at hand, the solution to the linear least squares problem is given by

$$\Gamma^* = \Psi \Xi^+ \Upsilon^T Z \tag{17}$$

where Ξ^+ stands for the Moore-Penrose pseudoinverse of Ξ. Repeating the above procedure for each matrix entry results in the polynomial approximations of the matrices $A(\theta)$, $B(\theta)$, $C(\theta)$, $D(\theta)$ that can be used for subsequent analysis and design of controllers.

IV. Numerical Example

In this section, the proposed procedure is applied to the NREL 5MW reference wind turbine model [16]. The aim is to find an LPV model encapsulating the wind turbine dynamics operating at the full load region. Large scale MIMO LTI models with 877 states are computed by the aeroelastic code HAWCStab2 for wind speeds equidistant 1 m/s ($\theta^{(i)} \in \{12, 13, \dots, 25\}$). The model is parameterized by the mean wind speed $\theta := \bar{V}$. A fifth-order polynomial dependence of the LPV system matrices

$$\begin{bmatrix} A(\theta) & B(\theta) \\ C(\theta) & D(\theta) \end{bmatrix} = \begin{bmatrix} A_0 & B_0 \\ C_0 & D_0 \end{bmatrix} + \sum_{d=1}^{5} \begin{bmatrix} A_d & B_d \\ C_d & D_d \end{bmatrix} \theta^d \tag{18}$$

gives a fair trade-off between interpolation accuracy and polynomial order. Due to the different units of inputs and outputs, the LTI systems should be suitably normalized before the order is reduced. Parameter-independent scales are applied to all LTI models such that expected signal excursions are normalized to 1. The generator torque input was scaled to 5% of the rated torque. The pitch angle input and wind speed input remained unscaled. The rotor angular velocity is scaled to the maximum excursion desired in closed-loop, 5 % of its nominal value. The lateral tower top displacement was scaled with the H_∞-norm of the inputs to this output channel.

Bode plots of the original, intermediate and final reduced order models for an operating point $\theta = 15$ m/s are depicted in Fig. 2. The intermediate model with 410 states resulted from modal truncation and residualization of the original system. A balanced truncation with residualization further reduced the size to 14 states. The magnitude plots have an excellent agreement in the frequencies of interest. The residualization in both steps assisted to a better fit of the low frequency content of the tower displacement output.

The balanced realization "misses" a low frequency anti-ressonance related to the transfer function from wind speed input to tower displacement output. Notice the differences in magnitude and more pronouncedtly phase around 10^{-2} Hz. However, this anti-ressonance does not contribute significantly to the input-output behaviour of the MIMO system. A comparison of the minimum and maximum singular values is depicted in Fig. 3 and shows an excellent agreement.

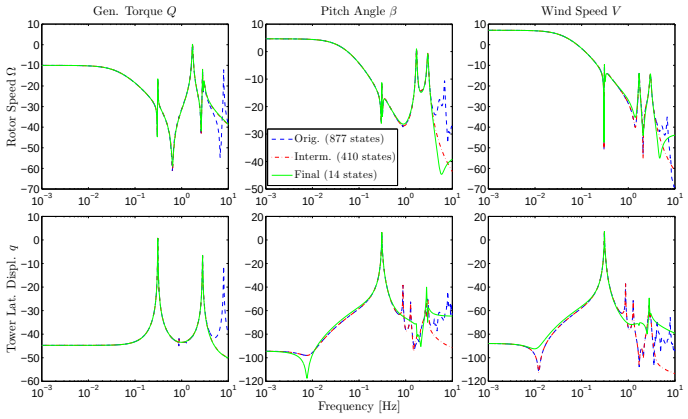

(a) Magnitude

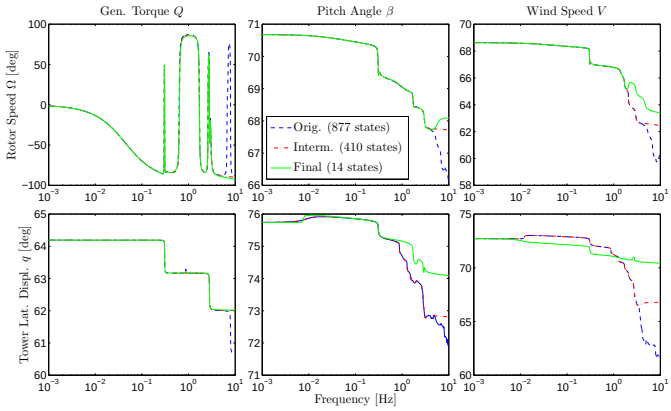

(b) Phase

Fig. 2. Bode plots of the original, intermediate and final reduced order models for a mean wind speed of 15 m/s.

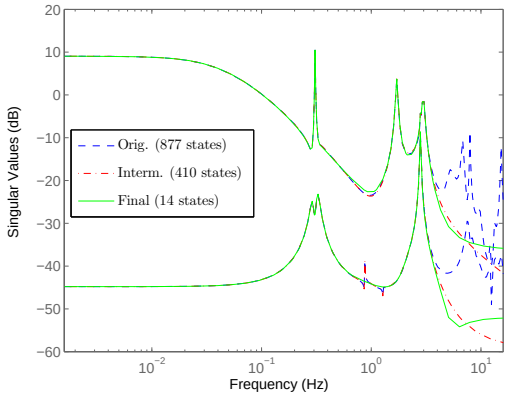

Fig. 3. Singular values of the original, intermediate and final reduced order models for a mean wind speed of 15 m/s.

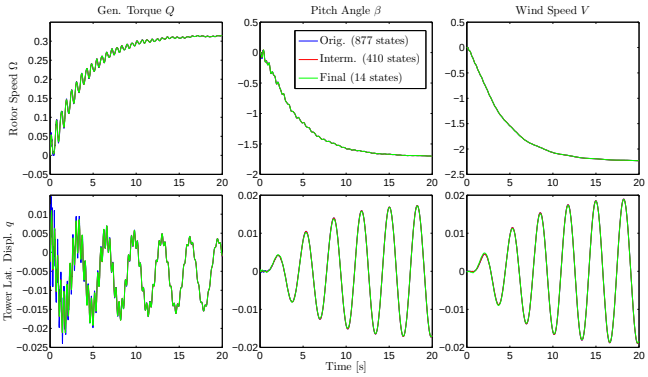

Fig. 4. Step responses of the original, intermediate and final reduced order models for a mean wind speed of 15 m/s.

Step responses of the original, intermediate and final reduced order models for a mean wind speed of 15 m/s are depicted in Fig. 4. Except for some high frequency content in the signal from generator torque to tower position, the responses are identical.

The location of the poles of the LPV system for a $2N_s$ grid of equidistant operating points is illustrated in Fig. 5. The arrows indicate how the poles move for increasing mean wind speeds. A smooth evolution of the poles along the full load region is noticeable.

The relative difference of the Hankel singular values of the interpolated LPV system and the reduced order system defined as

$$\sigma_{rel,r,i} = \frac{\sigma_{int,r,i} - \sigma_{r,i}}{\sigma_{r,i}} \times 100, \quad i = 1, \ldots, N_s \qquad (19)$$

serves as a measure of the quality of the interpolation. A good fit can be corroborated by some metrics of $\sigma_{rel,r,i}$ given in Tab. I. The mean difference in the Hankel singular values is only 0.27% and the maximum difference just 2.75%.

V. Conclusion & Future Work

This paper presents a procedure to obtain a reduced-order LPV model of a wind turbine from a set of high-order LTI models. Finding ways to encapsulate high-fidelity LTI aeroelastic models as an LPV system is an important step to increase the utilization of recent advances in LPV control by the wind turbine industry. The proposed procedure starts by model reduction of the high-order LTI systems at different values of the parameter space. Manipulations of the state-space coordinates follows, in order to arrive at low-order consistent LTI systems for subsequent interpolation. The reduced-order LPV system has a suitable size for analysis and synthesis of controllers and presents smoothly varying dynamics along the scheduling parameter range.

A subject for future work is to initially interpolate the set of high-order LTI models and later apply an appropriate reduction method to realize a reduced order LPV model. Preserving structure reduction methods applied directly in the second order vector equations of motion in an interesting topic to be studied. Model complexity versus required polynomial degree and a comparison with models obtained by first-principles is also subject of future work.

References

[1] F. Rasmussen, M. Hansen, K. Thomsen, T. Larsen, F. Bertagnolio, J. Johansen, H. A. Madsen, C. Bak, and A. Hansen, "Present status of aeroelasticity of wind turbines," *Wind Energy (DOI: 10.1002/we.98)*, vol. 6, 2003.

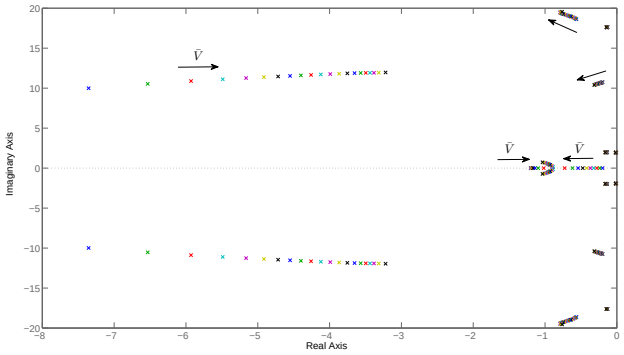

(a) Pole Map

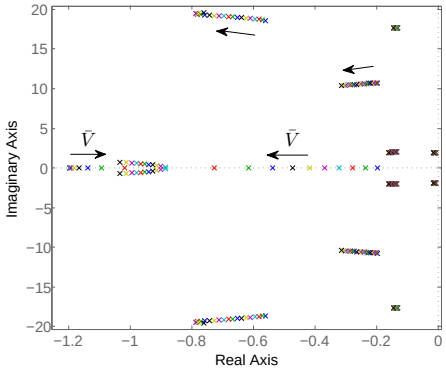

(b) Detail

Fig. 5. Pole location of the LPV model for frozen values of the varying parameter θ.

TABLE I

DIFFERENCE IN THE HANKEL SINGULAR VALUES BETWEEN THE LPV AND REDUCED ORDER SYSTEM FOR FROZEN VALUES OF θ.

Max	Min	Mean	Std. dev
2.75	0.001	0.27	0.57

[2] L. Pao and K. Johnson, "Control of wind turbines: Approaches, challenges, and recent developments," *IEEE Control Systems Magazine*, vol. 31, pp. 44–62, 2011.

[3] F. Bianchi, H.D.Battista, and R. Mantz, *Wind turbine control systems: Principles, modelling and gain scheduling design.* Springer-Verlag, London, 2007.

[4] K. Ostergaard, B. P., and J. Stoustrup, "Linear parameter varying control of wind turbines covering both partial load and full load conditions," *Int J Robust Nonlinear Contr*, vol. 19, p. 92116, 2009.

[5] F. Adegas, C. Sloth, and J. Stoustrup, "Structured linear parameter varying control of wind turbines," in *Control of Linear Parameter Varying Systems with Applications*. Springer-Verlag, London, 2012.

[6] J. S. Shamma and M. Athans, "Gain scheduling: Potential hazards and possible remedies," *IEEE Control Syst. Magazine*, vol. vol. 12, no. 3, p. 101107, 1992.

[7] M. Hansen, "Aeroelastic properties of backward swept blades," in *Proc. of the 49th AIAA Aerospace Sciences*, Orlando, Florida, 2011.

[8] S. Gugercin and A. C. Antoulas, "A survey of model reduction by balanced truncation and some new results," *Int. J. Control*, vol. 77, pp. 748–766, 2004.

[9] W. Gawronski, *Dynamics and Control of Structures: A Modal Approach*, Springer, Ed. Springer, 1998.

[10] A. Laub, M. Heath, C. Paige, and R. Ward, "Computation of system balancing transformations and other applications of simultaneous diagonalization algorithms," *IEEE Transactions on Automatic Control*, vol. Vol.32, Issue 2, pp. 115–122, 1987.

[11] K. Zhou, J. Doyle, and K. Glover, *Robust and Optimal Control*. Prentice Hall, 1996.

[12] M. Lovera and G. Mercere, "Identification for gain-scheduling: A balanced subspace approach," in *Proc. American Control Conference*, 2007.

[13] D. Luenberger, "Canonical forms for linear multivariable systems," *IEEE Transaction on Automatic Control*, vol. 12(3), p. 290293, 1967.

[14] T. Kailath, *Linear Systems*. Prentice Hall, 1980.

[15] *Documentation of the MATLAB Control System Toolbox, State-Space Models, canon function.*

[16] J. Jonkman, S. Butterfield, W. Musial, and G. Scott, "Definition of a 5-mw reference wind turbine for offshore system development," National Renewable Energy Laboratory, Tech. Rep., 2009.